ACETIC ACID AS A CATALYST IN THE SYNTHESIS OF BENZOXANTHENES

Meryl Maria George,[a] R. Shah Aakruti,[a] P. Iniyavan,[a] S. Sarveswari[a] and V. Vijayakumar[a]*

Keywords: Multicomponent reactions; acetic acid; benzoxanthenes.

Multi-functionalized xanthenes were synthesised using arylaldehydes and 1,3-dicarbonyl compounds through multi-component reactions using acetic acid as the catalyst and all these newly synthesized compounds have been characterized using ^{1}H NMR, ^{13}C NMR and IR spectral data.

* Corresponding Authors
Fax: +91 416 224 3091
E-Mail: kvpsvijayakumar@gmail.com
[a] Centre for Organic and Medicinal Chemistry, VIT University, Vellore-632014, Tamilnadu, India

Introduction

The multicomponent reactions (MCR) are extremely significant due to their broad range of applications in pharmaceutical chemistry for drug discovery. MCRs are extremely convergent, producing a remarkably high increase of molecular complexity in just one step. Xanthenes and its derivatives are important in the area of medicinal chemistry. Xanthenes have wide range of biological and therapeutic properties such as antibacterial, antiviral and anti-inflammatory actions as good as in Photodynamic therapy. Furthermore, due to their useful spectroscopic properties, they were used as dyes in laser technologies and in fluorescent materials for visualization of bio molecules. It generated great attention due to its interesting biological activity.[1-8]

Acetic acid is one of the simplest carboxylic acid, which has more applications in industrial chemical, mainly used in the production of cellulose acetate for photographic film and polyvinyl acetate for wood glue, as well as synthetic fibres and fabrics[9]. In the continuation of our earlier interest on xanthenes[10-13] in the present work, we report an efficient and convenient procedure for the synthesis of xanthenes employed by the union of aldehyde and 1,3-dicarbonyl compounds in the presence acetic acid as homogeneous catalyst under thermal conditions.

Experimental

Material

All the chemicals were purchased from Sigma Aldrich and used without further purification. TLC was performed on preparative plates of silica gel (s.d.fine). Visualization was made with iodine chamber. The purity of the products was also confirmed by TLC.

Instrumentation

Melting points were recorded on Elchem Microprocessor in open capillary tubes and uncorrected. The IR spectra recorded on a Perkin Elmer 781 Spectrophotometer using KBr pellets, and only noteworthy absorption levels (reciprocal centimeters) were listed. The NMR spectra were recorded on a Bruker Avance 400 MHz spectrometer using TMS as internal standard (chemical shifts δ in ppm).

General procedure for the synthesis of xanthenes

A mixture of cyclodione 0.25g(2 mmol) / dimethyldione 0.28g(2 mmol) and arylaldehydes in acetic acid was heated at 60°C. The progress of the reaction was monitored by TLC. After completion of the reaction, the reaction mixture was cooled to room temperature. The crude product was quenched into crushed ice mixture and further it was neutralized with 10% $NaHCO_3$ solution, solids are filtered, purified through crystallisation using pet. ether. The products were characterized by IR, NMR spectroscopic data and the melting point of compounds was noted.

3,4,6,7-tetrahydro-9-(3,4-dimethoxyphenyl)-3,3,6,6-tetra methyl-2*H*-xanthene-1,8(5*H*,9*H*)-dione (3a)

IR (KBr,cm^{-1}) ν_{max}: 1667, 1504, 1449, 999; ^{1}H NMR (400 MHz, $CDCl_3$) δ_H: 1.00 (s, 6H, -CH_3),1.10 (s, 6H, -CH_3), 2.18 (d, 2H, *J* = 16.4 Hz, -$CH_{2\ axial}$), 2.44 (d, *J* = 16.4 Hz, 2H, -CH_2 axial), 2.46 (m, 4H, -CH_2 equatorial), 3.80 (s, 3H, -OCH_3 of aryl), 3.86 (s, 3H, -OCH_3 of aryl), 4.70 (s, 1H, -CH), 6.71 (d, 1H, *J* = 8.4 Hz, aryl proton at C6′ *ortho*), 6.75 (d, 1H, *J* = 8.4 Hz, aryl proton at C5′ *meta*), 7.20 (d, 1H, *J* = 4 Hz, aryl proton at C2′ *ortho*); ^{13}C NMR (100 MHz, $CDCl_3$) δ_C: 27.3, 29.4, 31.2, 32.2, 40.9, 50.8, 55.8, 55.9, 110.8, 112.3, 115.8, 120.1, 134.0, 147.4, 148.4, 162.2, 196.6.

3,4,6,7-tetrahydro-9-(3,4,5-trimethoxyphenyl)-3,3,6,6-tetra methyl-2*H*-xanthene-1,8(5*H*,9*H*)-dione (3b)

IR (KBr,cm^{-1}) ν_{max}: 2816, 1667, 1504, 999; ^{1}H NMR (400 MHz, $CDCl_3$) δ_H: 1.03 (s, 6H, -CH_3), 1.12 (s, 6H, -CH_3), 2.24 (m, 4H, CH_2), 2.47 (m, 4H, CH_2), 3.77 (s, 3H,-OCH_3), 3.85 (s, 6H,-OCH_3), 4.71 (s, 1H, CH), 6.51 (d, 2H,

aryl protons); ^{13}C NMR (100 MHz, $CDCl_3$) δ_C: 27.2, 28.9, 32.2, 40.9, 50.7, 56.1, 60.3, 105.1, 115.6, 136.6, 139.8, 152.8, 162.4, 196.6.

9-(4-Biphenylyl)-3,4,5,6,7,9-hexahydro-1*H*-xanthene-1,8 (2*H*)-dione (3c**)**

IR (KBr,cm^{-1}) ν_{max} 1667, 1483, 1360, 1011; ^{1}H NMR (400 MHz, $CDCl_3$) δ_H: 2.00-2.30 (m, 4H, -CH_2), 2.33-2.42 (m, 4H, -CH_2), 2.56-2.70 (m, 4H, -CH_2), 4.85 (s, 1H, CH), 7.26-7.52 (m, 9H, ArH).

3,4,6,7-tetrahydro-9-(3-hydroxyphenyl)-3,3,6,6-tetramethyl-2*H*-xanthene-1,8(5*H*,9*H*)-dione (3d**)**

IR (KBr,cm^{-1}) ν_{max} 2963, 1659, 1597, 1199; ^{1}H NMR (400 MHz, $CDCl_3$) δ_H: 1.00 (s, 6H, -CH_3), 1.10 (s, 6H, -CH_3), 2.20 (d, 2H, J = 16.4 Hz, -$CH_{2\ axial}$), 2.25 (d, 2H, J = 16.4 Hz, -$CH_{2\ axial}$), 2.46 (m, 4H, $CH_{2equatorial}$) 4.73 (s, 1H, CH), 6.58 (d, 1H, J = 7.7 Hz, ArH), 6.70 (d, 1H, J = 7.7 Hz, ArH), 7.02 (s, 1H, ArH), 7.05 6.58 (t, 1H, J = 7.7 Hz, ArH); ^{13}C NMR (100 MHz, $CDCl_3$) δ_C: 27.4, 29.2, 31.7, 32.3, 40.9, 50.7, 77.4, 113.6, 115.6, 116.3, 119.7, 129.2, 145.6, 156.0, 162.7, 197.0.

9-(4-Biphenylyl)-3,3,6,6-tetramethyl-3,4,5,6,7,9-hexahydro-1*H*-xanthene-1,8(2*H*)-dione (3e**)**

IR(KBr,cm^{-1}) ν_{max} 2955, 1668, 1412, 999; ^{1}H NMR (400 MHz, $CDCl_3$) δ_H: 1.02 (s, 6H, -CH_3), 1.10 (s, 6H, -CH_3), 2.16 (d, 2H, J = 16.2 Hz, -$CH_{2\ axial}$), 2.35 (d, 2H, J = 16.4 Hz, -$CH_{2\ axial}$), 2.44 (m, 4H, $CH_{2equatorial}$) 4.95 (s, 1H, CH), 6.95 (d, J = 9.6 Hz, 2H, ArH), 7.02 (m, J = 9.6 Hz, 1H, ArH), 7.15 (dd, J = 8.4 Hz, 1.6 Hz, 2H, ArH), 7.26 (dd, J = 8.4 Hz, 1.6 Hz, 2H, ArH), 7.38 (d, J = 8.4 Hz, 2H, ArH); ^{13}C NMR (100 MHz, $CDCl_3$) δ_C: 27.4, 29.3, 32.1, 40.8, 50.7, 76.7, 113.3, 126.8, 129.9, 132.8, 134.0, 163.2, 196.6.

9-(2,4-dichlorophenyl)-3,3,6,6-tetramethyl-3,4,5,6,7,9-hexa hydro-1*H*-xanthene-1,8(2*H*)-dione (3f**)**

IR (KBr,cm^{-1}) ν_{max} 1667, 1466, 1408, 567; ^{1}H NMR (400 MHz, $CDCl_3$) δ_H: 1.00 (s, 6H, -CH_3), 1.09 (s, 6H, -CH_3), 2.23 (m, 8H, CH_2), 4.7 (s, 1H, CH), 6.51 (m, 3H, ArH).

Results and Discussion

The benzoxanthenes (**3a-e**) were synthesized through the cyclocondensation reaction of 5,5-dimethylcycloheaxan-1,3-dione (**1**) (2mmol), arylaldehyde (**2a-e**) (1 mmol) in acetic acid (Scheme 1). The progress of the reaction was monitored by TLC. The attempt was found to be successful since it affords the desired product. To improve the yield the same reaction was attempted under different solvents such as ethanol, chloroform, acetic acid and found that acetic acid act as better solvent as well as the catalyst. All the synthesized compounds have been characterized using IR, ^{1}H NMR spectral data (included in experimental section). The compound 9-(4-hydroxy-3,5-dimethoxyphenyl)-3,3,6,6-tetramethyl-3,4,5,6,7,9-hexahydro-1*H*-xanthene-1,8(2*H*)-dione (**3a**) was considered as a representative example and its spectral characterization described below.

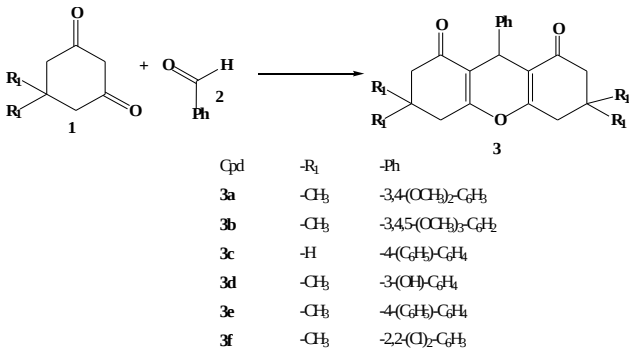

Cpd	-R_1	-Ph
3a	-CH_3	-3,4-$(OCH_3)_2$-C_6H_3
3b	-CH_3	-3,4,5-$(OCH_3)_3$-C_6H_2
3c	-H	-4-(C_6H_5)-C_6H_4
3d	-CH_3	-3-(OH)-C_6H_4
3e	-CH_3	-4-(C_6H_5)-C_6H_4
3f	-CH_3	-2,2-$(Cl)_2$-C_6H_3

Scheme 1. Synthesis of Benzoxanthenes

Proton Chemical Shift Assignment: The careful examination of ^{1}H NMR spectrum of **3a** (Fig. 1) reveals that the two singlets appeared at δ 1.00 ppm and 1.10 ppm integrating for six protons each were due to the methyl protons at C-11, 11′ and C-12, 12′.

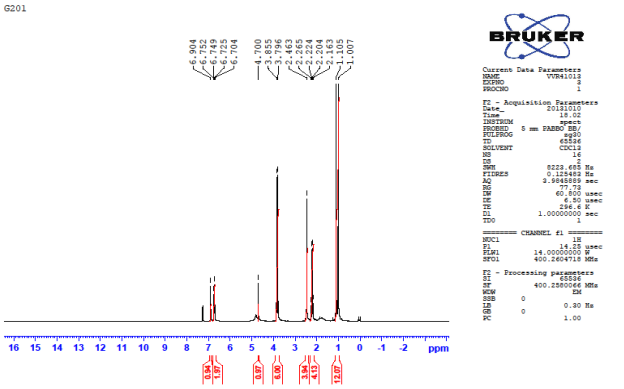

Figure 1. ^{1}H NMR spectrum of 3,4,6,7-tetrahydro-9-(3,4-dimethoxyphenyl)-3,3,6,6-tetramethyl-2*H*-xanthene-1,8(5*H*,9*H*)-dione (3a).

The doublets at 2.18 ppm and 2.44 ppm integrating for two protons each with the coupling constant of 16.4 Hz were due to the axial protons of the cyclohexane ring part (at C-8, C-8′, C-10, C-10′), whereas its equatorial protons appeared as multiplet at 2.46 integrating for four protons. The singlet appeared at 3.80 ppm and 3.86 ppm integrating for three protons each is due to the methyl protons of methoxyl group on aryl ring. The signal at δ 4.70 ppm appeared as singlet integrating for one proton has been assigned as proton at C-4. The three signals appeared between δ 6.70-6.90 ppm is due to the aryl protons and assigned as follows; The doublet at 6.71 ppm integrating for one proton with the coupling constant of 8.4 Hz is due to the C6′ *ortho* of aryl ring, The another doublet integrating for one proton at 6.75 ppm with the J = 8.4 Hz was assinged as aryl proton at C5′ *meta*. The remaining doublet at 7.20 which also integrates for one proton was due to the C2′ *ortho* of the aryl ring.

 DOI: 10.17628/ecb.2014.3.414-416

Carbon Chemical Shift Assignment: The ^{13}C NMR spectrum of **3a** revealed that signals at 27.26 ppm and 29.35 ppm correspond to the carbons at C-11, 11′ and C-12, 12′ respectively. The signals at 31.23 and 32.20 ppm are due to the carbons at C-10, C-10′ and C-9 and C-9′ respectively. Signal at 50.75 ppm may be bue to the carbons at C-8 and C-8′. Signals at 55.76 and 55.88 ppm are due to the methoxyl carbon of aryl ring. Signals at 110.83 and 162.10 ppm are due to the C3, C5 and C2, C6 carbons respectively. The signals at 120.11, 136.99, 147.45 and 148.43 are due to the aryl carbons. The signal at 162.19 ppm correspond to carbons at C-2 and C-6. The signal at 196.50 ppm correspond to carbonyl carbons. Similarly all other compounds in the series **3b-e** also be characterized and included in the experimental section. The above discussion clearly revealed the formation of the desired compounds

Conclusion

In conclusion the acetic acid was found to be a best solvent cum catalyst in the synthesis of benzoxanthenes and afford the better yield than other methods.

Acknowledgements

Authors are thanking the VIT management for providing facilities to carry the work in the chemistry department and thanking the SIF-Chemistry, VIT University for providing IR, NMR facilities to record the spectra.

References

[1]Peres, V., Nagem, T. J., Oliveira, F. F., *Phytochemistry*, **2000**, *55*, 683.

[2]Na, Y. J., *Pharm. Pharmacol.*, **2009**, *61*, 707.

[3]Pinto, M. M., Sousa, M. E., Nascimento, M. S., *Curr. Med. Chem.*, **2005**, *12*, 2517.

[4]Woo, S., Jung, J., Lee, C., Kwon, Y., Na, Y., *Bioorg. Med. Chem. Lett.*, **2007**, *17*, 1163.

[5]Asano, J., Chiba, K., Tada, M., Yoshii, T., *Phytochemistry*, **1996**, *41*, 815.

[6]Matsumoto, K., Akao, Y., Ohguchi, K., Ito, T., Tanaka, T., Iinuma, M., Nozawa, Y., *Bioorg. Med. Chem.*, **2005**, *13*, 6064.

[7]Pouli, N., Marakos, P., *Anticancer Agents Med. Chem.* **2009**, *9*, 77.

[8]Akao, Y., Nakagawa, Y., Iinuma, M., Nozawa,Y., *Int. J. Mol. Sci.*, **2008,** *9*, 355.

[9]Hosea, C., Robin, S., Tanke, G., Paul, T., Ullmann's Encyclopedia of Industrial Chemistry, 2011, DOI: 10.1002/ 14356007.a01_045.pub2.

[10]Palakshi Reddy, B., Vijayakumar, V., Narasimhamurthy, T., Suresh, J. and Nilantha Lakshman, P.L., *Acta Cryst.*, **2009**, *E65***,** o916.

[11]Loh, W-S., Fun, H-K., Palakshi Reddy, B., Vijayakumar, V., and Sarveswari, S., *Acta Cryst.* **2011,** *E67*, o35.

[12]Fun, H.K., Loh, W-S., Rajesh, K., Vijayakumar, V., and Sarveswari, S., *Acta Cryst.* **2011**, *E67*, o1876.

[13]Fun, H.-K., Ooi, C.W., Palakshi Reddy, B., Vijayakumar, V., and Sarveswari, S., *Acta Cryst.* **2012**. *E68*, o2367.

Received: 03.03.2014.
Accepted: 01.04.2014.

CATALYTIC DEGRADATION OF METHYLENE BLUE BY NANOSTRUCTURED CrO(OH) PREPARED BY HYDROTHERMAL METHOD

Rafia Azmat[a] and Ailiya Saeed[b]

Keywords: Nano tubes; chromium oxide; catalytic activity; degradation; methylene blue

Nano flat branched tube structure CrO(OH) (340-447 nm) demonstrated very good catalytic bustle in dye hazardous effluent treatment of textile industry. CrO(OH) Nanoparticles(NPs) have been synthesized using hydrothermal treatment of $K_2Cr_2O_7$ in a mixed aqueous alcohol system. It was observed that solvent composition and the temperature exhibited imperative effects on the configuration of the end products. Conducting tests demonstrated that the single phase nano-branched particles can be synthesized at elevated reaction temperature and higher percent composition of ethanol with water (>50%). The experiment validates catalytic efficiency of the synthesized CrO(OH) NPs as a catalyst in oxidation of the basic dye methylene blue (MB). Further, the impacts of other parameters were also investigated, including catalyst dosage, H_2O_2 dosage, catalyst circulation, concentration of dye and acidic media. After reaction of 30 minutes, degradation of methylene blue reached over 80% for most catalyst samples. Spectral analysis proposed that the degradation of MB followed by demethylation. It was observed that the catalytic activity was much advanced than that of the commercial potassium dichromate powder. Characterization of nanoparticle prepared was confirmed by EDS, SEM images and FTIR while effectiveness by UV-Visible spectroscopy.

Corresponding Authors
E-Mail: rafiasaeed200@yahoo.com
[a] [a]Department of Chemistry & [b]Deaprtment of Chemical Engineering, [a]University of Karachi 75270, Karachi Pakistan
[b] [b]NED University of Engineering & Technology Karachi

Introduction

Nanoparticle exploration is presently a space of powerful scientific research, regarding its probable applications in dyes, electronic fields, optical, and biomedical researches[1]. They act as an excellent connection between atomic or molecular structures and bulk materials. The properties of several conventional materials altered when designed as a nanoparticle[2].This is because that they have larger surface area/gram weight as compared to material by which nanoparticle was prepared and become more reactive. The properties of compounds altered when their mass reaches to nano-scale because the composition of atoms at the surface of a material becomes substantial[3]. The use of nanoparticle as a catalyst in dye de-coloration is a new emerging technique that involved interrelation with the assembly and the reactions of nanoparticles and their compounds.

Literature reports[2-11] that nanoparticles of different material can be synthesized which showed unique properties linked with assemblies of atoms or molecules on a very miniature scale series amongst individual building blocks and the bulk material (from 1 to 1000 nm). The efficiency of particle may be high as compared to the material used for synthesis which may be related with the significance of quantum effects. Silver nanoparticles (Agnp) [12] were prepared by wet chemical reduction method using chitosan bio-stabilizer having 90 % deacetylation and sodium borohydride as the reducing agent. FTIR, FESEM, HRTEM, UV-Visible, SPR spectroscopy measurements were used for the nanoparticles characterization. The catalytic efficiency of the Agnp was investigated for the oxidative degradations of nine different intensely colored dyes. It was reported that the Chitosan-Agnp incorporated advanced oxidation process (AOP) exhibited much significant results, that these may be used in the bleaching processes of organic pollutants and colorants in aqueous system. SnO_2[6] nanoparticles were synthesized via hydrothermal process and used for the photo catalytic decoloration of Acid Red 27 (AR27) in presence of ultraviolet (UV) irradiation. The average crystallite sizes of SnO_2 nanoparticles' derived from X-ray analyses which were synthesized for 2, 12 and 24 h were about 3.73, 5.31 and 7.6 nm, respectively. The high surface area of about 183, 120 and 90 (m^2 g^{-1}) were analysed by Brunauer-Emmett-Teller (BET)[6] method.

Photocatalytic degradation of Navy Blue HE2R (NB) dye was monitored through modified sol-gel route for synthesis of Au and γ-Fe_2O_3 modified TiO_2 nanoparticles (NPs)[7] at low temperature and characterized by X-ray diffraction, Raman and UV-VIS spectroscopy studies. That showed the presence of gold and iron oxide phases along-with the anatase TiO_2 phase. Exposure of the dye to the UV light in the presence of pure and gold NPs attached TiO_2 catalysts caused dye degradation of about ~20 % and ~80 %, respectively, in the first couple of hours. In the presence of γ-Fe_2O_3 NPs attached TiO_2, a remarkable ~95 % degradation of the azo dye was observed only in the first 15 min of UV exposure.

This paper aimed to the synthesis of nanoparticle of CrO(OH) prepared hydrothermally from $K_2Cr_2O_7$ as no report was available for the thermal synthesis and application of degradation or oxidation of dyes. Methylene blue which is basic cationic dye was selected for ascertaining their presentations, and to explore the catalytic enactment of the synthetic nanoparticle on the degradation, as an organic pollutant. The activity of nanoparticles was investigated on various process parameters for complete decoloration and substantial dye degradation.

Materials and methods

All chemicals in this work including, dye, oxalic acid, H_2O_2, $K_2Cr_2O_7$ and ethanol were of A.R. grade. Solutions were prepared in deionized water and diluted for getting desired concentration at the time of kinetics runs.

Preparation of nanoparticles

All chemicals used as received without further purification. 1.0 g-4.0 g $K_2Cr_2O_7$ was put into a 100/250 ml volumetric flask into a hydrothermal water bath. The mixed aqueous ethanol solutions were prepared by taking absolute ethanol and distilled water with ethanol volume percent ranging from 1 % to 100 %. 45 ml of the aqueous ethanol solution was transferred to the conical flask. Then, the mixture was allowed to react at 100–160 C^0 for 8–24 h. The consequential precipitates were washed and filtered with distilled water and dried at 70 ^{0}C in an oven for 5 h. The yield of the CrO(OH) product was about 96.3 %. Number of series of dye solutions was prepared in which amount of dichromate nanoparticle was constant. That dye's concentration was selected with correlation coefficients R^2=0.980 as described by Zhang et al.[12] Amount of nanoparticle was taken about 0.01-0.04 g.

The oxidation processes leading to the degradation of dye in presence of various influential parameters[3-18] were investigated to check the efficiency of the particle.

Characterization

FTIR spectra

The above prepared samples were characterized by Fourier transforms infrared (FTIR) transmission spectra which was recorded on a Perkin-Elmer 16PC FTIR spectrometer from 4000 to 400 cm^{-1}. Samples were mixed with KBr powder for FTIR measurements. Background correction was made using a blank KBr pellet as the reference. Initially FTIR of simple potassium dichromate was observed then, FTIR of synthetic nanoparticle of CrO(OH)was taken for comparison.

SEM Images

SEM observations were carried out on JEOL-2010. Surface areas of the samples were determined by BET measurements on nitrogen adsorption at 77 K with a Beckman Coulter Surface Area Analyzer SA 3100. Figs. 1-2 showed low and high resolution images in which (A) represents the cluster of nanoparticle at 10 kVx15,000-30,000 with 0.5-1 µm. Analysis of SEM images of nanoparticle done by EDS technique

EDS Image

EDS spectrum showed the characteristic peak of oxygen reflecting the catalytic activity of synthesized nanoparticle.

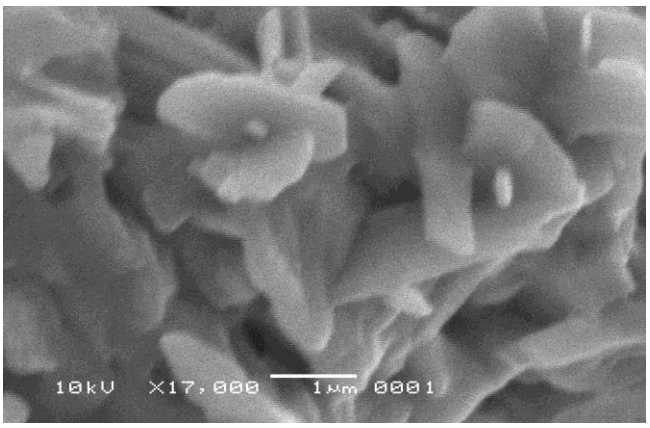

Figure 1. SEM image of synthetic nanoparticle of CrO(OH) in aqueous with 50 % ethanol mixed solvent system

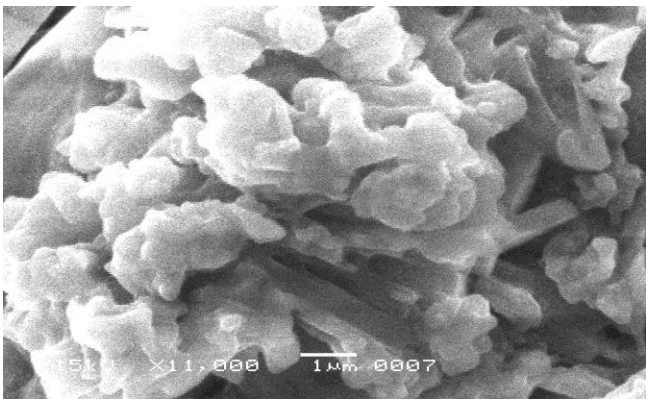

Figure 2. High resolution of SEM image of synthetic nanoparticle of CrO(OH) in aqueous ethanol mixed solvent system showing branched flattened structure indicating large surface

Results and Discussion

Characterization of CrO(OH) nanoparticles

An important previous work on the synthesis of 1D nanostructure was used by hydrothermal method and obtained single crystal nanoparticle on a small scale[12]. As no report was available on the thermal synthesis of CrO(OH) nanoparticles, the characterizations of particles were done by FTIR spectra, UV- Visible, SEM and EDS technique. The FT-IR spectrum of $K_2Cr_2O_7$ before hydrothermal treatment with ethanol was obtained and compared with FT-IR spectrum of CrO(OH) nanoparticles. The spectrum of CrO(OH) NPs. showed one broad peak at 3396.64 cm^{-1} (OH-bending modes), a peak at 920 cm^{-1} (adsorbed water), and peaks at 1450.11 and 1508, (CH_3 bending due to the presence of ethanol residue).

The results of FT-IR and SEM investigation showed that CrO(OH) powders have branched crystallized nano-flattened tube like structure and pores which were appropriate surfaces for catalytic activity (Figs. 1, 2). It can be related with chromium oxide surface having periodic polar single-layers of O and OH and Cr ions which can easily be monitored in the EDS peaks of NPs. This may create strong quantum and strong electrostatic field perpendicular to chromium oxide surface which is active and cause the adsorption of the dye molecules from the

solution, and help in the decolorization (Fig. 3). The catalytic activity was optimized under various optimum parameters like concentration of dye, amount of nanoparticle, hydrogen peroxide, and oxalic acid.

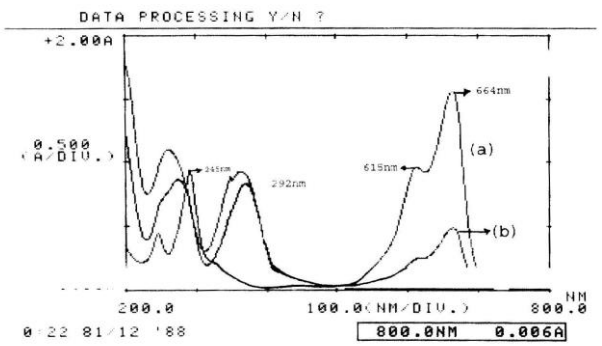

Figure 3. Spectral change of the dye MB after time interval of 30 min: a=peak before oxidation, b= after oxidation

Variable concentration of dye[14] viz; 50, 100, 150, 200, 250 and 300 ppm were checked for catalytic activity of CrO(OH) nanoparticles. It was found that decoloration efficacy of the particles was up to 200 ppm within 30 min. At higher concentration of the dye, de-coloration efficacy was decreased from 250 to 300 ppm as reported earlier[14-17] This indicated that at lower dye concentration, all surfaces were available for adsorptiom[13-17]. Also OH^- and active O^{2-} species were acted rapidly for dye removal whereas at higher concentrations, the number of available adsorption places was filled and therefore decolorization efficacy was lowered[17].

The efficacy of the CrO(OH) NPs were accelerated by the addition of hydrogen peroxide. This reduced the time of the decoloration from 30 to 10 min. The catalytic degradation reaction was conducted by taking 10 ml (200 mg L^{-1}) of MB solution in a 250 ml flask in which 0.04 g of CrO(OH) NPs was used as a catalyst with 60 ml of distilled water[12]. Then 10 ml of 30 % H_2O_2 solution, was added to the mixture, and allowed to react at room temperature with continuous stirring. 1 ml of reacting mixture for a regular time interval was pipetted into a volumetric flask and diluted with 25 ml of distilled water before subjecting to optical analysis. Catalytic surface was removed by centrifuging in order to avoid the tendency of particle to scatter the instance light ray. The centrifuged dye solution was then placed into a quartz cell (path length 1.0 cm) and the spectral change was measured with a ultraviolet–visible (UV–Vis) spectrophotometer Shimadzu UV-160 A. A linear calibration curve for the dye concentrations was obtained by monitoring the peak intensity at λ_{max} = 664 nm for a series of standard solutions according to the Beer's law. The total disappearance of color showed the degradation of MB dye (Fig. 3).

Catalytic activity of nanoparticles was also checked in acidic medium using oxalic acid and found that acidic medium showed significant influence in the process efficiency for the basic organic dye. Generally, $K_2Cr_2O_7$ work as a strong oxidizing agent in acidic medium but the synthetized CrO(OH) nanoparticles were very effective adsorbents for decolorizing basic cationic MB as compared to simple $K_2Cr_2O_7$ powder. The high process efficacy of nanostructured CrO(OH) in an acidic medium may be attributed due to the more H ion that can probably increase the electrostatic attraction between MB and nanoparticles. The amount of CrO(OH) NPs was varied from 0.01-0.04 g. It was observed that 0.04 g of particle showed very rapid de-coloration in just 20 min (Fig. 4). However, a probable mechanism based on catalytic reaction has been discussed in reaction pathway.

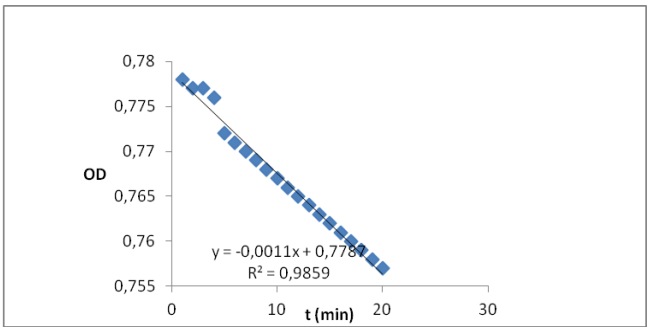

Figure 4. Effect of amount of CrO(OH) NPs (0.04g) on de-coloration of MB

The catalytic performance of NPs for the oxidation of MB dye was presented in Fig. 3. UV–Vis spectral change of dye MB and H_2O_2 reaction mixture recorded with respect to time as a function of the CrO(OH) NPs amount[14]. Initially, the spectrum was scanned in absence of H_2O_2 at t=0 for MB of 200 mg L^{-1} where characteristic peaks at 245, 292, 615 and 664 nm were appeared. These peaks reflect that initially degradation followed by demethylation (peak at 615 nm) and then further reaction in presence of CrO(OH) nanoparticle leads to complete degradation. It was observed that when H_2O_2 was added, absorption peaks of MB dropped promptly (Fig.3) in a few minutes only. While remaining peaks of spectrum at 292 and 245 nm may be covered by strong absorption of H_2O_2 in the range of 185-300 nm as reported earlier[12] or these peaks may be related with the degraded product of basic dye MB.

The observed visual color variation of mixture from blue to grey and colorless strongly support the oxidation gradually leads to the degradation. It was observed that reaction gets slow down with the passage of time with the hyperbolic shift in original peak of dye at 664 nm 30 minutes. These peaks may be correlated with the demethylation[18] of MB where basic structure of the dye was retained and only axochrome of the dye was laminating from the basic structure. The shifts of absorption band from blue to colorless showed the catalytic degradation of MB within 30 min, the band at 615 nm became very broadband weak and no obvious new band was observed, suggesting nearly complete degradation of MB. The bands at 245 and 292 nm showed complete shift from visible to UV region which may be of degraded product.

It is well known that the main product of MB oxidation is SO_4^-ion[12]. Mineralization of dye into SO_4^-ions indicates that free radicals (HO, HOO, or O_2) generated in this reaction most probably, interact with S atom in the middle heterogeneous ring of the dye which leads to the degradation of the dye. Therefore the SO_4 -ions were simply tested by using $BaCl_2$ for evaluation of the efficiency of the catalytic efficiency of CrO(O)H NPs for degradation of MB. The white precipitate of $BaSO_4$ indicated that MB has been fully

 DOI: 10.17628/ecb.2014.3.417-421

mineralized during the catalytic oxidation process. It was proposed that the high decoloration efficacy of NPsmay follow the generation of oxidative stress due to the free radical (HO, HOO, or O_2^-) produced during reaction. Therefore the probable mechanism for dye oxidation/degradation with nanoparticle and H_2O_2 was the generation of very high and speedy OH radical and O which was more effective in acidic medium. This reaction may also be into account for reducing time of decoloration. The catalyst may be regenerated due to desorption mechanism followed by degradation of dye.

Reaction Pathway

The possible mechanism of catalytic activity of the CrO(OH) particles involves the adsorption and desorption phenomena. Initially adsorption of MB takes place on the surface of catalyst where interaction with HO, HOO, or O_2^- radical leads to the degradation of dye. This process regenerates the catalyst. The addition of H_2O_2 into the mixture of dye and CrO(OH) particles releases OH, OOH and O_2 which induces high oxidizing capability which will regenerate the catalyst effectively and the catalyst will have more surface area to adsorb the dye according to Eqn. 1.[18]

$$MB + H_2O_2 \xrightarrow{GOOHNPs} MBH + OH + O \qquad (1)$$

These nascent free radical species (OH, O) possess high oxidizing capability and cause destructive oxidation of the organic dye according to Eqn. 2. This is a probable reason for reducing the time of decoloration of MB and oxidation takes place via C-C bond breakage and S-O interaction of MB.

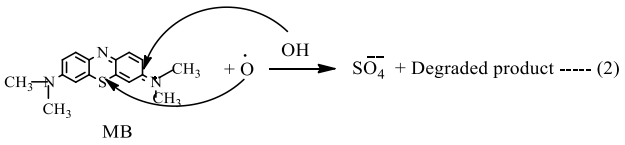

Also, the insignificant molecules from the dye degradation were desorbed off from the nanoparticle surface and the catalyst is regenerated in this way.

An experiment was also performed for further awareness of this CrO(OH) nanoparticle catalytic reaction mechanism. In the exploration, the CrO(OH) nanoparticle catalyst and H_2O_2 were quiet kept in the sealed glass flask while the MB solution was contained in another flask. A bent U-tube as described by[12] was used to join the both flasks to the transfer of O_2 produced in the first flask into the bottom of the MB solution in the second flask. Continuous bubbling of O_2 in the MB solution was observed with the addition of H_2O_2 into the first flask. After 1 h duration of observation, no apparent color change of the blue dye solution was recorded as reported earlier.[12] This experiment ratifies that the free radicle species (e.g., HO, HOO, or O_2^- radical,) produced near the catalyst surface and involved in the degradation of MB. This reaction confirmed the activity of CrO(OH) nanoparticles in MB degradation comparing it to simple potassium dichromate powder in the presence of acids. The CrO(OH) nanoparticles have higher catalytic activity than the commercial micro-scaled $K_2Cr_2O_7$ powder.

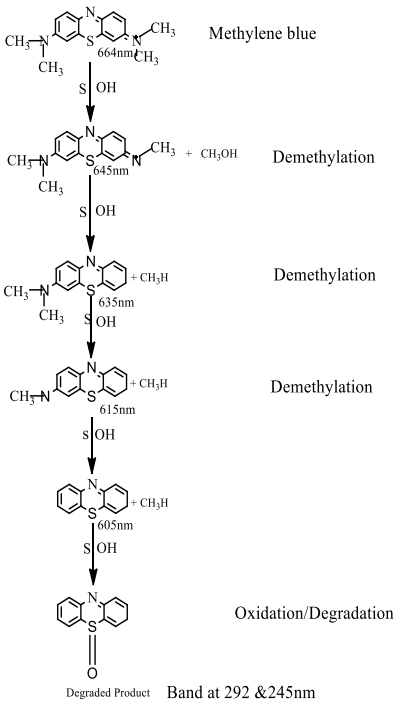

Scheme 1. A probable mechanism of catalytic decoloration of MB with CrO(OH) nanoparticles

Conclusion

It was concluded that CrO(OH) nanoparticles produced from $K_2Cr_2O_7$ in aq. EtOH under hydrothermal conditions showed an effective decoloration activity in methylene blue dye. The catalyst can be regenerated for its reuse.

Acknowledgement

The author is very thankful to Dean Faculty of Science for providing financial assistance to this project. Author is highly thankful for research assistance to Ms. Shumaila Shahab during this project.

References

[1]Aneesh, P. M., Vanaja, K. A., Jayaraj, M. K., *Proc. of SPIE*, **2007,** *IV*, 6639, 66390J-1

[2]En-Qin, G., Li, Z., Mai-Zhi, Y., Sheng-Min, C., *Acta Phys. Chim. Sinica*, **2001**, *17(2)*, 177-180.

[3]Liao, Q., Tannenbaum, R., Wang, Z. L., *J. Phys. Chem.*, **2006**, *110B*, 14262-14265.

[4]Quynh, H. T. T., Vu, L. V., Canh, T. D., Long, N. N., *J. Phys. Conf. Ser.* **2009,** *187* :1-7

[5]Hayash, H., Hakuta, Y., *Materials* , **2010,** *3*, 3794-3817

[6]Kandjani, A. E., Salehpoor, P., Tabriz, M. F., Arefian, N. A. and Vaezi, M. R., *Mat. Sci.-Poland.*, **2010,** *28(2)*, 377-391

[7]Tushar, J., Manjusha, K., Pravarthana, D., Wdan, R., Pragati ,T., *J. Nanosci. Nanotech.*, **2012,** *12(2)*, 928-936

[8]Aziz, M., Abbas, S. S., Rosemaria, W., Baharom, W., Zuraidah, W., Mahmud, W., *Mater. Lett.*, **2012,** *74*, 62-64

[9]Wang, Y., Xu, G., Ren, Z., Wei, X., Weng, W., Du, P., Shen, G. , Han, G., *J. Am. Ceramic Soc.* ,**2008,** *91(11)*, 3795-3799.

[10]Jinxin, Z., Gaoling, Z., Gaorong, H., *Frontiers Chem. China*, **2007,** *2(1)*, 98–101.

[11]Araújo, V. D., Avansi, W., Carvalho, H. B. de., Moreira, M. L., Longo, E., C., Ribeiro, E., Bernardi, M. I. B., *Cryst.Eng.Comm*, **2012,** *14*, 1150-1154.

[12]Zhang, W., Yang, Z., Liu, Y., Tang, S., Han, X., Chen, M. *J. Crystal Growth*, **2004,** *263(1–4)*, 394–39.

[13]Wang,B., Huang, X.., Zhu, Z., Huang, H., Dai, J., *Appl. Nanosci.*, **2012**, *24*, 423-427.

[14]Azmat, R., Saleem, N., *Frontiers Chem. China*, **2011,** *6(2)*, 120-126.

[15]Azmat, R., Tanwir, Q., Mohammed, F.V., Ahmed, T., *Frontiers Chem. China*, **2011,** *6(2)*, 84-90

[16]Azmat, R., Uddin, F., *Asian J. Chem.*, **2012,** *24(7)*, 2833-2838

[17]Qamer, N., Azmat, R., Naz ,R., *Pak. J. Pharm. Sci.* **2013**, *26(1)*, 59-66

[18]Azmat, R., Ph. D., Dissertation. University of Karachi **2004**

Received: 16.03.2014.
Accepted: 01.04.2014.

SYNTHESIS AND SPECTROSCOPIC STUDY OF DIVALENT METAL COMPLEXES WITH 4-HYDROXY-6- METHYL-3-((Z)-4-METHYLPHENYLAZO)-2H-PYRAN-2-ONE LIGAND

Mahmoud Najim Al-Jibouri,[a] Taghreed M. Musa[a] and Al-Ameen Bariz Omar Ali[a]]

Keywords: azo dye, metal complexes, 4-hydroxy-6- methyl-3-((Z)-4-methylphenylazo)-2H-pyran-2-one ligand

Six chelate complexes of 4-hydroxy-6-methyl-3-((Z)-4-methylphenylazo)-2H-pyran-2-one (HL) ligand with Mn(II), Co(II), Ni(II), Cu(II) and Zn(II) were synthesized and characterized by elemental analysis, magnetic susceptibility measurements, electronic, ^{1}H, ^{13}C NMR and IR spectral studies. The ligand is coordinated to the metals through its deprotonated pyrane-oxygen and the azo-group. Mn(II), Co(II), Cu(II) and Ni(II) complexes have octahedral geometry around the central atoms. The molar conductance measurements on chloride-ion containing Zn(II) and Cd(II) complexes confirmed that chloride ions are bound in the coordination sphere, and the most probable geometry around the central atoms is likely to be tetrahedral.

* Corresponding Authors
E-Mail: mahmoudnajim71@yahoo.com
[a] Chemistry Department, College of Science, Al-Mustansiriya University, Baghdad, Iraq

Introduction

Azo compounds, characterized by the presence of one or more azo (–N=N–) groups in the molecule, are widely used as dyes and form complexes with various metals.[1-11] The azo compounds are usually prepared by the reaction of diazo species obtained in the diazotisation of aromatic primary amines and a coupling agent.[2] The versatile ligating behaviour of azo compounds had evoked considerable interest because its metal complexes have shown better usability in dye industry than the parent azo dyes.[3-11] Furthermore, the toxicity of azo dyes used as parent or complexed materials in dye industry is generally lower than the toxicity of the starting compounds, e .g. the azo-compounds formed from diazotized benzidines with maleic ester cannot be converted back to benzidine in human body which suggests that these dyes are not mutagenic as the parent amines.[8]

Since the metal-azo dyes complexes are more specific and selective than the pure azo dyes due to their better fiber affinity and improved light fastness, therefore the structure and properties of various pyrazolone-like derivatives have been studied.[4-8] For example, complexes of Ni(II), Co(II), Mn(II), Cu(II), La(III), Ce(III), Th(IV) or VO_2(V) cations with 4-*p*-methoxyphenylazopyrazolone, Cu(II) and Co(II) complexes of 1-isonicotinoyl-3-methyl-4-phenylazopyrazolones,[4,5] or the synthesis and characterization of macrocyclic ligands prepared by the condensation of dehydroacetic acid with 1,2-phenylenediamine and 1,3-propylenediamine were reported.[7.]

p-Tolylazo-4-hydroxy-6-methylpyran-2-one and its complexes with Mn(II), Co(II), Ni(II), Cu(II), Cd(II) and Zn(II) have not been characterized so far.

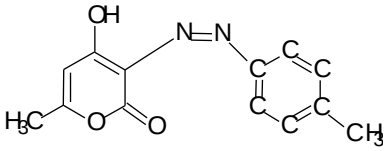

Figure 1. Structure of the 4-hydroxy-6-methyl-3-[(*Z*)-(4-methylphenyl)azo]-2*H*-pyran-2-one ligand

Experimental

Materials and methods

All the chemicals used for synthetic purposes were of Analar grade. Solvents like methanol, nitric acid, chloroform, N,N-dimethylformamide and ethanol were Sigma Aldrich products and used as received. Commercial methanol was purified by distillation.

The chloride salts of Mn(II), Ni(II), Cu(II), Cd(II) and Zn(II) were used for the synthesis of the complexes.

Synthesis of 3-(4-methylphenyl)azotriacetic lactone, HL

4-Methylaniline (0.01 mol, 1.08 g) was first diazotised with $NaNO_2$ and HCl, and the resulting solution was slowly added dropwise to a well cooled alkaline solution of 4-hydroxy-6-methyl-2-pyranone (0.02 mol, 1.266 g). The mixture was allowed to stand for 2 h. The product, 6-methyl-3-((Z)-(4-methylphenyl)azo)-4-hydroxypyrane, HL, was filtered, washed successively with 0.001 M HCl then with distilled water (Scheme 1) . The product was recrystallized from methanol and stored over anhydrous calcium chloride in a desiccator. The molecular formula is $C_{12}H_{13}N_2O_3$, Elem. Anal.: Found (calcd.): %C=62.33 (63.93), %N=10.66 (11.47), %H=4.22(4.95).

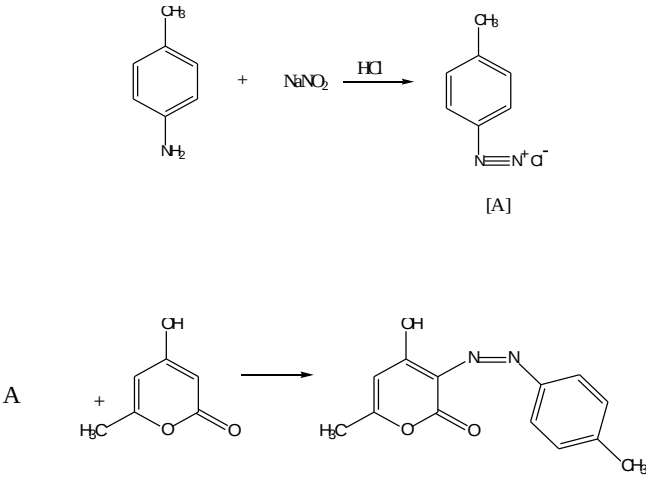

Scheme 1. Synthesis of HL azo ligand

Synthesis of metal complexes

Methanolic solutions of metal salts were added dropwise to the solution of HL ligand in the same solvent under stirring. The mixture was refluxed on a steam bath for about 2-3 hours. The metal salt to ligand ratio was kept at 1:2. The precipitated complexes were filtered, washed with water, methanol and dried. These were recrystallized from CH_3Cl-CH_3OH mixture and stored over anhydrous $MgSO_4$ in a desiccators (Scheme 2).

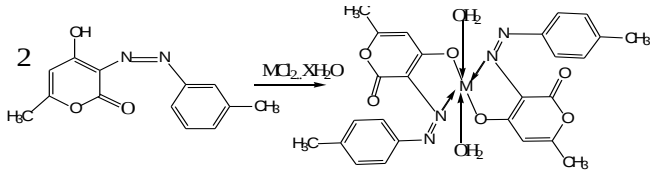

M=Mn(II), Co(II), Ni(II), Cu(II)

Scheme 2. Synthesis of M(II) (M=Cu, Ni, Mn, Co) complexes with HL azo ligand**.**

Physical measurements

The elemental analyses (CHN) of the free ligand were carried out using Carlo Elba CHN analyzer. The metal content analyses were conducted using FAAS on Shimadzu 670AA flame atomic spectrometer with standard addition method.[12] The UV–visible spectra were recorded using 0.001 M solutions of ligand and complexes in methanol and DMF, respectively. The IR spectra of the compounds were recorded in KBr discs. The NMR spectra were obtained using DMSO-d_6 as solvent and TMS as internal standard on a Bruker 300MHz NMR spectrometer. The magnetic susceptibility was determined at room temperature on Sherwood magnetic susceptibility instrument which was calibrated $Hg[Co(NCS)_4]$. The chloride-ion content of the zinc(II) and Cd(II) chelates were determined by conductometric titration after dissolving the complexes in least volume of HNO_3 and dilution with 10 % ethanol.

Results and discussion

The synthesis route for the metal complexes can be seen in Scheme 3. The complexes are stable solids in air, with varying shades of brown coloration and their structures were established from their elemental analyses, infrared, electronic, or NMR spectra and magnetic moment measurements. The results obtained from CHN and metal content analysis (Table 1 and Figure 2) are in good agreement with the data calculated for 1:2 metal-ligand ratio for Mn, Co, Ni or Cu and and 1:1 ratio for Zn or Cd complexes. [12] The complexes are completely soluble in DMF and DMSO, partially soluble in other polar solvents such as acetonitrile and methanol but are completely insoluble in non-polar organic solvents. The low molar conductance values obtained (10-33 Ω^{-1} cm^2 mol^{-1}) for the complexes in DMF indicates their non-electrolyte nature.[13] The decomposition points of complexes are high enough thus the loss of water is probably proceeded even before melting/observable decomposition.

In all the complexes one of the azo nitrogens and the oxygen of deprotonated enolic hydroxyl group take part in the coordination with the central metal ions (Figure 1). The Zn(II) and Cd complexes were diamagnetic and all others showed expected magnetic moment values.

NMR spectra

Both the ^1H and ^{13}C NMR spectra of the ligand confirmed the proposed structure and all the peaks could be assigned.[12] The Figure 2 shows the ^1H NMR spectrum of Cd(II)complex that records clear shift in signals of –OH, -CH=C-O- and less shift in absorptions of Ar-H resonances in the regions 6.4-7.8 ppm and 12.33 ppm, respectively. Furthermore, the shielded resonances of $–CH_3$ groups were recorded at 2.3-3.3 ppm. The distinct changes in the absorptions of ^1H NMR for the ligand support the coordination nitrogen –N=N- in β-position and –OH of 2-pyranone moiety upon deprotonation.[13]

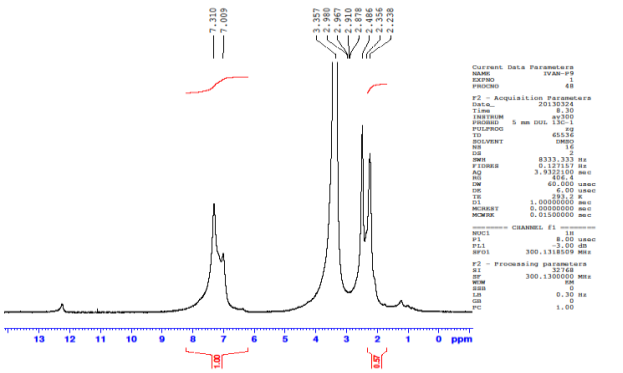

Figure 2. ^1H NMR spectrum of Cd(II)complex in DMSO-d_6 solution

FTIR spectra

The important IR spectral bands and their assignment are shown in Table 2. The free ligand in KBr shows a broad band at 3500 cm^{-1} which belongs to an intra hydrogen-bound OH-group, thus it confirms the existence of the enol tautomeric form of the free azo ligand.

 DOI: 10.17628/ecb.2014.3.422-425

Table 1. Physical properties and elemental analysis of the prepared ligand HL and its metal complexes.

Compound	Molecular weight, g mol^{-1}	Color	M.P., °C	Λ, S mol^{-1} cm^2	M-content, % Calcd. (found)	Cl-content, % Calcd. (found)
HL	244.3	Dark yellow	122-124	8		
[$MnL_2(H_2O)_2$]	577.5	Dark brown	244-246	12	9.51(9.01)	
[$CoL_2(H_2O)_2$]	581.5	Red	266^d	20	10.13(9.22)	
[$NiL_2(H_2O)_2$]	581.3	Dark yellow	288^d	33	10.10(9.55)	
[$CuL_2(H_2O)_2$]	586.2	Red	320^d	17	10.84(10.44)	
[$ZnLCl(H_2O)$]	362.1	Orange	317^d	19	18.06(16.11)	9.79(9.09)
[$CdLCl(H_2O)$]	409.2	Brown	279^d	30	27.46(26.55)	8.66(8.36)

d=decomposition

Table 2. Selected infrared vibrations of HL ligand and its metal complexes (cm^{-1}).

Compound	**νC=O, ν-OH**	**νC=CH, νN=N-**	**νM-N, νM-O**	**νAr-C-H, νC-O (pyranone)**
HL	1690-1678(s), 3500(br)	1630, 1520-1480		3010(w), 2966(m), 1215
[$MnL_2(H_2O)_2$]	1680-1658(s), 3520	1620, 1500-1420	550(m), 470(w)	3060(w), 2982(m), 1216
[$CoL_2(H_2O)_2$]	1670-1640(s), 3612	1590, 1480-1470	488, 422	3066, 2952, 1206
[$NiL_2(H_2O)_2$]	1675-1662(s), 3522	1591, 1501-1469	476, 410	3100, 2872, 1222
[$CuL_2(H_2O)_2$]	1653-1639(s), 3444(br)	1588, 1511-1433	560(w), 455(m)	3050, 2950,1189
[$ZnLCl(H_2O)$]	1675-1645(s), 3550	1604, 1544-1501	477-455, 422(m)	3108(w), 1198(s)
[$CdLCl(H_2O)$]	1680-1641(s), 3255(m)	1533, 1450-1433	489(m), 400(w)	3022(w), 1118(m)

s=strong, m=medium, br=broad, w=weak

The strong absorptions at 1520-1480 cm^{-1} and 1690-1678 cm^{-1} regions are typical for the an –N=N– and C=O pyranone moieties, respectively.[16] The strong absorptions in the region 1215 cm^{-1} may be attributed to C–O–C stretching corresponded to triacetic lactone strcture.[17]

Decreasing wavenumber values belong to the –C=O and -N=N- groups in the IR spectra of the complexes clearly indicates a bidentate monobasic coordination of the HL ligand through oxygen of the deprotonated –OH group and the β-N-atom of the –N=N-group, respectively. The strong absorptions in the range of 1544-1420 cm^{-1} entirely reveals the shifting of electron pair of -N=N- group toward metal ions. All the metal(II) complexes showed a broad absorptions in the region 3220-3612 cm^{-1}which entirely belong to the coordinated water molecules.[16]

The far-infrared spectra of metal complexes in CsI discs showed weak absorptions in the regions 412-560 and 400-470 cm^{-1}confirming the presence M-N and M-O bonds, and the spectra of Zn and Cd-complexes contains the vibrations belongs to M-Cl, M-N and M-O bonds as well.

Electronic spectral data and magnetic moments

The electronic absorption bands of complexes are very similar to the bands of the ligand. This showed that no structural changes occurred on complexation, however, a slight shift in the absorption maxima of >C=O and -N=N bands may have occurred as the consequence of their participation in the coordination. The dark yellow solution of HL in methanol displays two high intensity peaks at 233 and 410 nm. These bands belong to the chromophores –N=N- group and substituted benzenoid ring.[15,19]

The cobalt complex was brown in color with a red tinge. This is typical for the octahedral geometry around cobalt(II).[19,20] The appearance of the band at 572 may be due to $^4T_{lg}(F) \rightarrow {}^4A_{2g}$ transition in an octahedral environment, although the magnetic moment value (3.82 B.M) was found to be too low for an octahedral geometry.[19,20]

The Mn(II) complex showed spectral bands which were overlapped with CT bands. The band observed at 540 nm could very well be due to $^6A_{1g} \rightarrow {}^4T_{1g}$ transition. The magnetic moment value of 5.54 B.M. indicated octahedral geometry.[18]

Table 3. Electronic spectra, molar conductance and magnetic moments of the prepared metal complexes

Compound	**λ_{max} nm**	**ν, cm^{-1}**	**Λ, S cm^2 mol^{-1}**	**μ, B.M.**
HL	333 410	30030 24390	-	-
[$MnL_2(H_2O)_2$]	299 540	33448 18518	25	5.54
[$CoL_2(H_2O)_2$]	315 572	31746 17482	14	3.82
[$NiL_2(H_2O)_2$]	396 656	25252 15243	19	2.65
[$CuL_2(H_2O)_2$]	267 388	37253 25773	33	1.70
[$ZnLCl(H_2O)$]	280 355	35714 28169	10	0
[$CdLCl(H_2O)$]	300 440	33333 25000	18	0

λ=molar conductance in DMF solutions at 0.001 M concentration.

 DOI: 10.17628/ecb.2014.3.422-425

The spectrum of Ni(II) complex was very conspicuous with bands at 396 nm and 656 nm belonging to the $^3A_{2g} \rightarrow {}^3T_{1g}(P)$ and the $^3A_{2g} \rightarrow {}^3T_{1g}(F)$ transitions respectively.[21-22] These bands are characteristic for octahedral geometry around nickel. The magnetic moment value of 2.65 B.M also pointed out the octahedral geometry for Ni(II) complexes. The brown colored copper complex showed bands at the lower end of the visible region. This complex has a magnetic moment of 1.70 BM**.**

The solutions of zinc(II)and cadmium (II) complexes in DMF showed high intensity peaks in the regions 280-300 and 355-400 nm that may be ascribed to intra-ligand charge transfer INCT and LMCT transitions respectively.[23,24]

Conclusion

The octahedral geometry for Cu(II), Ni(II), Co(II) or Mn(II) complexes and tetrahedral geometry for Zn(II) or Cd(II)-complexes was proposed on the basis of elemental analyses, molar conductivity measurements, magnetic measurements and NMR or FTIR spectra. The infrared spectral studies revealed that the β-nitrogen of N=N group and the enolized oxygen atom of pyranone ring participate in bonding with the metal ions forming a five-membered ring chelates.

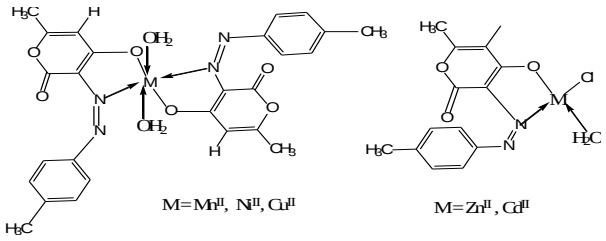

Scheme 3. Structures of M(II) complexes with 4-hydroxy-6-methyl-3-[(*Z*)-(4-methylphenyl)azo]-*2H*-pyran-2-one**.**

References

[1]Szymczyk, M., Freeman, H. S., *Dyes Pigm.*, **2007,** *2(1)*, 8-15.

[2]Szymczyk, M., El-Shafei, A., Freeman, H. S., *Rev. Prog. Color*, **2004**, *34(1)*, 39-57.

[3]Mustroph, H., Stollenwerk, M., Bressau, V., *Angew. Chem. Int. Ed.*, **2006,** *45(13)*, 2016-35.

[4]Latif, A. S. A., Hassib, H. B., *J. Therm. Anal. Calor.*, **2002**, *68(3)*, 983-995.

[5]Kuncheria, B. and Indrasenan, P., *Ind. J. Chem*., **1988**, *27A*, 1005-1007.

[6]Li, X., Wu, Y., Gu, D., Gan, F., *Dyes Pigm.*, **2010,** *86(2)*,182-9.

[7]Karipcin, F., Dede, B., Percin-Ozkorucuklu, S., Kabalcilar, E., *Dyes Pigm*., **2010,** *84*, 14-19.

[8]De France, B. F., Carter, M. H. and Josephy, P. D., *Fd. Chem. Toxic*., **1986,** *24(2)*, 165-169.

[9]Latif, A. S. A., Hassib, H. B., *J. Therm. Anal. Calor*., **2009,** *68(3)*, 983-995.

[10]Latif, A. S. A., *Synth. React. Inorg. Met-Org. Nano Chem*., **2001,** 31(8), 1355-1374.

[11]Seth, S. and Aravindakshan, K. K., *Spectrochim. Acta Part A. Mol. Biomol. Spectr*., **2013**, 112, 276-279.

[12]Drago, R. S., *Physical Methods in Inorganic Chemistry*, Affiliated East-West Press Pvt. Ltd., **1968**, New Delhi, India.

[13]Geary, W. J., *Coord. Chem. Rev.*, **1971**, *7(1)*, 81.

[14] Budzikiewicz, H., Djerassi, C. and Williams, D. H., *Mass spectrometry of Organic Compounds*, Holden-Day, **1967**, San Francisco.

[15]Lycka, A., Lunák, Jr. S., Aysha, T., Holusa, R., Hrdina, R., *Tetrahedron Lett*., **2010,** *51*, 3149-51.

[16]Dyer, J. R., *Application of absorption spectroscopy of organic compounds*, Prentice Hall, Eaglewood Cliffs, N. J., **1965**.

[16]Nakamato, K., *Infrared and Raman Spectra of Inorganic and Coordination Compounds*, Wiley, **1986**, New York.

[17]Pavia, D. L., Lampman, G. M., Kriz, G. S., *Introduction to Spectroscopy*, 2nd Edn., Saunders Golden Sunburst Series, Harcourt Brace College Publishers, **1996**, New York, USA.

[17]Baerham, T. J., *NMR Spectra of Simple Heterocycles*, Wiley, **1973**, New York.

[18] Silverstein, R. M., Webster, F. X., *Spectrometric Identification of Organic Compounds*, John Wiley & Sons, **1998**, New York.

[19]Batterham, T. J., *NMR Spectra of Simple Heterocycles* (Taylor, E. C. and Weissberger, A., eds). *General Heterocyclic Chemistry Series*, John Wiley & Sons, Inc. New York, USA, **1973**.

[20]Greenwood, N. N., Earnshow, A. *Chemistry of the Elements*, Pergamon Press:oxford.,1994, 1348.

[21]Dua, R. L. and Syamal, A., *Elements of Magnetochemistry*, **1992**.

[22]Sutton, D., *Electronic Spectra of Transition Metal Complexes*, McGraw-Hill, **1968**, London.

[23]Szymczyk, M., Freeman, H. S., *Dyes Pigm*., **2007**, *72(1)*, 8-15.

[24]Szymczyk, M., El-Shafei, A., Freeman, H. S., *Rev. Prog. Color***., 2004,** *34(1*

Received: 22.04.2014.
Accepted: 05.04.2014.

PROPERTIES OF WATER/*N*-PROPANOL/IONIC SURFACTANT/PHENYLACETYLENE MICELLAR SYSTEMS

Monzer Fanun,[a]*, Ahmad Shakarnah,[a] Michael Schwarze,[b] Reinhard Schomäcker,[b], Zackaria Nairoukh,[c] and Jochanan Blum[c]

Keywords: phase behavior, nanoemulsions, hydrodynamic diameter, dynamic light scattering, hydration of alkynes

Water/*n*-propanol/ionic surfactant /phenylacetylene micellar systems were formulated. The surfactants were the anionic, sodium dodecyl sulfate and the cationic cetyltrimethylammonium bromide. The ratio (w/w) of *n*-propanol/surfactant equals 2/1. The extent of the micellar region as function of temperature was determined. The particle hydrodynamic diameter of the oil-in-water micellar systems measured using dynamic light scattering and was found to decrease with temperature. In the diluted region, nanoemulsions systems were observed. Hydration of alkynes found to be highly influenced from the ionic nature of the surfactant. Cationic surfactants accelerate the addition of water to alkynes while anionic surfactants decease the reaction rate.

Corresponding Authors
Tel: + 972522406061;
Fax: + 972 22 79 69 60
E-mail address: *Fanunm@gmail.com or mfanun@science.alquds.edu*
[a] Colloids and Surfaces Research Center, Al-Quds University, East Jerusalem 51000, Palestine
[b] Institut für Chemie, Technische Universität Berlin, Strasse des 17. Juni 124, D-10623 Berlin, Germany
[c] Institute of Chemistry, The Hebrew University of Jerusalem, Jerusalem 91904, Israel

Introduction

Catalytic hydration of alkynes was widely investigated and reported.[1] Liquid-phase semi hydrogenation of phenylacetylene under mild conditions was done in the presence of organophilic Pd-montmorillonite catalysts synthesized in a micellar system based on the cationic surfactant cetyltrimethylammonium bromide.[2] Palladium nanoparticles incorporated in a hydrotalcite proved to be efficient catalysts for the liquid-phase semi hydrogenations phenylacetylene.[3] Palladium nanoparticles also proved to be active and selective catalysts for the liquid-phase semi hydrogenations of phenylacetylene, 3-butyn-1-ol, 4-octyne and 1-phenyl-1-butyne.[4,5] Phase transfer catalyzed reaction of phenylacetylene occurring under mild conditions with carbon monoxide, aqueous base, toluene as the organic phase, and catalytic amounts of nickel cyanide as the metal catalyst and cetyltrimethylammonium bromide as the surfactant affords unsaturated acids in reasonable yields.[6] Brönsted acidic ionic liquids have been successfully developed as task specific ionic liquids for hydration of alkynes (e.g. phenylacetylene) under mild conditions to give high yields of ketones as a selective product.[7] Gold nanoparticles exhibit high activity and stability in the hydrogenation of phenylacetylene into styrene in the phenylacetylene-styrene mixture.[8,9] A new simple protocol for the hydration of alkynes that is expected to reduce the hazards associated with industrially important processes was recently reported.[10] A possible mechanism of hydration of phenylacetylene in near-critical water was proposed.[11] A three-phase emulsion-solid state-transport method (EST) system can be applied successfully for catalytic hydrogenation, cyclotrimerization, decarbonylation, hydroformylation and carbon-carbon coupling of hydrophobic substrates in aqueous microemulsions.[12-16] In this study we continue our works to formulate new nanoemulsions composed of water/*n*-propanol/ionic surfactant/phenylacetylene to be used as a reaction media for the hydration of phenylacetylene. The surfactants used were the anionic sodium dodecyl sulfate (SDS) and the cationic cetyltrimethylammonium bromide (CTAB). The objective is to study the effect of the surfactants head group on the phenylacetylene hydration in oil-in-water nanoemulsions

Experimental

Materials

Phenylacetylene (PAC), cetyltrimethylammonium bromide (CTAB) and *n*-propanol were purchased from Sigma-Aldrich Chemical Company. Sodium dodecyl sulfate (SDS) was purchased from Ridel de Haën. All the components were used as supplied without further purification. Triply distilled water was used for all experiments.

Methods

Phase behavior at constant temperature

A four-component system behavior is described in pseudo ternary phase diagrams in which the weight ratio of surfactant/cosurfactant is fixed. The determination of the phase behavior was performed in a thermostated bath ($T \pm$ 0.1 K). Ten weighted samples composed of mixtures of (surfactant + cosurfactant) and oil were prepared in culture tubes sealed with Viton -lined screw caps at predetermined weight ratios of oil/ surfactant/cosurfactant. The mixtures were titrated with water and were equilibrated during a time interval of up to 24 h. The different phases were determined visually and optically using crossed polarizer's method. Appearance of turbidity was considered as an indication for phase separation. The phase behavior was determined only after sharp interfaces had become visible. The completion of

this process was hastened by centrifuging the samples. Every sample that remained transparent and homogeneous after vigorous vortexing was considered as belonging to the one phase region.[17-19]

Particle size determination

Particle size measurements were performed using Zetasizer Nano S (ZEN 1600, Malvern Instruments Ltd., Worcestershire, United Kingdom) for the measurements of size of dispersed particles in solution. The equipment includes a 4 mW, 633 nm He-Ne laser. Size measurement range between 0.6nm to 6 nm, size measurement angle equals 173º, concentration range for size measurement was between 0.1ppm (0.00001 vol%) – 40 wt% and temperature measurement range between 275 K to 363 K. 1.5 ml micellar samples was introduced in a disposable polystyrene cuvettes and measured at temperatures range between 298 and 323 K by steps of 5 K. The particle hydrodynamic diameter is calculated from the translational diffusion coefficient (d_H) using the Stokes-Einstein relationship:

$$d_H = \frac{k_B T}{6\pi\eta D} \quad (1)$$

where

d_H is the hydrodynamic diameter,
k_B is Boltzmann's constant,
T is the absolute temperature and
η is the solvent viscosity.

The results are averages of three experiments.

Emulsification of the substrates

Typically, a mixture of triply distilled water (TDW, 89.3 wt.%), and a suitable surfactant (3.3 wt.%) was stirred at room temperature. Then, the substrate (0.8 wt.%) was added drop wise under vigorous stirring. The emulsion, so formed, was titrated with *n*-propanol until a clear transparent mixture was obtained (usually 6.6 wt.%). A calculated amount of the desired acid was added to the microemulsion in order to obtain a 0.33 M microemulsion.

General procedure for the hydration of alkynes

The above microemulsion of the substrate was placed in either an autoclave or in a pressure vessel and heated with stirring to the desired temperature for the required length of time. The reaction vessel was cooled to room temperature and the microemulsion was treated with NaCl (2 g), which caused phase separation. The aqueous phase was extracted with Et_2O (2×15 mL) and the combined organic phases were neutralized with aqueous $NaHCO_3$, dried ($MgSO_4$), concentrated and chromatographed on silica gel. The products were then analyzed by ^1H NMR, MS, and GC in the usual manner and compared with authentic samples.

Results and Discussion

Phase behavior

Figures 1 and 2 present the phase behaviors of water/ sodium dodecylsulfate/*n*-propanol/ phenylacetylene and water / cetyltrimethylammonium bromide / *n*-propanol/ phenylacetylene systems at 298 K, respectively. The ratio (w/w) of *n*-propanol/ surfactant equals 2/1. As shown in the Figures, the one phase micellar system appears from the first addition of water and continues to appear until 40 wt.% water in the case of sodium dodecyl sulfate based system. In the case of cetyltrimethylammonium bromide based system, the one phase continues until 25 wt.% water for high surfactant+cosurfactant contents (above 50 wt%), while for low surfactant+cosurfactant contents (below 50 wt%) the one phase continues until 10 wt.% water.

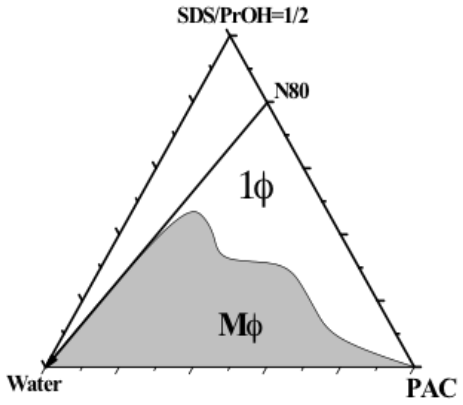

Figure 1. Pseudo ternary phase diagram of the water/n-propanol/ sodium dodecyl sulfate /phenylacetylene system at 298 K. The mixing ratio (w/w) of n-propanol/surfactant equals 2/1. The one phase region is designated by 1ϕ, and the multiple phase regions are designated by (Mϕ). N80 is the dilution line where the weight ratio of (surfactant + propanol)/ phenylacetylene equals 4/1.

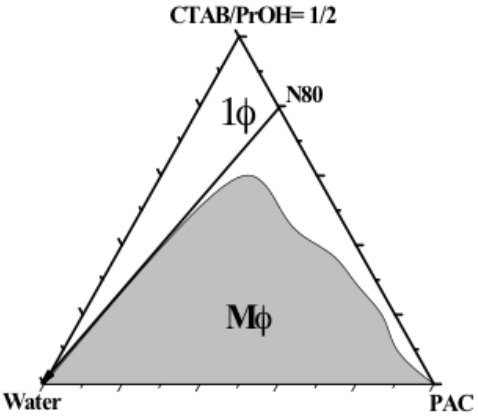

Figure 2. Pseudo ternary phase diagram of the water/n-propanol/ cetyltrimethylammonium bromide /phenylacetylene system at 298 K. The mixing ratio (w/w) of n-propanol/surfactant equals 2/1. The one phase region is designated by 1ϕ, and the multiple phase regions are designated by (Mϕ). N80 is the dilution line where the weight ratio of (surfactant + propanol)/ phenylacetylene equals 4/1.

 DOI: 10.17628/ecb.2014.3.426-429

Similar findings on the behavior of sodium dodecyl sulfate in the presence of other aromatic oils were reported.[18,19] The area of the one phase region, A_T (%), varies slightly with temperature. Similar behavior of the dependence of the phase behavior on temperature of ionic surfactants was reported elsewhere.[18,19]

Diffusion properties

We estimated the hydrodynamic diameter (d_H) of the micellar system in the water-rich region at water volume fraction equals 0.90 and above using equation 1. The variation in the values of the hydrodynamic diameter (d_H) at water volume fractions of 0.90 and 0.95 for the studied system as function of temperature is shown in Figures 3 and 4. As shown in Figures, the hydrodynamic diameter decreases with temperature. The values of the hydrodynamic diameter indicate that the micellar systems formed are nanoemulsions. These systems will be used as alternative reaction media for the hydration of phenylacetylene.

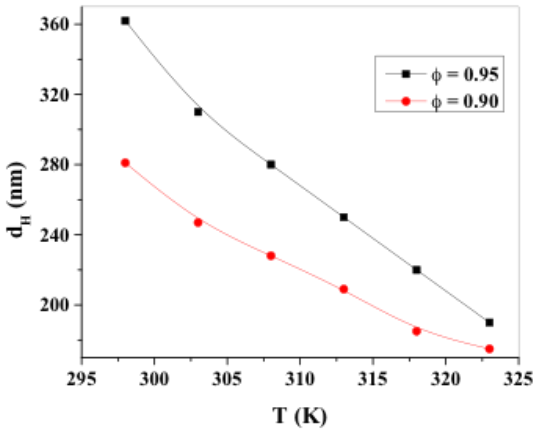

Figure 3. Variation of the particle hydrodynamic diameter as function of temperature for water/n-propanol/ sodium dodecyl sulfate / phenylacetylene oil-in-water nanoemulsions along N80 dilution line.

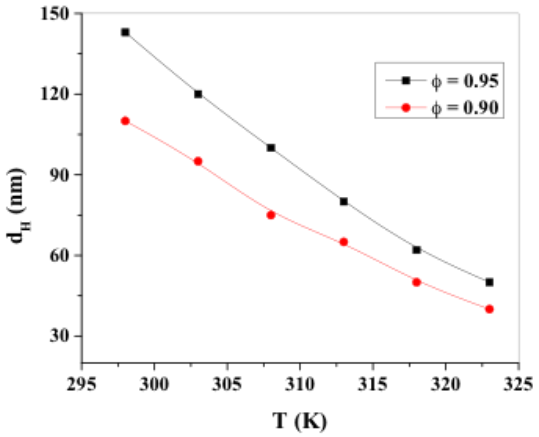

Figure 4. Variation of the particle hydrodynamic diameter as function of temperature for water/n-propanol/ cetyltrimethylammonium bromide/phenylacetylene oil-in-water nanoemulsions along N80 dilution line.

Hydration of phenylacetylene

Highly efficient hydration of alkynes has beenperformed in water upon addition of a suitable surfactant that solubilizes the substrate. From previous studies, it had been showed that hydration of alkynes depends on the ionic nature of the surfactants.[10] In this report we introduced two different types of surfactants, anionic and cationic surfactants. Some representative results summarized in Table 1 indicate that hydration of phenylacetylene is more efficient upon the addition of cetyltrimethylammonium bromide.

Table 1. Dependence of the hydration of phenylacetylene on the nature of the surfactants [a]

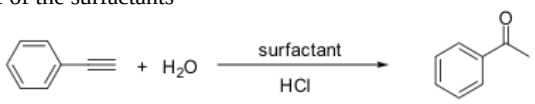

Entry	Surfactant	Isolated PhCOMe [%][b]
1	SDS	72
2	CTAB	87

[a] Reaction conditions as described in section 2 except that all experiments were performed for only 3 h at 140 ºC [b] Average of at least two experiments that did not differ by more than ± 3%.

Conclusions

New nanoemulsions were developed for performing hydration reactions of phenylacetylene that will lead to a significant reduction in the vast amount of organic solvents used currently, and consequently increase the safety and diminish the cost of chemical processes. Since the particle size of the micellar system is an important parameter in determining the yield of hydration reaction of phenylacetylene, the results presented in this study recommend performing these reactions at water volume fractions above 0.90 or at surfactant contents slightly above the critical micelle concentration and at high temperatures. The influence of the nature of the surfactant was investigated in the alkynes hydration process. It was found that the cationic surfactants increase the reaction rate.

Acknowledgment

We gratefully acknowledge the financial support of this trilateral study by the Deutsche Forschungsgemeinschaft (DFG) through grant SCHO 687/8-2.

References

[1]Hintermann, L., Labonne A., *Synthesis* **2007** , *8*, 1121-1150

[2]Mastalir, A., Kiraly, Z., Berger F., *Appl. Catal. A: General*, **2004** , *269*, 161-168

[3]Lou, X., Li, L., Deng, J., Guo, T., Yang W., *Chem. Commun.*, **2010**, *46*, 2745-2747.

[4]Mastalir, A., Kiraly Z., *J. Catal.*, **2003**, 220, 372-381

[5]Papp, A., Molnar, A., Mastalir, A., *Appl. Catal. A: General*, **2005**, *289*, 256-266.

[6]Amer, I., Alper H., *J. Organomet. Chem.*, **1990**, *383*, 573-577.

[7]Kore, R., Kumar, T. J. D., Srivastava, R., *J. Mol. Catal., A.*, **2012**, *360*, 61-70.

[8]Nikolaev, S. A., Permyakov, N. A., Smirnov, V. V., Yu. Vasilkov, A., Lanin, S. N., *Kinet. Catal.*, **2010**, *51*, 288-292.

[9]Sergio, S. , Jones, A. L., Mohr, F., Laguna M., *Organometallics*, **2007**, *26*, 952-957.

[10]Nairoukh, Z., Avnir, D., Blum J., *ChemSusChem*, **2013**, *6*, 430 –432.

[11]Li, S., Chang, Y.J., Wang, Y., Dai L.Y., *Chin. Chem. Letters* **2011**, *22*, 393-396.

[12]Abu Reziq, R., Avnir, D., Blum J., *Angew. Chem. Int. Ed*., **2002**, *41*, 4132-4134.

[13]Nairoukh, Z., Fanun, M., Schwarze, M., Schomäcker, R., Blum J., *J. Mol. Catal. A*., **2014**, *382*, 93- 98.

[14]Dahoah, S., Nairoukh, Z., Fanun, M., Schwarze, M., Schomäcker, R., Blum, J. , *J. Mol. Catal. A*., **2013**, *380*, 90-93.

[15]Tsvelikhovsky, D., Blum J., *Eur J. Org. Chem.*, **2008**, *12*, 2117-2122.

[16]Nairoukh, Z. , Blum J., *J. Mol. Catal. A*., **2012**, *358*, 129-133.

[17]Fanun, M., Shakarnah, A., Meltzer, D., Schwarze, M., Schomäcker, R., Blum, J., *Tenside Surf. Deterg.*, **2011**, *48*, 400-407.

[18]Fanun, M., Shakarnah, A., Mustafa, O., Schwarze, M., Schomäcker, R., Blum, J., *Eur. Chem. Bull.*, **2012**, *1*, 141-145.

[19]Fanun M., Shakarnah, A., Mustafa, O., Schwarze, M., Schomäcker, R., Blum, J., *Eur. Chem. Bull.*, **2013**, *2*, 606–610.

Received: 05.03.2014.
Accepted: 05.04.2014.

NOVEL HETEROCYCLIC COMPOUNDS DERIVED FROM ACETOACETANILIDE TOGETHER WITH THEIR ANTITUMOR EVALUATIONS

Karam A. El-Sharkawy[a]* and Eman M. Samir[b]

Keywords: pyrazol, pyridazine, thiophene, 1, 2, 4 triazine, cytotoxic activity.

The reaction of acetoacetanilide **(1)** with cyclohexanone **(2)** gave compound **3** which it was reacted with the active methylene reagents **4a, b** afforded cyclohexylidene derivatives **5a, b**. The latter products were reacted with elemental sulfur in presence of basic catalyst to produce thiophene derivatives **6a, b**. Also compound **1** reacted with diazonium salts **7a, b** then compounds **8a**, **b** were produced respectively, compounds **8a, b** were directed toward the reaction with malononitrile **(4a)**, ethyl cyanoacetate **(4b)** in either ammonium acetate or piperdine to form compounds **9a-d** and **10a-d** respectively**,** also compounds **8a, b** reacted with either phenylisothiocanate **(11)** afforded compounds **13a, b** or hydrazine derivatives **14a, b** to produce compounds **15a-d**. The newly synthesized compounds were evaluated for antitumor activity.

Corresponding Authors
Tel: 00201004712543
Fax: 00238371543
E-mail: karamsyn@yahoo.com
[a] Chemistry Department, Faculty of Biotechnology, October University for Modern Sciences and Arts(MSA), El-Wahat Road, 6 October City, Egypt.
[b] National Organization for Drug Control & Research P.O. 29, Cairo, Egypt

Introduction

A large number of medicinal compounds which have been discovered belong to a major class of heterocycles containing sulphur and (or) nitrogen. Thiophene and its derivatives constitute one of the major classes in heterocyclic chemistry, thus some of these compounds has interesting biological properties such as cytotoxic, antitumor activity,[1,2] anti-inflammatory and analgesic agents,[3,4,6] antimicrobial[5,6] and antiprotozoal activity,[7,8] pyridazine derivatives has antimicrobial activity,[9] on the other hand the fused 1,2,4 triazine derivatives has Antiproliferative activity,[10] moreover pyrazole derivatives has many biological significant such as Antiproliferative activity.[11]

In this article from our view as continuation of such efforts directed towards the synthesis of new heterocyclic compounds based on the presence of acetoacetanilide derivatives, and the screening of their antitumor activity against three different cell lines. The structures of the newly synthesized compounds were established using IR, NMR & Mass spectrometry techniques.

Results and discussion

In the present work we report the uses of acetoacetanilide through some heterocyclic synthesis followed by cytotoxic evaluations of the newly obtained compounds. Thus, acetoacetanilide **(1)** reacted with cyclohexanone **(2)** in benzene/AcOH containing ammonium acetate gave the Knoevenagel condensation product **3**. The structure of compound **3** was confirmed based on the analytical and spectral data. Thus, the ^{1}H NMR spectrum of compound **3** showed two multiplets at δ 1.77-1.79 & 2.11-2.16 ppm indicating the five CH_2 groups, a singlet at δ 2.27 ppm corresponding to CH_3 group, a multiplet at δ 7.25-7.36 ppm for the C_6H_5 group and a singlet, D_2O-exchangeable at δ 9.63 ppm for the NH group. Compound **3** reacted with either malononitrile **(4a)** or ethyl cyanoacetate **(4b)** afforded compounds **5a** and **5b** respectively. The existence of the methyl group in conjugation with the cyano group enhances the reactivity of the first.

Thus, the reaction of compounds **5a** and **5b** with elemental sulfur in 1,4-dioxan containing a catalytic amount of triethylamine to give the thiophene derivatives **6a** and **6b** respectively. The analytical and spectral data of compounds **6a** and **6b** were consistence with their respective structures. Thus, the ^{1}H NMR spectrum of **6a** showed two multiplets at δ 1.73-1.76 & 1.91-1.98 ppm indicating the five CH_2 groups, a singlet at δ 4.54 ppm indicating two H of NH_2 group, a singlet at δ 6.73 ppm corresponding to 1H (thiophene ring), a multiplet at δ 7.27-7.38 ppm for the C_6H_5 group and a singlet, D_2O-exchangeable at δ 9.32 ppm for the NH group.

The reaction of compound **1** with either 3-cyano-4,5,6,7-tetrahydrobenzo[*b*]thiophene-2-diazonium chloride **(7a)** or 3-ethoxycarbonyl-4,5,6,7-tetrahydrobenzo[*b*]thiophene-2-diazonium chloride **(7b)** gave the hydrazo derivatives **8a** and **8b** respectively (cf. Scheme 1) . The reaction of the synthesized compounds **8a** or **8b** with either malononitrile **(4a)** or ethyl cyanoacetate **(4b)** in the presence of ammonium acetate at 120 °C gave the Knoevenagel condensation products **9a-d** respectively. On the other hand carrying the same reaction but in refluxing ethanol containing piperidine gave the pyridazine derivatives **10a-d** respectively (cf. Scheme 2).

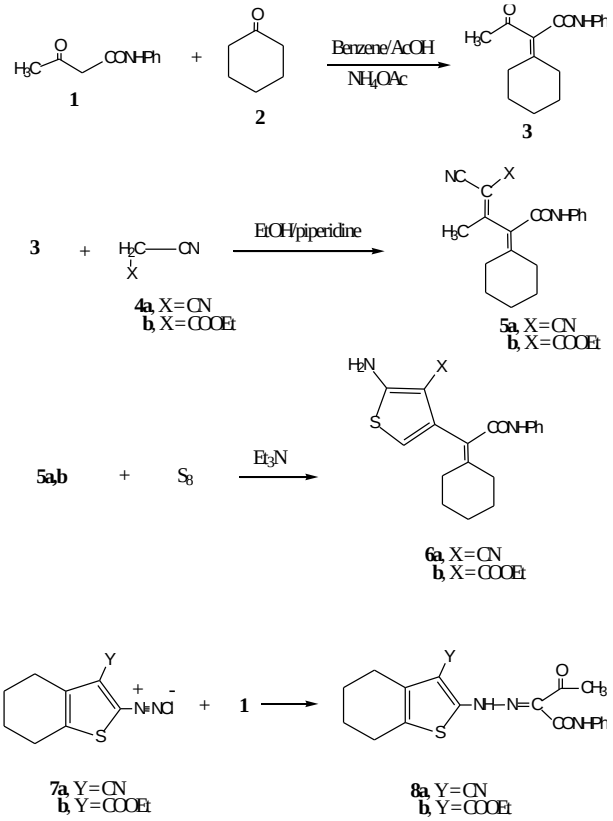

Scheme 1. Synthesis of compounds **3-8a,b**

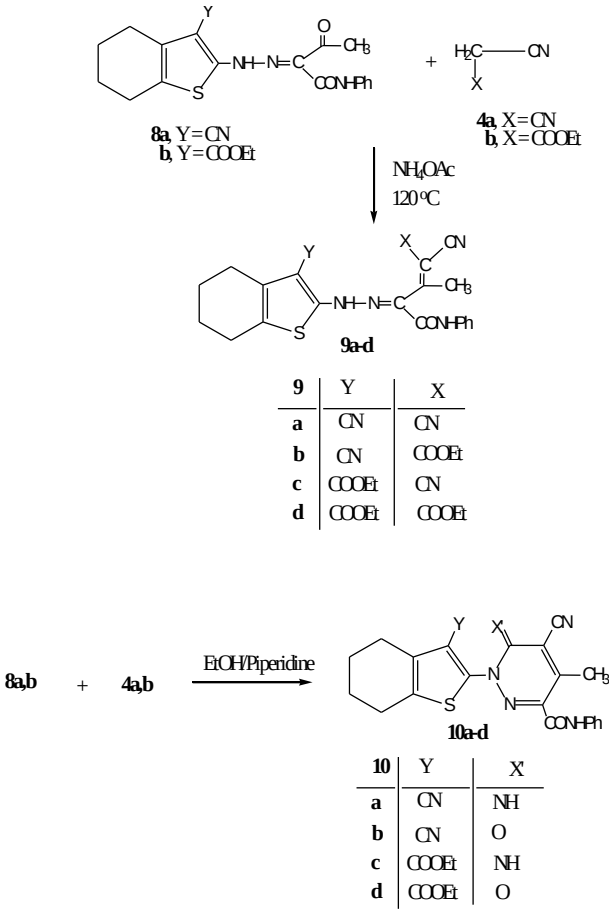

9	Y	X
a	CN	CN
b	CN	COOEt
c	COOEt	CN
d	COOEt	COOEt

10	Y	X'
a	CN	NH
b	CN	O
c	COOEt	NH
d	COOEt	O

Scheme 2. Synthesis of compound **9a-d, 10a-d**

Formation of the latter products might be explained in terms of first formation of the acyclic intermediates **9a-d** followed by their cyclization.

The structures of compounds **10a-d** were established on their respective analytical and spectral data. Thus, the ^{1}H NMR spectrum of **10a** as specific example showed two multiplets at δ 1.64-1.68 & 2.05-2.12 ppm indicating to the four CH_2 groups, a singlet at δ 2.34 ppm corresponding to the CH_3 group, a multiplet at δ 7.27-7.42 ppm for the C_6H_5 group and two singlets, D_2O-exchangeable at δ 8.25 and 9.30 ppm for the two NH groups.

The reaction of either compound **8a** or **8b** with phenylisothiocyanate **(11)** in presence of 1,4-dioxan containing triethylamine afforded 1,2,4-triazine derivatives **13a** and **13b** respectively. The analytical and spectral data of compound **13a** were in agreement with the assigned structures.

Finally the reaction of either compound **8a** or **8b** with either hydrazine hydrate **(14a)** or phenylhydrazine **(14b)** gave the pyrazole derivatives **15a-d** respectively (cf. Scheme 3).

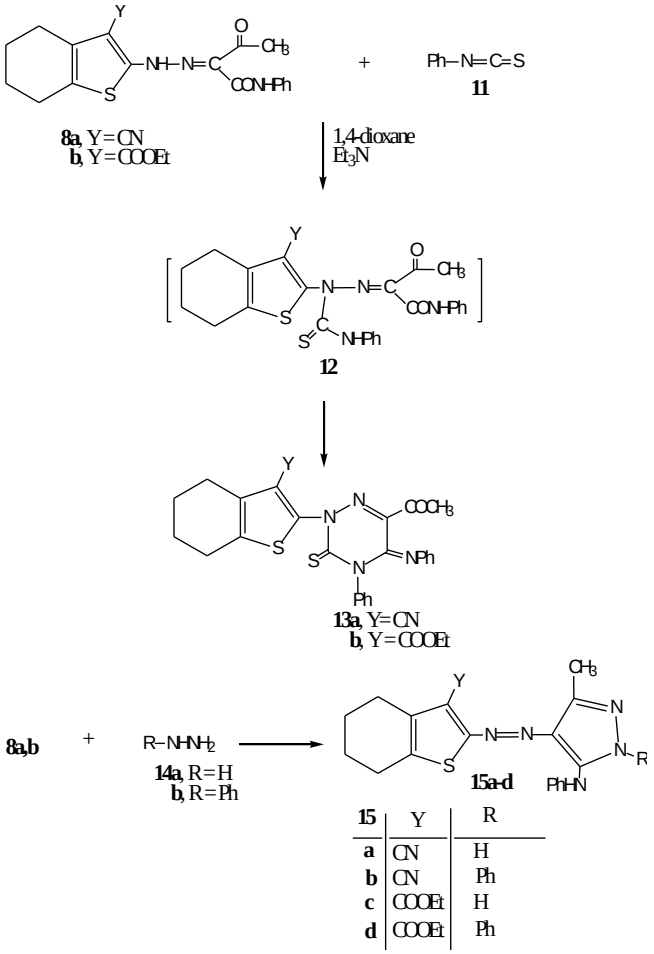

15	Y	R
a	CN	H
b	CN	Ph
c	COOEt	H
d	COOEt	Ph

Scheme 3. Synthesis of compounds **13a, b-15a-d**

 DOI: 10.17628/ecb.2014.3.430-436

Antitumor activity tests

Reagents: L-glutamine and Fetal bovine serum (FBS) were from Gibco Invitrogen Co. (Scotland, UK). RPMI-1640 medium was from Cambrex (New Jersey, USA). Doxorubicin, dimethyl sulfoxide (DMSO), penicillin, streptomycin and sulforhodamine B (SRB) were from Sigma Chemical Co. (Saint Louis, USA).

Cell cultures. Three human tumor cell lines, MCF-7 (breast adenocarcinoma), NCI-H460 (non-small cell lung cancer), and SF-268 (CNS cancer) were used. MCF-7 was obtained from the European Collection of Cell Cultures (ECACC, Salisbury, UK) and NCI-H460 and SF-268 were kindly provided by the National Cancer Institute (NCI, Cairo, Egypt). They grow as monolayer and routinely maintained in RPMI-1640 medium supplemented with 5% heat inactivated FBS, 2 mM glutamine and antibiotics (penicillin 100 U mL^{-1}, streptomycin 100 µg mL^{-1}) at 37 °C in a humidified atmosphere containing 5% CO_2. Exponentially growing cells were produced by plating 1.5 x 10^5 cells mL-1 for MCF-7 and SF-268 and 0.75 x 10^4 cells ml^{-1} for NCI-H460, followed by 24 h of incubation. The effect of the vehicle solvent (DMSO) on the growth of cell lines which it was evaluated in all tests by exposing untreated control cells to the maximum concentration (0.5%) of DMSO used in each assay.

Tumor cell growth assay: The effects of the newly synthesized compounds **3–15a-d** on the in vitro growth of human tumor cell lines were evaluated according to the procedure adopted by the National Cancer Institute (NCI, USA) in the '*In vitro* Anticancer Drug Discovery Screen' that uses the protein-binding dye sulforhodamine B to assess cell growth[12]. Briefly, exponentially cells growing in 96-well plates were then exposed for 48 h to five serial concentrations of each compound starting from a maximum concentration of 150 µM. Following this exposure period adherent cells were fixed, washed and stained. The bound stain was solubilized and the absorbance was measured at 492 nm in a plate reader (Bio-Tek Instruments Inc., Powerwave XS, Wincoski, USA). For each test compound and cell line, a dose response curve was obtained and the growth inhibition of 50 % (GI_{50}) corresponding to the concentration of the compounds that inhibited 50% of the net cell growth was calculated as described elsewhere[13]. Doxorubicin was used as a positive control and tested in the same manner.

Results are given in concentrations that were able to cause 50 % of cell growth inhibition (GI_{50}) after a continuous exposure of 48 h and show means ± SEM of three-independent experiments performed in duplicate.

Effect on the Growth of Human Tumor Cell Lines

The effect of the newly synthesized compounds **3-15a-d** was evaluated on the *in vitro* growth of three human tumor cell lines representing different tumor types namely, breast adenocarcinoma (MCF-7), non-small cell lung cancer (NCI-H460) and CNS cancer (SF-268) after a continuous exposure for 48 h. The results were introduced in **Table 1**.

Table 1. Effect of compounds **3-15a-d** on the growth of three human tumor cell lines

Compound	GI_{50}, µmol L^{-1}		
	NCI-H460	**MCF-7**	**SF-268**
3	27.6 ± 2.4	16.9 ± 4.8	16.8 ± 2.6
5a	0.02 ± 0.002	0.01 ± 0.002	0.02 ± 0.001
5b	12.1 ± 0.8	10.3 ± 2.6	6.3 ± 0.8
6a	0.4 ± 0.2	0.2 ± 0.01	0.2 ± 0.06
6b	4.2 ± 1. 4	6.1 ± 2.4	4.0 ± 1.2
8a	12.6 ± 0.6	14.5 ± 0.8	8.7 ± 2.4
8b	22.4 ± 8.1	24.2 ± 2.8	28.3 ± 4.2
9a	0.01 ± 0.002	0.01`± 0.004	0.01 ± 0.001
9b	1.6 ± 0.4	2.2 ± 0. 8	4.0 ± 0.2
9c	6. 1 ± 2.4	8. 1 ± 2.1	4.2 ± 1.3
9d	0.9 ± 0.2	0.1 ± 0.02	0.3 ± 0.05
10a	8. 1 ± 2.2	6.2 ± 1.1	8.20 ± 2.4
10b	0.4 ± 0.2	0.2± 0.06	0.5 ± 0.01
10c	32.0 ± 1.6	40.0 ± 0.4	10.5 ± 1.2
10d	0.01 ± 0.003	0.02 ± 0.001	0.01 ± 0.001
13a	0.2 ± 0.01	0.1 ± 0.02	0.2 ± 0.02
13b	10.6 ± 4.6	8.5 ± 2.8	6.7 ± 1.4
15a	20.4 ± 8.1	22.2 ± 2.8	20.3 ± 4.2
15b	0.01 ± 0.008	0.01`± 0.006	0.01 ± 0.002
15c	2.6 ± 0.6	4.2 ± 0.2	8.0 ± 1.4
15d	0.01 ± 2.4	0.1 ± 0.01	0.2 ± 0.03
Doxorubicin	0.04 ± 0.008	0.09 ± 0.008	0.09 ± 0.007

The all compounds were able to inhibit the growth of the tested human tumor cell lines in a dose-dependent manner. The results indicated through **Table 1** revealed that compounds **5a**, **9a**, **10d** and **15b** showed the highest inhibitory effect against all three tumor cell lines, such activity is higher than the reference doxorubicin. While compounds **6a** and **13a** showed high inhibitory effects against three different cell lines, which are less than the corresponding reference doxorubicin. Compounds **3**, **5b**, **8a**, **8b**, **9c**, **10a**, **10c**, **13b** and **15a** showed the lowest inhibitory effect. The remaining compounds showed a moderate growth inhibitory effect. Comparing compound **5a** and **5b** it is obvious that the presence of the CN group in compound **5a** is responsible for their reactivity over **5b**. Similarly comparing of **6a** with **6b**, **8a** with **8b** and **13a** with **13b** it is obvious that the introduction of the CN group in **6a**, **8a** and **13a** showed higher inhibitory effect towards the three cell lines than that of **6b**, **8b** and **13b**. On the other hand comparison of inhibitory effect of compounds **9a-d**, one can say that compound **9a** with the X = Y = CN showed the highest inhibitory effect among the four compounds such reactivity is higher than that of the reference doxorubicin. Comparison of compounds **10a-d** showed that the effect of X^- = O and Y= COOEt like in **10d** the maximum inhibitory result among the four compounds was obtained. However, when X^- = O and Y = CN as in case of **10b** the inhibitory effect was lowered but it hasn't large amount as the compound is still of the most active compounds among the all test compounds. On the other hand the introduction of NH group like in **10a** decreases the reactivity and such observation was shifted towards lower reactivity in case of **10c** where X = NH and Y = COOEt. Similarly, comparison of compounds **15a-d** showed that when R = Ph and Y= CN like in **15b** the maximum inhibitory effect among the four compounds was obtained.

However, when R = Ph and Y = COOEt as in case of **15d** the inhibitory effect was lowered but it hasn't large amount as the compound is still of the most active compounds among all test compounds. On the other hand introduction of un-substituted compound like in **15a** decreases the reactivity and such observation was shifted towards lower reactivity in case of **15c** where R = H and Y = COOEt.

Experimental

All melting points were determined in open capillaries and are uncorrected. Elemental analyses were performed on a Yanaco CHNS Corder elemental analyzer (Japan). IR spectra were measured using KBr discs on a Pye Unicam SP-1000 spectrophotometer. ^{1}H NMR spectra were measured on a Varian EM 390-200 M*Hz* instrument in CD_3SOCD_3 as solvent using TMS as internal standard and chemical shifts were expressed as δ ppm. Mass spectra were recorded on Kratos (75 eV) MS equipment (Germany).

2-Cyclohexylidene-3-oxo-N-phenylbutanamide (3)

To a dray solid of acetoacetanilide **(1)** (5.31g, 0.03 mol) containing ammonium acetate (0.50 g) cyclohexanone **(2)** (2.94 g, 0.03 mol) was added. The reaction mixture was heated in an oil bath at 120ºC for 1h then left to cool then triturated with ethanol and the formed solid product was collected by filtration.

Compound **3:** Pale brown crystals from ethanol, yield: 96 % (7.406 g); mp: 120 ºC. IR (KBr): υ/cm^{-1} = 3448-3320 (NH), 3050 (CH-aromatic), 2991(CH_3), 2885(CH_2) 1695, 1687 (2CO). ^{1}H NMR (DMSO-d_6): δ = 1.77-1.79 (m, 6H, 3CH_2), 2.11-2.16 (m, 4H, 2CH_2), 2.27 (s, 3H, CH_3), 7.25-7.36 (m, 5H, C_6H_5), 9.63 (s, 1H, NH, D_2O-exchangeable). MS (relative intensity) m/z: 257 (M^+, 21%). Analysis for $C_{16}H_{19}NO_2$ Calcd: C, 74.68; H, 7.44; N, 5.44. Found: C, 74.93; H, 7.29; N, 5.83 %.

4,4-Dicyano-2-cyclohexylidene-3-methyl-N-phenylbut-3-enamide (5a) and ethyl-4-(phenylcarbamoyl)-2-cyano-4-cyclohexylidene-3-methylbut-2-enoate (5b)

General procedure: To a solution of compound **3** (2.57 g, 0.01 mol) in ethanol (50 ml) containing piperidine (0.5 ml), either malononitrile **(4a)** (0.66 g, 0.01 mol) or ethylcyanoacetate **(4b)** (1.13 g, 0.01 mol) was added. The reaction mixture was heated under reflux for 3 h then left to cool and the solid product was formed in each case upon pouring onto ice/water containing few drops of hydrochloric acid, the solid product was collected by filtration.

Compound **5a**: Yellow crystals from ethanol, yield: 86 % (2.624 g); mp: 134 °C. IR (KBr): υ/cm^{-1} = 3466-3323 (NH), 3054 (CH-aromatic), 2980 (CH_3), 2918 (CH_2), 2223-2220 (2 CN), 1687 (CO), 1633 (C=C). ^{1}H NMR (DMSO-d_6): δ = 1.75-1.79 (m, 6H, 3CH_2), 1.87-1.91 (m, 4H, 2CH_2), 2.28 (s, 3H, CH_3), 7.29-7.41 (m, 5H, C_6H_5), 9.88 (s, 1H, NH, D_2O-exchangeable). MS (relative intensity) m/z: 305 (M^+, 17.5%). Analysis for $C_{19}H_{19}N_3O$ Calcd: C, 74.73; H, 6.27; N, 13.76. Found: C, 74.85; H, 6.11; N, 13.93 %.

Compound **5b**: Yellow crystals from ethanol, yield: 84 % (2.958 g); mp: 104 °C. IR (KBr): υ/cm^{-1} = 3484-3312 (NH), 3058 (CH-aromatic), 2985 (CH_3), 2916 (CH_2), 2222 (CN), 1690, 1687 (2CO), 1636 (C=C). ^{1}H NMR (DMSO-d_6): δ = 1.13 (t, 3H, J = 7.44 Hz, CH_3), 1.72-1.77 (m, 6H, 3CH_2), 2.12-2.18 (m, 4H, 2CH_2), 2.35 (s, 3H, CH_3), 4.22 (q, 2H, J = 7.44 Hz, CH_2), 7.28-7.40 (m, 5H, C_6H_5), 9.73 (s, 1H, NH, D_2O-exchangeable). MS (relative intensity) m/z: 352 (M^+, 30.6%). Analysis for $C_{21}H_{24}N_2O_3$ Calcd: C, 71.57; H, 6.86; N, 7.95. Found: C, 71.73; H, 6.68; N, 8.21 %.

2 - (5 - Amino-4 - cyanothiophen - 3 - yl)- 2- cyclohexylidene-N-phenylacetamide (6a) and 2-amino-4-(cyclohexylidene-phenyl-carbamoyl-methyl) thiophene-3-carboxylic acid ethyl ester (6b)

General procedure: To a solution of each compound **5a** (0.915 g, 0.003 mol) or compound **5b** (1.06 g, 0.003 mol) in 1,4-dioxan (40 ml) containing triethylamine (0.5 ml), elemental sulfur (0.1 g, 0.003 mol) was added. The reaction mixture was heated under reflux for 1.5 h then poured onto ice/water containing few drops of hydrochloric acid and the formed solid product was collected by filtration.

Compound **6a**: Buff crystals from acetic acid, yield: 72 % (0.728g); mp: 180-182 ºC. IR (KBr): υ/cm^{-1} = 3473-3318 (NH_2, NH), 3058 (CH-aromatic), 2882 (CH_2), 2224 (CN), 1686 (CO), 1633 (C=C). ^{1}H NMR (DMSO-d_6): δ = 1.73-1.76 (m, 6H, 3CH_2), 1.91-1.98 (m, 4H, 2CH_2), 4.54 (s, 2H, NH_2, D_2O exchangeable), 6.73 (s, 1H, thiophene ring), 7.27-7.38 (m, 5H, C_6H_5), 9.32 (s, 1H, NH, D_2O-exchangeable). MS (relative intensity) m/z: 337 (M^+, 21.2%). Analysis for $C_{19}H_{19}N_3OS$ Calcd: C, 67.63; H, 5.68; N, 12.45; S, 9.50. Found: C, 67.85; H, 5.82; N, 12.62; S, 9.29 %.

Compound **6b**: Pale yellow crystals from acetic acid, yield: 81 % (0.933g); mp: 215-217 ºC. IR (KBr): υ/cm^{-1} = 3469-3322 (NH_2, NH), 3058 (CH-aromatic), 2970 (CH_3), 2892 (CH_2), 1693, 1685 (2CO), 1634 (C=C). ^{1}H NMR (DMSO-d_6): δ = 1.12 (t, 3H, J = 7.09 Hz, CH_3), 1.65-1.73 (m, 6H, 3CH_2), 2.62-2.67 (m, 4H, 2CH_2), 4.26 (q, 2H, J = 7.09 Hz, CH_2), 4.71 (s, 2H, NH_2, D_2O exchangeable), 6.65 (s, 1H, thiophene ring), 7.27-7.38 (m, 5H, C_6H_5), 9.39 (s, 1H, NH, D_2O-exchangeable). MS (relative intensity) m/z: 384 (M^+, 12.4%). Analysis for $C_{21}H_{24}N_2O_3S$ Calcd: C, 65.60; H, 6.29; N, 7.29; S, 8.34. Found: C, 65.88; H, 5.98; N, 7.52; S, 8.02 %.

2-(2-Hydrazinyl-4,5,6,7-tetrahydrobenzo[*b*]thiophene-3-cyano)-3-oxo-N-phenyl-butanamide (8a) and 2-(2-hydrazinyl -4,5,6,7-tetrahydrobezo [*b*] thiophene-3-ethoxy-carbonyl)-3-oxo-N-phenylbutanamide (8b)

General procedure: A cold solution of either of 3-cyano-4,5,6,7-tetrahydrobenzo[*b*]thiophene-2-diazonium chloride **(7a)** or 3-ethoxy carbonyl -4,5,6,7-tetrahydrobenzo [*b*] thiophene-2-diazonium chloride **(7b)** [obtained by adding sodium nitrite (1.49 g, 0.02 mol) solution to a cold solution of either 2-amino-3-cyano-4,5,6,7-tetrahydrobenzo[*b*] thiophene (3.56 g, 0.02 mol) or ethyl 2-amino-4,5,6,7-tetrahydrobenzo [*b*] thiophene-3-carboxylate (4.51 g, 0.02 mol) in acetic/hydrochloric acid (10:3) with continuous stirring] was added to a cold solution (0-5 ºC) of acetoacetanilide **(1)** (3.56 g, 0.02 mol) in ethanol (50 ml) containing sodium hydroxide (10 ml, 10 %). The reaction mixture was stirred at room temperature for 1 h and the solid product was formed, collected by filtration.

Compound **8a**: Orange crystals from DMF, yield: 63 % (4.617 g); mp=108-110 ºC. IR (KBr): υ/cm^{-1} = 3482-3341 (2 NH), 3053 (CH-aromatic), 2981 (CH_3), 2887 (CH_2), 2220 (CN), 1688, 1684 (2CO), 1636 (C=C). ^{1}H NMR (DMSO-d_6): δ = 1.71-1.75 (m, 4H, 2CH_2), 2.16-2.22 (m, 4H, 2CH_2), 2.37 (s, 3H, CH_3), 7.32-7.41 (m, 5H, C_6H_5), 8.72, 9.15 (2s, 2H, D_2O-exchangeable, 2NH). MS (relative intensity) m/z: 366 (M^+, 11.8%). Analysis for $C_{19}H_{18}N_4O_2S$ Calcd: C, 62.28; H, 4.95; N, 15.29; S, 8.75. Found: C, 62.44; H, 5.22; N, 15.39; S, 8.82 %.

Compound **8b**: Orange crystals from DMF, yield: 75 % (6.197 g); mp: 169-171 ºC. IR (KBr): υ/cm^{-1} = 3472-3363 (2 NH), 3056 (CH-aromatic), 2974 (CH_3), 2894 (CH_2), 1692, 1684 and 1681 (3CO), 1636 (C=C). ^{1}H NMR (DMSO-d_6): δ = 1.16 (t, 3H, J = 7.62 Hz, CH_3), 1.62-1.73 (m, 4H, 2CH_2), 2.27-2.34 (m, 4H, 2CH_2), 2.42 (s, 3H, CH_3), 4.23 (q, 2H, J = 7.62 Hz, CH_2), 7.28-7.42 (m, 5H, C_6H_5), 8.32, 9.36 (2s, 2H, D_2O-exchangeable 2NH). MS (relative intensity) m/z: 413 (M^+, 27.4%). Analysis for $C_{21}H_{23}N_3O_4S$ Calcd: C, 61.00; H, 5.61; N, 10.16; S, 7.75. Found: C, 61.28 ; H, 5.42; N, 10.31; S, 7.93 %.

2-(2-Hydrazinyl-4,5,6,7-tetrahydrobenzo[*b*]thiophene-3-cyano)-4,4-dicyano-3-methyl-N-phenyl-but-3-enamide (9a), ethyl 4-(phenylcarbamoyl)-4-(2-hydrazinyl-4,5,6,7-tetrahydrobenzo[*b*]-thiophene-3-cyano)-2-cyano-3-methyl-but-2-enoate (9b), 2-(2-hydrazinyl-4,5,6,7-tetrahydrobenzo[*b*]thiophene-3-ethoxycarbonyl)-4,4-dicyano-3-methyl-N-phenyl-but-3-enami-de (9c) and ethyl 4-(phenylcarbamoyl)-4-(2-hydrazinyl-4,5,6,7-tetrahydrobenzo[*b*]thiophene-3-ethoxycarbonyl)-2-cyano-3-methylbut-2-enoate (9d)

To a dray solid of either compound **8a** (1.01 g, 0.003 mol) or **8b** (1.24 g, 0.003 mol) containing ammonium acetate (0.50 g), either malononitrile **(4a)** (0.2 g, 0.003 mol) or ethylcyanoacetate **(4b)** (0.34 g, 0.003 mol) was added. The reaction mixture was heated in an oil bath at 120 ºC for 1h then left to cool, triturated with ethanol and the solid product was formed and collected by filtration.

Compound **9a**: Pale yellow crystals, yield: 68 % (0.845 g); mp: >290ºC IR (KBr): υ/cm^{-1} = 3449-3323 (2NH), 3055 (CH-aromatic), 2955 (CH_3), 2890 (CH_2), 2227-2220 (3CN), 1693 (CO), 1633 (C=C). ^{1}H NMR (DMSO-d_6): δ = 1.66-1.69 (m, 4H, 2CH_2), 2.25-2.31 (m, 4H, 2CH_2), 2.40 (s, 3H, CH_3), 7.29-7.40 (m, 5H, C_6H_5), 8.42, 9.29 (2s, 2H, D_2O-exchangeable, 2NH). MS (relative intensity) m/z: 414 (M^+, 15.7%). Analysis for $C_{22}H_{18}N_6OS$ Calcd: C, 63.75; H, 4.38; N, 20.28; S, 7.74. Found: C, 63.92; H, 4.66; N, 20.32; S, 7.49 %.

Compound **9b**: Pale yellow crystals from ethanol, yield: 78 % (1.08 g); mp: 238-240 ºC. IR (KBr): υ/cm^{-1} = 3480-3323 (2NH), 3053 (CH-aromatic), 2968 (CH_3), 2883 (CH_2), 2223, 2220 (2CN), 1690, 1687 (2CO), 1621 (C=C). ^{1}H NMR (DMSO-d_6): δ = 1.13 (t, 3H, J = 7.31 Hz, CH_3), 1.64-1.70 (m, 4H, 2CH_2), 2.14-2.18 (m, 4H, 2CH_2), 2.28 (s, 3H, CH_3), 4.22 (q, 2H, J = 7.31 Hz, CH_2), 7.24-7.40 (m, 5H, C_6H_5), 8.29, 9.33 (2s, 2H, D_2O-exchangeable 2NH). MS (relative intensity) m/z: 461 (M^+, 22.5%). Analysis for $C_{24}H_{23}N_5O_3S$ Calcd: C, 62.46; H, 5.02; N, 15.17; S, 6.95. Found: C, 62.39; H, 4.91; N, 14.92; S, 7.04 %.

Compound **9c**: Yellow crystals from ethanol, yield: 84 % (1.162 g); mp: 266-268 ºC. IR (KBr): υ/cm^{-1} = 3478-3320 (2 NH), 3058 (CH-aromatic), 2972 (CH_3), 2888 (CH_2), 2226, 2221 (2CN), 1692, 1689 (2CO), 1636 (C=C). ^{1}H NMR (DMSO-d_6): δ = 1.16 (t, 3H, J = 7.48 Hz, CH_3), 1.62-1.73 (m, 4H, 2CH_2), 2.17-2.21 (m, 4H, 2CH_2), 2.32 (s, 3H, CH_3), 4.31 (q, 2H, J = 7.48 Hz, CH_2), 7.30-7.43 (m, 5H, C_6H_5), 8.27, 9.39 (2s, 2H, D_2O-exchangeable 2NH). MS (relative intensity) m/z: 461 (M^+, 34.5%). Analysis for $C_{24}H_{23}N_5O_3S$ Calcd: C, 62.46; H, 5.02; N, 15.17; S, 6.95. Found: C, 62.62; H, 5.29; N, 15.33; S, 7.22 %.

Compound **9d**: Yellow crystals from 1,4 dioxane, yield: 66 % (1.006 g); mp: 188-190 ºC. IR (KBr): υ/cm^{-1} = 3489-3322 (2 NH), 3056 (CH-aromatic), 2964 (CH_3), 2883 (CH_2), 2220 (CN), 1690, 1687 and 1681 (3CO), 1638 (C=C). ^{1}H NMR (DMSO-d_6): δ = 1.13, 1.16 (2t, 6H, CH_3), 1.60-1.75 (m, 4H, 2CH_2), 1.97-2.05 (m, 4H, 2CH_2), 2.21 (s, 3H, CH_3), 4.20, 4.25 (2q, 4H, 2CH_2), 7.24-7.40 (m, 5H, C_6H_5), 8.30, 9.37 (2s, 2H, D_2O-exchangeable 2NH). MS (relative intensity) m/z: 508 (M^+, 26.5%). Analysis for $C_{26}H_{28}N_4O_5S$ Calcd: C, 61.40; H, 5.55; N, 11.02; S, 6.30. Found: C, 61.39 ; H, 5.69; N, 11.29; S, 6.49 %.

5-Cyano-1-(3-cyano-4,5,6,7-tetrahydrobenzo[*b*]thiophen-2-yl)-1,6-dihydro-6-imino-4-methylpyridazine-3-(N-phenyl-carbox-amide) (10a), 5-cyano-1-(3-cyano-4,5,6,7-tetrahydrobenzo[*b*]-thiophen-2-yl)-1,6-dihydro-4-methyl-6-oxo-pyridazine-3-(N-phenylcarboxamide) (10b), ethyl 2-(3-phenylcarbamoyl) -5-cyano-6-imino-4-methyl-pyridazin-1(6*H*)-yl)-4,5,6,7-tetrahyd-robenzo[*b*]thiophene-3-carboxylate (10c) and ethyl 2-(3-phenyl-carbamoyl)-5-cyano-4-methyl-6-oxo-pyridazin-1(6*H*)-yl)-4,5,6,7-tetrahydrobenzo[*b*]thiophene-3-carboxylate (10d)

General procedure: To a solution of either compound **8a** (1.01 g, 0.003 mol) or **8b** (1.24 g, 0.003 mol) in ethanol (50 ml) containing piperidine (0.5 ml) either malononitrile **(4a)** (0.2 g, 0.003 mol) or ethyl cyanoacetate **(4b)** (0.34 g, 0.003 mol) was added. The reaction mixture was heated under reflux for 6 h then left to cool and the formed solid product in each case, upon pouring onto ice/water containing few drops of hydrochloric acid was collected by filtration.

Compound **10a**: Pale brown crystals from ethanol, yield: 76 % (0.944 g); mp: 150-152 ºC. IR (KBr): υ/cm^{-1} = 3458-3321 (2 NH), 3056 (CH-aromatic), 2946 (CH_3), 2862 (CH_2), 2229, 2220 (2CN), 1690 (CO), 1660 (C=N), 1636 (C=C). ^{1}H NMR (DMSO-d_6): δ = 1.64-1.68 (m, 4H, 2CH_2), 2.05-2.12 (m, 4H, 2CH_2), 2.34 (s, 3H, CH_3), 7.27-7.42 (m, 5H, C_6H_5), 8.25, 9.30 (2s, 2H, D_2O-exchangeable, 2NH). MS (relative intensity) m/z: 414 (M^+, 23.3%). Analysis for $C_{22}H_{18}N_6OS$ Calcd: C, 63.75; H, 4.38; N, 20.28; S, 7.74. Found: C, 63.56; H, 4.39; N, 20.19; S, 7.93 %.

Compound **10b**: Yellow crystals from ethanol, yield: 83 % (1.034 g); mp: 140-141 ºC. IR (KBr): υ/cm^{-1} = 3469-3340 (NH), 3052 (CH-aromatic), 2978 (CH_3), 2874 (CH_2), 2226, 2220 (2CN), 1693, 1688 (2CO), 1638 (C=C). ^{1}H NMR (DMSO-d_6): δ = 1.62-1.68 (m, 4H, 2CH_2), 2.17-2.22 (m, 4H, 2CH_2), 2.38 (s, 3H, CH_3), 7.28-7.38 (m, 5H, C_6H_5), 9.30 (s, 1H, D_2O-exchangeable, NH). MS (relative intensity) m/z: 415 (M^+, 37.2%). Analysis for $C_{22}H_{17}N_5O_2S$ Calcd: C, 63.60; H, 4.12; N, 16.86; S, 7.72. Found: C, 63.89; H, 4.32; N, 16.95; S, 7.51 %.

Compound **10c**: Yellow crystals from ethanol, yield: 76 % (1.051 g); mp: 164-166 ºC. IR (KBr): υ/cm^{-1} = 3534-3349 (2 NH), 3056 (CH-aromatic), 2956 (CH_3), 2906 (CH_2), 2222 (CN), 1689, 1686 (2CO), 1665 (C=N), 1636 (C=C). ^{1}H NMR (DMSO-d_6): δ = 1.12 (t, 3H, J = 6.89 Hz, CH_3), 1.64-1.72 (m, 4H, 2CH_2), 2.13-2.17 (m, 4H, 2CH_2), 2.23 (s, 3H, CH_3), 4.20 (q, 2H, J = 6.89 Hz, CH_2), 7.26-7.40 (m, 5H, C_6H_5), 8.29, 9.37 (2s, 2H, D_2O-exchangeable, 2NH). MS (relative intensity) m/z: 461 (M^+, 17.6%). Analysis for $C_{24}H_{23}N_5O_3S$ Calcd: C, 62.46; H, 5.02; N, 15.17; S, 6.95. Found: C, 62.72; H, 5.32; N, 15.49; S, 7.21 %.

Compound **10d**: Yellow crystals from ethanol, yield: 73 % (1.012 g); mp:152-154 ºC. IR (KBr): υ/cm^{-1} = 3476-3336 (NH), 3056 (CH-aromatic), 2980 (CH_3), 2892 (CH_2), 2221 (CN), 1693, 1689 and 1684 (3CO), 1638 (C=C). ^{1}H NMR (DMSO-d_6): δ = 1.11 (t, 3H, CH_3), 1.62-1.73 (m, 4H, 2CH_2), 2.12-2.15 (m, 4H, 2CH_2), 2.27 (s, 3H, CH_3), 4.23 (q, 2H, CH_2), 7.28-7.43 (m, 5H, C_6H_5), 9.39 (s, 1H, D_2O-exchangeable, NH). MS (relative intensity) m/z: 462 (M^+, 21.8%). Analysis for $C_{24}H_{22}N_4O_4S$ Calcd: C, 62.32; H, 4.79; N, 12.11; S, 6.93. Found: C, 62.46 ; H, 5.09; N, 12.39; S, 6.69 %.

2-(6-Acetyl-4,5-dihydro-4-phenyl-5-(phenylimino)-3-thio-1,2,4-triazin-2-(3*H*)-yl)-4,5,6,7-tetrahydrobenzo[*b*]-thiophene-3-carbonitrile (13a) and ethyl 2-(6-acetyl-4,5-dihydro-4-phenyl-5-(phenylimino)-3-thio-1,2,4-triazin-2(3*H*)-yl)-4,5,6,7-tetrahydrobenzo[*b*]thiophene-3-carboxylate (13b)

General procedure: To a solution of either compound **8a** (1.01 g, 0.003 mol) or **8b** (1.24 g, 0.003 mol) in 1,4-dioxan (40 ml) containing catalytic base "triethylamine" (0.5 ml), phenylisothiocyanate **(11)** (0.41 g, 0.003 mol) was added. The reaction mixture was heated under reflux for 3 h then left to cool and the formed solid product in each case, upon pouring onto ice/water containing few drops of hydrochloric acid was collected by filtration.

Compound **13a**: Orange crystals from DMF, yield: 77 % (1.116 g); mp: 185-187 ºC. IR (KBr): υ/cm^{-1} = 3053 (CH-aromatic), 2973 (CH_3), 2888 (CH_2), 2220 (CN), 1689 (CO), 1634 (C=C). ^{1}H NMR (DMSO-d_6): δ = 1.73-1.75 (m, 4H, 2CH_2), 1.98-2.06 (m, 4H, 2CH_2), 3.01 (s, 3H, CH_3), 7.34-7.46 (m, 10H, 2C_6H_5). MS (relative intensity) m/z: 483 (M^+, 14.5%). Analysis for $C_{26}H_{21}N_5OS_2$ Calcd: C, 64.57; H, 4.38; N, 14.48; S, 13.26. Found: C, 64.41; H, 4.08; N, 14.32; S, 13.44 %.

Compound **13b**: Orange crystals from DMF, yield: 75 % (1.193 g); mp: 233-235 ºC. IR (KBr): υ/cm^{-1} = 3056 (CH-aromatic), 2958 (CH_3), 2893 (CH_2), 1692, 1687 (2CO), 1636 (C=C). ^{1}H NMR (DMSO-d_6): δ = 1.14 (t, 3H, J = 7.42 Hz, CH_3), 1.61-1.74 (m, 4H, 2CH_2), 2.19-2.24 (m, 4H, 2CH_2), 3.05 (s, 3H, CH_3), 4.21 (q, 2H, J = 7.42 Hz, CH_2), 7.28-7.41 (m, 10H, 2C_6H_5). MS (relative intensity) m/z: 530 (M^+, 26.2%). Analysis for $C_{28}H_{26}N_4O_3S_2$ Calcd: C, 63.37; H, 4.94; N, 10.56; S, 12.08. Found: 63.42; H, 5.19; N, 10.36; S, 11.84%.

4-((3-Cyano-4,5,6,7-tetrahydrobenzo[*b*]thiophen-2-yl)diazenyl)-3-methyl-5-phenylamino-1*H*-pyrazol (15a), 4-((3-cyano-4,5,6,7-tetrahydrobenzo[*b*]thiophen-2-yl)diazenyl)-3-methyl-1-phenyl-5-phenylamino-1*H*-pyrazol (15b), 4-((3-ethoxycarbonyl-4,5,6,7-tetrahydrobenzo[*b*]thiophen-2-yl)diazenyl)-3-methyl-5-phenylamino-1*H*-pyrazol (15c) and 4-((3-ethoxycarbonyl-4,5,6,7-tetrahydrobenzo[*b*]thiophen-2-yl)di-azenyl)-3-methyl-1-phenyl-5-phenylamino-1*H*-pyrazol (15d)

General procedure: To a solution of either compound **8a** (1.01 g, 0.003 mol) or **8b** (1.24 g, 0.003 mol) in ethanol (50 ml) either hydrazine hydrate **(14a)** (0.15 ml, 0.003 mol) or phenyl hydrazine **(14b)** (0.33 g, 0.003 mol) was added. The reaction mixture in each case was heated under reflux for 3 h then poured onto ice/water containing few drops of hydrochloric acid and the formed solid product was collected by filtration.

Compound **15a**: Pale brown crystals from ethanol, yield: 76 % (0.826 g); mp: 205-207 ºC. IR (KBr): υ/cm^{-1} = 3458-3321 (2NH), 3056 (CH-aromatic), 2966 (CH_3), 2884 (CH_2), 2229 (CN), 1660 (C=N), 1636 (C=C). ^{1}H NMR (DMSO-d_6): δ = 1.62-1.67(m, 4H, 2CH_2), 1.88-1.93 (m, 4H, 2CH_2), 2.13 (s, 3H, CH_3), 7.26-7.37 (m, 5H, C_6H_5), 8.78, 9.61 (2s, 2H, D_2O-exchangeable, 2NH,). MS (relative intensity) m/z: 362 (M^+, 16.8%). Analysis for $C_{19}H_{18}N_6S$ Calcd: C, 62.96; H, 5.01; N, 23.19; S, 8.85. Found: C, 63.14; H, 4.99; N, 22.94; S, 8.61 %.

Compound **15b**: Yellow crystals from ethanol, yield: 75 % (0.986 g); mp: 245-247 ºC. IR (KBr): υ/cm^{-1} = 3439-3321 (NH), 3056 (CH-aromatic), 2952 (CH_3), 2858 (CH_2), 2223 (CN), 1633 (C=C). ^{1}H NMR (DMSO-d_6): δ = 1.61-1.66 (m, 4H, 2CH_2), 2.03-2.07 (m, 4H, 2CH_2), 2.24 (s, 3H, CH_3), 7.24-7.47 (m, 10H, 2C_6H_5), 9.22 (s, 1H, D_2O-exchangeable, NH). MS (relative intensity) m/z: 438 (M^+, 19.2%). Analysis for $C_{25}H_{22}N_6S$ Calcd: C, 68.47; H, 5.06; N, 19.16; S, 7.31. Found: C, 68.73; H, 4.83; N, 19.12; S, 7.22%.

Compound **15 c**: Yellow crystals from ethanol, yield: 76 % (0.934 g); mp: 169-171 ºC. IR (KBr): υ/cm^{-1} = 3573-3329 (2 NH), 3052 (CH-aromatic), 2947 (CH_3), 2868 (CH_2), 1690 (CO), 1649 (C=N), 1632 (C=C). ^{1}H NMR (DMSO-d_6): δ = 1.14 (t, 3H, J = 7.48 Hz, CH_3), 1.62-1.70 (m, 4H, 2CH_2), 2.17-2.24 (m, 4H, 2CH_2), 2.38 (s, 3H, CH_3), 4.21 (q, 2H, J = 7.48 Hz, CH_2), 7.29-7.39 (m, 5H, C_6H_5), 8.30, 9.33 (2s, 2H, D_2O-exchangeable, 2NH). MS (relative intensity) m/z: 409 (M^+, 33.4%). Analysis for $C_{21}H_{23}N_5O_2S$ Calcd: C, 61.59; H, 5.66; N, 17.10; S, 7.83. Found: C, 61.48; H, 5.42; N, 17.22; S, 7.89 %.

Compound **15d**: Yellow crystals from ethanol, yield: 68 % (0.99 g); mp: 175-177 ºC. IR (KBr): υ/cm^{-1} = 3482-3329 (NH), 3053 (CH-aromatic), 2971 (CH_3), 2880 (CH_2), 1688 (CO), 1632 (C=C). ^{1}H NMR (DMSO-d_6): δ = 1.12 (t, 3H, CH_3), 1.60-1.67 (m, 4H, 2CH_2), 2.18-2.25 (m, 4H, 2CH_2), 2.35 (s, 3H, CH_3), 4.22 (q, 2H, CH_2), 7.26-7.38 (m, 10H, 2C_6H_5), 9.46 (s, 1H, D_2O-exchangeable, NH). MS (relative intensity) m/z: 485 (M^+, 27.1%). Analysis for $C_{27}H_{27}N_5O_2S$ Calcd: C, 66.78; H, 5.60; N, 14.42; S, 6.60. Found: C, 66.52 ; H, 5.32; N, 14.15; S, 6.78 %.

 DOI: 10.17628/ecb.2014.3.430-436

Acknowledgment

The authors would like to thank the research group working at the Medicinal Department at the National Research Center, Dokki, Egypt, for recording the pharmacological data of the synthesized products. Moreover, the effort of Dr. Mohammed Othman, MSA University-Biochemistry Department, is greatly appreciated for his kind revisions for the pharmacological data.

References

[1]Shchekotikhin, A. E., Glazunova, V. A., Dezhenkova, L. G., Luzikov, Y. N., Sinkevich, Y. B., Kovalenko, L. V., Buyanov, V. N., Balzarini, J., Chun Huang F., Jer Lin J., -Shan Huang, H., Shtil, A. A. and Preobrazhenskaya, M. N., *Bioorg.Med. Chem.,***2009,** *17***,** 1861.

[2]Dallemagne, P., Khanh, L., ellah Alsadi, A., Varlet, I., Collot, V., Paillet, M., Bureau, R. and Rault, S., *Bioorg. Med. Chem.*, **2003,** *11*, 1161.

[3]Fakhr, I. M .I., Radwan, M. A. A., El-Batran, S., Abd El-Salam, O. M. E. and El-Shenawy, S. M., *Eur. J. Med. Chem.*, **2009,** *44*, 1718.

[4]Molvi, K. I., Vasu, K. K., Yerande, S. G., Sud -arsanam, V. and Haque, N., *Eur. J. Med. Chem.*, **2007,** *42*, 1049.

[5]Abreu, A., Paula, M. T. F., Luis, S. M. and Maria-Joao, P. O., *Tetrahedron*, **2004,** *60*, 11821.

[6]Alagarsamy, S. M., Ramsechu, K. V. and Solomon, K., *Eur. J. Med. Chem.*, **2006,** *41*, 1293.

[7]Bharti, N., Husain, K., Garza, M. T .G., Cruz-Vega, D. E., Castro-Garza, J., Mata-Cardenas, B. D., Naqvia, F. and Azama, A., *Bioorg. Med. Chem. Lett.*, **2002,** *12*, 3475.

[8]Valderrama, J., Fournet, A., Valderrama, C., Bastias, S., Astudillo, C., Rojas de Arias, A., Inchausti, A. and Yaluff, G., *Chem. Pharm. Bull. (Tokyo)*, **1999,** *47(9)*, 1221.

[9]Elkholy, M. Y., *Heterocyclic Comm.* **2011,** *11*, 89.

[10]Barrja, P., Diana, P., Lauria, A., Montalbano, A., Almerico, A. A., Dattolo, G. and Cirrincione, G., *Anticancer Res.*, **2004**, *24*, 3775.

[11]Poreba, K., Opolski, A., Wietrzyk, J. and Kowalska, M., *Arch. Pharm. (Weinheim)*, **2001**, *334***,** 219.

[12]Skehan, P., Storeng, R., Scudiero, D., Monks, A., McMahon, J., Vistica, D., Warren, J. T., Bokesch, H., Kenney, S. and Boyd, M. R. J., *Natl. Cancer Inst*., **1990,** *82*, 1107.

[13]Monks, A., Scudiero, D., Skehan, P., Shoemaker, R., Paull, K., Vistica, D., Hose, C., Langley, J., Cronise, P., Vaigro-Wolff, A., Gray-Goodrich, M., Campbell, H., Mayo J. and Boyd, M. J., *Natl. Cancer Inst.***, 1991,** *83*, 757.

Received: 12.04.2014.
Accepted: 04.05.2014.

ANTI-CORROSIVE ACTIVITIES OF SOME NOVEL SURFACTANTS BASED ON VEGETABLE OILS

V. M. Abbasov,[a] I. T. Ismayilov,[a,b] Hany M. Abd El-Lateef,[a,c] and S. F. Akhmadbeyova[a]

Keywords: corrosion inhibition; surfactants; vegetable oils; fatty acids; adsorption; mild steel

Corrosion inhibition by surfactant molecules are related to the surfactant's ability to aggregate at interfaces and in solution. In this article, the adsorption and corrosion inhibition of series of commercial fatty acid surfactants synthesized based on vegetable oils (sunflower, cottonseed, corn and palm oil) onto mild steel is investigated at 50 ºC in CO_2-saturated brine. The inhibition efficiencies of the tested compounds showed good inhibition and protection of the carbon steel even at low concentrations. The corrosion inhibition tendency correlated to the chemical structure of the compounds.

Corresponding Authors
E-mail: Hany_shubra@yahoo.co.uk
[a] Mamedaliev Institute of Petrochemical Processes, National Academy of Sciences of Azerbaijan, AZ1025 Baku, Azerbaijan
[b] Faculty of Chemistry, Lomonosov Moscow State University, 119991, GSP-1, 1-3 Leninskiye Gory, Moscow, Russia
[c] Chemistry Department, Faculty of Science, Sohag University, 82524 Sohag, Egypt

Introduction

The study of CO_2 corrosion started a few decades ago and cannot be considered well resolved yet. Carbon steel is widely used as tubing or as pipeline in the oil and gas industry, and is usually eroded heavily, especially when the corrosion electrolyte contains CO_2.[1] In the oil extraction and processing industries, inhibitors have always been considered to be the first line of defense against corrosion. Most of the inhibitors currently used in producing wells are organic nitrogenous compounds. In that sense, use of surfactants as inhibitors is one of the best-known methods of corrosion protection.[2-4] Corrosion inhibition by surfactant molecules is related to the surfactant's ability to aggregate at interfaces and in solution.

In the present work, we have synthesized novel surfactants isolated from vegetable oils (sunflower (**A**), cottonseed (**B**), corn (**C**) and palm (**D**) oils) and studied their anti-corrosive properties in carbon dioxide environments at 50 °C. The surfactants were prepared in different compositions **(Scheme1)** based on vegetable oils and diethanolamine as in Ref.[5] The structures of synthesized surfactants were confirmed by physical-chemical spectroscopic methods.

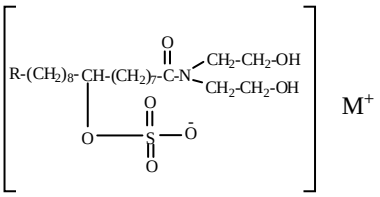

Scheme 1. Molecular structure of the synthesized anionic surfactants, where M=Na^+ (Inhibitor I), K^+ (Inhibitor II), NH_4^+ (Inhibitor III), -NH-CH_2CH_2OH (Inhibitor IV),-N-$(CH_2CH_2OH)_2$ (Inhibitor V).

Experiments

Linear polarization resistance corrosion rate (LPR) (bubble-test method) involves evaluating the corrosion of a given metal in simulated brine saturated with CO_2 at a temperature equivalent to that in the field. During the test, CO_2 gas is sparged continuously into the test solution. The rate of corrosion is determined instantaneously with the LPR technique, in which a small direct-current voltage is applied to a pair of identical electrodes and the resultant current is measured. A limitation of the bubble-test method is that it does not provide information on the effect of shear stress on the performance of a given corrosion inhibitor.

Results and Discussion

Figure 1 shows that, the change in corrosion rate (CR) with time for low carbon steel in 1%NaCl solution saturated with CO_2 containing different concentrations form inhibitor **I** at 50 °C synthesized based on all four oils. The inhibitor was added after 1 hour of exposure because at this time the corrosion potential got stable, allowing the measurement of the corrosion rate (CR) prior the injection of the inhibitor. The initial CR, without inhibitor, was measured to be between 3.45 and 5.03 mm/year. It can be observed from Figure **1** that the CR, in the absence of inhibitor, tends to increase with time. The increase in CR has been attributed to the galvanic effect between the ferrite phase and cementite (Fe_3C) which is a part of the original steel in the non-oxidized state and accumulates on the surface after the preferential dissolution of ferrite (α-Fe) into Fe^{2+} **[6].** Fe_3C is known to be less active than the ferrite phase. Therefore, there is a preferential dissolution of ferrite over cementite, working the former as the anode and latter as the cathode, favoring the hydrogen evolved reaction (HER) during the corrosion process.[6,7]

Corrosion parameters were calculated on the basis of LPR test. The inhibition efficiency (*IE*) and degree of surface coverage were calculated according to the following equations:[5]

$$IE,\% = 100\,\frac{CR_0 - CR_i}{CR_0} \quad (1)$$

$$\theta = 1 - \frac{CR_i}{CR_0} \quad (2)$$

where

θ = Surface coverage,

CR_o is the corrosion rate without inhibitor and

CR_i the corrosion rate when inhibitor is present.

It can be seen that the presence of inhibitors results a high decrease in the rate of corrosion. In the case of these surfactants, the corrosion rate decreases as the inhibitor concentration increases, getting maximum inhibition efficiency ranged between 91.9 and 99.90 % at 100 ppm after 20 hour of exposure.

The results showed that all synthesized inhibitors were good inhibitors and their inhibition efficiencies were significantly increased with increasing the concentration of surfactant. The increase of inhibitor efficiency with increasing the concentration can be interpreted on the basis the adsorption amount and the coverage of surfactants molecules, increases with increasing concentration. The inhibition efficiency of the investigated inhibitors which synthesized based on vegetable oils was increased in the following order (after 20 hours):

A_{II}> A_I> A_{III}> A_{IV} >A_V based on sunflower oil

B_{II}> B_I> B_V> B_{IV} >B_{III} based on cottonseed oil

C_{II}> C_{IV}> C_V> C_I >C_{III} based on corn oil

D_V> D_{IV}> D_{II}> D_{III} >D_I based on palm oil

There was an increase in the efficiency of corrosion inhibition with increasing concentration, Due to their containment of C=O, oxygen, nitrogen and sulfur groups these molecules contribute towards inhibition, and effectively protecting the surface. Adsorption of these surface active molecules forms thin inhibitor films on the metal surface which in order relatively isolate the metal surface from the corrosive environment causing much reduced corrosion rates. Inhibition efficiency of these films depends on various factors including but not limited to corrosivity of the environment, concentration of the active inhibitor molecules, any synergetic effects with other molecules present in the environment and/or flow/shear effects.

The surface coverage rates (θ) are found to depend on the concentrations of the inhibitors. The surface coverage rates are increased with the increase of the surfactant concentrations. This indicates that the inhibitory action of the investigated inhibitors against carbon steel corrosion can be attributed to the adsorption of these molecules on the metal surface, limits the dissolution of carbon steel, and the adsorption amounts of surfactants on carbon steel increase with concentrations in the corrosive solutions.

The results also showed that, the inhibition efficiencies in the case of surfactants obtained on the basis of palm oil are higher compared with those of inhibitors obtained on the basis of cottonseed, corn and sunflower oils at the same conditions. This behavior may be due to the difference in fatty acids compositions of oils. The fatty acid composition of oils from vegetable sources varies depending on plant origin and sort (Table **1**).[8]

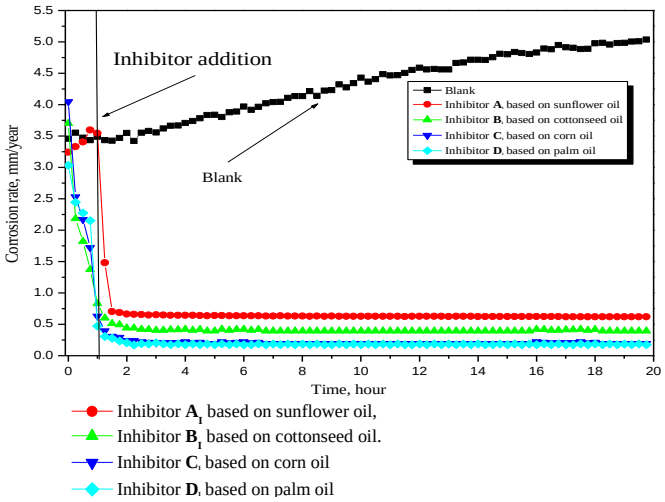

Figure 1. Variation of the corrosion rate with time for carbon steel in 1 % NaCl solution saturated with CO_2 containing different concentrations of inhibitor (I) at 50 °C.

In order to obtain the isotherm, the linear relation between θ values and C_{inh} must be found. Attempts were made to fit the θ values to various isotherms including Langmuir, Temkin, Frumkin and Flory–Huggins. By far the best fit is obtained with the Langmuir isotherm. This model has also been used for other inhibitor systems **[9, 10].** According to this isotherm, θ is related to C_{inh} by **[11]:**

$$\frac{C_{inh}}{\theta} = C_{inh} + \frac{1}{K_{ads}} \quad (3)$$

Where

K_{ads} is the equilibrium constant of the inhibitor adsorption process and

C_{inh} is the inhibitor concentration.

Plots of C_{inh}/θ versus C_{inh} yielded a straight line as shown in Fig. 2, which suggested that the adsorption of inhibitors on metal surface obeyed Langmuir adsorption isotherm model. This isotherm assumed that the adsorbed molecules occupied only one site and there was no interaction with other molecules adsorbed. The linear regression coefficients (R^2) and the slopes parameter variations were calculated. All correlation coefficient (R^2>0.9597) indicated that the inhibition of carbon steel by these inhibitors was attributed to the adsorption of surfactant molecule on the metal surface. However, the slopes of the C_{inh}/θ versus C_{inh} plots were close to 1 and showed a little deviation from unity which meant non-ideal simulating[12] and unexpected from Langmuir adsorption isotherm. They might be the results of the interactions between the adsorbed species on the metal surface.[13, 14].

Table 1. Fatty acid composition of the oils (percent by weight of total fatty acids).

Oil	Unsatd/ Satd. ratio	Saturated acids					Unsaturated acids		
		Capric C10:0	Lauric C12:0	Myristic C14:0	Palmitic C16:0	Stearic C18:0	Oleic C18:1	Linoleic C18:2	α-Linolenic C18:3
Sunflower(A)	7.3	-	-	-	7	5	19	68	1
Cottonseed (B)	2.8	-	-	1	22	3	19	54	1
Corn (C)	6.7	-	-	-	11	2	28	58	1
Palm (D)	1.0	-	-	1	45	4	40	10	-

The values of K obtained from the Langmuir adsorption isotherm are calculated, together with the values of the Gibbs free energy of adsorption (ΔG^0_{ads}) calculated from

$$K_{ads} = \frac{1}{55.5}\exp\left(-\frac{\Delta G^0_{ads}}{RT}\right) \quad (4)$$

where

R is the universal gas constant,

T the thermodynamic temperature and

the value of 55.5 is the concentration of water in the solution.

The high values of K_{ads} for the studied surfactants indicate stronger adsorption on the metal steel surface in CO_2-saturated brine. Large values of K_{ads} imply more efficient adsorption and hence better inhibition efficiency.[4] The large value of K_{ads} obtained for the studied surfactants agree with the high inhibition efficiency obtained.

The negative ΔG^0_{ads} values are consistent with the spontaneity of the adsorption process and the stability of the adsorbed layer on the carbon steel surface. Generally, values of ΔG^0_{ads} up to -20 kJ mol^{-1}, the types of adsorption was regarded as physisorption, the inhibition acted due to the electrostatic interactions between the charged molecules and the charged metal, while the values around -40 kJ mol^{-1}or smaller were associated with chemisorption as a result of sharing or transfer of electrons from organic molecules to the metal surface to form a coordinate type of bond (chemisorption).[15] The values of ΔG^0_{ads} in our measurements for all inhibitors synthesized based on all oils were found around -40 kJ mol^{-1}, thus the adsorption mechanism of the surfactants on carbon steel in 1% NaCl solution saturated with CO_2 was typical chemisorption.

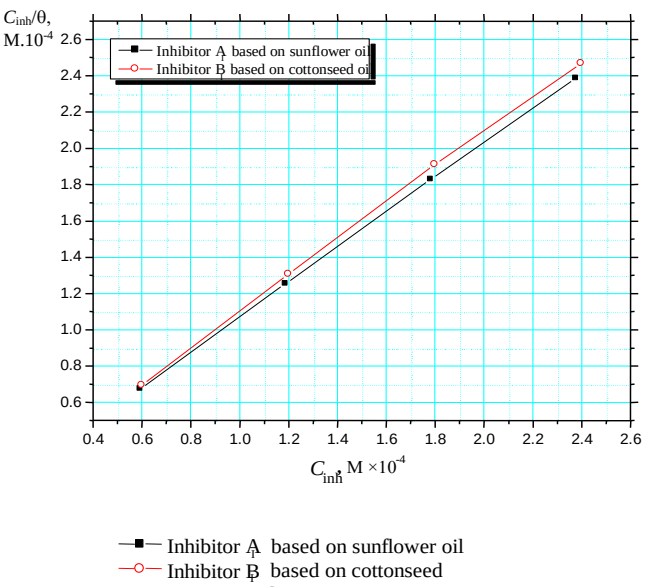

Figure 2. Langmuir adsorption isotherms for carbon steel in 1 % NaCl saturated wirh CO_2 in the presence of different inhibitors at 50 °C.

The corrosion process is inhibited by the adsorption of these surfactants on carbon steel surface. Inhibition efficiency increased with increase in concentration of the surfactants, getting maximum inhibition efficiency ranged between 91.9 and 99.90 % at 100 ppm after 20 hour of exposure.

The inhibition efficiencies in the case of inhibitors obtained based on sunflower oil are higher compared with those of inhibitors obtained based on sunflower, corn and palm oils at the same conditions. This behavior may be due to the difference in fatty acids compositions of two oils.

The adsorption of synthesized surfactants on carbon steel surface obeyed Langmuir adsorption isotherm. The high value of adsorption equilibrium constant and negative value of standard free energy of adsorption suggested that surfactants are strongly adsorbed on carbon steel surface, and are chemically adsorbed on the metal surface.

Conclusions

Linear polarization corrosion rate was employed to study the corrosion inhibition of carbon steel in CO_2-saturated solutions using some novel surfactants as corrosion inhibitors synthesized based on vegetable oils.

All inhibitors were found to be effective inhibitors for carbon steel corrosion in CO_2-saturated solutions.

References

[1]Abbasov, V. M., Abd El-Lateef, H. M., Aliyeva, L. I., Ismayilov, I. T., Qasimov, E. E., *J. Korean Chem. Soc*., **2013**, *57 (1)*, 25-34.

[2]Abbasov, V. M., Abd El-Lateef, H. M., Aliyeva, L. I., Ismayilov, I. T., *NACE Corrosion*, **2013,** Florida, USA, No.2129.

[3]Abd El-Lateef, H. M., Abbasov, V. M., Aliyeva, L. I., Qasimov, E. E., and Ismayilov, I. T., *J. Surf. Interfac. Mater.* **2012**, *1*, 1–11.

[4]Abd El-Lateef, H. M., Abbasov, V. M., Aliyeva, L. I., Ismayilov, T. I., Qasimov, E. E., Ahmadov, T. U., *Global J. Phys. Chem.*, **2012**, *3(14)*, 1-12.

[5]Ismayilov, I. T., Abd El-Lateef, H. M., Abbasov, V. M., Aliyeva, L. I., Efremenko, E. N., Qasimov, E. E., Mamedhanova, S. A., *Adv. Mater. Corros*., **2012**, *1*, 22-29.

[6]Crolet, J. Thevenot, N. Nesic, S., *Corrosion*, **1998**, *54*, 194-203.

[7]Videm, K. Kvarekvaal, J. Perez, T. Fitzsimons, G., *NACE Corrosion*, Houston, Texas, **1996**, Paper No. 1.

[8]Johansson, I., Svensson, M., *Current Opin. Coll. Interfac. Sci.*, **2001**, *6(2)*, 178-188.

[9]Kissi, M. Bouklah, M. Hammouti, B. Benkaddour, M., *Appl. Surf. Sci*., **2006**, *252*, 4190.

[10]Machnikova, E., Whitmire, K. H., Hackerman, N., *Electrochim. Acta*, **2008,** *53*, 6024–6032.

[11]Badawy, W. A. Ismail, K. M. Fathi, A. M., *Electrochim. Acta*, **2006,** *51*, 4182– 4189.

[12]Migahed, M. A., Monhamed, H. M., Al-Sabagh, A. M., *Mater. Chem. Phys.*, **2003**, *80*, 169.

[13]Azim, A., Shalaby, L. A., Abbas, H., *Corros. Sci.*, **1974**, *14*, 21–24.

[14]Szklarska-Smialowska, Z. Mankowski, J., *Corros. Sci.*, **1978,** *18*, 953.

[15]Yurt, A., Ulutas, S., Dal, H., *Appl. Surf. Sci.*, **2006**, *253*, 919.

Received: 14.03.2014.
Accepted: 06.04.2014.

ELECTRICAL CONDUCTIVITY OF SALICYLALDEHYDE THIOSEMICARBAZONE AND ITS Pd(II), Cu(II) AND Ru(III) COMPLEXES

Ramadan M. El-Bahnasawy,[a] Lobna M. Sharaf El-Deen,[b] Abdou S. El-Table,[a] Mohammed A. Wahba[c]*and Abd El-Monsef I Abd El-Mensef[a]

Keywords: use the Keywords style for the list of keywords, separating with a comma each items.

Salicylaldehyde thiosemicarbazone complexes of Pd(II), Cu(II) and Ru(III) have been characterized by elemental analyses, molar conductance, infrared, NMR, electronic spectra and thermal analyses. The data show the formation of two different types of complexes with 1:1 and 1:2 metal:ligand stoichiometries. The *dc* electrical conductivity of the ligand and the complexes was measured at varying temperatures. The results obtained were explained and discussed in terms of proposed semicondutive behaviour of the complexes and a probable occurrence of phase transition. The activation energies were calculated for the ligand and the complexes.

* Corresponding Authors
E-Mail: mohamedwahba12@gmail.com
[a] Chemistry Department, Faculty of Science, El-Menofya University, Egypt.
[b] Physics Department, Faculty of Science, El-Menofya University, Egypt.
[c] Inorganic Chemistry Department, National Research Center, Egypt.

Introduction

The synthesis of transition metal complexes with thiosemicarbazone ligands has been receiving considerable attention due to the potentially useful chemotherapeutic properties of both ligands and complexes as antimalarial, antitumor and antibacterial activities.[1-3] The chemistry of thiosemicarbazone has received considerable attention because of their variable bonding modes, promising biological implications, structural diversity, and ion–sensing ability.[4,5]

Thiosemicarbazones usually behave as chelating ligands against transition and non-transition metal ions binding through sulphur and nitrogen atoms, although in few cases they act as unidentate ligand with sulphur as the binding atom.[6] Platinum group metal complexes show a broad spectrum of pharmacological activity.[7] It was found that their dibasic tridentate thiosemicarbazones with ONS donor sites are of immense importance as they possess a wide spectrum of medicinal properties and can also give dimetallic or polymeric species with unusual structural and magnetic properties.[8]

In this paper, we report the synthesis and characterization of some salicylaldehyde thiosemicarbazone complexes of Pd, Cu and Ru. The d.c. electrical conductivity and thermal analyses have been correlated and their ΔE_g for conduction have been discussed.

Experimental

The ligand was prepared by mixing equimolecular amounts of thiosemicarbazide and salicylaldehyde in absolute methanol and refluxing on a water bath for two hours, the condensation products was filtered off, crystallized form methanol and dried under vacuum. The metal complexes were prepared by mixing 1:1 or 1:2 molar ratios of Cu(II), Pd(II) and Ru(III) salts and the ligand, respectively, in absolute methanol. The mixtures were refluxed on a water bath for a time depending on the nature of metal cation used. The formed complexes were filtered off, washed several times with pure dry methanol, and dried under vacuum. Elemental analyses (C, H, Cl) were performed at the micro-analytical unit of the University of Cairo. Pd and Cu were determined by established methods.[9] DTA. and TGA were carried out on a Shimadzu DT-30 and DT-50 thermal analyzers. Molar conductance was measured in DMF (DMSO for Pd complexes) using a Bibby conductometer type MC-1. The electronic and IR spectra were recorded on Perkin Elmer Lambda 4B UV-VIS. and infrared spectrophotometers, respectively. Magnetic susceptibilities were measured by the modified Gouy method using $Hg[Co(CNS)_4]$ as a calibrating agent and a Johnson Mathey magnetic susceptibility balance. Diamagnetic corrections were made using Pascal's constants.[10] The magnetic moments were calculated from the equation: $\mu_{eff}=2.84(\chi_m^{corr}T)^{1/2}$ the electrical conductivity was measured as given earlier using Keithly 616 electrometer.

Biological activity. The preliminary screening test was performed by the disk diffusion methods.[11,12] Whatmann No.1 filter paper discs (6 mm diameter) were sterilized by autoclaving for one hour at 120 ˚C. The sterile discs were placed on the surface of the cold solid medium in Petri-dishes inoculated with the microorganism and then incubated at 28 ºC. The inhibition of the microbial growth was evaluated after 24 hours.

Results and discussion

The elemental analyses, physical and analytical data of the investigated complexes were summarized in Table 1. All the complexes are quite stable at room temperature and non-hygroscopic in nature. The complexes are freely soluble in DMF, DMSO, and pyridine. The values indicates that the molar conductance complexes I and IV are non-electrolytes, whereas complexes II and III are univalent electrolytes. The insolubility of the complexes in common organic solvents and non-melting nature indicate that they are polymeric or ionic.[13]

Electronic spectra and magnetic moment

Pd(II) complexes are diamagnetic suggesting square planar geometry for these complexes. Electronic spectral data and assignment (Table 1) are also indicative of square planar geometry. Also, Ru(III) complex magnetic moment is 0.96 B.M. Which is less than the low spin d^5 configuration indicating magnetic exchange interaction between Ru(III) ions, this could be explained by a dimer formation through chloride bridges.[14]

The ligand exhibits a solid state electronic spectral band at 389 nm which is assigned to n-π* transition associated with the thiosemicarbazone moiety $C=N^1$. This band is blue shifted to ca. 323 nm and 370 nm in palladium complexes respectively.[15] Also, the complexes show a non ligand band at ca. 411 nm due to charge transfer.[15]

In the UV-VIS spectrum of the ligand solution, the absence of π-π* of C=S group at 238 nm[16] indicates the thiol form[17] and the presence of two bands at 343 and 332 nm assigned to n-π* transition of azomethine chromophore confirming that the ligand contains the azine group and the ligand in the solution is present in its thiol form (Figure 1).

In the complexes (I and III), the band assigned to the n-π* at 345 nm greatly decreases in the intensity indicating that $C=N^1$ group is coordinated to the metal ion. The absence of the band corresponding to the $C=N^2$ group is a good evidence that the ligand in these complexes is present in the thione form, this is supported by the appearance of C=S band at 224 nm. The intraligand bands for complexes II and IV are present at ca. 343 and 333 nm corresponding to n-π* transition of $C=N^2$ and $C=N^1$ groups with large molar absorptiveness due to the increased conjugation of the ligand and the absence of π-π* of C=S indicates that complex II contains the ligand in the thiol form. The complexes show also non-ligand bands due to charge transfer at 370-407 nm.[18] The spectrum of the copper(II) complex displays the d-d transition band at 622 nm, suggesting square planar geometry.[19] This also supported by the lower value of the effective magnetic moment (μ=1.13 B.M) due to metal-metal interaction[20] in the dimeric structure.

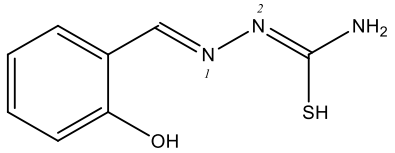

Figure 1. Structure of the ligand

1H NMR spectra

The ^{1}H NMR spectrum of the ligand in DMSO shows the phenolic OH proton at 11.4 ppm and the NH proton at 9.9 ppm, these two peaks disappeared in the presence of D_2O. The spectra of complexes I and II in DMSO are similar to that of the ligand except that in the spectrum of complex I the signal due to OH proton disappeared while that of the NH proton appeared. This indicates that the palladium is bonded to the phenolic OH and azomethine nitrogen; on the other hand the spectrum of complex II shows the presence of the phenolic OH at the same position while the NH protons disappeared.

Table 1. Analytical and electronic spectral data of salicylaldehyde thiosemicarbazone and its Cu, Pd, and Ru complexes

Compound	Colour	MP or (d.p.) ºC	Λ_m	Elect-rolyte nature	Found (calcd.) %[b]				Intraligand and Charge Transfer (molar absorptivities*10^{-4})				μ_{eff} B.M.
					C	H	M	Cl	C.T.	n→π* $C=N^1$	π→π* $C=N^2$	n→π* C=S	
Ligand [H_2L]	Bright yellow	219-221	3	[a]	49.3 (49.5)	4.9 (4.8)	- -	- -		343 (3.00)	332 (2.8)		-
Complex I [Pd(HL)Cl]	Brown	>300	60	[a]	28.7 (28.6)	2.7 (2.4)	32.6 (31.7)		387 (062)	345 (0.56)		223	Dia
Complex II [Pd(H_2L_2)Cl_2]	Orange	275	151	1:1	33.3 (33.2)	3.2 (3.2)	18.3 (18.8)	13.4 (12.5)	383 (1.2)	344 (2.6)	333 (2.2)	-	Dia
Complex III [Cu(HL)Cl]	Dirty green	280	121	1:1	32.4 (32.8)	3.5 (2.7)	20.9 (21.7)	12.8 (12.1)	622 (0.07) 407 (0.26) 371 (0.4)	346 (0.32)		225	1.13
Complex IV [RuLCl·H_2O]	Black	>300	41	[a]	27.6 (27.6)	3.2 (2.6)	29.5 (29.1)	9.8 (10.2)	407 (0.33) 370 (0.28)	347 (0.37)	338 (0.41)	-	0.96

[a] Non-conducting solution, [b] % H_2O 5.7 (5.2).

 DOI: 10.17628/ecb.2014.3.441-446

IR spectra

The ligand

The IR spectrum of the ligand (Table 2) exhibits phenolic group frequencies ν(OH), oop(OH) and ν(C-O) at 3440, 950 and 1273 cm^{-1} respectively and exhibits also a strong band at 1612 cm^{-1} assigned to (C=N).[21] The appearance of a band at 1056 cm^{-1} is assigned to (C=S)[22] which is a good evidence that, in the solid state the ligand is a mixture of free syn and hydrogen bonded anti forms (Figure 2).

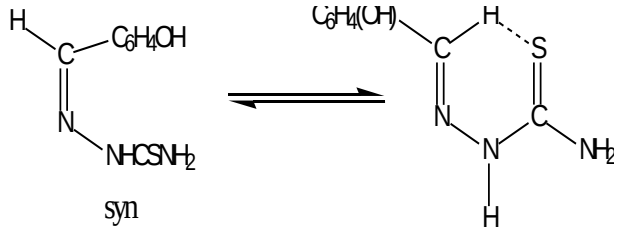

Figure 2. Ligand structure in the solid state

The complexes

Comparison of the IR spectra of I and III complexes with that of the free ligand reveals the absence of bands corresponding to phenolic (OH) and (C=N) groups. The band assigned to (C=S) is shifted to lower frequencies compared to that of the ligand; while the (C-O) band is shifted to higher frequency indicating that the phenolic OH is deprotonated and that Pd and Cu are bonded through the azomethine nitrogen,[17,20] C=S[22] and phenolic oxygen.[23]

In the spectrum of complex II, bands corresponding to free phenolic OH, which is proved by the violet color appearing during the addition of aqueous $FeCl_3$ solution to its alcoholic solution. On the other hand, the disappearance of ν(C=S) and δ(N-H) and appearing of three news bands at 2587, 601 and 1595 cm^{-1} assigned to V(S-H),[24] ν(C-S)[25,26] and ν(C=N-N=C)[27], respectively, indicating that palladium is coordinated through the azomethine nitrogen and thiol sulphur whereas the phenolic OH is still free. In the Ru complex the disappearance of ν(OH), ν(NH), (C=S) accompanied by the appearance of bands at 1595, 619 cm^{-1} due to ν(C=N-N=C)[27] and ν(C-S)[25,26] indicates that Ru is bonded through O, N and S atoms. The presence of water in Ru complex is indicated by the presence of a broad band around 3400 cm^{-1} which could be assigned to δ(OH) stretching.[28] The presence of non-ligand bands at ca (503-510) (522-543), (414-430) cm^{-1} proves coordination through O,[23] N,[21] S.[25,26]

Based on the previously discussed elemental analyses, conductance, magnetic moment, electronic and IR spectra, the structure of the investigated complexes can be represented as in Figure 3.

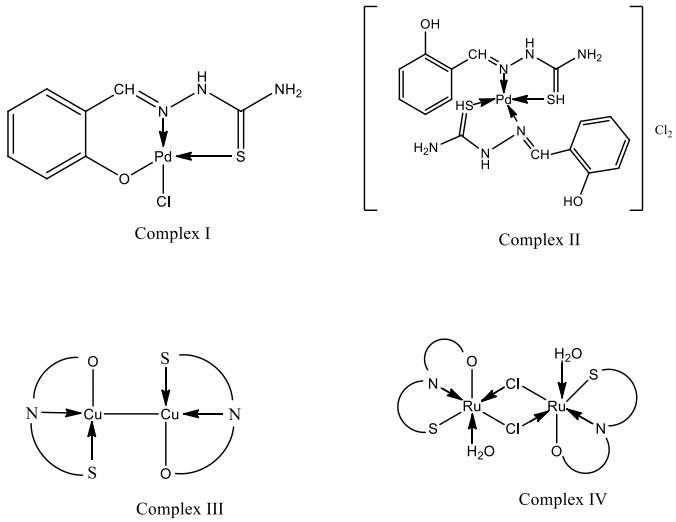

Figure 3. Proposed structure for the investigated complexes

Thermal analyses

Salicylaldehyde thiosemicarbazone is thermally stable up to 225˚C. The medium endothermic peak at 220 ºC (without weight loss) is due to its melting. The exothermic peak at 237 ºC with 25.5% weight loss may be due to the loss of one molecule of thiosemicarbazide from two molecules of the ligand according to scheme 1.

Table 2. IR spectral data of salicyaldehyde thiosemicarbazone and its Cu, Pd and Ru complexes

Compound	ν(OH) δ(OH)	ν (NH)	ν (S-H) ν (C-S)	ν (C=N)	ν (C=S)	ν (M-O)	ν (M-N)	ν (M-S)
Ligand [H_2L]	3340(S) (950)m	3317(s) 3170(d)	- -	1612	1056(m)	-	-	-
Complex I [Pd(HL)Cl]	- -	3302(w) 3133(w)	- -	1599(m)	1036(m)	503(m)	522(w)	414(m)
Complex II [$Pd(H_2L_2)Cl_2$]	3415(s) (946) (m)	3327 3255	2587 (601)	1595(m)	-	-	543	423
Complex III [Cu(HL)]Cl	- -	3378 3178	- -	1604	1028	517	532	433
Complex IV [$RuLCl{\cdot}H_2O$]	broad	3262 3139	- (619)	1604	-	510	530	440

 DOI: 10.17628/ecb.2014.3.441-446

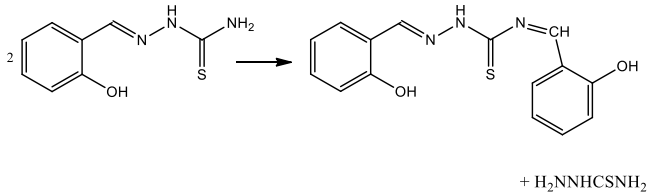

Scheme 1. Thermal decomposition of the Ligand

Complex I decomposes at 370-390 ºC after rearrangement at 300 ºC and before its melting at 320 ºC (Table 3). The decomposition is similar to that of the ligand that occurs by losing one thiosemicarbazide molecules from two molecule of complex according to Scheme 2.

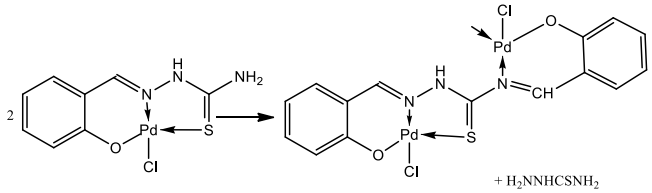

Scheme 2. Thermal decomposition of complex I.

Complex II: after rearrangement at 200 ºC, it melts at 260-285 ºC losing two molecules of HCl resulting in the formation of the 1:2 inert complexes according to Scheme 3.

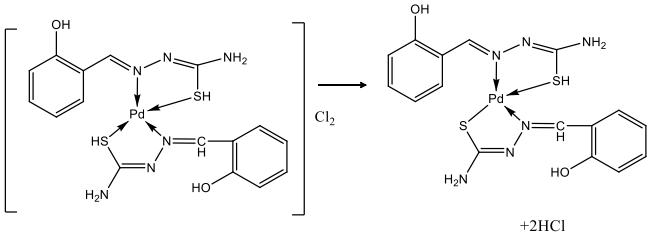

Scheme 3. Thermal decomposition of complex II.

D.C. electrical conductivity

The I-V (current intensity-voltage) characteristic curves of the ligand (Figure 4) and its complexes were measured in the temperature range of 20-180 ºC and the voltage range of 0-400 volts. From this Figure, it is clear that, the I-V curves obey the well known Ohm's law in certain temperature and voltage ranges. The amount of respond current, which reflects the sample conductivity, was found to vary from a sample to another, and the current-voltage dependence seems to be approximately linear in certain ranges. In ranges, which almost follow the linear I-V range, we found that by increasing the applied voltage by very small amount, the current is sharply increased causing the so called switching voltage and it was a function of temperature. To elucidate this observation we built new sample holder with pin electrode to measure accurately the I-V curves in the switching range.

Figure 5 shows the temperature dependence of the d.c. electrical conductivity of the ligand and complexes. From this figure, it is clear that, the samples exhibit a semiconducting behaviour in a certain temperature range from which the activation energies ΔE were calculated using the well known Arrhenius equation.

From these measurements: we observe that the conduction mechanism of the ligand and complex I is electronic where the conductivities at 110 ºC is of the order of -10.1 and -10.6 Ω^{-1} cm^{-1} respectively and the activation energies are about 0.55 and 0.53 eV, respectively. For complexes II, III and IV, where the conductivities were very high, the activation energies for conduction were very low. In these complexes values of log σ at t = 110 ºC are -7.8, -2.27, and -1.35 Ω^{-1} cm^{-1}, respectively and the activation energies are 0.29, 0.12, and 0.43 eV, respectively. These complexes have two halogens in their structures which enhance the conductivity and may act as an agent charge carrier transport.

Table 3. Thermal analyses data of the ligand and its Pd complexes

Formula	M. wt	Temp. ºC	%wt. loss Calc. (Found)	DTA peaks	Temp. ºC	Assignment
Ligand [H_2L]	195	220	-	endo(m)	220	Due to melting
$C_8H_9N_3O_5$		220-256	23.3 (25.5)	exo (m)	237	Loss of thisemicarbazide according to scheme 1
		270-500	-	-	-	Stable
[Pd(HL)Cl]	336	80	- (-)	-	80	Due to rearrangement
		320	13.5 (16.0)	endo	320	Due to melting
		370-390		exo(br)	390	Loss of thiosemicarbazide according to scheme 2
		390-500		-	-	Stable
[Pd(H_2L_2)Cl_2]	567.5	100	-	endo	100	Due to rearrangement
		260	-	endo	260	Due to rearrangement
		260-285	12.9 (13.0)	exo	270	Loss of 2HCl molecules according to Scheme 3
		285-395	-	-	-	Stable
		395-500	-	-	-	Further decomposition

 DOI: 10.17628/ecb.2014.3.441-446

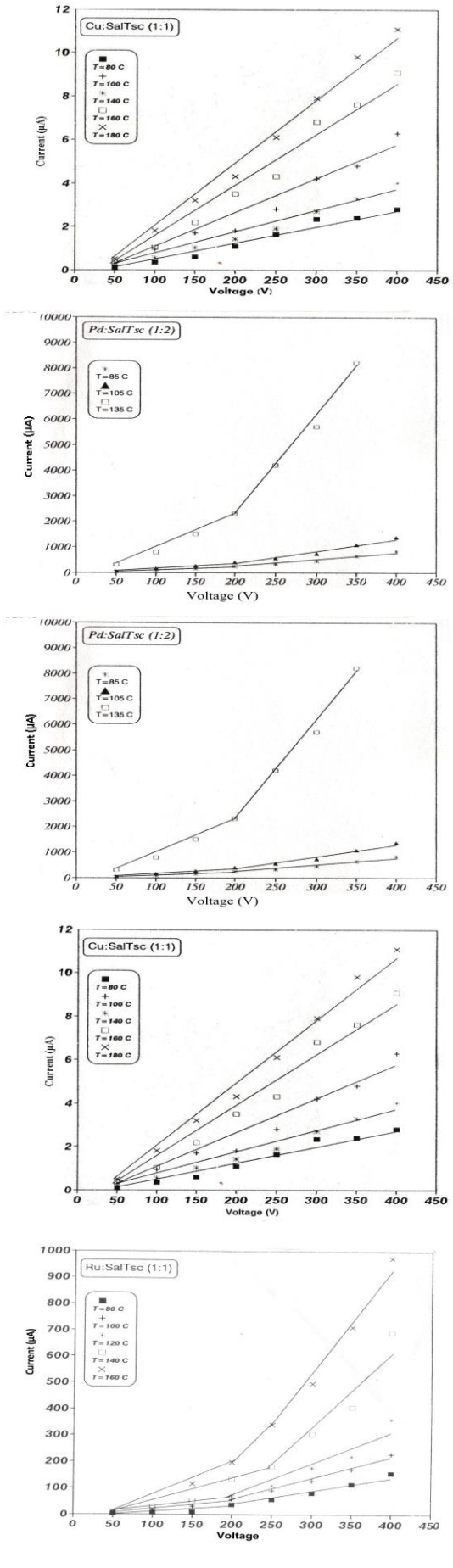

Figure 4. *I-V* characteristic lines of salicylaldehyde thiosemicarbazone (SalTSC) and its complexes

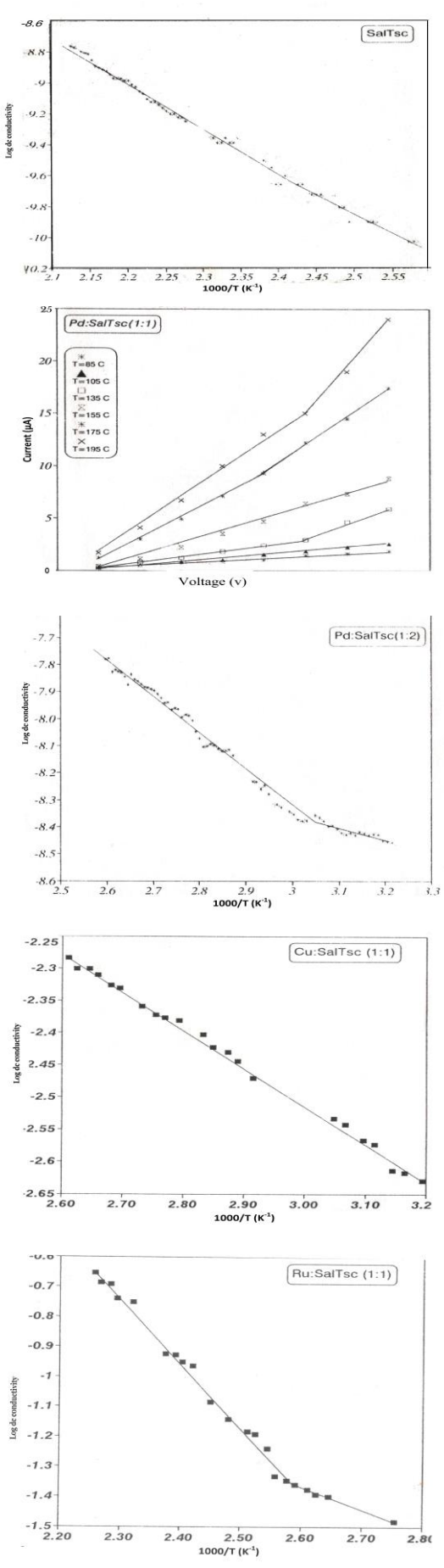

Figure 5. log *dc* conductivity vs. 1000/*T* of salicylaldehyde thiosemicarbazone (SalTSC) and its complexes

 DOI: 10.17628/ecb.2014.3.441-446

Biological activity

The biological activity of the ligand and its complexes are summarized in Table 4. From this table, it is clear that the ligand has antimicrobial activity nearly as the control (DMSO), which means that it has activity neither to gram positive nor negative bacteria. Also, the Ru complex is inactive against both of them. On the other hand the copper complex has a very high antimicrobial against gram-positive and gram-negative bacteria, whereas, the palladium complex shows less activity than the copper complex against both. This is agreeing with what reported by Scovill et al.[29] that complexed thiosemicarbazone, especially copper(II) and iron(III) are more active than uncomplexed ones. Also, it is clear from Table 4 that neither the ligand nor its complexes have activity against fungi.

Table 4. The preliminary screening of antimicrobial activity of salicylaldehyde thiosemicarbazone and its complexes

Compound	Gram +ve	Gram -ve	Fungi
	Bacillus subtillus	Escherichia Coli	Candida Libolica
Ligand	6.0	7.0	6.0
Complex I	9.3	8.1	6.0
Complex II	11.1	9.0	6.0
Complex III	16.0	16.0	6.0
Complex IV	6.0	6.0	6.0
Complex V	6.0	6.0	6.0
DMSO	6.0	6.0	6.0

References

[1]Khanye, S. D., Baojie Wan Scott, G. Franzblau, Gut, J., Rosenthal, P. J., Smith, G. S., Chibale, K., *J. Organomet. Chem.*, **2011**, *696*, 3392.

[2]Kovala-Demertzi, D., A, B., MA, D., M., C. *Chemotherapy*, **2007**, *53*, 148.

[3]Khandani, M., Sedaghat, T., Erfani, N., Haghshenas, M. R., Khavasi, H. R., *J. Mol. Struct.*, **2013**, *1037*, 136.

[4]Mishra, D., Naskar, S., Michael, G., Chattopadhyay, S. K. *Inorg. Chim. Acta*, **2006**, *359*, 585.

[5]Casas, J. S., Garcia-Tasende, M. S., Sordo, J., *Coord. Chem. Rev. 2*, **2000**, *209*, 197.

[6]Singh, K., and Tandon, J., *Monatsh. Chem.*, **1992**, *123*, 315.

[7]Cutillas, N., Yellol, G. S., Haro, C. D., Vicente, C., Rodríguez, V., Ruiz, J., *Coord. Chem. Rev. 2*, **2013**, *257*, 2784.

[8]Syamal, A., Ahmad, S., Bariniazi, M. A., *J. Indian Chem. Soc.*, **1983**, *60*, 493.

[9]A. I. Vogel, (Ed.) *Vogel's textbook of quantitative inorganic analysis. 4th ed.* 1986.

[10]Wilkins, J. L. a. R. G., Interscience, New York, 1960.

[11]West, D. X., Huffman, D. L., Saleda, J. S., Liberta, A. E., *Transition Met. Chem.*, **1992**, *17*, 568.

[12]Gould, J. C., Bowie, J. K., *Edinb. Med. J.*, **1952**, *159*, 178.

[13]Geary, W. J., *Coord. Chem. Rev.*, **1971**, *7*, 81.

[14]El-Saied, F. A., El-Bahnasawy, R. M., Azzem, M. A., El-Sawaf, A. K., *Polyhedron*, **1994**, *13*, 1781.

[15]West, D. X., Liberta, A. E., Saleda, J. S., *Trans. Met. Chem.*, **1992**, *17*, 568.

[16]Balakrishnan, K., Aravindakshan, K. K., *J. Indian Chem. Soc.*, **1991**, *68*, 187.

[17]Chandra, S., Singh, R., *Synth. React. Inorg, Met-Org. Chem.*, **1987**, *17*, 869.

[18]West, D. X., Romack, T. J., Liberta, A. E., *Transition Met. Chem.*, **1992**, *17*, 256.

[19]Mesubi, M. A., *J. Coord.*, **1984**,*13*, 179.

[20]Biradar, N. S., Havinale, B. R., Inorg. Chim. Acta, **1976**, 17, 157.

[21]Singh, K., Singh, R. V., Tandon, J. P., *Polyhedron*, **1988**, *7*, 151.

[22]Singh, V. P., Singh, R. V., Tandon, J. P., *J. Prakt. Chem.*, **1989**, *4*, 690.

[23]Mahapatra, B. B., Pujari, S. K., *Ind. J. Chem.*, **1983**, *22A*, 525.

[24]Ali, M. A., Bose, R., *J. Inorg. Nucl. Chem.*, **1977**, *39* 265.

[25]Khan, B. T., Zakeeruddin, S. M., *Transition Metal Chemistry*, **1991**, *16*, 119.

[26]Thakur, Y., Narinjha, B., *J. Inorg. Nucl. Chem*, **1980**, *42* 449.

[27]Patil, M. S., Shah, J. R., *J. Indian Chem. Soc.*, **1981**, *58*, 944.

[28]Shukla, P. R., K, S. V., Jaiswal, A. M., and Narain, J. J., *Ind Chem Soc.*, **1983**, *60*, 321.

[29]Scovill, D. L. K., Franchino, C.F., *J. Med. Chem.*, **1982**, *22*, 1261.

Received: 12.03.2014.
Accepted: 06.04.2014.

SYNTHESIS AND CHARACTERIZATION OF TRANSITION METAL COMPLEXES WITH AZO LIGAND DERIVED FROM 4-HYDROXY-6-METHYL-2-PYRANONE

Mahmoud Najim Al-Jibouri[a]

Keywords: Azo dyes derived from 4-hydroxy-6-methyl-2-pyranone; transition metal complexes; synthesis.

A series of metal (Cr(III), Fe(III), Mn(II), Co(II), Ni(II), Cu(II) and Zn(II)) complexes with 4-[(Z-(4-hydroxy-6-methyl-2-oxo-2H-pyran-3-yl]-1-methyl-2-phenyl-1,2-dihydro-3H-pyrazol-3-one were prepared by azo coupling of diazotised 4-aminoantipyrine with 4-hydroxy-6-methyl-2-pyranone. The free ligand and its metal complexes were fully characterized on the basis of elemental analyses and ^{1}H NMR, FTIR and UV-Visible spectroscopy. The keto-enol tautomer azo ligand [HL] was a mixture of E and Z isomers as suggested by ^{1}H NMR and FT-IR spectroscopy. The chelating properties of the new azo ligand were studied towards Cr(III), Fe(III), Co(II), Ni(II), Cu(II) and Zn(II) ions, and the spectral data revealed that the nitrogen and oxygen atoms of –N=N-, C=O and –OH groups participated in bonding with the metal ions. The study of NMR, IR and electronic spectra indicated an octahedral structure for all metal complexes except zinc(II) complex, which has the tetrahedral structure.

Corresponding Authors
E-Mail: mahmoudnajim71@yahoo.com
[a] Chemistry department, College of Science-Al-Mustansiriya University

Introduction

The study of azo dyes of pyrazoline-2-one and pyran-2-one derivatives has been of much interest in recent years due to their antibacterial, antiviral, anticancer, antifungal, antihelminthes and insecticidal activities.[1] In particular, the tautomerism of pyran-2-one ligands show a dramatic increase in the diversity of biological properties.[2-4] For example, some of these organic derivatives have shown hypoxia-selective cytotoxicity and they could be potentially useful for the treatment of solid tumours. Besides, some derivatives have presented excellent *M. tuberculosis* growth inhibition values, leading generally the lack of the two –N=N- and –C=O groups to the loss of the *antimycobacterial* activity.[5-6]

In an effort to improve bioavailability and pharmacological and toxicological properties of azo dye of 4-aminoantipyrine, many authors focused their research on the synthesis, characterization and biological evaluation of metal complexes of this family of organic compounds.[7-9] The spectral and magnetic studies of iron(III) complexes of hydroxyaryl azodyes, derived from antipyrine, prompted Rawther and Nair[10] to suggest from the IR data that the OH groups take part in co-ordination together with –N=N– nitrogen and C=O of pyrazolone ring.[10]

Antipyrine Schiff base derivatives can serve as antiparasitic agents and their complexes with platinum(II) and cobalt(II) ions have been shown to act as antitumor substance[11].This prompted us to synthesize the Schiff base ligand, Fig. 1, containing the antipyrinyl moiety as well as the delocalized conjugated system followed by its reaction alone or mixed with 2-aminopyridine (2-ampy), 8-hydroxyquinoline (8-HOqu) or oxalic acid (Ox) with some di- and trivalent transition metal halides to gain insight into the mode of coordination and geometry of the obtained complexes. These studies lead to several complexes with higher pharmacological activity than the free ligands, especially iron complexes bearing anti-*Mycobacterium tuberculosis* activity.

Metal complexes of azo compounds could be divided into two categories, namely the ones in which the azo group is involved in bonding and the others in which it is not. The former are derived from azo compounds containing donor functions such as OH, NH_2, COOH, SH, etc., in a congenial position so as to form six or five membered chelates.[12] In view of the importance of such azo dye bearing NO donor atoms of pyran-2-one and pyrazoline moieties, we describe here the coordination behaviour of organic ligand derived from azo ligand of 4-hydroxy-6-methyl-pyran-2-one (HL) towards some transition elements (Mn(II), Cr(III), Fe(III), Co(II), Ni(II), Cu(II) (Scheme 1) and Zn(II).

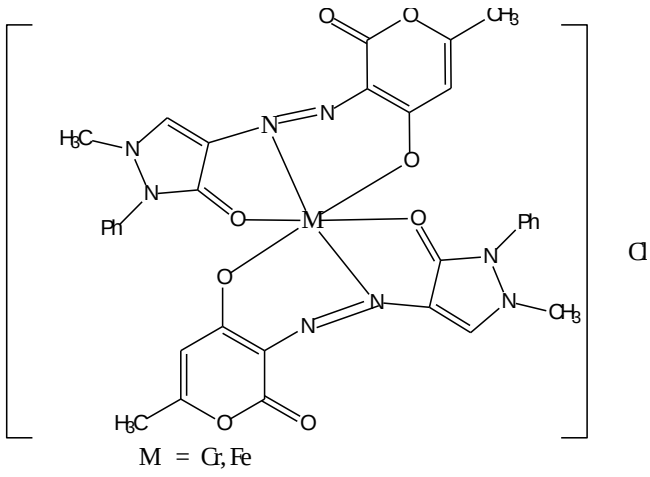

Figure 1. Proposed octahedral structure of Cr(III) and Fe(III) complexes of 4-[(Z-(4-hydroxy-6-methyl-2-oxo-2H-pyran-3-yl]-1-methyl-2-phenyl-1,2-dihydro-3H-pyrazol-3-one (HL) ligand, (if M=Mn, Co, Ni, or Cu(II), there is no Cl in the outer sphere..

Experimentals

UV-visible spectra were recorded on a Shimadzu UV-Vis spectrophotometer over 200-800 nm using 10^{-3} M solutions of ligands and complexes in methanol, which was used as reference.

IR spectra were recorded on a JASCO FTIR spectrophotometer 4100 in the range 400-4000cm^{-1}. Elemental analysis was carried out with a CHN Carlo-Erba 1106 elemental analyzer. The %Cl contents were measured via conductometric titrations against standard solution of silver nitrate after dissolving the Zn(II) and Cd(II) complexes in concentrated nitric acid then dilution with 5%v/v methanol.

Magnetic susceptibility values were determined at room temperature on a Merck type instrument which was calibrated using Hg[Co(NCS)4] with Magnet Bruker magnetic susceptibility balance via Faradays method to deduce the magnetic moments of the solid metal complexes. The NMR spectra of free ligand was recorded in DMSO-d_6 solvent on Bruker 300MHz spectrometer.

Synthesis of diazonium salt of antipyrine

The reagents and solvents were of analytical grade and used without further purification. 4-Aminoantipyrine (0.01 mole) was diazotised by dissolving it in 1:1 HCl and adding $NaNO_2$ (0.01 mol) solution keeping the temperature at 0-5 °C. This product was dried over anhydrous $MgSO_4$ and verified for purity (TLC).

Synthesis of HL ligand

4-Aminoantipyrine (1.32 g, 0.01 mole) was diazotised and its diazonium salt was spontaneously added slowly dropwise to a well cooled alkaline solution (pH=8.5) of 4-hydroxy-6-methyl-2-pyranone (1.26 g, 0.01 mole). The mixture was allowed to stand for 1 h. The pale brown product of HL ligand formed was filtered, washed successively with very dilute HCl and water, then recrystallised from boiling ethanol and stored over anhydrous $CaCl_2$ in a desiccator (yield 80 %, m.p. 120-122 °C) (Scheme 1).

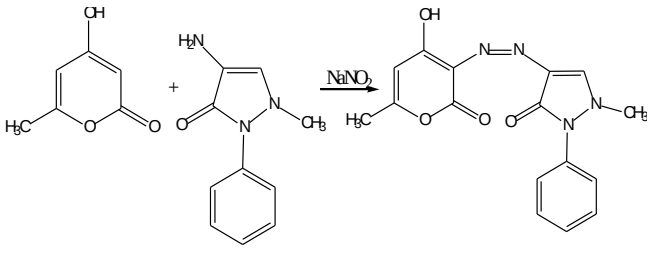

Scheme 1. Synthesis of HL ligand.

Synthesis of metal complexes

To a methanolic solution (10 ml) of HL (1 mmole, 0.345g) a metal salt solution (1 mmole, $CrCl_3.6H_2O$, $FeCl_3.6H_2O$, $MnCl_2.4H_2O$, $MCl_2.6H_2O$ (M=Co, Ni), $CuCl_2.2H_2O$ and $ZnCl_2$) in methanol was added dropwise under stirring.

The mixture was refluxed on a steam bath for about 2-3 hours. The metal to ligand ratio was kept at 1:2 for all metal ions except for zinc(II) where it was kept at 1:1. The deep colour complexes were filtered, washed with water, methanol and finally dried in an oven. The complexes were recrystallised from CH_3CN–EtOH (1:3) mixture and stored over anhydrous $CaCl_2$ in a desiccators. ^{1}H NMR (300 MHz, DMSO-d_6, δ, ppm): 2.4 (S, *J*=8 Hz, 3H, -CH_3-antipyrine), 3.4(s, 3H, CH3-pyranone), 4.5-4.76 (S, 1H, CH=C-antipyrine,), 6.9-7.2 (m, *J*=12Hz, 5H, Ar-*H*), 8.4 (d, *J*=6 Hz, 1H, OH), 8.9 (s, H, H-C=C-pyranone).

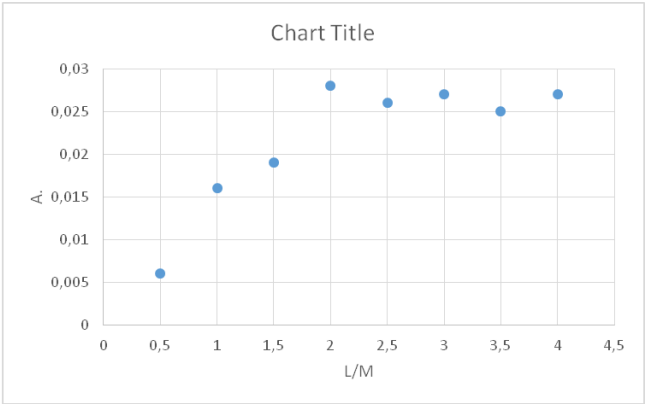

Figure 2. The absorbance-molar ratio relationship in the case of Cu(II)-L^{1-} system (λ=560 nm)

Results and discussion

The following representative equations illustrate the formation of some of the complexes obtained

$$2HL+MCl_3.6H_2O \longrightarrow [ML_2]Cl,\ M(III)=Cr \text{ and } Fe$$

$$2HL+MCl_2.nH_2O \longrightarrow [ML_2],\ M(II)=Mn, Co, Cu \text{ and } Ni$$

The synthesis route for the metal complexes is shown in Scheme 1. The complexes are stable solids in air, with varying shades of colouration and their structures were established from their elemental analyses, infrared and electronic and NMR spectra and magnetic moment values.

The results of the elemental analysis are in good agreement with the calculated values of 1:2 metal to ligand except for zinc(II) complexes in which 1:1 ratio was established. The complexes are completely soluble in DMF and DMSO, partially soluble in other polar solvents such as acetonitrile and methanol but are completely insoluble in non polar organic solvents. Low molar conductance values between 27.2 and 38.3 Ω^{-1} cm^2 mol^{-1} obtained for the complexes in DMF indicated that they are non-electrolytes and the nature of chlorine to metal bonds can be described as coordinative.[13]

However, the chromium and iron(III) complexes show molar conductance values in the range 75-85 Ω^{-1} cm^2 mol^{-1} confirming the electrolytic behavior in 1:1 ratio and support the presence of chloride ions in the outer sphere of the Cr(III) and Fe(III) complexes.[14] The analytical data and other physical properties of the complexes are recorded in Table 1.

 DOI: 10.17628/ecb.2014.3.447-451

Table 1. Physical properties and elemental analysis of the prepared ligand HL and its metal complexes.

Compound	M.W. g mol^{-1}	Colour	M.P. °C	C% Calc. (found)	H% Calc. (found)	N% Calc. (found)	M% Calc. (found)	Cl% Calc.(found)
HL	358	Pale brown	120-122	53.63(52.67)	3.92(3.21)	15.64(15.11)		-
[CrL_2]Cl	798	Dark green	250-252	53.045(52.17)	3.45(3.00)	15.08(15.71)	6.54(6.14)	4.44(4.33)
[FeL_2]Cl	803.5	Brown	290d	47.22(46.99)	3.30(2.72)	13.94(13.90)	6.98(5.82)	4.42(4.78)
[MnL_2]	766	Dark red	296d	50.40(49.62)	3.40(3.66)	14.66(14.77)	7.08(6.63)	-
[CoL_2]	768	Dark pink	306d	50.05(49.44)	3.91(3.44)	14.60(14.72)	7.29(6.94)	-
[NiL_2]	770	Orange	307d	49.37(49.00)	3.83(3.11)	14.40(15.11)	7.96(8.87)	-
[CuL_2]	777.6	Dark brown	290d	49.38(45.66)	3.50(2.65)	14.41(14.88)	8.20(8.09)	-
[ZnLCl]	452.5	Red	311d	24.69 (24.00)	2.80(2.13)	12.31(12.55)	13.26 (12.6)	7.84(8.33)

d=decomposition

^{1}H NMR spectra of the free azo ligand

The ^{1}H NMR absorptions of the ligand in DMSO-d_6 is shown in Figure 3. The proton NMR spectrum of the ligand can be classified into three distinct classes, the methyl (N-CH_3), (C=C-H) and hydroxyl (-OH) protons appear as singlet peaks and in the ranges 1.97-2.02, 8.9 ppm and 8.4 ppm respectively. [15-18] The broad singlet peaks found between 3.6-4.56 ppm are due to protons of –CH3 related to pyran and N-CH_3 moiety respectively.However the multiple peak in the region 6.9-7.22 ppm could be attributed to resonance of aromatic and pyrazoline protons. More ever, the Figure 4 shows the ^{13}C resonance of HL ligand, that records the absorptions at 155, 131, 121 to 25 ppm that are corresponded to C=O, C=N, C-N-C=C- and CH_3 groups respectively. The data obtained from ^{13}C NMR (Figure 4) with results of ^{1}H NMR together supports the the expected structure of azo ligand.

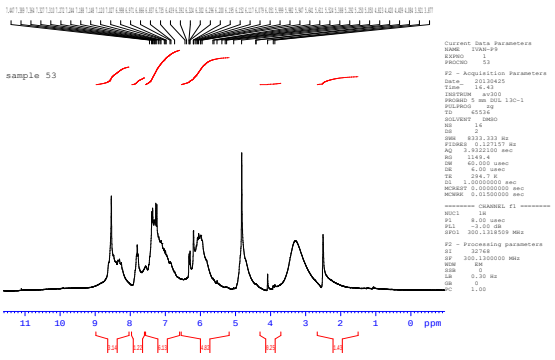

Figure 3. ^{1}H NMR spectrum of HL ligand in DMSO-d_6

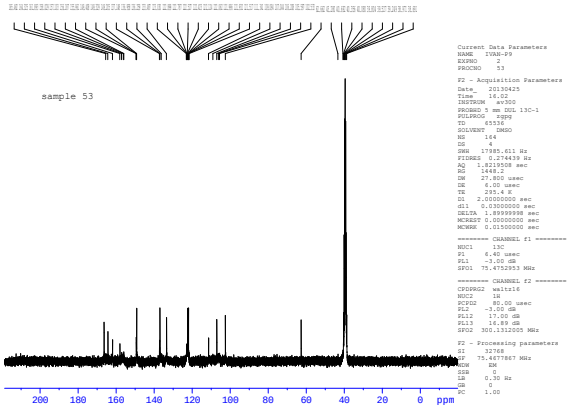

Figure 4. ^{13}C NMR spectrum of HL ligand in DMSO-d_6

IR spectra

The important IR spectral bands and their assignment are given in Table 2. The free ligand in KBr disc shows broad band at 3470 cm^{-1} which belongs to OH, thus it confirms the keto-enol tautomerism of the free azo ligand. The strong absorptions at 1450-1510 cm^{-1} and 1730-1655 cm^{-1} are typical for –N=N– and C=O(pyranone) moieties respectively.[19] The band due to C–O–C stretch of the pyranone ring was observed at 1115-1122 cm^{-1}. In the IR spectra of the complexes, the band in the region ~ 1700-1625 cm^{-1} gives a clear indication of chelated C=O group suggesting involvement of carbonyl oxygen of pyrazolone ring in the coordination with metal ions.

Table 2. FT-IR data of azo ligand and its metal complexes.

Symbol	νC=O,νOH	ν C=C, νN=N-	νM-N, νM-O	Other bands, νC-H, C-O
HL	1730, 1653, 3470	1630, 1440-1510(s)		3100(w), 2966, 1115-1122
CrL_2Cl	1690(s)-1645	1590,1433-1490	533(w), 420(m), 260-300	3033(w), 2972(m), 1110
MnL_2	1678-1633(s)	1570,1420-1500	530,428	3023, 2982, 1200
FeL_2Cl	1655-1642(s)	1541-1599(s),1444	555(w), 470, 336	3030, 2882, 1122
CoL2	1674-1633(s)	1568-1606, 1433	555(w), 473(w)	3040, 2950, 1120
NiL_2	1685-1625(s)	1585-1614(s), 1422	538, 430(w)	3094(br), 1111
CuL_2	1700-1661(s)	1566-1606(s),1418	560(m), 450(w),	3022(w), 1118
ZnLCl	1680-1633(s)	1544-1588(s), 1419	545, 450(m), 265(w)	2675(m), 1109(s)

s=strong, m=medium, br=broad, w=weak

 DOI: 10.17628/ecb.2014.3.447-451

As well as, the downshift in –N=N- vibration supports the participation of nitrogen atom in β-position in bonding with the metal ions. The weak to medium bands at 560-530 and 420-477 cm^{-1} were due to vibrational modes of M-N and M-O bands, respectively. [20-21]

Electronic spectra and magnetic moments of metal complexes

The free azo ligand solution in methanol displays two distinct peaks at 280 and 375 nm that are characterized of –N=N-, C=O and other chromophore groups.[22] The magnetic moment value of Cr(III) complex was 3.44 B.M suggested an octahedral geometry.[22-23] The conspicuous electronic spectral bands were at 470-580 nm due to $^4A_2g(F) \rightarrow {}^4T_1g(F)$ and $^4A_2g(F) \rightarrow {}^4T_2g(F)$ transitions, respectively, that remarkably gave additional support to octahedral geometry of the Cr(III) complex. The brown solution of iron(III) complex in DMF showed spectral bands which were overlapped with CT bands. The bands observed at 577 nm could very well be due to $^6A_1g \rightarrow {}^4T_1g$ transition. The magnetic moment value of 5.64 B.M indicated the octahedral geometry. [23]The spectrum of Ni(II) complex was characteristic of an octahedral geometry with prominent bands at 380 nm ($^3A_2g \rightarrow {}^3T_1g(P)$ and 670 nm ($^3A_2g \rightarrow {}^3T_1g(F)$). The magnetic moment of 2.78 B.M. also suggested an octahedral geometry. The Cu(II) complex was brown in colour due to strong C.T bands tailing off into the blue end of the visible region. The magnetic moment value (1.74 B.M.) lies well within the expected range (1.7-2.2 B.M.). The dark red solution of Zn(II) complex was diamagnetic and the spectral peaks were all similar to those of the ligand as d-d transitions were absent.[24] As the same d-d transitions for Cr(III), Fe(III), Mn(II) and Cu(II) complexes, the cobalt(II) and nickel(II) solutions in DMF exhibit spin-allows transitions in the regions 400-530 and 560-610 nm confirming the $^4T_1g \rightarrow {}^4T_2g(F)$, $^4T_1g \rightarrow {}^4A_2g(F)$ and metal to ligand charge transfer LMCT transitions, respectively, these agree well with the observed values of magnetic moments.[25] The red solution of zinc(II) complex in DMF showed high intensity peaks at 225 and 367 nm due to electronic transitions of –C=C, C=O, and N=N- chromophores and LMCT, respectively.[25]

Table 3. Electronic spectra, molar conductance and magnetic moments of the prepared metal complexes

Compound	λ_{max}, nm	ν, cm^{-1}	Λ, S cm^2 mol^{-1}	μ, B.M.
HL	375	26666	10	-
	280	35714		
[CrL_2]Cl	344	29069	65	3.44
	570	17543		
	580	17241		
[FeL_2]Cl	300	33333	58	5.64
	577	17331		
[MnL_2]	341	29325	40	5.5
	433	23094		
[CoL_2]	400	25000	23	3.44
	533	18761		
[NiL_2]	288	34722	25	2.98
	566	17667		
	610	16393		
[CuL2]	340	29411	22	1.74
	560	17857		
[ZnLCl]	367	27247	28	0
	225	44444		

λ=molar conductance in DMF solutions at 0.001 M concentration.

Conclusion

A series of novel chromium(III), iron(III), manganese(II), cobalt(II), nickel(II), copper(II) and zinc(II) complexes with a new azo ligand 4-[(Z-(4-hydroxy-6-methyl-2-oxo-2H-pyran-3-yl]-1-methyl-2-phenyl-1,2-dihydro-3H-pyrazol-3-one were synthesized. The free ligand and the isolated solid metal complexes were fully characterized on the basis of C.H.N.M. elemental analyses, ^1H and ^{13}C NMR, FTIR and UV-Visible spectroscopic results. The formula of metal complexes were found to be $[ML_2]Cl_n$, for the M=Cr, Fe(III) if n=1 and M=Mn, Co, Ni and Cu(II) for n=0, while the zinc(II) complex has tetrahedral geometry with the formula [ZnLCl]. The infrared spectral data revealed that the new azo compound HL behaves as tridentate Lewis base via the β-nitrogen atom of –N=N- group and two oxygen atoms of –deprotonated OH and –C=O of 2-pyranone and pyrazoline moieties, respectively. According to the results obtained from elemental analyses, molar conductivity measurements in DMF solutions and magnetic susceptibility data, the octahedral structures for all metal(II) complexes except the zinc(II), which has tetrahedral structure, were proposed.

References

[1]Chalaca, M. Z., Figueroa-Villar, J. D., Ellena, J. A. and Castellano, E. E., *Inorg. Chim. Acta*, **2002,** *328*, 45.

[2]Bouchama, A., Bendaâs, A., Chiter, C., Beghidja A. and Djedouani, A., *Acta Cryst., Section E*, **2007**, *63(9)*, 1205-1207.

[3]Khalil, A., Hassan, M. A., Mohamed, M. M., Elsayed, A. M., *Dyes Pigments*, **2005**, *66*, 241-245.

[4]Weisberger, A., Wiley R. H., Wiley, P., Eds. *The chemistry of heterocyclic compounds. Pyrazolinones, pyrazolidones and derivatives*, John Wiley, New Yorк. **1964**

[5]Gupta, D. R. and Gupta, R. S., *J. Ind. Chem. Soc*., **1966,** *43(5)*, 377-379.

[6]Gupta, D. R. and Ojha, A. C., *J. Ind. Chem. Soc*., **1970**, *47(12)*, 1207-1208.

[7]Rawther, S. and Nair, M. R. G., *J. Ind. Chem. Soc.*, **1992,** *69*, 157-161.

[8]Hassib, H. B., Abdel Latif, S. A., *Spectrochim. Acta, Part A*. **2003**, *59*, 2425-2434.

[9]Kratzl, K., Fostel H. and Sobczak, R., Monatsh. Chem., **1972**, *103(9)*, 677.

[10]Makedonski, P. B., Johannes, H. H., Wichem, J., Grahn, W., Kowalsky, W., *Dyes Pigments*, **2004**, *16*, 109-119.

[11]Aysha, T., Lycka, A., Lunák, S. Jr., Machalický, O., Elsedik, M. and Hrdina, R., *Dyes Pigments*, **2013,** *98*, 547-556.

[12]Gup, R., Kirkan, B., *Spectrochim. Acta*, **2005**, *62*, 1188-1195.

[13]Geary, W. J., *Coord. Chem. Rev.*, **1971**, *7(1)*, 81-122 .

[14] Kruger P. J. and Smith, D. W. *Can. J. Chem.*, **1967**, *45(14)*, 1611-1618.

[15]Porter, Q. N. and Baldas, J., *Mass Spectrometry of Heterocyclic compounds* (Weissberger, A. and Taylor, E. C., eds) Wiley-Inter Science, John. Wiley and Sons, Inc., USA, **1971**.

[16]Budzikiewicz, H., Djerassi, C. and Williams, D. H., *Mass spectrometry of Organic Compounds*, Holden-Day, **1967**, San Francisco.

[17]Dyer, J. R. *Application of absorption spectroscopy of organic compounds*, Prentice Hall, , Eaglewood Cliffs, N. J. **1965**

[18]Batterham, T. J., *NMR Spectra of Simple heterocycles* (Taylor, E. C. and Weissberger, A., eds. *General Heterocyclic Chemistry Series*, John Wiley and Sons, Inc. New York, USA. **1973**.

[19]Silverstein, R. M., Webster, F. X., *Spectrometric Identification of Organic Compounds*, John Wiley and Sons, Inc., New York**,1998**.

[20]Nakamato, K., *Infrared and Raman Spectra of Inorganic and Coordination Compounds*, Wiley, New York, **1986**.

[21]Drago, R. S. *Physical Methods for Chemists*, 2nd. edition, Saunders Colleges Publishing, New York. **1977**.

[22]Sutton, D., *Electronic Spectra of Transition Metal Complexes*, McGraw Hill, , London, **1968**.

[23] Dutta, R. L. and Syamal, A., *Elements of Magnetochemistry*, **1992**

[24]Cotton, F. A. and Wilkinson, G., *Advanced Inorganic Chemistry*, John Wiley, New York, **1980**.

[25]Seth, S., Aravindakshan, K. K., Spectrochim. Acta Part A Mol. Biomol. Spectr., **2013,** *2(1)*, 415-422.

Received: 10.03.2014.
Accepted: 06.04.2014.

CRYSTAL STRUCTURES AND STABILITY OF HYDRATES AND DEUTERIOHYDRATES OF QUINOLINE N-OXIDES

Vladimir P. Andreev[a], Dmitry O. Zaitsev[b], Yurii A. Velikodny[c], and Vladimir V. Chernyshev[c,d]

Keywords: quinoline N-oxide; 2-methylquinoline-N-oxide; 4-methylquinoline-N-oxide; crystallohydrates ; deuteriohydrates; dehydration, crystal structure; powder X-ray diffraction

The protiated (H_2O) and deuteriated (D_2O) crystallohydrates of quinoline N-oxide, 2-methylquinoline N-oxide and 4-methylquinoline N-oxide demonstrate different behavior at ambient conditions, namely, the deuteriated dihydrates undergo solid state transformation into crystalline anhydrous or hemihydrate forms, while protiated dihydrates loss 3D periodicity. In attempts to explain this phenomenon, the crystal structures of the six compounds – namely, quinoline N-oxide and quinoline N-oxide dihydrate, 2-methylquinoline N-oxide hemideuteriohydrate and 4-methylquinoline N-oxide dihydrate, 4-methylquinoline N-oxide and 4-methylquinoline N-oxide dihydrate – were analyzed.

* Corresponding Author
Phone: +7-495-9393654
E-Mail: Vladimir@struct.chem.msu.ru
[a] Department of Molecular Biology, Biological and Organic Chemistry; Faculty of Ecology and Biology, Petrozavodsk State University, Lenina av. 33, Petrozavodsk 185910, Russian Federation
[b] Department of General Chemistry, Faculty of Ecology and Biology, Petrozavodsk State University, Lenina av. 33, Petrozavodsk 185910, Russian Federation
[c] Department of Chemistry, M.V.Lomonosov Moscow State University, 1-3 Leninskie Gory, Moscow 119991, Russian Federation
[d] A. N. Frumkin Institute of Physical Chemistry and Electrochemistry RAS, 31 Leninsky prospect, Moscow 119071, Russian Federation

Introduction

The field of isotope effects has expanded exponentially in the last years.[1] A quick glance in recent publications shows that researchers examine isotope effects on hydrogen bond structure,[2,3] conformational changes,[4] the end product of organic reaction,[5,6] volumetric properties of dilute solutions[7] among many others phenomena. Moreover, the effect of the replacement of hydrogen (H) with deuterium (D) in biological systems is well documented,[8,9] and the possible role of naturally occurring D in the living organism has been investigated. As brief examples of the latter, Somlyai with colleagues[10] have shown that naturally occurring deuterium is essential for the normal growth rate of cells, and Olgun[11] concluded that deuteronation may interfere with the conformations and functions of many macromolecules and contribute to some pathologies like heavy water toxicity and aging. The aforementioned examples demonstrate the need for more detailed studies on the nature of these effects with the use of quantum chemical calculations.

The reliability of the results obtained by these computational methods in the case of bulky three-dimensional object has to be supported by the preliminary calculations of model crystalline samples, for example, such as hydrated and deuteriated quinoline N-oxide and its derivatives.

Recently, we have published the results of spectral and thermochemical investigation of physicochemical properties of quinoline N-oxide crystallohydrates with H_2O and D_2O.[12] We established that at boiling quinoline N-oxide in D_2O proceeds chemical reaction affording isoindoline-1,3-dione (phthalimide), that was not a case at boiling quinoline N-oxide in H_2O. Also we have found, that quinoline N-oxide form a stable dihydrate with two independent and energetically different H_2O molecules, and complete dehydration of quinoline N-oxide occurs when temperature reaches 150 °C. Later we have discovered that deuteriated quinoline N-oxide, which is isostructural with the dihydrated protiated form, transforms into anhydrous crystalline form at ambient conditions within an hour. The same difference in the dehydration processes has been observed for protiated (H_2O) and deuteriated (D_2O) crystallohydrates of 2-methylquinoline N-oxide and 4-methylquinoline N-oxide. Trying to find the possible reasons of this difference in conditions of dehydration between the protiated and deuteriated crystallohydrates of quinoline N-oxides, the crystal structures of the six compounds – namely, quinoline N-oxide (**1**) and quinoline N-oxide dihydrate (**1d**, **d** – dihydrate),[13] 2-methylquinoline N-oxide hemideuteriohydrate ($0.5D_2O$) (**2h**, **h** – hemideuteriohydrate) and 2-methylquinoline N-oxide dihydrate (**2d**), 4-methylquinoline N-oxide (**3**) and its dihydrate (**3d**) – were analyzed. Compounds **1**, **2h** and **3** were obtained as microcrystalline powders from the corresponding dideuteriohydrates ($.2D_2O$) after one hour exposure at ambient conditions (T = 25 °C).

Experimental

All reagents were of commercial quality and were used as received. Solvents were dried and purified using standard techniques.

Compounds **1**, **2** and **3** were initially obtained as amorphous viscous mass from the corresponding quinolines by oxidation with the hydrogen peroxide in accordance with the known procedure.[14] N-oxides dihydrates were obtained by recrystallization from H_2O. Deuterohydrates were obtained by dehydration of hydrates in the presence of P_2O_5 to the constant mass and dissolution of the obtained N-oxides in the minimal amount of D_2O at room temperature. The solutions thus obtained were stored in the presence of P_2O_5 until formation of heterogenic mixture of the crystals and liquid phase. Selected crystals were quickly grinded into powder and measured on powder diffractometer within 5 min to be sure the samples are isostructural to corresponding dihydrates **1d**, **2d** and **3d**. Powder samples of the compounds **1, 2h** and **3** were obtained from the corresponding deuterohydrates **1d**, **2d** and **3d** after they were kept for 1 h in an open air at ambient conditions.

X-Ray Crystallography

The solid state crystal structures of compounds **2d** and **3d** (Table 1) were obtained from X-ray single-crystal diffraction data, collected using a CAD4 (CuK_α radiation) diffractometer. Crystal structures of compounds **1, 2h** and **3** (Table 2) were determined by powder diffraction methods.[15] with the use of powder patterns measured with a G670 Guinier camera diffractometer (CuK_α radiation) at ambient conditions (T = 295(2) K).

Table 1. Crystal data for **2d** and **3d** (single-crystal samples).

	2d	**3d**
CCSD number	978214	978216
Empirical formula	$C_{10}H_9NO.2H_2O$	$C_{10}H_9NO.2H_2O$
FW	195.21	195.21
Crystal size, mm^3	0.50x0.15x0.10	0.20x0.20x0.10
Crystal form, colour	prism, colourless	prism, colourless
Crystal system	Monoclinic	Triclinic
Space group	*P2₁/c*	*P-1*
Unit cell dimensions		
a/ Å	6.772(5)	6.815(4)
b/ Å	15.829(5)	8.940(4)
c/ Å	9.608(2)	9.100(4)
α/ °	90	107.83(3)
β/ °	106.39(4)	110.45(4)
γ/ °	90	92.03(4)
V/ $Å^3$	988.0(8)	488.2(5)
Z	4	2
Radiation	CuK_α	CuK_α
μ/ mm^{-1}	0.807	0.816
No. reflns collected/independent	2474/1870 [*R(int)* = 0.117]	2014/1846 [*R(int)* = 0.036]
No. params/restraints	140/6	141/6
Final *R* indices	*R(F)* = 0.062 (876 reflns with *I*>2σ(*I*)), *wR*(F^2) = 0.212	*R(F)* = 0.068 (1059 reflns with *I*>σ(*I*)), *wR*(F^2) = 0.259
GOF	1.021	1.038

The crystal structures of **2d** and **3d** were solved with *SHELXS97* using direct methods, completed by subsequent Fourier syntheses, and refined with *SHELXL97*[16] by full-matrix least-squares procedures on F^2. All non-hydrogen atoms were refined with anisotropic displacement parameters. C-bound H atoms were placed in idealized positions and refined using a riding model. The crystalline water H atoms were located on a difference map and refined with O–H bond lengths restrained to 0.85(4) Å.

The monoclinic (**1** and **2h**) and triclinic (**3**) unit-cell dimensions were determined from powder patterns using three indexing programs: TREOR90,[17] ITO[18] and AUTOX.[19] Based on systematic extinctions the space groups for **1** and **2h** were determined to be *Pn* and *C2/c*, respectively. For **3**, centrosymmetric space group *P-1* was assigned. The unit-cell parameters and space groups were further tested using a Pawley fit[20] and confirmed by crystal structure solution. The crystal structures have been solved with the use of simulated annealing technique.[21] The molecular model for quinoline N-oxide has been taken from the Cambridge Structural Database (CSD, Version 5.33),[22] and molecular models for 2- and 4-methylquinoline N-oxides were taken from the refined structures **2d** and **3d**, respectively. In the subsequent direct space search for each compound, the rigid molecular model without H atoms was used with the six varied degrees of freedom. In **2h**, the water O atom situated on a twofold rotational axis has been located on a difference Fourier map. The solution found was fitted with the program MRIA[23] in the bond-restrained Rietveld refinement using a split-type pseudo-Voigt peak profile function[24] and March-Dollase[25] formalism of preferred orientation correction.

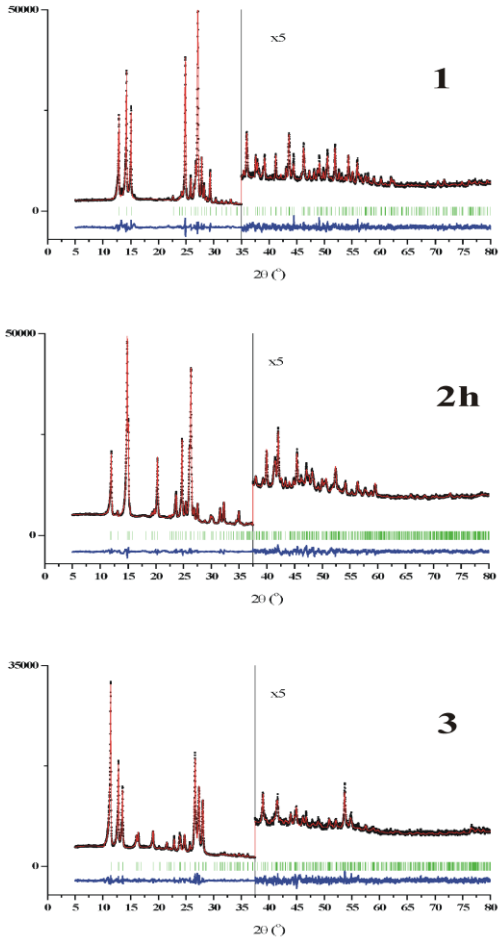

Figure 1. The final Rietveld plots for the patterns of **1** (top), **2h** (middle) and **3** (bottom) showing the experimental (black dots), calculated (red) and difference (blue) curves. The vertical bars denote calculated positions of the diffraction peaks.

 DOI: 10.17628/ecb.2014.3.452-456

Table 2. Crystal data for **1d**,[13] **1**, **2h** and **3** (powder samples).

	1d[13]	**1**	**2h**	**3**
CCSD number	193774	978212	978213	978215
Empirical formula	$C_9H_7NO.2H_2O$	C_9H_7NO	$C_{10}H_9NO.0.5D_2O$	$C_{10}H_9NO$
FW		145.16	169.19	159.18
Particle morphology, colour	prism, colourless	platelets, colourless	prism, colourless	prism, colourless
Crystal system	Monoclinic	Monoclinic	Monoclinic	Triclinic
Space group	*P2₁/n*	*Pn*	*C2/c*	*P-1*
Unit cell dimensions				
a, Å	9.484(3)	12.6462(14)	12.7754(15)	7.7500(8)
b, Å	16.235(5)	3.7354(7)	9.7518(8)	8.6446(12)
c, Å	6.907(2)	7.4642(9)	14.6743(17)	6.8282(8)
α, º	90	90	90	103.93(2)
β, º	118.25(2)	100.297(17)	112.81(2)	105.26(2)
γ, º	90	90	90	65.31(2)
V/ Å^3	936.8(8)	346.92(9)	1685.2(3)	396.50(8)
Z	4	2	8	2
Radiation	$CuK_{\alpha1}$	$CuK_{\alpha1}$	$CuK_{\alpha1}$	$CuK_{\alpha1}$
μ, mm^{-1}		0.744	0.728	0.697
$2\theta_{min} - 2\theta_{max}$, increment		5.00 – 80.00, 0.01	5.00 – 80.00, 0.01	5.00 – 80.00, 0.01
No. params/restraints		73/45	79/53	77/51
$R_p/R_{wp}/R_{exp}$**		0.038/0.051/0.018	0.022/0.028/0.015	0.030/0.040/0.019
GOF		2.658	1.734	1.937

** R_p, R_{wp} and R_{exp} are defined according to Ref.[29]

Restraints were applied to the intramolecular bond lengths and contacts (<2.8 Å), the strength of the restraints was a function of interatomic separation and, for intramolecular bond lengths, corresponded to r.m.s. deviation 0.02 Å. Additional restraints were applied to the planarity of the molecular skeleton, with the maximal allowed deviation from the mean plane 0.03 Å. All non-H atoms were refined isotropically. In all structures, H and D atoms were positioned geometrically (C-H 0.93-0.96 Å; O-D 0.88 Å) and not refined. The diffraction profiles for all compounds after the final bond-restrained Rietveld refinements are shown

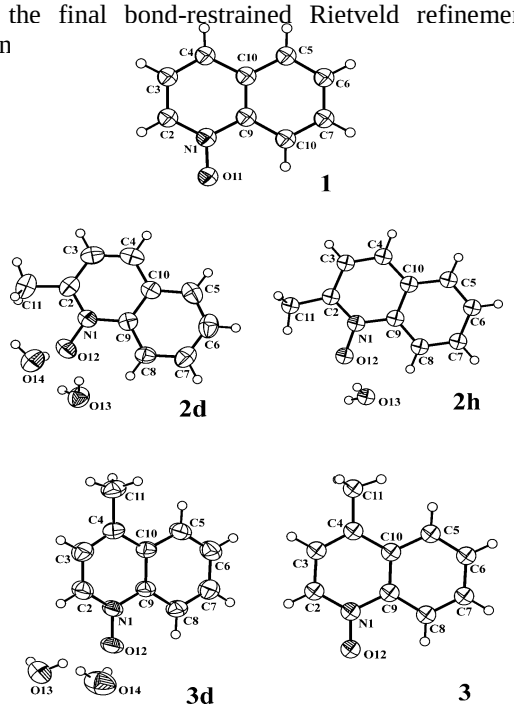

Figure 2. The content of asymmetric unit in the investigated compounds showing the atomic numbering and 50 % probability displacement ellipsoids for **2d** and **3d**, and spheres for **1**, **2h** and **3**.

Results and Discussion

The crystal structures **1**, **2h**, **2d**, **3** and **3d**[26] (Figure 2, drawn with *PLATON*[27]) are new, and, therefore, they will be briefly discussed here.

In **1**, the short axis *b* [= 3.7354(7) Å] reveals an existence of π…π interactions between the quinoline N-oxide molecules, which form stacks in [010]. Weak intermolecular C – H …O interactions (Table 3) link further these stacks into layers parallel to (101) (Figure 3; Figures 3 – 7 drawn with *Mercury*[28]).

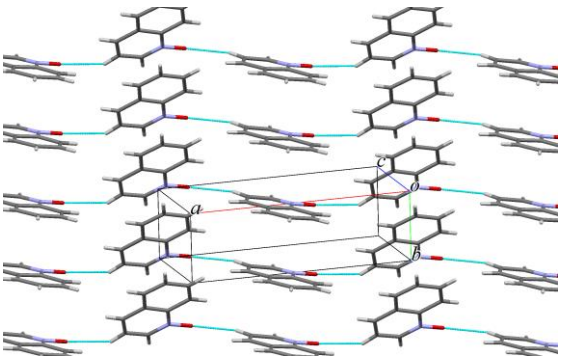

Figure 3. A portion of the crystal packing in **1**, showing the stacks of the molecules and weak C – H…O interactions as green thin lines.

In **2h**, the lattice water molecule (D_2O) situated on two-fold rotational axis is hydrogen-bonded (Table 3) with two 2-methylquinoline N-oxide (*M*) molecules thus forming the 2*M*.D_2O structural unit. Further, these 2*M*.D_2O units interact through π…π interactions proved by short distance of 3.643(8) Å between the centroids of aromatic rings, so 2*M*.D_2O units are arranged into chains extended in [10-1] (Figure 4). Finally, weak intermolecular C–H …O hydrogen bonds (Table 3) consolidate the crystal packing.

Table 3. Hydrogen-bonding geometry (Å, º) in **1**, **2h**, **2d** and **3d**.

	D−H…A	D−H	H…A	D…A	D−H…A
1	C3−H3…O11^{i}	0.93	2.58	3.236(14)	128
2h	O13−D13…O12	0.88	2.00	2.866(12)	167
	C3−H3…O13^{ii}	0.93	2.45	3.320(10)	155
	C5−H5…O13^{iii}	0.93	2.57	3.325(11)	139
2d	O13−H131…O14^{iv}	0.85(3)	1.97(4)	2.817(5)	174(4)
	O13−H132…O12	0.85(4)	1.98(3)	2.815(5)	165(4)
	O14−H141…O12	0.85(4)	1.99(3)	2.836(5)	173(4)
	O14−H142…O13^{v}	0.85(2)	2.02(2)	2.861(5)	171(3)
3d	O13−H131…O12	0.85(5)	1.94(5)	2.778(5)	167(5)
	O13−H132…O14^{iv}	0.84(6)	2.09(6)	2.819(7)	145(6)
	O14−H141…O12	0.85(6)	1.96(7)	2.797(6)	169(7)
	O14−H142…O13^{vi}	0.85(5)	1.94(5)	2.784(6)	170(8)

Symmetry codes: (i) x+1/2, -y, 1/2+z; (ii) –1/2+x, 1/2+y, z; (iii) -1/x, -1/2+y, z; (iv) –1+x, y, z; (v) 1+x, 1/2-y, /2+z; (vi) -x, -y, -z.

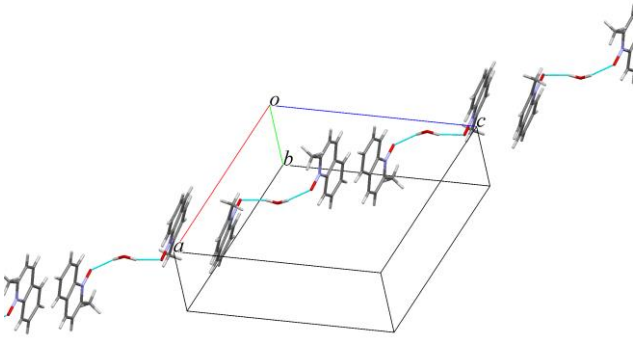

Figure 4. A portion of the crystal packing in **2h**, showing the 2*M*.D$_2$O structural units (*M* = 2-methylquinoline N-oxide) linked through π…π interactions into chains in [10-1]. Thin green lines denote O – H…O hydrogen bonds.

In **2d**, the 2-methylquinoline N-oxide molecules form stacks in [100] with the short distances of 3.614(8) and 3.755(9) Å between the centroids of aromatic rings within the stack. The lattice water molecules filling the space between the stacks are involved in O – H…O hydrogen bonding (Table 3) thus consolidating the crystal packing (Figure 5).

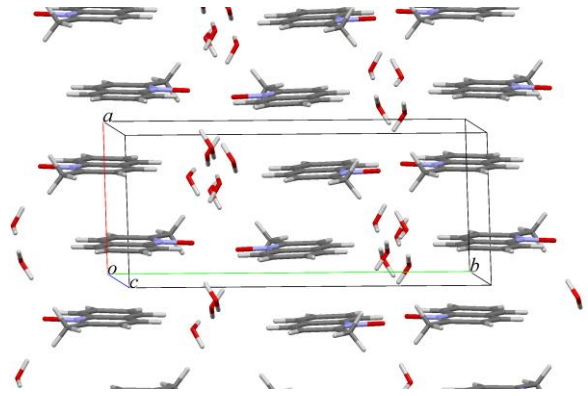

Figure 5. A portion of the crystal packing in **2d**, showing the stacks of the molecules and lattice water molecules filling the space between them.

In **3**, the 4-methylquinoline N-oxide molecules form stacks in [001] with the shortest distances of 3.516(7) and 3.690(9) Å between the centroids of aromatic rings within the stack. The weak Van der Waals interactions consolidate further the crystal packing (Figure 6).

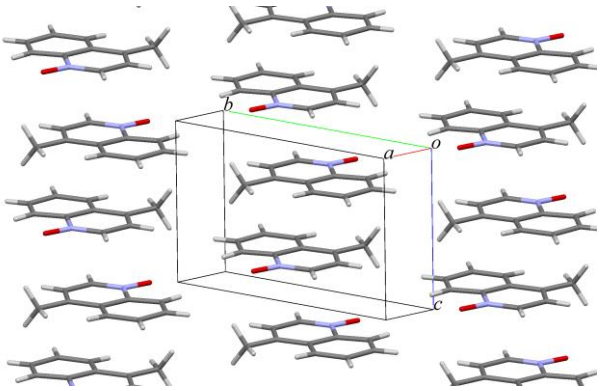

Figure 6. A portion of the crystal packing in **3**, showing the stacks of the molecules.

The crystal packing of **3d** is similar to that in **2d**. The 4-methylquinoline N-oxide molecules form stacks in [100] with the short distances of 3.669(7) and 3.696(7) Å between the centroids of aromatic rings within the stack. The lattice water molecules fill the space between the stacks and participate in O – H…O hydrogen bonding (Table 3) thus consolidating the crystal packing (Figure 7).

The crystal structures of the five compounds discussed in this paper (**1**, **1d**, **2d**, **3** and **3d**) contain stacks of the molecules, which aggregate further either through O–H…O hydrogen bonds in the dihydrates **1d**, **2d** and **3d**, or *via* weak non-classical C – H…O hydrogen bonds and Van der Waals interactions in the anhydrous forms **1** and **3**. Comparing the crystal structures of **1d** and **3d** with their anhydrous forms **1** and **3**, respectively, one can suggest a simple model of the dehydration process based on the destruction of O – H(D)…O hydrogen bonds, elimination of the H(D)$_2$O molecules from the channels between the stacks and subsequent convergence, or collapse, of the stacks.

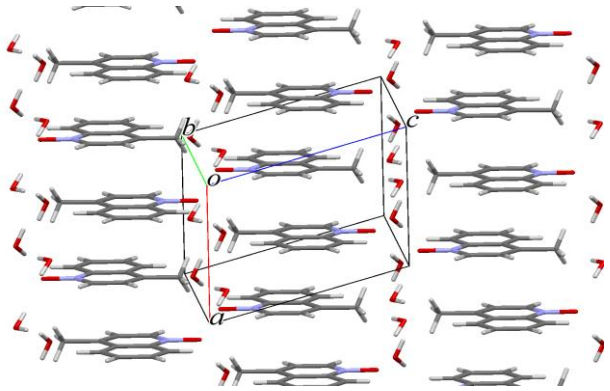

Figure 7. A portion of the crystal packing in **3d**, showing the stacks of the molecules and lattice water molecules filling the space between them.

This model assumes that π …π interactions are most important in our compounds, because they pack the molecules into stacks which serve as rigid building blocks in further solid state transformations. However, the transformation **2d** → **2h** can not be described in the framework of the aforementioned model of dehydration. Indeed, stacks of the 2-methylquinoline N-oxide molecules observed in **2d** are absent in **2h**. It means that stacks of the quinoline N-oxide molecules can not be considered as rigid building blocks in the hydration/dehydration process. A proper model for such process should take into account a competition between various intermolecular interactions.

Our attempts to obtain at ambient conditions anhydrous forms **1**, **2**, **3** and a hemihydrate form **2h**, starting from the corresponding dihydrates (.2H_2O) resulted in their transformation into liquid state caused by an absorption of atmospheric water molecules. Attempts to reproduce these solid state transformations at room temperature *in vacuo* failed too – all crystallites were destroyed and transformed into amorphous state. Therefore, we conclude that protiated (H_2O) and deuteriated (D_2O) dihydrates of (2- and 4-methyl) quinoline N-oxides demonstrate different behavior at ambient conditions, namely, the deuteriated dihydrates undergo solid state transformation into crystalline anhydrous or hemihydrate forms, while protiated dihydrates loss 3D periodicity. A comparison of the crystal structures of crystallohydrates **1d**, **2h**, **2d**, **3d** and anhydrous forms **1** and **3** does not allow us to explain properly this phenomenon – further experimental studies are required.

References

[1]Kohen, A., Limbach, H.-H., (Eds), *Isotope Effects in Chemistry and Biology*. CRC Press/Taylor and Francis Group: Boca Raton, FL, **2006**.

[2]Rich, C. C., McHale, J. L., *Phys. Chem. Chem. Phys.*, **2012**, *14*, 2362.

[3]Arai, H., Horikawa, Y., Sadakane, K., Tokushima, T., Harada, Y., Senba, Y., Ohashi, H., Takata, Y., Shin, S., *Phys. Chem. Chem. Phys.*, **2012**, *14*, 1576.

[4]Hatano, N., Watanabe, M., Takekiyo, T., Abe, H., Yoshimura, Y., J. *Phys. Chem. A*, **2012**, *116*, 1208.

[5]Dougan, B.A., Xue, Z.L., *Science China – Chem.*, **2011**, *54*, 1903-1908.

[6]Segapelo, T. V., Guzei, I. A., Spencer, L. C. and Darkwa, J., *Inorg. Chem. Commun*., **2011**, *14*, 1706.

[7]Ivanov, E.V., *J. Chem. Thermodyn.*, **2012**, *47*, 162.

[8]Rundel, P.W., Ehleringer, J.R., Nagy, K.A., *Stable isotopes in Ecological Research*, Springer, New York, **1988**.

[9]Katz, J.J., Crespi, H.L., in: *Isotope Effects in Chemical Reactions* (C.J. Collins and N.S. Bowman, Eds.), Van Nostrand Reinhold, New York, pp. 286-363, **1971.**

[10]Somlyai, G., Jancso, G., Jakli, G., Vass, K., Barna, B., Lakics, V., Gaal, T., *FEBS Lett*. **1993**, *317*, 1.

[11]Olgun, A., *Theor. Biol. Med. Model*., **2007**, 4.

[12]Gubarev, Yu. A., Lebedeva, N. Sh., Andreev, V. P., Girichev, G.V., *Russ. J. General Chem*., **2008**, *79*, 1183.

[13]Ivashevskaja, S. N., Aleshina, L. A., Andreev, V. P., Nizhnik, Y. P., Chernyshev, V. V., *Acta Cryst.*, **2002**, *E58*, o920.

[14]Ochiai, E., *J. Org. Chem*., **1953**, *18*, 534.

[15](a) Harris, K. D. M.; Tremayne, M.; Lightfoot, P.; Bruce, P. G., *J. Am. Chem. Soc*.**, 1994**, *116*, 3543; (b) Harris, K. D. M.; Tremayne, M.; Kariuki, B. M., *Angew. Chem., Int. Ed*., **2001**, *40*, 1626; (c) Chernyshev, V. V., *Izv. Akad. Nauk, Ser. Khim.*, **2001**, 2171 (In Russian) [*Russ. Chem. Bull.*, **2001**, *50*, 2273]; (d) David, W. I. F., Shankland, K., McCusker, L. B., Baerlocher, C., (Eds.) *Structure Determination from Powder Diffraction Data*, OUP/IUCr, **2002**; (e) Cheung, E. Y., Kitchin, S. J., Harris, K. D. M., Imai, Y., Tajima, N., Kuroda, R., *J. Am. Chem. Soc.*, **2003**, *125*, 14658; (f) Tremayne, M. *Phil. Trans. Roy. Soc.*, **2004**, *362*, 2691; (g) Favre-Nicolin, V., Cerny, R., *Z. Kristallogr*., **2004**, *219*, 847; (h) Tsue, H., Horiguchi, M., Tamura, R., Fujii, K., Uekusa, H., *J. Synth. Org. Chem. Japan*, **2007**, *65*, 1203; (i) David, W. I. F., Shankland, K., *Acta Cryst*., **2008**, *64*, 52.

[16]Sheldrick, G. M., *Acta Cryst.*, **2008**, *A64*, 112.

[17]Werner, P.-E., Eriksson, L., Westdahl, M., *J. Appl. Cryst.*, **1985**, *18*, 367.

[18]Visser, J. W., *J. Appl. Cryst.*, **1969**, *2*, 89.

[19](a)Zlokazov, V. B., *J. Appl. Cryst*., **1992**, *25*, 69; (b) Zlokazov, V. B., *Comput. Phys. Commun.*, **1995**, *85*, 415.

[20]Pawley, G. S., *J. Appl. Cryst.*, **1981**, *14*, 357.

[21]Zhukov, S. G., Chernyshev, V. V., Babaev, E. V., Sonneveld, E. J., Schenk, H., *Z. Kristallogr*., **2001**, *216*, 5.

[22]Allen, F. H., *Acta Cryst*., **2002**, *B58*, 380.

[23]Zlokazov, V. B., Chernyshev, V.V., *J. Appl. Cryst*., **1992**, *25*, 447.

[24]Toraya, H., *J. Appl. Cryst.*, **1986**, *19*, 440.

[25]Dollase, W. A., *J. Appl. Cryst*., **1986**, *19*, 267.

[26]The crystal structures **1**, **2h**, **2d**, **3** and **3d** were deposited with CCDC (Nos. 978212-978216). These data can be obtained free of charge via http://www.ccdc.cam.ac.uk/data_request/cif, or by e-mailing data_request@ccdc.cam.ac.uk, or by contacting The Cambridge Crystallographic Data Centre, 12 Union Road, Cambridge CB2 1EZ, UK; fax: +44(0)1223-336033.

[27]Spek, A. L. *J. Appl. Cryst.* **2003**, *36*, 7.

[28]Macrae, C. F., Bruno, I. J., Chisholm, J. A., Edgington, P. R., McCabe, P., Pidcock, E., Rodriguez-Monge, L., Taylor, R., van de Streek, J., Wood, P. A., *J. Appl. Cryst*., **2008**, *41*, 466.

[29]Young, R. A., Wiles, D. B., *J. Appl. Cryst.*, **1982**, *15*, 430.

Received: 19.03.2014.
Accepted: 07.04.2014.

A NEW EPOXY RESIN BASED EMULSION PRIMER

E. V. Shynkarova and V. D. Koshevar

Keywords: emulsion; epoxy resins; corrosion protection; primer

Metal structures are easily destroyed under the environmental influence. A new protective material, an anticorrosive primer based on an emulsion resin ED-20 dispersed in water has been developed and tested.

* Corresponding Authors
Fax: 8017 284 27 34
E-Mail: schinkarova@igic.bas-net.by
[a] Institute of General and Inorganic Chemistry, National Academy of Sciences of Belarus, Republic of Belarus, Surganova Street, 9/1, Minsk, 220072.

Introduction

Epoxy resins- the most important film-forming materials for paints and varnishes – are widely used for corrosion protection because of their unique properties which are: high adhesion of epoxy coatings (PC) to the most of construction materials, good physical and mechanical properties, low shrinkage during curing and resistance to hydrolysis due to absence of easily saponifiable group in their molecules. In addition, liquid epoxy resins have low toxicity and relatively low energy consumption is needed to emulsify them in an aqueous medium.

The epoxy resin based compositions are the most promising and environmentally friendly for coatings.[1] Further, the developments in the production of epoxy resins and their use for coatings comply with both ecological (Directive 2004/42/EC of the European Parliament) and the economical considerations.

Recently, a number of companies including Russians are engaged in manufacturing the industrial coatings based on various resins (alkyd, epoxy, polyurethane) emulsified in water.[2,3] Benefits of coatings formed from aqueous emulsions of epoxy: excellent resistance to corrosion, high adhesion to various surfaces.

The technologies for developing industrial resin (epoxy, alkyd, polyurethane) emulsions is getting attention in the Republic of Belarus because allnecessary conditions such as raw materials, equipment and the market are easily available. JSC "Lakokraska" (Lida) now manufactures the equipment for emulsification of resins. One of the limiting factors for the application of aqueous emulsions of resins in Belarus is the lack of domestic development of coatings based on it.

The purpose of this study is to report on import replacement of protective material in an epoxy emulsion primer which protects the metal from corrosion.

Experiments

In developing highly corrosion reistant primer one has to ensure high protective properties and environmental safety. The pigment based on a mixture ferrite of calcium and zinc obtained from the galvanic waste from Belarusian enterprises is environmentally friendly.

There are two components of the primer which are mixed immediately prior to use. One part includes an anticorrosive pigment, filler, processing aids (wetting agent, defoamer, corrosion inhibitor, thickener) and hardener. This part of the primer was prepared by grinding the componentson a bead mill at a shaft speed 1200 min^{-1} for 1 h

The second part is a 60 % emulsion of epoxy resin obtained by the direct emulsification of the epoxy resin.[4] The epoxy resin ED-20 consisting of 21.3 % of epoxy groups with epoxy equivalent weight equal to 202 g $equiv^{-1}$ is used. The emulsifier (GOST 10587-84), surface-active substance Emulsogen LCN-287, and polymer microparticles were used for stabilizer . The emulsion was prepared by NDG-10 disperser with a peripheral speed of 20 m s^{-1}. Physical and technological characteristics of the epoxy emulsion are shown in Table. 1.

It should be noted that epoxy emulsion can only be used in coatings with special hardeners, which in most cases is the aqueous amine-containing composition. The chemical composition and structure of the hardener affects the properties of the coatings.

Early it was found[5] that the optimum cross-linking agent for this system is aminoadduktovy water-based hardener Epilink 701 (Netherlands), whose properties are shown in Table. 2.

Table 1. Physical and technical characteristics of the epoxy emulsion

Appearance	milky-white liquid
Dry residue	56.0±1 %
Dynamic viscosity at 20 ° C	0.8 Pa s
pH	7.5
Droplet size, microns	0.1-7

Table 2. Physico-chemical properties of hardener

Appearance	White emulsion
Dynamical viscosity at 25 ° C	5-10 mPa s
Amine value	130-165 mg KOH/g
Hydrogen equlvalent	250-350 g/mol

Before applying the primer its two parts are mixed together. The primer is applied by spraying on the steel. Metal samples were degreased with white spirit. Coatings cured at a temperature (20±2)º C "cold cure" for 2, 5, 7, 10 days. and (80±2)ºC "hot set" for 1 and 2 hours.

The following technical and technological properties of primers and coatings were studied:

Dynamical viscosity was measured by a VZ-246 viscosimeter with a nozzle diameter of 4 mm at temperature of 20±2 °C according to the GOST 8420 standard; Mass fraction of non-volatile substances at 105±2°C according to the GOST 17537 standard; Hardness of the coating according to the GOST 5233 standard; Adhesion by method of parallel cuts in accordance with GOST 15140 standard; Thickness of dry coating layer was determined by the GOST 6-10-403-77 standard; Resistance to static exposure of 20 % and a 3% solution of sodium chloride, water and engine oil in accordance with GOST 9.403; Impact strength of the coating according to GOST 4765-73.

Appearance of the coating after tests carried out in hostile environments was evaluated according to GOST 9.407 standard. Kinetics of curing was studied of coatings to modify the content gel fractions (insoluble fraction after crosslinking). Gel content was determined by extracting the soluble fraction of acetone in a Soxhlet apparatus for 24 hours.

Results and Discussion

The volume content of each component determines certain properties of the coating. Thus, for example, coatings of fillers or pigments in the coating characterize a pigment volume concentration (*PVC*) above which the quality of the coating deteriorates.[6]

PVC is given by:

$$PVC = \frac{\sum\left(\frac{m_p}{\rho_p}\right)_i}{\sum\left(\frac{m_p}{\rho_p}\right)_i + \sum\left(\frac{m_b}{\rho_b}\right)K}$$

where

m_p, m_b– weight, respectively, pigment and binder;

i – the amount of excipients;

ρ_p, ρ_b -the densities, respectively, of pigment and binder;

K – constant (dry residue of a binder).

We calculated the PVC of the primer on the above formula. The calculation is made of the ratio of 100 wt. parts hardener. The optimum composition was proved to be 38 %.

The kinetics of curing primer coatings have shown that there is slow growth of gel fraction in the "cold curing". The quantity of the insoluble fraction after 2 days crosslinking is 80 % after 5 days 87 % and after 7-10 days it is 94 %. The insoluble fraction after curing at 80 º C for 1.2 h is 96 %. It can be assumed that the gelation process is largely completed in "hot" curing PC for 1-2 hours..

The data obtained are in good agreement with the results of measuring the hardness of the investigated coatings. Hardness of the coating cured at (20±2)°C for 2 days equalled to 13 rel. units, the solidification is significantly increased with increasing cure . The greatest hardness acquired after curing for 7-10 days is *H*=0.3 rel. units. As a result of the "hot" curing of coatings, the hardness reached 0.5 rel. u

Key performance primers and coatings based on it are shown in Table. 3.

Table 3. Properties of epoxy primer and coatings based on it

Data	**Values**
Volume solids,%	50
Working viscosity VZ-4 primer, sec	25-30
Opacity, g m^{-2}	72
Drying time to degree 3 (20±2)ºC, h	3
Viability after mixing at temperatures (20±2)ºC, h, not less	1
Coating thickness, micron	
monolayer	30
two-layer	60
The time prior to application of subsequent layers at a temperature of (20±2)ºC, day	1
Color coating	brown
Adhesion of the coating to the substrate, pts	1
The coating hardness conv. and:	
after drying (20±2)ºC for 7 days.	0,3
after drying (80±2)ºC for 2 h	0,5
Conditional lightfastness, h	24
Impact strength of the coating cm, not less than	50
Resistance to static two-layer coating to water at (20±2)ºC, d, not less	30
Resistance to the effects of engine oil (20±2)ºC, not less	40
Resistance of the coating in a 20% sodium chloride solution at (20±2)ºC, h, not less	150
Resistance of the coating in a 3% sodium chloride solution at (20±2)ºC, h, not less	150

It is established that during the tests, listed in Table. 3, the environment preserved integrity of the coatings, there are no signs of cracking and blistering. After removal of coatings on metal, the traces of underfilm corrosion is not observed..

The coatings were tested for resistance to variable temperature, high humidity, salt spray and UV rays. Laboratory cyclic tests were carried out for 30 cycles (2880 h). Methods for carrying out one set of tests is presented in Table. 4.

Table 4. Technique one test cycle

№	Test equipment	Test conditions	Time
1	Salt spray chamber, mode A (salt spray test)	T =35±2 ºC, Solution: NaCl, c =50±5 g dm^{-3}, pH = 6.5-7.2	8 hour
2	Exposure to air	T = 15±30ºC Humidity not more than 80 %	16 hour
3	Salt spray chamber, mode B (test condensate)	T = 40±2 ºC Humidity in 100 %	8 hour
4	Exposure to air	T = 15±30 ºC Humidity not more than 80 %	16 hour
5	The apparatus of artificial weather	T = 40±2 ºC Ultraviolet radiation	8 hour
6	Exposure to air	T = 15±30 ºC Humidity not more than 80 %	16 hour
7	Camera cold	T =-20±2 ºC	8 hour
8	Exposure to air	T = 15±30 ºC Humidity not more than 80 %	16 hour

Dry film thickness was 80-90 μ. Sample test results are shown in Table. 5. The Table 5 shows that the coatings have high resistance to the variable temperatures, high humidity, salt spray and UV.

Table 5. The test results of samples

№	Data	Document	Value of the index according to GOST	The actual value of the index
1 2	Decorative properties of the coating	GOST 9.407-84 p. 2.2	No changes	Nochanges
3 4	Protective properties of the coating	GOST 9.407-84 p. 2.3	Lack of destruction	Coating damage is not observed

Conclusion

The developed primer is a new modern material. It provides excellent protection against corrosion of metallic structures in corrosive saline environments, and increases ecologically friendly and improved sanitary conditions.

References

[1]Eselev, A. D., Bobilev, V. A. *Coating Mater. Appl.*, **2008**, № . 10, 12-15.

[2]Dinissen, T. *Coating Mater. Appl.*, **2008,** №. 1-2, 58-62.

[3]Manner, V. V., Kulikova, M. V., Saprykin, O. A., **RU 2154081**, C09D163/02. **2000.**

[4]Koshevar, V. D. Shynkarova, E. V., Kazhuro, **BL 12535**, C 08J 3/02, C 08L 63/00. **2008**.

[5]Shynkarova, E. V., Koshevar, V. D., Budeyko, N. L., *Coating Mater. Appl.*, **2010,** №.4, 33-35.

[6]Fialkov, Y. Y., Zhitomir, A. N., Tarasenko, A. *Physical chemistry of non-aqueous solutions.* L.: Chemistry, **1973**. 376.

Received: 20.03.2014.
Accepted: 07.04.2014.

GREEN SYNTHESIS OF NOVEL PHTHALIMIDE DERIVATIVES OF *P*-AMINOSALICYLIC ACID AS POTENTIAL ANTI-TUBERCULOSIS AGENTS

Y. Dathu Reddy,[a]* P. Praveen Kumar,[a] B. Rama Devi,[a] Ch. Venkata Ramana Reddy[a] and P. K. Dubey[a]

Keywords: phthalic anhydrides; *p*-aminosalicylic acid; anti-tuberculosis agents; 4-(2-carboxybenzamido)-2-hydroxybenzoic acids; 4-(1,3-dioxoisoindolin-2-yl)-2-hydroxybenzoic acids

Green synthesis of novel compounds 4-(2-carboxybenzamido)-2-hydroxybenzoic acids **3a-3e** and 4-(1,3-dioxoisoindolin-2-yl)-2-hydroxybenzoic acids **4a-4e** have been developed in good yields which were analogues of *p*-aminosalicylic acid (used as anti-tuberculosis agent).

Corresponding Authors
E-Mail: dathureddyjntuh@gmail.com
[a] Department of Chemistry, Jawaharlal Nehru Technological University Hyderabad College of Engineering, Kukatpally, Hyderabad (A.P), India-500 085.

Introduction

Tuberculosis (TB), an infection of *Mycobacterium tuberculosis*, still remains the leading cause of worldwide deaths among infectious diseases.[1] One-third of the population is infected with *Mycobacterium tuberculosis* and the World Health Organization (WHO) estimates that within the next 20 years about 30 million people will be infected with the bacillus.[2] Considering TB problems, the WHO declared this disease a global health emergency in 1993.[3] It is commonly known that *Mycobacterium tuberculosis* has developed resistance to the majority of the existing drugs.[4] However, powerful new anti-TB drugs with new mechanisms of action have not been developed in the last forty years. Therefore, there is an urgent demand for a new class of anti-tubercular agent with a different mode of action and it has led medicinal chemists to explore a wide variety of chemical structures. p-Aminosalicylic acid (PAS) and its sodium salt are the drugs used to treat tuberculosis.[3,5] Brand names are Tubasal, Nemasol sodium, etc. However, its potency is less than that of the current five first-line drugs (isoniazid, rifampicin, ethambutol, pyrazinamide, and streptomycin) for treating tuberculosis but it is still useful in the treatment of multidrug-resistant tuberculosis.[5] PAS can cause some side effects including nausea, vomiting, abdominal pain, hepatitis and jaundice.[5] So a promising approach to minimize these side effects is still in so much interest via analogues formation. On the other hand, phthalimide derivatives have been widely reported to posses beneficial pharmaceutical effects, like analgesic,[6] anti-inflammatory[7] and antiviral,[8] etc.

Keeping the above details/facts in mind and in continuation of our earlier studies,[9] on preparation of new derivatives of phthalic anhydride, it was considered worthwhile to prepare phthalimide derivatives of aspirin and p-aminosalicylic acid as potentially biologically active compounds and as new chemical entities.

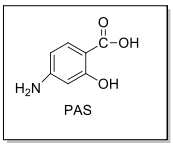

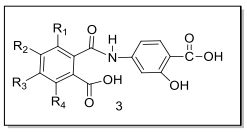

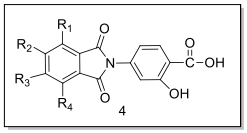

Experimental section

Melting points are uncorrected and were determined in open capillary tubes in sulphuric acid bath. TLC were run on silica gel – G and visualization was done using iodine or UV light. IR spectra were recorded using Perkin – Elmer 1000 instrument in KBr pellets. ^{1}H NMR spectra were recorded in DMSO – d_6 using TMS as internal standard with 400 MH_Z spectrometer. Mass spectra on an Agilent LC-MS instrument.

General procedure for preparation of 3a-3e

A mixture of **1a-1e** (10 mM), **2** (10 mM) and glycerol (20 ml) was heated at 40 ^oC for 10 min. At the end of this period, colourless solid separated out from reaction mixture which was collected by filtration, washed with hexane (10 ml) and dried. The crude product was recrystallized from a suitable solvent to obtain pure **3a-3e.**

3a: Yield = 2.58 g (85%), M.P: 220–222 ^oC; IR (KBr) : 3038-3353 cm^{-1} (broad, medium, -NH- and -OH groups put together), 1703 cm^{-1} (sharp, strong, -CO- of acid group), 1690 cm^{-1} (sharp, strong, -CO- of acid group), 1632 cm^{-1} (sharp, strong, -CO- of amide group); ^{1}H- NMR (DMSO-d_6, 400 MHz) : δ 7.0 (s, 1H, -NH, D_2O exchangeable), 7.4-8.0 (m, 7H, Ar-H), 10.6 (s, 1H, -OH, D_2O exchangeable), 11.5 (s, 1H, -COOH, D_2O exchangeable) 13.2 (s, 1H, -COOH, D_2O exchangeable); ^{13}C-NMR (DMSO-d_6, 400 MHz): δ

111.5, 112.3, 113.6, 116.7, 116.9, 122.7, 124.8, 127.6, 131.6, 133.3, 135.1, 140.2, 158.8, 172.6, 176.5; HRMS calcd for $C_{15}H_{11}NO_6$ $[M+H]^+$: 302.5215. Found: 302.5212.

3b: Yield = 3.71 g (85%), M.P: >220 ºC; IR (KBr) : 3050-3350 cm^{-1} (broad, medium, -NH- and -OH groups put together), 1705 cm^{-1} (sharp, strong, -CO- of acid group), 1695 cm^{-1} (sharp, strong, -CO- of acid group), 1630 cm^{-1} (sharp, strong, -CO- of amide group) ; ^{1}H- NMR (DMSO-d_6, 400 MHz) : δ 7.2 (s, 1H, -NH, D_2O exchangeable), 7.4-8.0 (m, 3H, Ar-H), 10.4 (s, 1H, -OH, D_2O exchangeable), 11.6 (s, 1H, -COOH, D_2O exchangeable) 13.4 (s, 1H, -COOH, D_2O exchangeable); ^{13}C-NMR (DMSO-d_6, 400 MHz): δ 111.3, 111.9, 112.6, 114.3, 115.8, 120.2, 123.4, 126.6, 130.6, 131.4, 134.2, 141.3, 157.0, 171.0, 176.0; HRMS calcd for $C_{15}H_7Cl_4NO_6$ $[M+H]^+$: 437.3232. Found: 437.3236.

3c: Yield = 5.12 g (83%), M.P: >220 ºC; IR (KBr) : 3050-3350 cm^{-1} (broad, medium, -NH- and -OH groups put together), 1710 cm^{-1} (sharp, strong, -CO- of acid group), 1690 cm^{-1} (sharp, strong, -CO- of acid group), 1640 cm^{-1} (sharp, strong, -CO- of amide group) ; ^{1}H- NMR (DMSO-d_6, 400 MHz): δ 7.2 (s, 1H, -NH, D_2O exchangeable), 7.4-8.0 (m, 7H, Ar-H), 10.4 (s, 1H, -OH, D_2O exchangeable), 11.5 (s, 1H, -COOH, D_2O exchangeable) 13.2 (s, 1H, -COOH, D_2O exchangeable); ^{13}C-NMR (DMSO-d_6, 400 MHz): δ 111.3, 111.9, 112.8, 114.4, 115.0, 117.7, 120.4, 123.4, 124.7, 126.3, 128.3, 136.2, 157.7, 171.0, 175.9; HRMS calcd for $C_{15}H_7Br_4NO_6$ $[M+H]^+$: 617.7313. Found: 617.7317.

3d: Yield = 2.77 g (80%), M.P: >220 ºC; IR (KBr) : 3050-3350 cm^{-1} (broad, medium, -NH- and -OH groups put together), 1705 cm^{-1} (sharp, strong, -CO- of acid group), 1695 cm^{-1} (sharp, strong, -CO- of acid group), 1625 cm^{-1} (sharp, strong, -CO- of amide group) ; ^{1}H- NMR (DMSO-d_6, 400 MHz): δ 7.4 (s, 1H, -NH, D_2O exchangeable), 7.4-8.0 (m, 6H, Ar-H), 10.4 (s, 1H, -OH, D_2O exchangeable), 11.7 (s, 1H, -COOH, D_2O exchangeable) 13.4 (s, 1H, -COOH, D_2O exchangeable); ^{13}C-NMR (DMSO-d_6, 400 MHz): δ 110.3, 111.2, 113.4, 115.6, 115.9, 120.2, 124.5, 126.9, 130.3, 132.3, 134.1, 141.1, 157.8, 173.4, 176.8; HRMS calcd for $C_{15}H_{10}N_2O_8$ $[M+H]^+$: 347.1216. Found: 347.1213.

3e: Yield = 2.77 g (80%), M.P: >220 ºC; IR (KBr) : 3030-3350 cm^{-1} (broad, medium, -NH- and -OH groups put together), 1700 cm^{-1} (sharp, strong, -CO- of acid group), 1690 cm^{-1} (sharp, strong, -CO- of acid group), 1630 cm^{-1} (sharp, strong, -CO- of amide group) ; ^{1}H- NMR (DMSO-d_6, 400 MHz) : δ 7.4 (s, 1H, -NH, D_2O exchangeable), 7.4-8.0 (m, 6H, Ar-H), 10.5 (s, 1H, -OH, D_2O exchangeable), 11.6 (s, 1H, -COOH, D_2O exchangeable) 13.6 (s, 1H, -COOH, D_2O exchangeable); ^{13}C-NMR (DMSO-d_6, 400 MHz): δ 112.2, 113.8, 114.2, 115.5, 118.0, 121.3, 124.2, 126.3, 132.5, 133.4, 133.2, 141.1, 159.8, 171.6, 173.3; HRMS calcd for $C_{15}H_{10}N_2O_8$ $[M+H]^+$: 347.1213. Found: 347.1217.

General procedure for preparation of 4a-4e

A mixture of **1a-1e** (10 mM), **2** (10 mM) and glycerol (20 ml) was heated for 2-2.5 h. At the end of this period, a colourless solid separated out from reaction mixture which was collected by filtration, washed with hexane (10 ml) and dried. The crude product was recrystallized from a suitable solvent to obtain pure **4a-4e.**

4a: Yield = 2.41 g (85%), M.P: >220 ºC; IR (KBr) : 3040-3350 cm^{-1} (broad, medium, -OH groups), 1700 cm^{-1} (sharp, strong, -CO- of acid group), 1690 cm^{-1} (sharp, strong, -CO- of acid group), 1635 cm^{-1} (sharp, strong, -CO- of amide group) ; ^{1}H- NMR (DMSO-d_6, 400 MHz): 7.4-8.0 (m, 7H, Ar-H), 11.4 (s, 1H, -OH, D_2O exchangeable), 13.6 (s, 1H, -COOH, D_2O exchangeable); ^{13}C-NMR (DMSO-d_6, 400 MHz): δ 110.6, 113.6, 116.5, 116.8, 123.7, 124.9, 126.1, 127.6, 132.7, 134.1, 140.1, 158.0, 158.3, 175.9; HRMS calcd for $C_{15}H_9NO_5$ $[M+H]^+$: 284.3018. Found: 284.3014.

4b: Yield = 3.58 g (85%), M.P: >220 ºC; IR (KBr) : 3030-3380 cm^{-1} (broad, medium, -OH groups), 1705 cm^{-1} (sharp, strong, -CO- of acid group), 1695 cm^{-1} (sharp, strong, -CO- of acid group), 1625 cm^{-1} (sharp, strong, -CO- of amide group) ; ^{1}H- NMR (DMSO-d_6, 400 MHz) : 7.4-8.0 (m, 3H, Ar-H), 11.2 (s, 1H, -OH, D_2O exchangeable), 13.4 (s, 1H, -COOH, D_2O exchangeable); ^{13}C-NMR (DMSO-d_6, 400 MHz): δ 112.4, 114.5, 115.5, 116.9, 120.5, 123.3, 125.2, 126.5, 130.4, 133.9, 142.1, 157.8, 158.2, 173.8; HRMS calcd for $C_{15}H_9Cl_4NO_5$ $[M+H]^+$: 422.2116. Found: 422.2119.

4c: Yield = 4.67 g (78%), M.P: >220 ºC; IR (KBr) : 3035-3350 cm^{-1} (broad, medium, -OH groups), 1705 cm^{-1} (sharp, strong, -CO- of acid group), 1680 cm^{-1} (sharp, strong, -CO- of acid group), 1630 cm^{-1} (sharp, strong, -CO- of amide group) ; ^{1}H- NMR (DMSO-d_6, 400 MHz) : 7.4-8.0 (m, 3H, Ar-H), 11.6 (s, 1H, -OH, D_2O exchangeable), 13.2 (s, 1H, -COOH, D_2O exchangeable); ^{13}C-NMR (DMSO-d_6, 400 MHz): δ 111.2, 112.5, 115.7, 118.6, 121.7, 122.6, 127.2, 128.8, 131.3, 136.2, 141.5, 156.9, 157.5, 174.3; HRMS calcd for $C_{15}H_9Br_4NO_5$ $[M+H]^+$: 599.1015. Found: 599.1018.

4d: Yield = 2.63 g (80%), M.P: >220 ºC; IR (KBr) : 3038-3353 cm^{-1} (broad, medium, -OH groups), 1700 cm^{-1} (sharp, strong, -CO- of acid group), 1685 cm^{-1} (sharp, strong, -CO- of acid group), 1620 cm^{-1} (sharp, strong, -CO- of amide group) ; ^{1}H- NMR (DMSO-d_6, 400 MHz): 7.4-8.0 (m, 6H, Ar-H), 11.0 (s, 1H, -OH, D_2O exchangeable), 13.6 (s, 1H, -COOH, D_2O exchangeable); ^{13}C-NMR (DMSO-d_6, 400 MHz): δ 110.5, 111.9, 113.2, 114.5, 122.8, 123.5, 124.6, 125.7, 130.5, 132.3, 142.8, 158.4, 158.9, 174.6; HRMS calcd for $C_{15}H_8N_2O_7$ $[M+H]^+$: 329.3315. Found: 329.3319.

4e: Yield = 2.63 g (80%), M.P: >220 ºC; IR (KBr) : 3020-3340 cm^{-1} (broad, medium, -OH groups), 1700 cm^{-1} (sharp, strong, -CO- of acid group), 1695 cm^{-1} (sharp, strong, -CO- of acid group), 1625 cm^{-1} (sharp, strong, -CO- of amide group) ; ^{1}H- NMR (DMSO-d_6, 400 MHz): 7.4-8.0 (m, 6H, Ar-H), 11.0 (s, 1H, -OH, D_2O exchangeable), 13.4 (s, 1H, -COOH, D_2O exchangeable); ^{13}C-NMR (DMSO-d_6, 400 MHz): δ 111.3, 112.4, 114.3, 115.6, 122.4, 124.4, 125.3, 126.8, 133.7, 135.3, 141.2, 157.9, 158.7, 174.8; HRMS calcd for $C_{15}H_8N_2O_7$ $[M+H]^+$: 329.3315. Found: 329.3319.

Results and Discussion

Phthalic anhydride **1a-1e** were reacted with 4-aminosalicylic acid **2** in glycerol at 40 ºC for 10 min to yield monoacid monoamide derivative i.e 4-(2-carboxybenzamido)-2-hydroxybenzoic acid **3a-3e,** respectively**.**

 DOI: 10.17628/ecb.2014.3.460-462

The latter were each transformed into the corresponding phthalimide 4-(1,3-dioxoisoindolin-2-yl)-2-hydroxybenzoic acid **4a-4e** in glycerol at 100 ºC for 2-2.5 h, involving a dehydrative ring closure, in high yields and in high purity**.**

Alternatively **4a** have been prepared by treatment of **1a** and **2** in glycerol at 100 ºC for 2 h**.** The structures of products have been established on the basis of spectral data. **(**Scheme 1) (Table 1) (Please see experimental section)**.** Then, the reaction of **1a and 2** to form **4a** was optimised by carrying out the reaction of **1a** (1 mmol) with **2** (1 mmol) in the presence of different solvents (glycerol, ethylene glycol, PEG-600 and DMF) at different temperatures (Table 1). However, reaction with glycerol at 100ºC for 2 h, unlike other solvents gave reasonably high yield (85%) of the product **4a** (Table 1, entry 3). Thus, glycerol was found to be best solvent for this reaction to form **4a** at 100 ºC for 2 h**.** After having optimized the reaction conditions, the generality of the reaction was confirmed by carrying out the condensation of several others **1a-1e** with **2** in glycerol as a solvent at 100ºC for 2-2.5 h yielding **4a-4e**. The structures of the products have been established on the basis of their spectral data. **(Scheme 1)** (Please see experimental section).

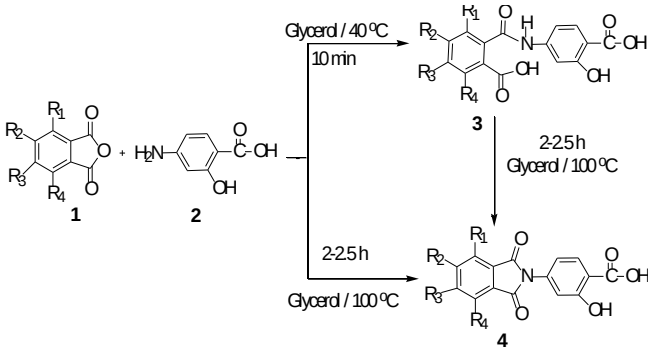

1	=	R_1	R_2	R_3	R_4
1a	=	H	H	H	H
1b	=	Cl	Cl	Cl	Cl
1c	=	Br	Br	Br	Br
1d	=	H	NO_2	H	H
1e	=	NO_2	H	H	H

Scheme 1. Synthesis of **3a-3e** and **4a-4e**.

Conclusion

Facile and green process for the preparation of potential anti-tuberculosis compounds have been developed. These compounds are structural analogues of *p*-aminosalicylic acid. The overall yields of these compounds are very good.

Table 1. Effect of solvent on reaction of **1a** with **2** yielding 4a.

Entry	Solvent	*T*, °C	Time, min	Yield of 4a, %
1	Glycerol	40	6	70
2	Glycerol	80	4	80
3	Glycerol	100	2	85
4	Ethylene glycol	40	6	45
5	Ethylene glycol	80	4	80
6	Ethylene glycol	100	2	80
7	PEG-600	40	6	60
4	PEG-600	80	4	75
5	PEG-600	100	2	80
6	DMF	40	5	60
7	DMF	80	3	70
8	DMF	100	2	75

Acknowledgement

Authors are very thankful to the authorities of **Jawaharlal Nehru Technological University Hyderabad** for providing laboratory facilities and for encourgement.

References

[1]Guzel, O., Terzioglu, N., Capan, G., Salman, A., *Arkivoc.*, **2006**(12), 98-110.

[2]Savini, L., Chiasserini, L., Gaeta, A., Pellerano, C., *Biorg. Med. Chem.*, **2002,** *10*, 2193-2198.

[3]Souza, M. V. N. D., *Recent Pat. Antiinfect. Drug. Discov.*, **2006**, *1*, 33-44.

[4]Trivedi, A. R., Dodiya, D. K., Ravat, N. R., Shah, V. H., *Arkivoc.*, **2008**(11), 131-141.

[5]Reed, M. D., Blumer, J. L., *Pediatr. Clin. North Am.*, **1983**, *30(1)*, 177-193.

[6]Okunrobo, L. O., Usifoh, O. C., Okpo, S. O., *Pak. J. Pharm. Sci.*, **2006**, *19*, 28.

[7]Pandey, V. K., Raj, N., *Curr Sci.*, **1984**, *53*, 256-268.

[8]Alaa, A. M., Abdel, A., *Eur. J. Med. Chem.*, **2007**, *42*, 614-626.

[9](a)Reddy, Y. D., Reddy, Ch. V. R., Dubey, P. K., *RSC Adv.*, **2014**, *4*, 2974-2979; (b) Reddy, Y. D., Kumar, P. P., Devi, B. R., Dubey, P. K., Kumari, Y. B., *Lett. Drug. Des. Discov.*, **2013**, *10*, 226-238; (c) Reddy, Y. D., Kumar, P. P., Devi, B. R., Dubey, P. K., Kumari, Y. B., *Lett. Org. Chem.*, **2013**, *10*, 70-76; (d) Kumar, P. P., Devi, B. R., Dubey, P. K., *Curr. Catal.*, **2012**, *10*, 202-205.

Received: 16.03.2014.
Accepted: 08.04.2014.

X-RAY CRYSTALLOGRAPHY OF BIS(*O*-ETHYLXANTHATO)-BIS(3,5-DIMETHYLPYRIDINE)NICKEL(II)

Kuldeep Singh,[a] Gurpreet Kour,[b] Ritu Sharma,[b] Renu Sachar,[b] Vivek K. Gupta,[a] Rajni Kant [a]*

Keywords: Octahedral coordination, direct methods, crystal structure; bis(*O*-ethylxanthato)bis(3,5-dimethylpyridine)nickel(II)

A six-coordinated Ni(II) complex, bis(*O*-ethylxanthato)bis(3,5-dimethylpyridine)nickel(II), [$C_{20}H_{28}N_2NiO_2S_4$], has been synthesized by the reaction of bis(*O*-ethylxanthato)nickel(II) with 3,5-dimethylpyridine in acetone. The Ni atom in the title complex is octahedrally coordinated within a trans-N_2S_4 donor set, with the Ni atom located on a centre of inversion. The structure of the title compound was elucidated by a single-crystal X-ray diffraction method. The compound crystallizes in the triclinic space group *P-1* with unit-cell parameters: a = 7.1750(3) Å, b = 9.3864(5) Å, c = 9.6914(4) Å and α = 84.962(4)°, β = 73.017(4)°, γ = 75.172(4)°. The crystal structure was solved by direct methods and refined by full-matrix least-squares procedures to a final *R*-value of 0.0238 for 2162 observed reflections. The asymmetric unit comprises half a molecule. The pyridine ring is coplanar, and is held almost perpendicular to the dithiocarbonato group. Molecules in the crystal are packed together to form layers.

* Corresponding Authors
Fax: +91 191 243 2051
E-Mail: rkvk.paper11@gmail.com
[a] X-ray Crystallography Laboratory, Post-Graduate Department of Physics & Electronics, University of Jammu, Jammu Tawi - 180 006, India
[b] Department of Chemistry, University of Jammu, Jammu Tawi-180 006, India

Introduction

Xanthates comprise an important class of 1,1-dithiolate ligands with many applications ranging from flotation agents to rubber vulcanizers.[1] Bivalent metal xanthates are known to form stable adducts with nitrogen donors which exhibit a variety of coordination geometries.[2] Metal xanthates are extensively used as pharmaceuticals, fungicides, pesticides, rubber accelerators, corrosion inhibitors, agricultural reagents and quite recently in therapy for HIV infections.[3,4] They forms a chelate with virtually all transition elements, and has proved to be a versatile chelating agent for the separation and extraction of metals in analytical chemistry and mineral flotation.[5] Coordination complexes of xanthato ligands with a variety of transition as well as non-transition metals have been reported.[6,7] As a part of our continuous research in this area, the title complex was prepared in the crystalline form and its various geometrical parameters were investigated.

Experimental Methods

Synthesis

Potassium *O*-ethylxanthate is prepared by reacting potassium hydroxide, carbon disulfide and ethyl alcohol according to the method available in the literature.[8] The complex bis(*O*-ethylxanthato)nickel(II) was prepared by stirring an aqueous solutions of nickel(II)chloride (2.37 g, 0.01 mol) and potassium *O*-ethylxanthate (3.2g, 0.02mol). Green precipitates of bis(O-ethylxanthato)nickel(II) were obtained which were filtered and dried in a vacuum desiccator. A solution of bis(*O*-ethylxanthato)nickel(II) (0.78 g, 0.0026 mol) in 50 mL of acetone was treated with excess of 3,5-dimethylpyridine and stirred for 30 min. The colour of the reaction mixture changed from brown to green. After allowing the solution to stand overnight at room temperature, bright green crystals of bis(*O*-ethylxanthato)bis(3,5-dimethylpyridine)nickel(II) were obtained.

X-ray Data Collection, Crystal Structure Determination and Refinement

X-ray intensity data of 14136 reflections (of which 2367 unique) were collected on a CCD area-detector diffractometer (*X'calibur system-Oxford diffraction make, U.K.*) which is equipped with graphite monochromated MoKα radiation (λ=0.71073 Å). The crystal used for data collection was of dimensions 0.3 x 0.2 x 0.2 mm^3. The cell dimensions were determined by least-squares fit of angular settings of 10746 reflections in the θ range 3.46 to 29.03°. The intensities were measured by ϕ and ω scan mode for θ ranges 3.47 to 26.00°. 2162 reflections were treated as observed ($I > 2\sigma(I)$). Data were corrected for Lorentz and polarization factors. The structure was solved by direct methods using *SHELXS97* software.[9] A total of 1024 phase sets were refined with the correct phase set having an absolute figure of merit, M(abs) = 1.262 and combined figure of merit CFOM = 0.045. Multisolution tangent refinement was carried out using 849 *E*-values with E >1.2. An E-map drawn with the correct set of phases revealed all the non-hydrogen atoms of the molecule. The R-factor based on the 849 E -values was R_E = 0.222. Full-matrix least-square refinement of the structure was carried out with *SHELXL97* software.[9] *Ortep-3 for Windows* software [10] was used for making the thermal ellipsoids.[10] The geometry of the molecule was calculated using *PLATON*[11] and PARST[12] software. CCDC-953601 contains the

supplementary crystallographic data for this paper. These data can be obtained free of charge from The Cambridge Crystallographic Data Centre via www.ccdc.cam.ac.uk/ data_request /cif.

Table 1. Crystal data and other experimental details for (**1**)

CCDC	953601
Chemical formula	$C_{20}H_{28}N_2NiO_2S_4$
Formula weight	515.39
Temperature	293(2) K
Measurement	X'Calibur System (now varian)
Radiation, Wavelength	MoKα, 0.71073 Å
Unit cell dimensions	a = 7.1750(3) Å, b = 9.3864(5) Å , c = 9.6914(4) Å α = 84.962(4)°, β = 73.017(4) ° γ = 75.172(4)°
Crystal system, Space group	P-1
Unit cell volume	603.38(5) $Å^3$
Density (calculated)	1.418 g cm^{-3}
Absorption coefficient	1.168 mm^{-1}
F (000)	270
θ range for entire data collection	3.47 < θ < 26.00°
Range of indices	-8 < *h* < 8, -11 < *k* < 11, -11 < *l* < 11
Reflections collected / unique	14136/ 2367
Reflections observed ($I>2\sigma(I)$)	2162
R_{int}	0.0269
R_σ	0.0156
Weighing scheme	$I\backslash[\sigma^2(F_o^2) + (0.0316P)^2 +$ 0.2328P] where $P=(F_o^2+2F_c^2)/3$
No. of parameters refined	136
Final *R*	0.0238
$WR(F^2)$	0.0623
Goodness-of-fit	1.054
$(\Delta/\sigma)_{max}$	0.001 for OSF
Final residual electron density	-0.168 < Δρ < 0.239 $Å^{-3}$

Table 2. Selected bond lengths (Å) and angles (°) for non-hydrogen atoms (e.s.d.'s are given in parentheses)

Bond lengths		**Bond angles**	
Ni1-N1	2.114(1)	N1-Ni1-S2	89.99(4)
Ni1-S2	2.4468(4)	N1-Ni1-S3	89.70(4)
Ni1-S3	2.4653(4)	S2-Ni1-S3	73.38(1)
S2-C8	1.683(2)	C8-S3-Ni1	82.39(6)
S3-C8	1.687(2)	C8-O1-C9	119.56(14)
O1-C8	1.333(2)	C8-S2-Ni1	83.04(6)
O1-C9	1.457(2)	C8-O1-C9	119.56(14)
N1-C1	1.331(2)		
N1-C5	1.335(2)		

Results and Discussion

A general view of the molecule indicating atom numbering scheme (thermal ellipsoids drawn at 40% probability level) is shown in Figure 1. *Ortep-3 for Windows* software[10] was used for making the thermal ellipsoids. Crystal data, along with data collection and structure refinement details are summarized in Table 1. Selected bond lengths and angles are given in Table 2.

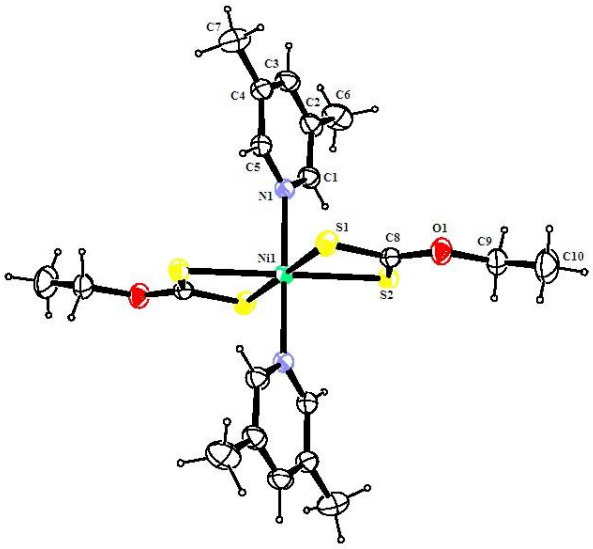

Figure 1. ORTEP view of the molecule with displacements ellipsoids drawn at 50% probability level. H atoms are shown as small spheres of arbitrary radii.

The asymmetric unit comprises of half molecule. The nickel atom is located at the inversion centre. The Ni(II) atom in the complex is six coordinated by two pyridine N atoms from two 2-dimethylpyridine ligands, and by four S atoms from two different xanthate ligands, exhibiting a distorted octahedral configuration of the Ni (II) atom.[13] The Ni1-N1 bond length of 2.115(3) Å, and the Ni-S distances, which for Ni1-S2= 2.447(4) and Ni1-S3 = 2.465(4) Å are normal for this type of compound. The two sulphur-carbon distances show double bond character due to the delocalization over the two C-S bonds.[14]

The sulfur atoms and the Ni atom are lying in the same plane. The bond angle around the nickel atom are in the range of 73.38(4) to 180° and the bond angles in the pyridine ring vary from 117.1(2) to 123.5(2)°, the average value being 120.00(2)°. The pyridine ring (N1, C1 C2, C3, C4, C5) is perfectly *planar* with a maximum deviation of -0.003(2) Å (observed for atom C5). The two methyl groups bound to C2 and C4 atoms are lying in the same plane as that of pyridine ring and it is evident from the least-squares plane calculation of the pyridine ring where the deviation for

C6 and C7 atoms are marginal being -0.023(2) and 0.018(2) respectively. The O1-C8 bond distance [1.333(2) Å] is shorter than O1-C9 [1.457(2) Å] as a consequence of the hybridization of the carbon atom.[15] By and large, the values for bond distances and angles are in agreement with related structures.[16-18] The dihedral angle between the least-squares plane of dithio-group (Ni1, S1, C8, S2) and the pyridine ring is 89.58(4)° meaning thereby that both the units are held almost perpendicular to each other.

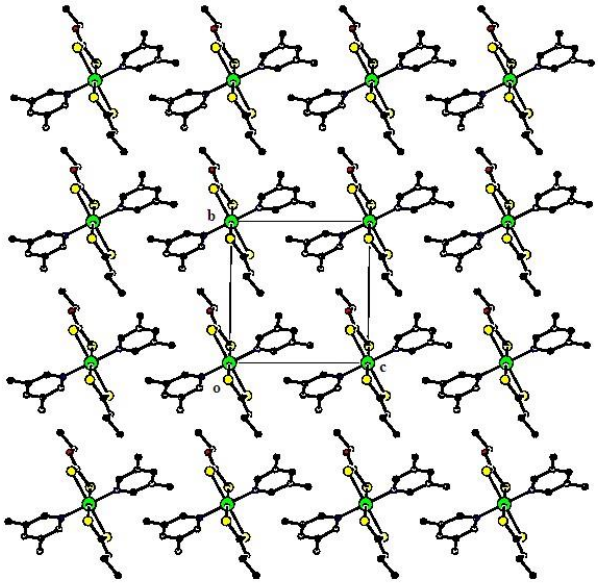

Figures 2. The crystal packing projected on the bc-plane

Packing of the molecules in the unit cell down b-axis is shown in Fig. 3. Molecules are arranged in a manner to form layers. Molecules within the layers are parallel to each other. The nickel atom is located at the each corner of the unit cell. In the absence of any significant hydrogen interaction, the packing of the molecule within thw unit cell stabalized with the help of Van der Waal forces.

Acknowledgements

One of the authors (Rajni Kant) acknowledges the Department of Science & Technology for single crystal X-ray diffractometer as a National Facility under Project No. SR/S2/CMP-47/2003.

References

[1] Tiekink, E. R. T., Haiduc, I., *Prog. Inorg. Chem*., **2005**, *54*, 127.

[2] Jiang, X. H., Zhang, W. G., Zhong, Y., Wang, S.L. *Molecules*, **2002**, *7*, 549.

[3] Victoriano, L. I., Cortes, H. B., *J. Coord. Chem.*, **1996**, *39*, 231.

[4]Ara, I., Bahij, F.E., Lachkar, M., Larbi, N.B., *Trans.Met.Chem.*, **2003**, 28, 908.

[5]Wolf, N., Roundhill, D. M., *Polyhedron*, **1994**, *13*, 2801.

[6]Travnicek, Z., Pastorek, R., Sindelar, Z., Marek, J., *J. Coord.. Chem.*, **1998**, *44*, 193-204.

[7]Ballester, L., Gutierrez, A., Perpinan, M. F., *Polyhedron*, **1996**, *15*, 1103.

[8]Furnniss, B. S., Hannaford, A. J., Smith, P. W. G., Tatchell, A. R., *Vogel's textbook of Practical Organic Chemistry,* 5th Edn. Pearson Education, London, **1989**.

[9]Sheldrick, G. M., *Acta Cryst*., **2008**, *A64*, 112.

[10]Farrugia, L. J., *J. Appl. Cryst.*, **2012**, *45*, 849.

[11]Spek, A. L., *Acta Cryst*., **2009**, *D65*, 148.

[12]Nardelli, M., *J. Appl. Cryst*., **1995**, *28*, 659.

[13]Zhu, H. L., Shao, S. C., Ma, J. L., Qiu, X. Y., Sun, L., Yang, S., *Acta Cryst.,*. **2003**, *E59*, m843.

[14]Jiang, X. H., Zhang, W. G., Zhong, Y., Wang, S. L. *Molecules*, **2002**, *7*, 549.

[15]Alam, N., Ehsan, M. A., Zeller, M., Mazhar, M., Arifin, Z. *Acta Cryst..*, **2011**, *E67*, m1064.

[16]Kapoor, S., Sachar, R., Singh, K., Gupta, V. K., Rajnikant *J. Chem. Crystallogr*., **2012**, *42*, 222.

[17]Kapoor, S., Kour, R., Sachar, R., Kant, R., Gupta, V. K., Kapoor, K., *Acta Cryst..*, **2012**, *E68*, m58.

[18]Singh, K., Kapoor, S., Sachar, R., Gupta, V. K., Rajnikant, *X-ray Struct Anal. Online*, **2012**, *28*, 43.

Received: 11.03.2014.
Accepted: 08.04.2014.

SYNTHESIS, DOCKING STUDIES, AND BIOLOGICAL EVALUATION OF ANTI-ULCER ACTIVITY OF 4-ALLYL-5-(4-R1)-PHENYLTHIOMETHYL-1,2,4-TRIAZOLE-3-YL-MERCAPTOACETIC ACID DERIVATIVES

Victoriya Georgiyants[a], Lina Perekhoda[a] , Narzullo Saidov[b] and Idibeg Kadamov[b]

Keywords: synthesis, anti-ulcer activity, rational drug design, triazoles.

A simple and efficient synthesis of 4-allyl-5-(4-R1)-phenylthiomethyl-1,2,4-triazole-3-yl-mercaptoacetic acid derivatives **7a-l** is described herein. This technique uses a direct alkylation 3-mercapto-4-allyl-5-(4-R1)-phenylthiomethyl-1,2,4-triazoles **5a-b**, with substituted chloracetic acid anilides **6a-k**, and 4'-bromo-2-chloroacetophenone **6l**. The probability of anti-ulcer activity of the newly synthesized substances **5a-b** and 7**a-l** was simulated by the computer program PASS and docking studies. The findings show that all substances of this group may be used for the treatment NSAID-induced ulcers.

*Corresponding Authors
Fax: +300506357443
E-Mail: perekhodalina@mail.ru
[a] National University of Pharmacy, Department of Pharmaceutical Chemistry, 53, Pushkinska St, Kharkiv, Ukraine 61002
[b] Tajic National University, Department of Pharmacy, Rudaki avenue,17, Dushanbe, Republic of Tajikistan, 734035

Introduction

The peptic ulcer disease is a serious gastrointestinal disorder that requires a targeted therapeutic strategy. The traditional medical approach to treating ulcers uses antacids, histamine-2 blockers, and proton pump inhibitors. Proton pump inhibitors are one of the most commonly prescribed classes of medications in the primary care setting and are often used in the treatment of acid-peptic diseases. Unfortunately, the use of these drugs can increase the risk of osteoporosis and the risk of certain allergies to foods. Besides, they block stomach acid production heighten the risk of an increasingly common infectious form of diarrhea.[1] Thus, the search for novel molecule templates with anti-ulcer activity that may lead to the creation of new drugs remains an important task of pharmaceutical and medicinal sciences.

Literature survey clearly demonstrate the high therapeutic potential of 1,2,4-triazole derivatives, good amount of information is available on antimicrobial,[2] anti-inflammatory,[3,4] analgesic,[5] neurotropic[6] and other types of biological activities of these compounds.[7-10] 3-Mercapto-1,2,4-triazole derivatives with alkyl, aryl, and acyl substituents at various positions exhibit one of highest level of activity in this class of compounds.[11-13] The interest of scientists in these derivatives is determined by their high reactivity. We believe that a perspective direction of modification of biological properties of 3-mercapto-1,2,4(4*H*)-triazole derivatives is introducing of acetanilide, acetophenone, and allyl substituents into their structure. Therefore, the synthesis of 4-allyl-5-(4-R1)-phenylthiomethyl-1,2,4-triazole-3-yl-mercaptoacetic acid derivatives presents particular interest. At the beginning of our research, the literature sources on their preparation were scarce. The purpose of this work is the synthesis of new derivatives of 1,2,4-(4*H*)-triazoles, prediction of their probable anti-ulcer activity by the computer program PASS, conducting the docking study, and comparison of their anti-ulcer activity *in vivo* on the acute alcohol-prednisolone model NSAID-induced ulcers in rats.

Experimental

Synthesis

In the initial stage of the research the precursors for the 3-mercapto-4-allyl-5-(4-R1)-phenylthiomethyl-1,2,4(4*H*)-triazoles **5a-b** synthesis were obtained. Alkylation thiophenols **1** with ethyl chloroacetate yielded esters **2,** which in turn were converted in the corresponding phenylthioacetic acid hydrazides **3** by hydrazinolysis. Reaction of **3** with allyl isothiocyanate led to corresponding substituted phenylthiosemicarbazides **4**. The merkapto-triazoles **5a-b** with excellent yields was obtained by cyclization of the substituted phenylthiosemicarbazides under basic homogeneous catalysis conditions. Compounds **5a-b** required no further purification and was used in the subsequent reactions.

The next stage of the research was the synthesis of potentially biologically active 4-allyl-5-(4-R1)-phenylthiomethyl-1,2,4-triazole-3-yl-mercaptoacetic acid derivatives **7a-l**. The target compounds were synthesized by alkylation of compounds **5a-b** with substituted chloroacetic acid anilides **6a-k** and α-chloracetophenone **6l.**[14,15] Various alkylating agents were used with the purpose to expand the collection of 1,2,4-triazole derivatives and identify the impact of structure modification on anti-ulcer activity by inserting a acetophenone instead of acetanilide residue. The synthetic route for the preparation of the new compounds is outlined in Scheme 1.

Table 1. Physical properties and other data

Com-pound	R	R^1	Yield, %	M.p., °C	Calculated, %		Formula	Found, %	
					N	S		N	S
5a	H	H	67.12	75-77	15.95	24.35	$C_{12}H_{13}N_3S_2$	15.,97	24.36
5b	H	4-CH_3	67.29	106-108	15.15	23.12	$C_{13}H_{15}N_3S_2$	15.16	23.13
7a	4-CH_3	H	66.67	148-150	14.13	16. 17	$C_{20}H_{20}N_4OS_2$	14.14	16.18
7b	4-CH_3	4-CH_3	76.20	140-142	13.65	15.62	$C_{21}H_{22}N_4OS_2$	13.67	15.64
7c	3-CH_3	4-CH_3	67.22	130-132	13.65	15.62	$C_{21}H_{22}N_4OS_2$	13.67	15.64
7d	3-CF_3	4-CH_3	67.99	158-160	12.06	13.80	$C_{21}H_{19}F_3N_4O_2S_2$	12.08	13.81
7e	3-OCH_3	4-CH_3	75.31	134-136	13.13	15.03	$C_{21}H_{22}N_4O_2S_2$	13.14	15.05
7f	2-CH_3; 3-Cl	4-CH_3	63.71	126-128	12.59	14.41	$C_{21}H_{21}ClN_4OS_2$	12.60	14.43
7g	2-CH_3	4-CH_3	76.92	120-122	14.09	16.13	$C_{20}H_{21}N_4OS_2$	14.11	16.15
7h	2-CF_3	4-CH_3	68.98	92-94	12.06	13.80	$C_{21}H_{19}F_3N_4OS_2$	12.08	13.82
7i	4-Br	4-CH_3	75.39	144-146	11.78	13.49	$C_{20}H_{19}BrN_4OS_2$	11.79	13.51
7k	2-CH_3; 4-CH_3; 6-CH_3	4-CH_3	69.94	120-122	12.77	14.62	$C_{23}H_{26}N_4OS_2$	12.79	14.64
7l	2-CH_3; 6-CH_3	4-CH_3	74.31	139-141	13.20	15.10	$C_{22}H_{24}N_4OS_2$	13.22	15.12

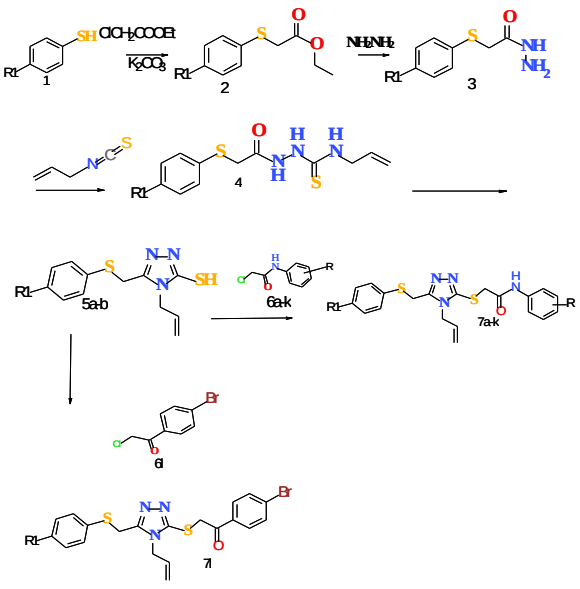

Scheme1. Synthesis route of title compounds

All research chemicals were purchased from the Sigma-Aldrich (USA) and used as such for the reactions. Reactions were monitored by thin layer chromatography carried out using pre-coated silica gel plates (E. Merck and Co., Darmstadt, Germany). The technique described above was found to be an efficient method for the preparation of 4-allyl-5-(4-R_1)-phenylthiomethyl-1,2,4-triazole-3-yl-mercaptoacetic acid derivatives **7a-l**.

General procedure for the synthesis of 3-mercapto-4-allyl-5-(4-R_1) -phenylthiomethyl-1,2,4(4*H*) -triazole (5a-b)

0.1 mol of substituted allyl isothiocyanate was added dropwise with vigorous stirring to a solution of 0.1mol of phenylthioacetic acid hydrazides **3** in 100 mL of ethanol. The reaction mixture was heated to reflux for 1 h, cooled and the precipitate of formed substituted phenylthio-semicarbazide **4** was filtered out and dried. To a suspension of 0.01 mol substituted phenylthiosemicarbazide **4** in 80 ml water were added 0.02 mol KOH. The reaction mixture was refluxed for 5 hours. After cooling, the solution was acidified with hydrochloric acid to pH = 3-4. The resulting precipitate merkaptotriazole was filtered, washed with water and dried.

General procedure for the synthesis of 4-allyl-5-(4-R_1)-phenyl-thiomethyl-1,2,4-triazole-3-yl-mercaptoacetic acid anilides (7a-k)

To a solution of 0.002 mol mercaptotriazole **5a-b** in 20 ml of ethanol was added 20 ml of an aqueous solution of 0.002 mol of KOH. To the resulting reaction mixture was poured with stirring an solution of 0.002 mol of substituted anilides chloracetic acid **6a-k** in ethanol. The resulting solution was heated to reflux for 1 h, cooled, poured into 200 ml of water. The precipitate of the product was filtered off and dried.

Synthesis of 4-allyl-5-(4-R_1)-phenylthiomethyl-1,2,4-triazole-3-ylthio-1-(4-bromo)-acetophenone (7l)

20 mL of an aqueous solution of 0.002 mole of KOH was added to a solution of 0.002 mol merkaptotriazole **5a** in 20 mL of ethanol. 0.002 mol of 4'-bromo-2-chloroacetopheno-

 DOI: 10.17628/ecb.2014.3.466-471

ne **6l** in ethanol was added to the resulting reaction mixture with stirring. The resulting solution was heated to reflux for 1 h, cooled, poured into 200 ml of water. The precipitate of the desired product was filtered off and dried.

All obtained compounds **5a-b** and **7a-l** after crystallization from ethanol or isopropanol are white crystalline substances with clear melting points, soluble in most organic solvents. Melting points (mp) were determined on a Kofler melting point apparatus. Purity of these compounds was checked by thin layer chromatography and supported by spectroscopic data. Physical properties and other data are shown in Table 1.

^{1}H NMR Structure determination

The ^{1}H NMR spectra were obtained on an NMR Spectrophotometer (Bruker Avance II 200 NMR) using DMSO-d6 as a solvent. Chemical shifts were expressed in parts per million relative to TMS as an internal standard.

The structure of compounds **5a-b** was confirmed by ^{1}H NMR spectroscopy. The singlet signal in the range 13.62 to 13.63 ppm is due to the proton mercapto group in compounds **5a-b**. The structures of compounds **7a-l** from **5a-b** also was confirmed by ^{1}H NMR spectrum. The mercapto group proton signal in compounds **7a-l** disappears. A singlet at 9.38 –10.60 ppm in substances synthesized **7a-l** spectrums has been confirmed presents amide group in structures obtained. The signals of aromatic protons were observed in the ranges 6.60 –7.78 ppm. As shown in Table 2, the signals of both methylene groups associated with sulfur atom in the synthesized compounds **5a-b** and **7a-l** as two singlets are common and occur in the spectra in the range δ 4,05 to 4,30 ppm.[16]

Theory/calculation

Pharmacological activity for all compounds synthesized was expected according to PASS computer program (Prediction of Activity Spectra for Substances).[17] All chemical structures were generated using ISIS DRAW 4.0 software. The chemical structures were stored in .mol format and were represented in PASS as a set of Multilevel Neighborhoods of Atoms (MNA-descriptors). MNA-descriptors were calculated iteratively for each atom of the structure using the following rules. The zero-level MNA descriptor was presented as an atom. The descriptor of the first level consists of the atom's zero-level descriptor and zero-level descriptors of its neighboring atoms sorted lexicographically. The prognosis showed a high probability of the anti-ulcer activity for these substances. The presumption can be made that all compounds of this group may exhibit high anti-ulcer (probable activity (*Pa*) from 0.523 to 0.621) and anti-helicobacter (*Pa* from 0.505 to 0.642) activities. The compound with highest probability of these activities is **7i**. The computer prediction results are shown in Table 3. As known, myofibroblasts are considered to play an important part in ulcer healing, expressing COX-2 and synthesizing prostaglandins when exposed to inflammatory stimuli. Prostaglandins have anti-secretory effect on gastric acid; and protect the lining of the stomach from the damaging effects of the acid. Therefore, ligands, which can prevent rapid metabolic conversion prostaglandins into inactive products, may be used for treating of NSAID-induced ulcer.[18]

The interaction of compounds **5a-b** and **7a-l** (as ligands) with protein 3DWW residues of enzyme human MPGES1 (as receptors) were studied by docking using SCIGRESS software.[19] As shown in Figure 1, enzyme human MPGES1 constitutes an inducible glutathione-dependent integral membrane protein as the endogenous ligand.[20.]

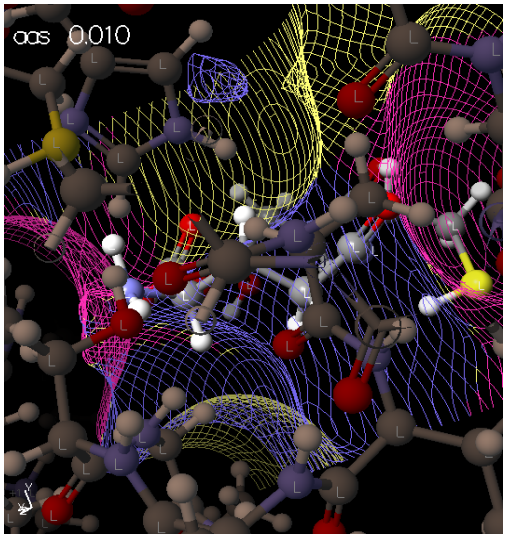

Figure 1. Ligand glutathione in active site protein 3DWW. Active site amino acid residues are represented as sticks colored according to residue type (Sequence protocol-Karplus and Schultz Flexibility).

Predicting the binding affinity and rank-ordering ligands in database screens was implemented by modified and expanded version of the SCIGRESS scoring function. Quantum docking method, in which both 3DWW and ligand are rigid, was adopted and binding energy values were compared with each other.[21]

The docking study was performed using Scigress Explorer 7.7 installed in a single machine running on a 3.4 GHz Intel Core 2 Duo Processor with 1GB RAM and 160 GB Hard Disk with Windows XP as the Operating System.

All ligands **5a-b** and **7a-l** were docked into the active site of the crystal structure of MPGES1 (PDB entry code 3DWW) using automated docking. The enzyme human MPGES1, which constitutes an inducible glutathione-dependent integral membrane protein modeled using the electron crystallographic structure at 3.5 Å resolution was downloaded from the RCSB Protein Data Bank (PDB ID: 3DWW) (www.pdb.org). Water molecules were removed and hydrogen added to crystal structure of protein before docking. After assigning charge and protonation state final refinement (energy minimization) was done using MM3 force field runs.

The docked 3D-structures of 3-mercapto-4-allyl-5-(4-R1)-phenytlhiomethyl-1,2,4(4*H*)-triazoles **5a-b** 4-allyl-5-(4-R1)phenylthiomethyl-1,2,4-triazole-3-il-mercaptoacetic acid anilides **7a-k** and 4-allyl-5-(4-R1)-phenylthiomethyl-1,2,4-triazole-3-ylthio-1-(4-bromo)-acetophenone **7l** were scored. Ligand structures **5a-b** and **7a-l** were drawn on Scigress Explorer using standard bond, lengths and angles. The ligands were stored in .csf format.

 DOI: 10.17628/ecb.2014.3.466-471

Table 2. ^{1}H NMR spectral characteristics of the synthesized compounds **5 a-b, 7a-l**

Compd.	CONH, s, 1H	Ar-H	NCH$_2$, 2H, d	CHCH$_2$, 1H, m	CHCH$_2$, 2H, dd	SCH$_2$, s, 2H	
5a	-	7.10-7.40, m, 5H;	4.65	5.7-6.0	5.0-5.2	4.21	13.62, s, 1H, SH
5b	-	7.10-7.30, dd, 4H;	4.65	5.7-6.0	5.0-5.2	4.11	13.63, s, 1H, SH; 2.13, s,3H, CH$_3$;
7a	10.10	7.05, d, 2H; 7.10-7.40, m, 7H;	4.65	5.8-6.0	4.9-5.3	4.05,	2.10, s, 3H, CH$_3$; 4.30, s, SCH$_2$, 2H
7b	10.20	6.98-7.11, m, 4H; 7.20-7.40, dd, 4H;	4.65	5.8-6.0	4.9-5.3	4.03	2.19, s, 6H,2xCH$_3$; 4.30, s, SCH$_2$, 2H
7c	10.21	6.85, d, 1H; 7.00-7.30, m, 7H;	4.65	5.8-6.0	4.9-5.3	4.05	2.19, s, 6H,2xCH$_3$; 4.30, s, SCH$_2$, 2H
7d	10.60	7.00-7.20, dd, 4H; 7.30-7.78, m; 3H, 8,08, s, 1H;	4.65	5.8-6.0	4.9-5.3	4.05	2.20, s, 3H, CH$_3$; 4.30, s, SCH$_2$, 2H
7e	10.25	6.60, d, 1H; 7.00-7.10, m, 3H; 7.20-7.40, dd, 4H;	4.65	5.8-6.0	4.9-5.3	4.05	2.20, s, 3H, CH$_3$; 3.53, 3H, s, OCH$_3$ 4.30, s, SCH$_2$, 2H
7f	9.85	7.10-7.30, m, 7H;	4.65	5.8-6.0	4.9-5.3	4.05	2.10, s, 3H, CH$_3$; 2.20, s, 3H, CH$_3$ 4.30, s, SCH$_2$, 2H
7g	9.58	7.00-7.30, m, 7H; 7.45, d, 1H;	4.65	5.8-6.0	4.9-5.3	4.05	2.10, s, 3H, CH$_3$; 2.20, s, 3H, CH$_3$ 4.30, s, SCH$_2$, 2H
7h	9.90	7.00-7.30, dd, 4H; 7.30-7.80, m, 4H;	4.65	5.8-6.0	4.9-5.3	4.10	2.20, s, 3H, CH$_3$; 4.30, s SCH$_2$, 2H,
7i	10.10	7.01-7.25, dd, 4H; 7.60-7.90, dd, 4H;	4.80	5.7-6.0	4.9-5.3	4.25	2.22, s, 3H, CH$_3$; 4.70, s, SCH$_2$, 2H
7k	9.38	6.60, c, 1H; 7.01-7.35, dd, 4H;	4.65	5.85-6.0	4.9-5.3	4.10	1.90, s,6H, 2xCH$_3$; 2.12, d, 6H, 2x CH$_3$ 4.30, s, SCH$_2$, 2H
7l	-	6.98-7.11, m, 5H; 7.35, d, 2H;	4.65	5.8-6.0	4.9-5.3	4.05	2.00, s,6H, 2xCH$_3$; 2.20, s, 3H, CH$_3$; 4.30, s SCH$_2$, 2H

The optimization of the cleaned molecules was done through MO-G computational application that computes and minimizes the energy of heat of formation. The MO-G computational application solves the Schrodinger equation for the best geometry of the ligand molecules. The augmented Molecular Mechanics (MM2/MM3) parameter was used for optimizing the molecules up to its lowest stable energy state. This energy minimization was done until the energy change is less than 0.001 kcal mol^{-1} or the molecules are updated almost 300 times. For automated docking of ligands into the active sites we used genetic algorithm with a fast and simplified Potential of Mean Force (PMF) scoring scheme. PMF uses atom types, which are similar to the empirical force fields used in Mechanics and Dynamics.

A minimization is performed by the Fast-Dock engine, which uses a Lamarkian genetic algorithm (LGA) so that individuals adapt to the surrounding environment. The best fits are sustained through analyzing the PMF scores. This process repeats for almost 3,000 generations with 500 individuals and 100,000 energy evaluations. Other parameters were left to their default values.

Structure-based screening involves docking of candidate ligands into protein targets, followed by applying a PMF scoring function to estimate the likelihood that the ligand will bind to the protein with high affinity or not. At the end of the docking study, the minimum Consensus score for the best ligand position for each of ligands was obtained.[22] Details are given in Table 4.

Table 3. Results predicted by computer program PASS

Compd.	Membrane protection	Antiulcer	Anti-helicobacter	Cholesterol lowering	Ovulation inhibitor
5a	0.750	0.546	-	-	-
5b	0.763	0.526	-	-	-
7a	0.674	0.551	0.564	0.525	0.508
7b	0.674	0.554	0.567	0.529	0.512
7c	0.687	0.549	0.560	0.512	-
7d	0.564		0.505	-	-
7e	0.609	0.523	0.518	0.515	0.514
7f	0.549	0.568	0.511	0.506	-
7g	0.610	0.560	0.543	0.532	-
7h	0.507	-	-	0.526	-
7i	0.781	0.621	0.642	-	-
7l	0.623	0.548	0.548	0.511	-
7k	0.622	0.552	0.550	0.530	-

Table 4. Consensus docking score

Compd.	5a	5b	7a	7 b	7 c	7 d	7 e	7 f	7 g	7 h	7 i	7 k	7l
Consensus docking score	-68.6	17.3	273.2	-7.2	-23.2	-70.5	-45.6	82.3	24.3	6.3	-16.8	107.5	234.7

Results and discussion

Results of docking studies have shown that molecule **7d** showed better binding energies than the others. The amino acids residues present in cavity of 3DWW protein mainly Arg70, 126, Gln134, Gsh 154, His 113, Tir 117,130, Glu 77, Arg110, Arg 126 (active site) were involved in the interactions with ligands. In the present work, 13 derivatives of 1,2,4-triazole were evaluated for their anti-ulcer activity through PASS program and docking studies. Later results were compared with experimental data on acute alcohol-prednizolon model NSAID-induced ulcers on rats, which suggests that only three derivatives of 1,2,4-triazole (compounds **7c**, **7d**, and **7i**) have substantial anti-ulcer activity.

Overall, this work illustrated that potential anti-ulcer compounds were found among new derivatives 1,2,4-(4*H*)–triazole. Compound **7i** was substantially more active than others and requires further study. In conclusion, excellent agreement between molecular docking combined with results of computer program PASS simulations and experimental affinities of these ligand series is apparent. The agreement of the computational and experimental results suggests that the docking studies and computer program PASS may become a valuable tool in the search for new drugs. The binding pattern can be further used as a tool for the structure-based novel anti-ulcer drug design.

Acknowledgements

The authors gratefully acknowledge the financial support from the National University of Pharmacy and the Tajic National University. The authors have declared no conflict of interest.

References

[1]Valle, D. L, *Peptic ulcer diseases and related disorders.* In: Braunwald, E., Fauci, A. S., Kasper, D. L., Hauser, S. L., Longo, D. L., Jameson, J. L., editors. *Harrison's principles of internal medicine.* 16-th ed. New York: McGraw-Hill. **2005**

[2]Navidpour, L., Shafaroodi, H., Amini K., Fazeli, M. R., Jamalifar, H., Shafiee, A., B*ioorg. Med. Chem*. **2006**, 14(8), 2507-2017.

[3]Saidov., N.B, Kadamov, I.M., Georgiyants, V.A., *Zh. Org. Farm. Khim*., **2013**, *11(1)*, 44-48.

[4]Abdel-Megeed, A. M., Abdel-Rahman., H. M, Alkaramany, G. E., *Eur. J. Med. Chem.* **2008**, *43(4)*, 642-647.

[5]L.Labanauskas, E.Ubrenaite, P.Gaidelis, A. Brukstus, *Farmaco.* **2004**, 59, 255-259.

[6]Saidov N. B., I. M. Kadamov, Georgiyants, V. A., *Zh. Org. Farm. Khim*., **2012**, *10(4)*, 25-28.

[7]Mathew, V., Giles, D., Keshavayya, J.et al,. *Arch. Pharm.* **2009**, *342(4)*, 210-220.

[8]Tozkoparan, B., Aktay, G., Yesilada E., *Arzneimittel-Forsch.*, **2001**, *51(6)*, 470-477.

[9]Karathikeyan, M.S., *Eur. J. Med. Chem*, **2009**, *44(2)*, 827-833.

[10]Saidov, N. B., Kadamov, I. M., Georgiyants, V. A., Taran, A. V., *Khim. Farm. Zh*., **2013**, *47(11)*, 11-15

[11]Labanauskas, L., Kalkas, V., Udrenaite, E., *Pharmazie*, **2001**, *56(8)*, 617-619.

[12]Tozkoparan, B., Kupeli, E., Izik, E., *Arzneimittel-Forsch.*, **2005**, *55(9)*, 533-540.

[13]Demchenko, A. M., Yanchenko, V. O., Shatirkina, T. V., Lozinskiy, M.O., *Farm. Zh.*, **2003**(2), 57-60.

[14]Joule, K., Mills J. A., *Heterocyclic Chemistry.* Blackwell Science, **2004**, 728.

[15]Garratt, P. J., Katntzky, A. R., Rees, C. W., *1,2,4-Triazoles. Comprehensive Heterocyclic Chemistry II*, Scriven, E. F., Ed. Pergamon: Oxford, **1995**

[16]Breitmaier, E., *Structure elucidation by NMR in organic chemistry*, 3rd ed. – John Wiley @ Sons Ltd, Chichester, **2002**.

[17]Poroikov, V., Filimonov, D., *Computer-aided prediction of biological activity spectra. Application for finding and optimization of new leads, Rational Approaches to Drug Design*, Eds. Holtje, H.-D. Sippl, W., Prous Science, Barcelona, **2001**, 403-407.

[18]Abraham, D. J. (ed.) *Burger's Medicinal Chemistry and Drug Discovery*, v.4 - *Drug Discovery and Drug Development* Sixth Edition. - A Wiley-Interscience Puplication, A John Wiley and Sons, Inc., **2003**.

[19]Scigress Explorer Ultra 7.7 *Bio Applications Getting Started Manual*, Fujitsu Limited, Poland, **2012**.

[20]Jegerschold, C., Pawelzik, S., Purhonen, P., Bhakat, P., Gheorghe, K. R., Gyobu, N., Mitsuoka, K., Morgenstern, R., Jakobsson, P. J., Hebert, H., *Proc. Natl. Acad. Sci. USA*, **2008**, *105*, 11110-11115.

[21]Chi Zhang, Song Liu, Qianqian Zhu, and Yaoqi Zhou, J., *Med. Chem*, **2005**, *48*, 2325-2335

[22]Clark, R. D., Strizhev, A., Leonard, M., Blake, J. F., Matthew, J. B., *J. Mol. Graphics Model*, **2002**, *20*, 281-295

Received: 15.03.2014.
Accepted: 08.04.2014.

THE STRUCTURE OF MIXED β-ARYL(FURYL)BENZOIN, 2-HYDROXY-2-(4''-CHLOROPHENYL)-1-(5'-*N*,*N*-DIMETHYLHYDRAZONYLFURYL-2')ETHANONE-1

Andrey Alexandrovich Anishchenko,[a] Vasiliy Georgievich Shtamburg,[b] Oleg Valerievich Shishkin,[c] Roman Ivanovich Zubatyuk,[c] Victor Vasilievich Shtamburg,[a] and Rem Grigorievich Kostyanovsky[d]

Keywords: β-benzoin, structure, isomerization

The structure of the thermal α→β benzoins isomerization product, 2-hydroxy-2-(4''-chlorophenyl)-1-(5'-*N*,*N*-dimethylhydrazonofuryl-2')-ethanone-1 has been proved by the XRD study. The possibility of the Me_2NN=CH-substituent conjugation with the carbonyl group via the furane ring take place due to the overall planarity this molecule fragment.

Corresponding Authors
Tel: +**380**-68-410-41-79
E-Mail: Koloxai@gmail.com
[a] Dnepropetrovsk Olesya Ghonchara National University, Dnepropetrovsk, Armeyskaya st. 22 "b", 49010. Ukraine.
[b] Ukrainian State Chemico-Technological University, Mostovaya st., 2/6,. 49038. Ukraine
[c] Institute for Single Crystals, National Academy of Sciences of Ukraine, 61001 Ukraine, Kharkov, Lenina ave, 60.
[d] N. N. Semenov Institute of Chemical Physics, Russian Academy of Sciences, 119991, Russian Federation, Moscow, Kosygina st., 4.

INTRODUCTION

Earlier we had reported that 4-chlorophenylglyoxal reacted with *N*,*N*-dimethylhydrazone of 2-furanecarbaldehyde yielding at -20 ^{0}C in ether solution the α-benzoin, 2-hydroxy-1-(4''-chlorophenyl)-2-(5'-*N*,*N*-dimethylhydrazonofuryl-2')-ethanon-1 **1**, which spontaneously isomerized at room temperature in β-benzoin, 2-hydroxy-2-(4''-chlorophenyl)-1-(5'-*N*,*N*-dimethylhydrazonofuryl-2')-ethanone-1 **2.**[1] The β-benzoin **2** is only product of the 4-chlorophenylglyoxal reaction with *N*,*N*-dimethylhydrazone of 2-furanecarbaldehyde at room temperature.[1] The letter "α" had been used to indicate the less stable isomer, the letter "β" had been used to indicate the more stable isomer.[2]

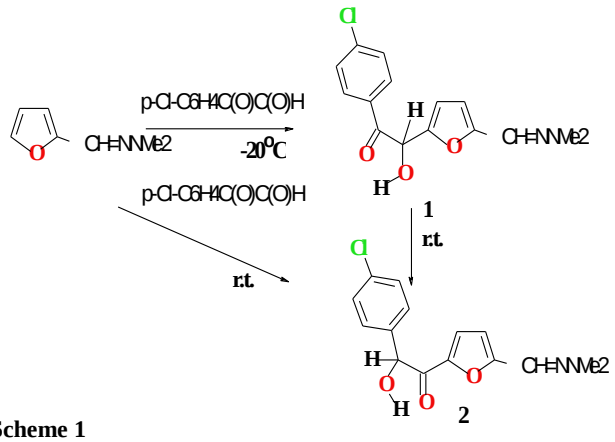

Scheme 1

The α-benzoin **1** and β-benzoin **2** structures were established by the data of NMR ^{1}H and MS spectra[1]. But the β-benzoin **2** structure remained unstudied.

EXPERIMENTAL

2-Hydroxy-2-(4''-chlorophenyl)-1-(5'-*N*,*N*-dimethylhydrazonylfuryl-2')-ethanone-1 (2)

The solution of *N*,*N*-dimethylhydrazone of 2-furanecarbaldehyde (13.0 mmol, 1.795 g) in PhH (5 ml) was added to the boiling solution of 4-chlorophenylglyoxal hydrate (10.0 mmol, 1.866 g) in PhH (20 ml). The reaction mixture was boiled during 30 min, than it was kept at 20 °C during 2 days, than PhH was evaporated *in vacuo*, the residue was washed hexane (20 ml), PhH (15 ml), yielding 2.168 g (70 %) 2-hydroxy-2-(4''-chlorophenyl)-1-(5'-*N*,*N*-dimethylhydrazonofuryl-2')-ethanone-1 **2**, orange crystals, mp. 145-146 °C, after crystallization from CH_2Cl_2 mp. 150-151 °C (cf. with mp. 150-151 °C[1]), identify with the sample of **2**[1] by NMR ^{1}H and MS.

The crystals of **1** were grew from CH_2Cl_2, monoclinic, $C_{15}H_{17}N_2O_3Cl\cdot0.25(CH_2Cl_2)$, at 298 K, a = 26.4863(19) Å, b = 5.7593(5) Å, c = 11.2223(9) Å, β = 103.999(8)°, V = 1661.0(2) Å^3, M_r = 325.01, Z = 4, space group C2, d_{calc} = 1.300 g/cm^3, μ(MoK$_\alpha$) = 0.245 mm^{-1}, F(000) = 680. Data were measured using Xcalibur 3 diffractometer (T=298 K, graphite-monochromated MoK$_\alpha$ radiation, 2θ/θ scan, $2\theta_{max}$=58.36°).

The structures were solved by direct method using the SHELXTL PLUS program package.[3] Refinement against F^2 in an anisotropic approximation (the hydrogen atoms isotropic in the riding model with U_{iso}=nU_{eq} of worn atom, n=1.5 for HO-group and Me-group, n = 1.2 for other hydrogen atoms) by a full matrix least-squares method for 6445 reflections was carried out to wR_2=0.136 (R_1=0.071for 1887 reflections with F>4σ(F), S=1.07).

 DOI: 10.17628/ecb.2014.3.472-473

RESULTS AND DISCUSSION

The XRD study data are evidence of β-benzoin structure of 2-hydroxy-2-(4''-chlorophenyl)-1-(5'-*N*,*N*-dimethylhydrazonofuryl-2')-ethanone-1 **2** (Figure 1, Tables1, 2). The Me_2NN=CH moiety conjugates with the benzoin carbonyl group via the furan ring bonds. The Me_2NN=CH moiety, the furan ring and the carbonyl group are oriented in the same plane, whereby this conjugation becomes possible. The middle quadratic deviation of these atoms from the plane of the conjugated bonds is equal 0.036 Å.

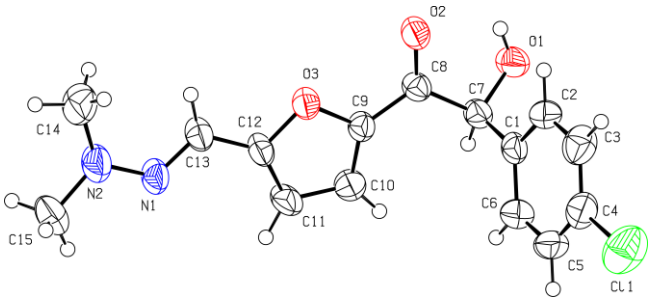

Figure 1. The structure of 2-hydroxy-2-(4''-chlorophenyl)-1-(5'-*N*,*N*-dimethylhydrazonofuryl-2')-ethanone-1 **2**.

This conjugation chain arises to charge transfer from nitrogen N(2) atom on O(2) oxygen atom. The structure of 2-hydroxy-2-(4''-chlorophenyl)-1-(5'-*N*,*N*-dimethylhydrazonofuryl-2')-ethanone-1 **2** can be more effectively described by the structure **2b** than the structure **2a** (Scheme 2).

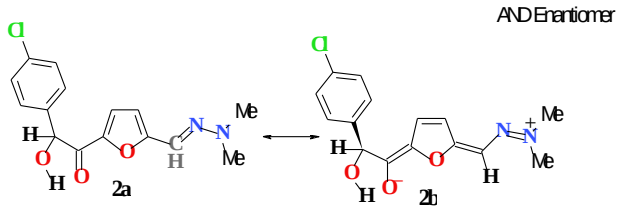

Scheme 2

It was found that in β-benzoin **2** N(2) atom has the nearly planar configuration. The sum of bond angles centered at this nitrogen atom (Σß) is 359°. The N(1)-N(2) bond is shortened to 1.322(4) Å (cf. with N-N bond length 1.45 Å[4]). The O(2)-C(8) bond is some elongated to 1.236 (5) Å (cf. with for C=O bond length 1.21 Å[4]).

The C(8)-C(9) bond and the C(12)-C(13) bond are some shortened to 1.433(5) Å and 1.431(5) Å relatively toward ordinary $C(sp^2)$-$C(sp^2)$ bond (1.47 Å.[4]] All these structure data mean the domination part of the resonance form **2b** in the β-benzoin **2** structure. It may suppose that arising of the long chain of the conjugation between Me_2N- and C=O-moiety is the moving force of the thermal α→β benzoins isomerization yielding β-benzoin **2.**[1]

The *para*-chlorophenyl substituent is perpendicular oriented to this conjugation plane (the C1-C7-C8-C9 torsion angle is -89.7(4)°.

In the resolved crystal of β-benzoin **2** the C(7) atom has absolute *S* configuration.

In the crystals molecules of β-benzoin **2** are linked in the chains along the *b* crystallographic direction due to intermolecular bifunctional hydrogen bonds O(1)-H(1)…O(1^{i}) [i: 3/2-x,-1/2+y,2-z] (H…O 2.33 Å, O-H…O 133°) and O(1)-H(1)…O(2^{i}) (H…O 2.14 Å, O-H…O 150°). Also in the crystal σ-hole bond Cl(1)…O(3^{ii}) [ii: 3/2-x, -1/2+y, 1-z] (Cl…O 3.18, C(4)-Cl(1)…O(3) 167°, C(12)-O(3)…Cl(1) 101°) take place.

Acknowledgement

This work was supported by the Russian Foundation for Basic Research (grant no. 13-03-90460) and Ukrainian Foundation for Fundamental Research (grant no. F-53/105-2013).

References

[1]Anishchenko, A.A., Shtamburg, V.G., Shtamburg, V.V., Mazepa, A.V., *Eur. Chem. Bull.*, **2013**, *2*, 361-366.

[2]Ide, W.S., Buck, J.S. in *Organic Reactions*, R. Adams (Ed.), Wiley, New York, **1948**, *4*, 269-304.

[3]Sheldrick, G. M. *Acta Cryst.*, **2008**, *A64***,** 112-122.

[4]Burgi, H.-B., Dunitz, J.D.. *Structure correlation*. Vol. 2. VCH. Weinheim. 1994, 741-784.

Received: 14.03.2014.
Accepted: 08.04.2014.

SPECTROSCOPIC, STRUCTURAL AND THERMAL CHARACTERIZATION OF CRYSTALLINE $[Cr(OC(NH_2)_2)_6]X_3$ (X = ClO_4, BF_4 AND Cl) COMPLEXES

Natalia Górska,[a] Edward Mikuli[a] and László Kótai[b]

Keywords: hexakis(urea-O)chromium(III) complexes; crystal structure; vibrational and electronic spectroscopy; phase transition; thermal decomposition

Three coordination compounds with urea ($CO(NH_2)_2$) ligands, namely $[Cr(urea)_6](ClO_4)_3$, $[Cr(urea)_6](BF_4)_3$, and $[Cr(urea)_6]Cl_3$ were investigated. In the temperature range of 130–320 K only the first two aforementioned complexes undergo one solid phase transition at: T^h_C =298.4 K and T^h_C=255.4 K (on heating), respectively. X-ray single crystal diffraction at 293 K demonstrates that $[Cr(urea)_6](BF_4)_3$ crystallises in the trigonal crystal system (*R*-3*c* space group) and is isostructural with the other two title compounds. Both the BF_4^- anions and $CO(NH_2)_2$ ligands are in the high temperature phase dynamically disordered. $[Cr(urea)_6](ClO_4)_3$, $[Cr(urea)_6](BF_4)_3$ and $[Cr(urea)_6]Cl_3$ are thermally stable up to ca. 500, 470 and 440 K, respectively, in argon atmosphere. $[Cr(urea)_6](ClO_4)_3$ decomposes explosively at ca. 550 K. $[Cr(urea)_6](BF_4)_3$ decomposes in three main stages with creation of Cr_2O_3 as a final product of decomposition at 1250 K. Whereas $[Cr(urea)_6]Cl_3$ decomposes in two main stages. The mixture of Cr, $CrCl_3$ and ClCrNH is created at 1270 K as a product of decomposition.

Corresponding Authors
Tel: +48 12 663 2265
E-Mail: gorska@chemia.uj.edu.pl
[a] Faculty of Chemistry, Jagiellonian University, Ingardena 3, 30-060 Kraków, Poland,
[b] Institute of Chemistry, Chemical Research Center, Hungarian Academy of Sciences, H-1525 Budapest, P.O. Box 17, Hungary

Introduction

It has been proved that metal-urea complexes are useful precursors to synthesize various nanocrystalline materials like metal oxides or nitrides.[1-3] $[Ti(urea)_6]Cl_3$ is a molecular precursor for nanocrystalline TiO_2 via thermal decomposition.[1] This complex is formed via C=O···Ti bonding and crystallizes in hexagonal space group *P*-3*c*1. It decomposes under stagnant air atmosphere in three main steps between 500 and 720 K. The final product of this decomposition, after oxidation of Ti^{3+} to Ti^{4+}, is crystalline TiO_2. In turn, $[Al(urea)_6]Cl_3$ decomposes under argon atmosphere in three main steps and the final decomposition product above 920 K is $(ClAlNH)_n$, which can be converted to nanocrystalline *c*- and *h*-AlN under NH_3 atmosphere.[2]

Crystal structure and thermal behaviour of six-coordinate compounds of the $[M(urea)_6]X_3$ type, with M = Mn^{3+}, Al^{3+}, Ti^{3+}, V^{3+} and X = ClO_4^-, ClO_3^-, NO_3^-, Cl^-, I^-, have been already investigated.[4-15] $[Mn(urea)_6](ClO_4)_3$ undergoes one phase transition between 290 and 317 K detected by different scanning calorimetry (DSC) method.[9] A second order phase transition has been also observed in $[Al(urea)_6](ClO_4)_3$ at ca. 295 K and in $[Ga(urea)_6](ClO_4)_3$ at ca. 301 K, by Mooy et al. using electron spin resonance (ESR) method.[10-12] These transitions are of the second order and antiferro-distortive and of displacive type. In the model proposed the phase transition was triggered by ordering of the oxygen atoms orientation in the perchlorate ions, half of which are assumed to be disordered above T_C .

The compounds of the $[M(urea)_6](ClO_4)_3$ type with M=Mn^{3+}, Al^{3+}, Ti^{3+} and V^{3+} are isomorphous at room temperature and crystallize in the hexagonal space group *R*-3*c* with *Z*=6.[11,13-15] In all mentioned compounds the perchlorate anions of tetrahedral symmetry are disordered. The structure consists of a two-dimensional close-packed arrangement of trigonally distorted octahedral $[M(urea)_6]^{3+}$ units in columns parallel to the *c* axis. In the columnar interstices the perchlorate ions are arranged in spiral fashion. The structure is loosely linked by hydrogen bonding net and van der Waals contacts.

The crystal structure of $[Ti(urea)_6](ClO_4)_3$ was also investigated at 90 K.[15] At this temperature it crystallizes in the same space group *R*-3*c*. The lattice parameter *c* is slightly smaller than the high-temperature value, but the parameter *a* is nearly twice as large as the one observed in high-temperature phase. The doubling value of parameter *a* is attributed to freezing out of the perchlorate ions below the phase transition temperature. So far, there is no information in literature about phase behaviour of the $[M(urea)_6](BF_4)_3$ compounds.

Among six coordination metal(III) complexes with ClO_4^- and BF_4^- tetrahedral anions, the phase polymorphism of $[M(NH_3)_6](ClO_4)_3$[16-18] and $[M(NH_3)_6](BF_4)_3$,[19-21] $[M(H_2O)_6](ClO_4)_2$,[22-23] and $[M(DMSO)_6](ClO_4)_2$[24-25] has been thoroughly investigated.

The main subject of the present paper is spectroscopic, structural and thermal characterization and investigation of phase polymorphism of three $[Cr(OC(NH_2)_2)_6]X_3$ ionic compounds, with ClO_4^-, BF_4^-, and Cl^- anions, using vibrational (FT-IR and FT-Raman) and electronic (UV-Vis) spectroscopies, X-ray single crystal diffraction (XRSCD), differential scanning calorimetry (DSC), and thermogravimetry analysis (TG/QMS).

Experimental

Materials and methods

Synthetic procedures. $[Cr(urea)_6]Cl_3$ (hereafter referred to as CrUCl) was prepared according to the method proposed by A. Werner.[26] $[Cr(urea)_6](ClO_4)_3$ (CrUClO) and $[Cr(urea)_6](BF_4)_3$ (CrUBF) were synthesized at room temperature by dissolving 1 gram of $[Cr(urea)_6]Cl_3$ in 20 ml of double distilled water and then stoichiometric amounts of aqueous solution of NH_4ClO_4 (99% purity, Sigma Aldrich) or $NaBF_4$ (99% purity, Sigma Aldrich), respectively, were added. The green precipitates formed as very fine needles were washed with distilled water and dried in air at 60 °C in order to remove water. They were stored in sealed containers in a desiccator over P_4O_{10}. The contents of carbon, nitrogen and hydrogen of the $OC(NH_2)_2$ (urea) ligands in the compounds investigated were determined from elemental analysis using a CHNS Vario Micro Cube instrument with a TCD detector. Calculated % for CrUCl: C, 13.89, N, 32.40; H, 4.66. Found %: C, 13.69, N, 32.23; H, 4.60. Calculated % for CrUClO: C, 10.14, N, 23.65; H, 3.40. Found %: C, 10.11, N, 23.46; H, 3.42. Calculated % for CrUBF: C, 10.71, N, 24.98; H, 3.60. Found %: C, 10.61, N, 24.89; H, 3.50. The presence of six urea ligands in the $[Cr(urea)_6]^{3+}$ cation unit of all three compounds investigated in the examined samples was confirmed.

FT-IR. Fourier transform middle infrared absorption (FT-MIR) spectra (4000–500 cm^{-1}) were performed using a Bruker VERTEX 70v vacuum spectrometer. The globar as a light source and a DTGS detector were used. The spectra were collected with a resolution of 2 cm^{-1} and 32 scans per each spectrum. The powdered samples were suspended in KBr pellets. Fourier transform far infrared absorption (FT-FIR) spectra (500–100 cm^{-1}) were collected for samples suspended in Apiezon N grease and placed on a polyethylene (PE) disc. The spectra were collected with a resolution of 2 cm^{-1} and 64 scans per spectrum.

FT-RS. Fourier transform Raman light scattering spectra were obtained with a Multi-RAM FT-Raman Bruker spectrometer at a frequency range 4000–50 cm^{-1}, with a resolution of 4 cm^{-1} and with 256 scans accumulated per each spectrum. A YAG Spectra-Physics Neodymium laser was used with incident radiation $\lambda = 1064$ nm.

UV-VIS. A Shimadzu UV–2101PC spectrophotometer equipped with ISR-260 attachment was used to record the electronic reflectance spectra in $BaSO_4$ pellets with $BaSO_4$ as a reference. The spectra were recalculated to absorbance units using the Kubelka–Munk transformation.

XRSCD. X-ray single crystal diffraction measurement was performed at 293 K for $[Cr(urea)_6](BF_4)_3$ using an Oxford Diffraction SuperNova four-circle diffractometer. Needle shaped green crystal of good quality was investigated. Crystallographic data have been deposited at the CCDC, 12 Union Road, Cambridge CB2 1EZ, UK. The deposition number is 995339.

DSC. Differential scanning calorimetry (DSC) measurements were conducted between 130 and 400 K using a Mettler-Toledo 822^e instrument. Powdered samples of $[Cr(urea)_6](ClO_4)_3$, $[Cr(urea)_6](BF_4)_3$, and $[Cr(urea)_6]Cl_3$ with masses of 8.45, 5.65, and 5.88 mg, respectively, were placed in hermetically sealed aluminium pans and measured with a scanning rate of 20 K min^{-1}. The transition temperatures were considered to be the peak temperature (T_{peak}) from the DSC curves on heating and cooling. Additional DSC measurement was conducted during heating for the $[Cr(urea)_6](ClO_4)_3$ sample placed in hermetically sealed aluminium pan with a hole on top with a scanning rate of 10 K min^{-1} in temperatures between 135 and 570 K. The sample mass was 2.63 mg. Additional DSC measurements were performed at 93–297 K with a Perkin Elmer PYRIS 1 DSC apparatus. The instrument was calibrated using the literature data for indium and water melting points. The enthalpy change (ΔH) was calculated by numerical integration of the DSC curve under the anomaly peak after a linear background arbitrary subtraction. The entropy change (ΔS) was calculated using the formula: $\Delta S = \Delta H/T_C$. The powdered samples were placed in aluminium vessels and closed by compression. The measurements were made both on heating and on cooling a freshly synthesized samples of $[Cr(urea)_6](ClO_4)_3$ and $[Cr(urea)_6](BF_4)_3$ of masses equal to 9.37 and 7.60 mg, respectively, with constant scanning rate of 20 K min^{-1}.

TGA. To characterize the samples further, thermal analysis was performed using thermogravimetry with simultaneous differential thermal analysis (TGA/DTG/SDTA) by means of a Mettler-Toledo TGA/SDTA 851e instrument. The gaseous products evolved from decomposition were identified on an on-line quadruple mass spectrometer (QMS) using a Balzer GSD 300T instrument. Powdered samples of $[Cr(urea)_6](ClO_4)_3$, $[Cr(urea)_6](BF_4)_3$, and $[Cr(urea)_6]Cl_3$ with masses of 3.719, 9.157, and 11.071 mg, respectively, were placed in open corundum crucible and measured with a scanning rate of 10 K min^{-1}. The measurements were performed at 300–1270 K with a constant flow (80 mL min^{-1}) of dry argon (99.999 %).

Results and discussion

Vibrational spectra (FT-IR and FT-RS)

The complex cation $[Cr(urea)_6]^{3+}$ is expected to have octahedral symmetry with the $OC(NH_2)_2$ ligands being coordinated to the central cation Cr^{3+} through oxygen atoms. The FT-IR and FT-RS band positions, their relative intensities and their tentative assignments are listed in Table 1. Comparison of the IR and Raman spectra of all three compounds are summarized in Fig. 1.

The proper assignment of the bands observed in FT-IR and FT-RS spectra of the chromium(III) compounds studied was done by comparison with the spectra obtained for pure urea and similar hexakis(urea-O)metal(III) coordination compounds published earlier.[1,2,27–29] Clearly, the strong C=O stretching vibration observed for free urea molecule at 1684 cm^{-1}, strongly coupled with $\delta_s(NH_2)$ mode, is shifted toward lower frequency in the case of urea molecules octahedrally coordinated to central metal through oxygen atoms. In turn, the C-N stretching vibration observed for free urea at 1466 cm^{-1} shifts toward higher frequency in case of all three compounds studied. Overall, the assignment proved that the molecular structures of the investigated compounds are such as expected.

 DOI: 10.17628/ecb.2014.3.474-481

Table 1. List of band positions of FT-IR and FT-Raman spectra of $[Cr(urea)_6]X_3$, where X = ClO_4^-, BF_4^-, and Cl^- with tentative assignments.

FT-IR, cm^{-1}			FT-Raman, cm^{-1}			Tentative assignments
ClO_4^- in 310 K	**BF_4^- in 293 K**	**Cl^- in 293 K**	**ClO_4^- in 293 K**	**BF_4^- in 293 K**	**Cl^- in 293 K**	
3491 st	3504 st	3451 vst	3485 w	3503 w	3442 sh	$\nu_{as}(NH_2)$
3477 sh			3479 w	3411 m		$\nu_{as}(NH_2)$
3374 st	3392 st	3352 vst	3397 m	3386 sh	3340 m	$\nu_s(NH_2)$
			3371 sh		3267 sh	$\nu_s(NH_2)$
3252 w	3261 w	3202 vst			3208 m	$\delta_s(NH_2)+\nu(CO)$
3199 w	3203 w					$\delta_s(NH_2)+\nu(CO)$
3133 w	3142 w					$\delta_s(NH_2)+\nu(CO)$
		2794 br,m				
1662 sh	1670 sh	1634 vst		1651 w,sh	1690 vw	$\delta_s(NH_2)$
1632 vst	1635 st		1630 w	1633 w	1647 w	$\delta_{as}(NH_2)$
					1618 w	$\delta_{as}(NH_2)/\nu(CO)$
1554 st	1557 st	1568 st	1566 w	1570 m	1580 sh	$\nu(CO)$
1545 sh	1548 sh	1553 sh	1557 m	1560 w,sh	1564 m	$\nu(CO)+\delta(NH_2)$
1510 m	1513 m	1499 st	1505 m	1507 m	1499 m	$\nu_{as}(CN)$
1500 sh		1466 st				
		1402				
	1296 w					
1150 sh	1155 sh	1161 sh	1144 vw	1150 w	1176 w	$\rho(NH_2)$
1091 st			1105 w			$\nu_{as}(ClO)F_2$
1036 sh	1043 vst	1034 sh	1042 st	1042 st	1040 st	$\nu_s(CN)$
	1029 vst,sh			1005 w,sh		$\nu_{as}(BF)F_2$
942 w,sh			938 vst			$\nu_s(ClO)A_1$
910 w,sh			911 sh			
825 vw,br			826 vw			
770 w	771 vw	764 m	774 w	784 vw		$\omega(CO)$
				770 vst		$\nu_s(BF)A_1$
758 w	758 w		760 w	758 vw	765 vw	$\tau_{as}(NH_2)$
	685w					
635 sh	631 st	634 m	629 st	628 st	631 st	
626 st			606 w,sh			$\delta_{as}(ClO)F_2$
	579 w	560 m				$\delta(CO)$
544 st	543 st	546 m	546 w	546 m	557 st	$\delta(CN)$
537 st		538 m	531 w		535 m	
	530 sh			530 m		$\delta_{as}(BF)F_2$
504	502 w					$\omega_a(NH_2)$
			465 st			$\delta_s(ClO)E$
450 w,br	425 m,br	462 m,br	458 st,sh			$\nu(M-O)$
377 st	371 st	389 st				
	349 sh			355 w		$\delta_s(BF)E$
311 w			309 w	308 w	312 w	
		252 w	273 vw	273 vw	280 vw	(O-Cr-O)
224 m	224 m	230 w	217 w			(O-Cr-O)
	216 sh	195 w		202 w	203 m	
	200 m					
198 m	192 m					
	185 w					
144 m	147 w	166 w	158 sh		167 m	Lattice
			114 vst	115 vst	103 vst	Lattice
			76 m,sh	73 m,sh	81 vst	Lattice

(vw – very weak, w – weak, sh – shoulder, m – medium, st – strong, vst – very strong, br – broad, ρ – rocking, τ – torsional, ω – wagging).

Electronic spectra (UV-Vis)

For further verification of the composition of the title compounds the UV-Vis spectra were measured. The results are presented in Fig. 2.

The electronic spectra of all three hexakis(urea-O)chromium(III) compounds, which have octahedral symmetry, are very similar and are essentially independent of the anion in the lattice. According to crystal field theory for the d^3 electronic configuration in octahedral ligand environment

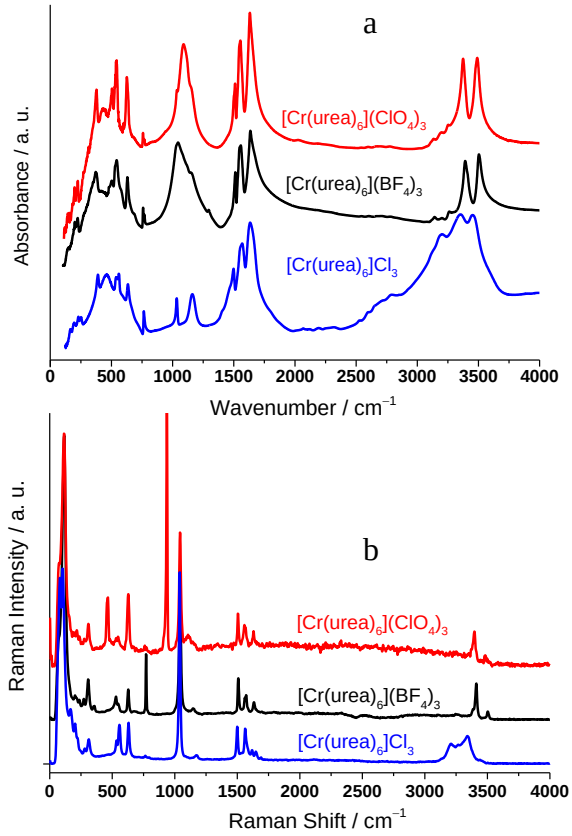

Figure 1. Comparison of experimental FT-IR (a) and FT-Raman (b) spectra of all three compounds investigated.

the lowest energy state for investigated compounds is designated to $^4A_{2g}$, thus exhibit three spin-allowed transitions from the ground state $^4A_{2g}$ to the excited states: $^4T_{2g}(F)$, $^4T_{1g}(F)$ and $^4T_{1g}(P)$, in order of increasing energy.[30-32] In the spectrum of [Cr(urea)$_6$](ClO$_4$)$_3$ there are indeed three main bands observed at: 608, 446, and 288 nm, which are attributed to $^4A_{2g} \rightarrow {}^4T_{2g}(F)$, $^4A_{2g} \rightarrow {}^4T_{1g}(F)$ and $^4A_{2g} \rightarrow {}^4T_{1g}(P)$ transitions, respectively. The band positions of the other two compounds investigated, namely [Cr(urea)$_6$](BF$_4$)$_3$ and [Cr(urea)$_6$]Cl$_3$, appear almost at the same wavelengths. The bands positions observed in the electronic spectra together with their assignments are presented in Table 2. The electronic spectra (Fig. 2) additionally confirm the proper composition of the title complexes.

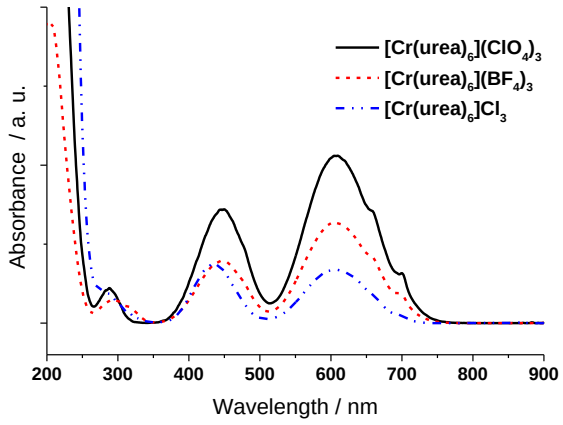

Figure 2. Electronic spectra obtained at room temperature for all three compounds investigated.

Table 2. Wavelengths and frequencies (nm/cm^{-1}) of the observed d-d transitions in Cr-urea complexes.

[Cr(urea)$_6$]X$_3$	$^4A_{2g} \rightarrow {}^4T_{2g}(F)$	$^4A_{2g} \rightarrow {}^4T_{1g}(F)$	$^4A_{2g} \rightarrow {}^4T_{1g}(P)$
Perchlorate	608/16447	446/22422	288/34722
Tetrafluoroborate	605/16529	448/22321	294/34014
Chloride	607/16474	434/23041	~273/36630

Crystal structure of [Cr(urea)$_6$](BF$_4$)$_3$ at 293 K

In order to check if [Cr(urea)$_6$](BF$_4$)$_3$ coordination compound is isostructural to [Cr(urea)$_6$](ClO$_4$)$_3$ and [Cr(urea)$_6$]Cl$_3$ investigated earlier[32] the X-ray single crystal diffraction measurement was performed. Table 3 presents experimental details of this experiment at 293 K.

Table 3. Crystallographic data for [Cr(urea)$_6$](BF$_4$)$_3$ at 293 K.

CCDC	995339
Crystallographic method	Single-crystal diffraction
Radiation	μ(MoKα) (λ = 0.71073 Å)
Empirical formula	$C_6H_{24}B_3F_{12}N_{12}O_6Cr$
Formula weight	672.80 g mol^{-1}
Crystal size	0.500 x 0.100 x 0.050 mm^3
Temperature	293(2) K
Crystal system	Trigonal
Space group	*R*-3*c* (No. 167)
Unit cell dimensions	*a* = 17.8250(5) Å
	b = 17.8250(5) Å
	c = 13.9010(8) Å
	$\alpha, \gamma = 90°, \beta = 120°$
Volume	3825.0(3) Å^3
D_{calc}	1.752 g cm^{-1}
Z	6
F_{000}	2034
Θ range for data collect.	2.28 to 27.62°
Reflections collected	8903
Independent reflections	989 (R_{int}=0.0416)
Refinement method	Full-matrix least-squares on F^2
Data/restrains/parameters	989/4/89
Goodness of Fit on F^2	1.208
Final *R* indices [I> 2sigma(I)]	R_1 = 0.0471, wR_2 = 0.1317
R indices (all data)	R_1 = 0.0608, wR_2 = 0.1578

The [Cr(urea)$_6$](BF$_4$)$_3$ compound studied crystallizes in the trigonal space group *R*-3*c* with lattice parameters *a* = b = 17.8250(5) Å, *c* = 13.9010(8) Å, and $\alpha, \gamma = 90°, \beta = 120°$, and *Z* = 6. Figure 3 presents a grow fragment in the unit cell and the molecular packing viewed along the c axis of [Cr(urea)$_6$](BF$_4$)$_3$. Each Cr^{3+} cation is coordinated by six urea molecules through oxygen atoms with all the Cr–O distances equivalent and equal to 1.963 Å and with the O–Cr–O bond angles ranging from 92.72 to 85.56°. All BF_4^- anions exhibit dynamical disorder at this temperature. Detailed geometrical parameters with atomic coordinates and isotropic displacement parameters are listed in Table 4 and selected bond lengths and angles are compared in Table 5.

 DOI: 10.17628/ecb.2014.3.474-481

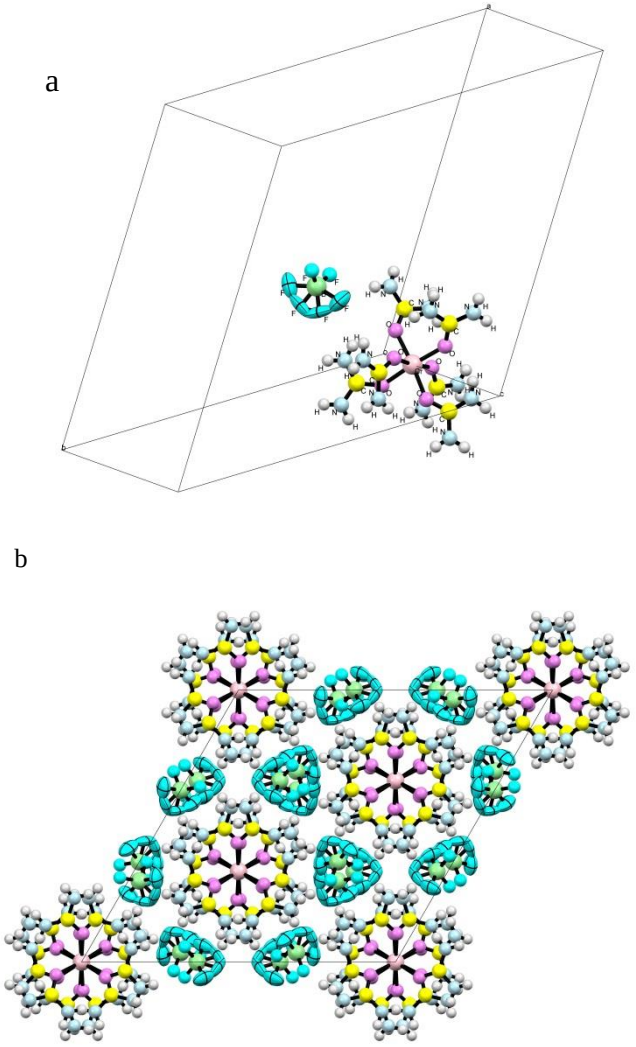

Figure 3. A view of (a) a grow fragment and (b) molecular packing of the unit cell along *c* axis of [Cr(urea)$_6$](BF$_4$)$_3$ at 293 K.

Phase transition investigations

Two temperature dependences of the heat flow (two DSC curves) of the [Cr(urea)$_6$](ClO$_4$)$_3$ and [Cr(urea)$_6$](BF$_4$)$_3$ samples registered during cooling (lower curves) and subsequent heating (upper curves) with a scanning rate of 20 K min^{-1} are presented in Fig. 4.

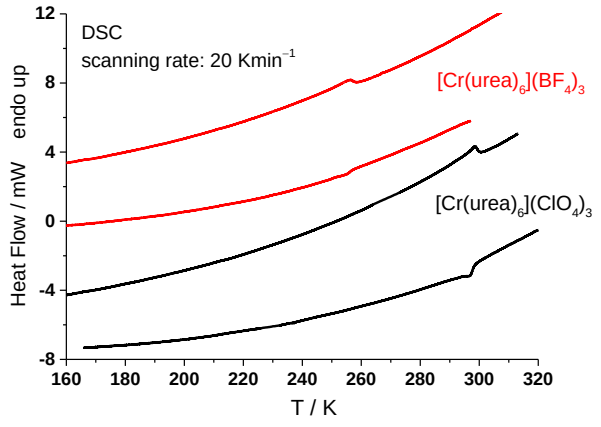

Figure 4. DSC curves for [Cr(urea)$_6$](BF$_4$)$_3$ and [Cr(urea)$_6$](ClO$_4$)$_3$ registered on cooling (lower curves) and heating (upper curves) with a scanning rate of 20 K min^{-1}.

Table 4. Atomic coordinates and equivalent isotropic displacement parameters U_{eq}/ (10^3 Å^2) for the structure obtained for [Cr(OC(NH$_2$)$_2$)$_6$](BF$_4$)$_3$ at 293 K.

Atom	*x*	*y*	*z*	*U*(eq)
Cr(1)	0.0000	0.0000	0.2500	0.033(1)
O(1)	0.1045(1)	0.0571(1)	0.1699(1)	0.042(1)
N(3)	0.1345(2)	-.0476(2)	0.1296(2)	0.062(1)
N(4)	0.2348(2)	0.0945(2)	0.1109(2)	0.061(1)
C(2)	0.1561(2)	0.0339(2)	0.1368(2)	0.042(1)
F(11)	0.3101(2)	0.2772(2)	0.0298(2)	0.091(1)
F(12A)	0.2224(4)	0.3121(1)	0.1144(12)	0.119(9)
F(12B)	0.2489(9)	0.2740(5)	0.1619(7)	0.114(5)
B(1)	0.2981(3)	0.3333	0.0833	0.055(1)
H(3A)	0.086(2)	-0.090(2)	0.142(3)	0.068(12)
H(4A)	0.249(2)	0.1468(14)	0.112(3)	0.061(10)
H(3B)	0.173(2)	-0.059(2)	0.111(3)	0.069(10)
H(4B)	0.271(2)	0.084(2)	0.081(3)	0.070(11)

U_{eq} is defined as one third of the trace of the orthogonalized U^{ij} tensor.

Table 5. Selected interatomic distances (Å) and angles (°) in [Cr(urea)$_6$](BF$_4$)$_3$ determined from XRSCD at 293 K.

Bond	Distances (Å)
Cr(1)–O(1)	1.9630(17)
O(1)–C(2)	1.268(3)
N(3)–C(2)	1.307(3)
N(4)–C(2)	1.323(4)
F(11)–B(1)	1.347(3)
F(12A)–B(1)	1.280(7)
F(12B)–B(1)	1.467(7)
N(3)–H(3A)	0.830(18)
N(3)–H(3B)	0.846(19)
N(4)–H(4A)	0.835(19)
N(4)–H(4B)	0.864(19)
Bond	**Angles (°)**
O(1)–Cr(1)–O(1)#1	85.56(10)
O(1)–Cr(1)–O(1)#2	90.97(8)
O(1)#1–Cr(1)–O(1)#2	174.97(9)
O(1)–Cr(1)–O(1)#3	90.97(8)
O(1)#1–Cr(1)–O(1)#3	92.72(10)
C(2)–O(1)–Cr(1)	133.74(17)
C(2)–N(3)–H(3A)	125(3)
C(2)–N(3)–H(3B)	118(3)
C(2)–N(4)–H(4A)	121(3)
C(2)–N(4)–H(4B)	124(2)
O(1)–C(2)–N(3)	122.2(2)
O(1)–C(2)–N(4)	118.5(3)
N(3)–C(2)–N(4)	119.3(3)
F(11)–B(1)–F(11)	116.0(4)
F(12A)–B(1)–F(12B)	51.3(5)

One small and broad anomaly at T^h_C=298.4 K (on heating) and T^c_C=296.7 K at (on cooling) can be observed for [Cr(urea)$_6$](ClO$_4$)$_3$. Also, one small and broad anomaly can be observed for [Cr(urea)$_6$](BF$_4$)$_3$, but it is shifted almost 40 K to lower temperature, namely: T^h_C=255.4 K (on heating)

 DOI: 10.17628/ecb.2014.3.474-481

and T^c_C=254.5 K at (on cooling). Thus, both compounds exhibit one solid-solid phase transition. We did not observe any phase transition in $[Cr(urea)_6]Cl_3$ in the temperature range investigated. The thermodynamic parameters of these transitions are shown in Table 6. Small thermal hysteresis (less than 2 degree) suggest that both phase transitions are rather of order-disorder type and are not connected with a large structural change.

Table 6. Thermodynamic parameters of the phase transition observed in $[Cr(urea)_6](ClO_4)_3$ and $[Cr(urea)_6](BF_4)_3$, obtained with a scanning rate of 20 K min^{-1}.

	T_C, K	ΔH, J mol^{-1}	ΔS, J K^{-1} mol^{-1}
$[Cr(urea)_6](ClO_4)_3$			
Heating	298.4	1784	6.0
Cooling	296.7	2009	6.8
$[Cr(urea)_6](BF_4)_3$			
Heating	255.4	1630	6.4
Cooling	254.5	1460	5.7

Interestingly, the observed phase transition in $[Cr(urea)_6](ClO_4)_3$ occurs at very similar temperature (T^h_C=298.4 K) to the ones observed in $[Ru(NH_3)_6](ClO_4)_3$ (T^h_C=290.3 K) detected by adiabatic calorimetry[17] and $[Cr(NH_3)_6](ClO_4)_3$ (T^h_C=293.5 K) detected by DSC.[18] In turn, the transition in $[Cr(urea)_6](BF_4)_3$ occurs at similar temperature (T^h_C=255.4 K) to the ones observed in $[Ru(NH_3)_6](BF_4)_3$ (T^h_C=241.6 K)[19], $[Co(NH_3)_6](BF_4)_3$ (T^h_C=271.7 K)[20], and $[Cr(DMSO)_6](BF_4)_3$ (T^h_C=247.4 K)[33], all of them detected by adiabatic calorimetry. It confirms an important role of the anion in phase transition mechanism.

Thermal stability (TG/ DTG/QMS)

DSC curve obtained during heating of the $[Cr(urea)_6](ClO_4)_3$ sample is presented in Fig. 5. The sample is stable up to about 500 K. Above this temperature large exothermic upturn above 550 can be observed which is a result of explosive decomposition. About the same temperature of decomposition was obtained by us for the sample measured in an open corundum crucible (without a lid). The inset to Fig. 5 shows a magnified view of heat flow between 250 K and 340 K. A small endothermic peak can be observed at about 300 K, which is associated with the solid-solid phase transition previously described.

The TG, DTG and QMS curves for $[Cr(urea)_6](BF_4)_3$ are presented in Fig.6. The masses of *m/e* = 43, 17, 16, 28, 44, 18, 27, 30, 26, 48, 19, and 46 correspond to fragments of HNCO, NH_3 or OH, O or NH_2, N_2, BNF or CO_2 or N_2O, H_2O, HCN, NO or BF, CN, BF_2, F, and NO_2, respectively. The thermal decomposition of the sample proceeds in three main stages. The sample is thermally stable up to about 470 K. Above this temperature in the range of 470–510 K it decomposes liberating two urea ligands. 83.6 % of the initial mass of the sample remains at 510 K, and this value corresponds well to the theoretical amount (82.2 %) of tetrakis(urea)chromium(III) tetrafluoroborate. In the second stage in the range of 510–655 K, most probably the next four urea molecules are liberated and the decomposition products of urea react with chromium(III) tetrafluoroborate creating an intermediate adducts.

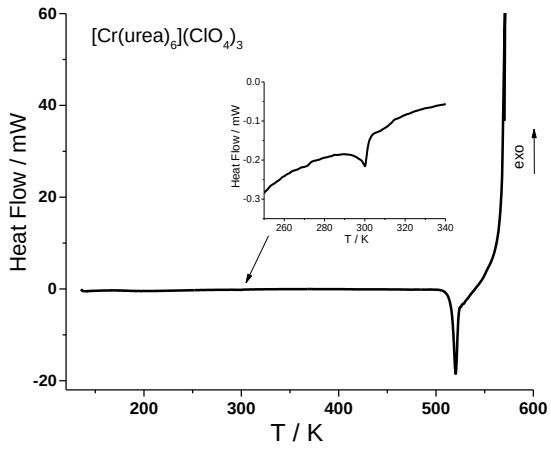

Figure 5. DSC curve for $[Cr(urea)_6](ClO_4)_3$ registered on heating with a constant rate of 10 K min^{-1}.

Both processes occur simultaneously but the exact mechanism of the second stage of decomposition is difficult to identify. In the third stage in the range of 655–1250 K, the intermediate adduct decomposes with further liberating of N_2, NO_2, F, CN, and HCN among others (see QMS lines in Fig. 6). The final product of thermal decomposition of $[Cr(urea)_6](BF_4)_3$ at 1250 K is chromium(III) oxide (Cr_2O_3) what was confirmed by us with FT-IR spectroscopy.

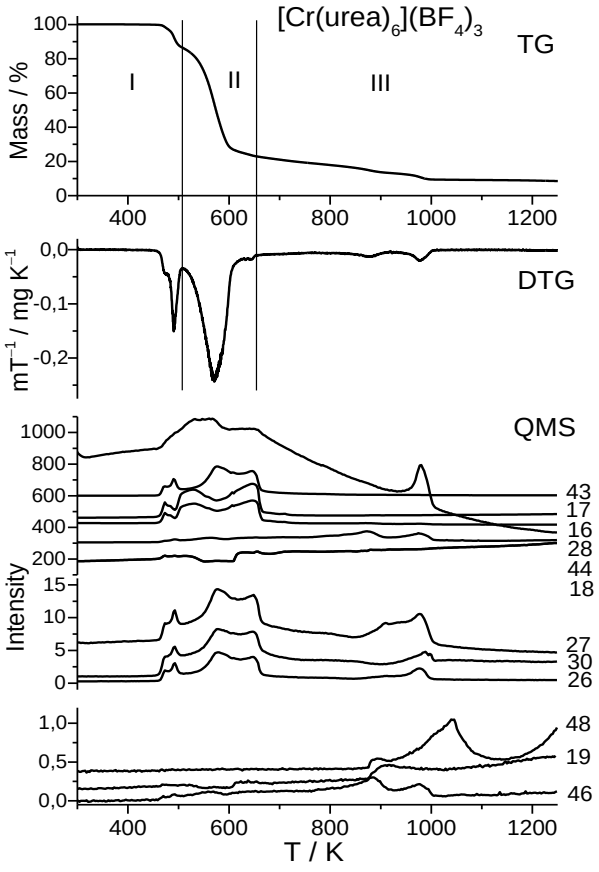

Figure 6. TG, DTG, and QMS curves obtained for $[Cr(urea)_6](BF_4)_3$ during heating with a constant rate of 10 K min^{-1}.

 DOI: 10.17628/ecb.2014.3.474-481

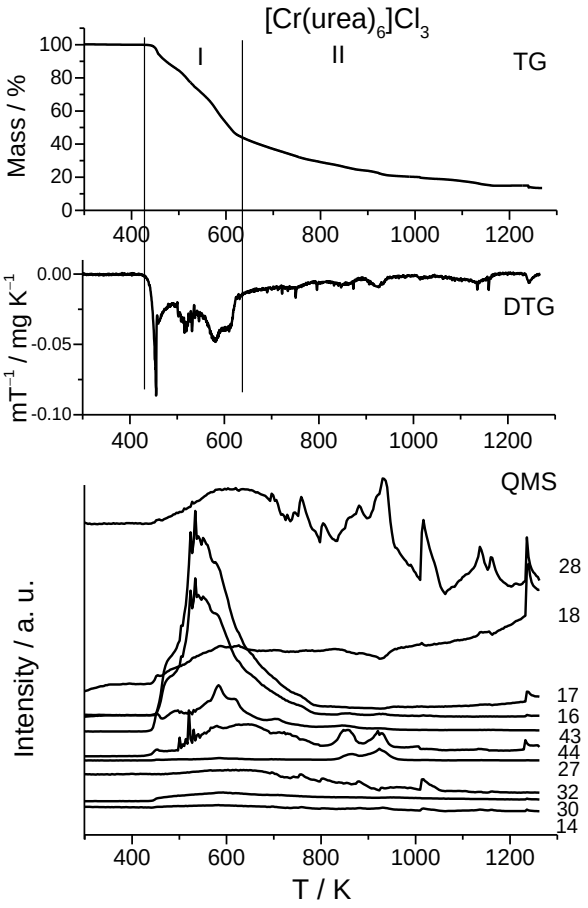

Figure 7. TG, DTG, and QMS curves obtained for [Cr(urea)$_6$]Cl$_3$ during heating with a constant rate of 10 Kmin^{-1}.

The TG-DSC analysis of [Cr(urea)$_6$]Cl$_3$ was already performed in the temperature range of 300–1070 K, in argon flow, at heating rate of 10 Kmin^{-1} by Qiu and Gao[34]. The compound is thermally stable up to 440 K. It decomposes in two main stages. In the first stage, between 440 and 620 K, the Cr–O coordination bonds break and disintegration of the urea molecules occurs with formation of solid CrCl$_3$·xNH$_3$. In the second stage, between 620 and 1070 K, most possibly the final solid (ClCrNH)$_n$ is created with releasing of volatile HCl and NH$_3$.

We reinvestigated the decomposition of [Cr(urea)$_6$]Cl$_3$ compound in the temperature range 300–1270 K using quadruple mass spectroscopy to analyze the gases evolved during TGA analysis. The TG, DTG, and QMS curves for [Cr(urea)$_6$]Cl$_3$ are shown in Fig. 7. The masses of *m/e* = 28, 18, 17, 16, 43, 44, 27, 32, 30, and 14 correspond to fragments of N$_2$, NH$_4$, NH$_3$, O or NH$_2$, HNCO, CO$_2$ or N$_2$O, HCN, O$_2$, NO, and N, respectively. The decomposition of the sample proceeds in two main stages. The TG curve shows that the composition is almost unchanged until 440 K. In the temperature range of 440–630 K it decomposes liberating and degrading the urea ligands and possibly creating an adduct such as CrCl$_3$·*x*NH$_3$. 45.0 % of the initial mass of the sample remains at 630 K what corresponds well to the CrCl$_3$·*x*NH$_3$ with *x* between 4 and 5. In the second stage, further degradation of urea molecules occurs together with constant releasing of chlorine. At 1270 K the thermal decomposition is not completely finished. 14.0 % of the initial mass of the sample remains at this temperature and we assume that the solid remaining is the mixture of metallic Cr, CrCl$_3$ and ClCrNH.

Conclusions

Apart from elemental analysis the spectroscopic analysis of FT-IR and FT-RS spectra together with electronic spectra (UV-Vis) confirmed proper composition of the investigated compounds.

[Cr(urea)$_6$](BF$_4$)$_3$ crystallizes at 293 K in trigonal crystal system in space group *R*-3*c* with *a* = *b* = 17.8250(5) Å, *c* = 13.9010(8) Å, and α, γ = 90°, β = 120°. Each Cr^{3+} cation is coordinated by six oxygen atoms deriving from urea molecules. The BF_4^- anions are dynamically disordered. The compound is isostructural with [Cr(urea)$_6$](ClO$_4$)$_3$ and [Cr(urea)$_6$]Cl$_3$.

One solid-solid phase transition has been detected in [Cr(urea)$_6$](ClO$_4$)$_3$ at: T^h_C=298.4 K and in [Cr(urea)$_6$](BF$_4$)$_3$ at: T^h_C=255.4 K. Both transitions are characterized by very small thermal hysteresis (ca. 1-2 K) and are most probably of order-disorder type.

In argon atmosphere, [Cr(urea)$_6$](ClO$_4$)$_3$ decomposes explosively just above 500 K. [Cr(urea)$_6$](BF$_4$)$_3$ decomposes in the range of 470–1250 K in three main stages with Cr$_2$O$_3$ being a final product of decomposition. The thermal decomposition of [Cr(urea)$_6$]Cl$_3$ proceeds in two main stages. The product of decomposition, which is still not finished at 1270 K, is a mixture of Cr, CrCl$_3$ and ClCrNH.

Acknowledgements

Thanks are due to Professor J. Szklarzewicz for UV-vis measurements. FT-IR and DSC (PYRIS 1) parts of the research were carried out with the equipment purchased thanks to the financial support of the European Regional Development Fund in the framework of the Polish Innovation Economy Operational Program (contract no. POIG.02.01.00-12-023/08).

References

[1]Li, J., Yang, X., Ishigaki, T., *J. Phys. Chem. B*, **2006**, *110*, 14611.

[2]Qiu, Y., Gao, L., *J. Am. Ceram. Soc*., **2004**, *87*, 352.

[3]Qiu, Y., Gao, L., *Int. J. Inorg. Mater*., **2004**, *19*, 63.

[4]Baker, J., Figgis, B. N., *Aust. J. Chem*., **1980**, *33*, 2377.

[5]Yersin, H., Otto, H., Gliemann, G., *Theoret. Chim. Acta*, **1974**, *33*, 63.

[6]Davis, P. H., Wood, J. S., *Chem. Phys. Lett*., **1969**, *4*, 466.

[7]Todorov, T., Petrova, R., Kossev, K., Macíček, J., Angelova, O., *Acta Cryst. C*, **1998**, *54*, 927.

[8]Figgis, B. N., Wadley, G. B., *J. Chem. Soc. Dalton Trans*., **1972**, 2182.

[9]Aghabozorg, H., Stoufer, R. C., Hall, J. H., *Amirkabir (J. Science & Technology)*, **1987**, *2*, 28.

[10]Mooy, J. H. M., de Jong, H. J., Glasbeek, M., van Voorst, J. D. W., *Chem. Phys. Lett*., **1973**, *18*, 51.

[11]Mooy, J. H. M., Krieger, W., Heijdenrijk, D., Stam, C. H., *Chem. Phys. Lett*., **1974**, *29*, 179.

[12]Mooy, J. H. M., Bolhuis, J., *Solid State Commun*., **1976**, *19*, 1005.

[13]Aghabozorg, H., Palenik, G. J., Stoufer, R. C., Summers, J., *Inorg. Chem*., **1982**, *21*, 3903.

[14]Figgis, B. N., Wadley, L. G. B., Graham, J., *Acta Crystallogr. B*, **1972**, *828*, 187.

[15]Figgis, B. N., Wadley, L. G. B., *Aust. J. Chem*., **1972**, *25*, 2233.

[16]Górska, N., Inaba, A., Hirao, Y., Mikuli, E., Hołderna-Natkaniec, K., *RSC Adv*., **2012**, *2*, 4283.

[17]Dołęga, D., Mikuli, E., Górska, N., Inaba, A., Hołderna-Natkaniec, K., Nitek, W., *J. Solid State Chem*., **2013**, *204*, 233.

[18]Mikuli, E., Górska, N., Wróbel, S., Ściesiński, J., Ściesińska E., *Z. Naturforsch. A*, **2007**, *62a*, 179.

[19]Dołęga, D., Mikuli, E., Inaba, A., Górska, N., Hołderna-Natkaniec, K., Nitek, W., *J. Solid State Chem*., **2013**, *197*, 429.

[20]Górska, N., Inaba, A., Hirao, Y., Mikuli, E., *J. Coord. Chem*., **2013**, *66*, 1238.

[21]Mikuli, E., Górska, N., Wróbel, S., Ściesiński, J., Ściesińska E., *J. Mol. Struct*., **2004**, *692*, 231.

[22]Mikuli, E., Migdał-Mikuli, A., Meyer, J., *J. Therm. Anal.*, **1998**, *54*, 93.

[23]Sinha, M. P., Pal, A., Dutta Roy, S. K., *J. Phys. C: Solid State Phys*., **1976**, *9*, 2783.

[24]Szostak, E., Migdał-Mikuli, A., Hołderna-Natkaniec, K., Gwoździk-Bujakowski, R., Kaczor, A., *J. Coord. Chem*., **2012**, *65*, 2732.

[25]Szostak, E., Migdał-Mikuli, A., *J. Therm. Anal. Cal*., **2010**, *101*, 601.

[26]Werner, A., *Lieb. Ann. Chem.*, **1902,** *322*, 296.

[27]Keuleers, R., Desseyn, H. O., Rousseau, B., Van Alsenoy, C., *J. Phys. Chem*., **1999**, *103*, 4621.

[28]Theophanides, T., *Coord. Chem. Rev*., **1987**, *76*, 237.

[29]Penland, R. B., Mizushima, S., Curran, C., Quagliano, J. V., *J. Am. Chem. Soc*., **1957**, *79*, 1575.

[30]Elving P. J., Zemel B., *J. Am. Chem. Soc*.,**1957**, *79*, 1281.

[31]Dingle, R., *J. Chem. Phys.*, **1969**, *50*, 1952.

[32]Witzke, H., *Theoret. Chim. Acta*, **1971**, *20*, 171.

[33]Górska, N., Inaba, A., Migdał-Mikuli, A., *Vib. Spectrosc*., **2012**, *62*, 222.

[34] Qiu, Y., Gao L., *Matter. Res. Bull*., **2003**, *38*, 1551.

Received: 15.03.2014.
Accepted: 08.04.2014.

STRUCTURE OF N-HYDROXY-4-PHENYLBUT-3-EN-2-IMINE

Preetika Sharma,[a] S. Samshuddin,[b] B. Narayana[b] and Rajni Kant[a]*

Keywords: oximes; intermolecular hydrogen bond; crystal structure; direct methods; N-hydroxy-4-phenylbut-3-en-2-imine

The title compound, N-hydroxy-4-phenylbut-3-en-2-imine [$C_{10}H_{11}NO$], was synthesized by reacting benzylideneacetone with hydroxylamine hydrochloride in the presence of base. The structure of the compound was characterized by single crystal XRD data. It crystallizes in the orthorhombic space group $Pbc2_1$ with unit-cell parameters: a= 5.591(6)Å, b=22.019(3)Å, c = 14.742(2) Å, β = 90.0º, Z = 4. The crystal structure has been elucidated by Direct methods and refined to a final R-value of 0.056 for 1535 observed reflections. In the crystal molecules are linked by two N-H...N intermolecular H-bonds forming dimer. Molecules in the unit cell are packed together to form well defined layers.

* Corresponding Authors
Fax: +91 191 243 2051
E-Mail: rkvk.paper11@gmail.com
[a] X-ray Crystallography Laboratory, Post-Graduate Department of Physics & Electronics, University of Jammu, Jammu Tawi - 180 006, India
[b] Department of Studies in Chemistry, Mangalore University, Mangalagangotri-574 199, India.

Introduction

Oximes are highly crystalline compounds that find applications in the protection, purification and characterization of carbonyl compounds.[1] The synthetic applications of oximes include their conversion into amides *via* Beckmann rearrangement, nitriles, nitro compounds, nitrones, amines, and azaheterocycles.[2-7] In coordination chemistry, oximes are act as a versatile ligand.[8] Moreover,oximes are also used as therapeutic agents in organophosphorus poisoning.[9]

Oximes are important intermediates for the preparation of primary amines by reduction. The primary amine generated can be used for the preparation of many heterocycles like quinoline, azetidinone, 1,2,4-triazole and 1,3,4-thiadiazole, benzothiazipines and thiazolidinone.[10] These heterocycles show various biological activities such as anti-cancer [11], anti-inflammatory[12], anti-allergics[13], anti-microbial[14] and anthelmintic.[15] In view of the importance of oximes and the fact that the crystal structure of the reduced form of the title compound viz. (E)-4-phenylbutan-2-one oxime[10] is known, we got interested in synthesis and the crystal structure determination of N-hydroxy-4-phenylbut-3-en-2-imine.

Experimental

Synthesis

The synthetic route for the title compound is presented in Scheme 1. A mixture of a 4 benzylideneacetone (1.46 g, 0.01 mole) and hydroxylamine hydrochloride (0.69 g, 0.01 mole) in 50 mL ethanolic sodium hydroxide was refluxed for 3 h, then cooled to room temperature. The precipitate that appeared was filtered off and recystallized from DMF. The single crystals were grown from DMSO by slow evaporation method and yield of the compound was 56 %. (m.p. 390 K).

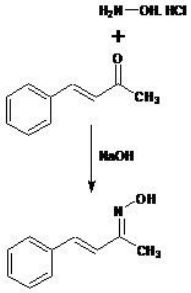

Scheme 1. Synthesis of the N-hydroxy-4-phenylbut-3-en-2-imine

X-Ray Structure determination

X-ray intensity data of 4425 reflections (of which 2378 unique) were collected at 293(2) K on *X*'calibur CCD area-detector diffractometer equipped with graphite monochromated Mo$K\alpha$ radiation (λ=0.71073 Å). The crystal used for data collection was of dimensions 0.30 X 0.20 X 0.10 mm. The intensities were measured by ω scan mode for θ ranges 3.95 to 26.98º. 1535 reflections were treated as observed (I>2σ(I)). Data were corrected for Lorentz-polarization and absorption factors. The structure was solved by direct methods using SHELXS97.[16]

All non-hydrogen atoms of the molecule were located in the best E-map. All the hydrogen atoms (except O1A, O1B, C10A and C10B H atoms) were geometrically fixed and allowed to ride on the corresponding non-H atoms with C-H= 0.93-0.98 Å and U_{iso} = 1.2 U_{eq}(C), except for the methyl groups where U_{iso}(H) = 1.5U_{eq}(C). The final refinement cycles converged to an R = 0.056 and wR(F2) = 0.144 for the observed 1535 reflections. Residual electron densities ranged from -0.177 to 0.168 eÅ^{-3}. Atomic scattering factors were taken from International Tables for X-ray Crystallography (1992, Vol. C, Tables 4.2.6.8 and 6.1.1.4). The crystallographic data are summarized in Table 1.

 DOI: 10.17628/ecb.2014.3.482-484

Table 1. Crystal data and other experimental details

CCDC Number	983555
Crystal description	Block
Crystal size	0.30 x 0.20 x 0.10 mm
Empirical formula	$C_{10}H_{11}NO$
Formula weight	322.40
Radiation, Wavelength	Mo *K*α, 0.71073 Å
Unit cell dimensions	*a* = 5.591(6), *b* = 22.019(3), *c* = 14.742(2) Å, α= 90.0º, β = 90.0º, γ= 90.0º
Crystal system, Space group	Orthorhombic,$Pbc2_1$
Unit cell volume	1814.9(4) $Å^3$
No. of molecules per unit cell, *Z*	4
Absorption coefficient	0.077 mm^{-1}
F(000)	688
θ range for entire data collection	3.95 < θ < 26.98
Reflections collected / unique	4425/ 2378
Reflections observed I > 2σ(I))	1535
Range of indices	*h*= -6 to 6, *k*= -27 to 24, *l*= -10 to 18
No. of parameters refined	276
Final R-factor	0.0557
wR(*F2*)	0.1442
R_{int}	0.0402
Rσ	0.0452
Goodness-of-fit	1.078
(Δ/σ)max	0.001
Final residual electron density	-0.177 < Δρ > 0.168 $eÅ^{-3}$-

Results and Discussion

An ORTEP[17] view of the title compound with atomic labelling is shown in Figure 1. The geometry of the molecule was calculated using the PLATON[18] and PARST[19] software. Selected bond lengths, bond angles and torsion angles are given in Table 2. Geometry of inter-molecular hydrogen bonds is given in Table 3.

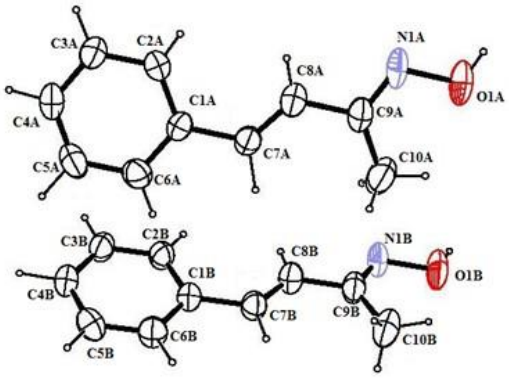

Figure 1. ORTEP view of the molecule with displacement ellipsoids drawn at the 40 % probability level. H atoms are shown as small sphere of arbitrary radii

The structure consists of two molecules in the asymmetric unit. Bond distances and bond angles are comparable with the reported structure (E)-4-phenylbutan-2-one oxime[10] except the bond distances C1A=C7A and C1B=C7B. The other geometrical parameters are comparable with some analogous structures.[20] The double bonds N1A=C9A and N1B=C9B are confirmed by their respective distances of 1.268(6) Å and 1.276(6) Å. The C7A=C8A (1.308 Å) and C7B=C8B (1.308 Å) bond distances are smaller than the standard value of 1.34Å.

The variation in bond angles around the atom C9A and C9B is primarily due to the existence of intermolecular hydrogen bond O-H...N. These O-H...N (O1A-H1...N1B and O1B-H2...N1A) intermolecular hydrogen bond are responsible for the formation of hydrogen bonded network thus, providing more stability to the molecules in the unit cell.

The best packing view has been obtained down a-axis i.e. bc plane (Figure 2).

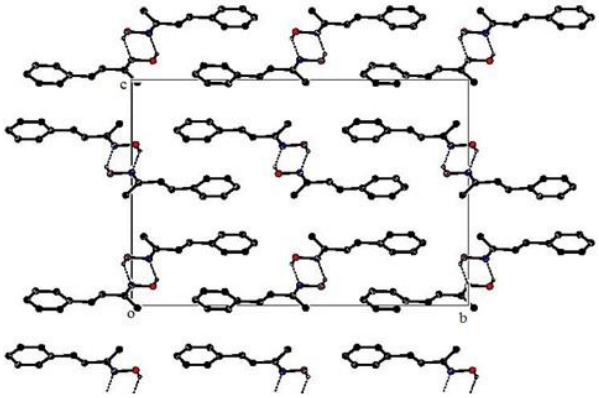

Figure 2. Packing diagram viewed down the a-axis

In the crystal packing, pairs of intermolecular hydrogen bonds (Table 3) link the molecules into dimmers (Figure 3) forming $R^2_2(6)$ ring motifs which are stacked along the *a* axis, forming a well defined layered structure (see Figure 2).

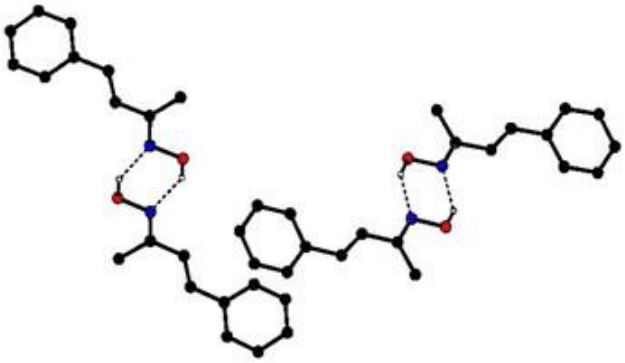

Figure 3. A plot of two molecules showing the formation of dimer by intermolecular N-H….N hydrogen bond (dashed lines).

Table 2. Selected bond lengths (Å) and bond angles (º) for non hydrogen atoms (e.s.d.'s are given in parentheses)

Bond distances, Å		**Bond angles,** º		**Torsion angles,** º	
N1A-O1A	1.410(5)	C8A-C9A-N1A	114.2(5)	C2B-C1B-C7B-C8B	179.4(5)
N1B-O1B	1.413(5)	C8B-C9B-N1B	113.4(5)	C2A-C1A-C7A-C8A	177.6(5)
C7A-C8A	1.308(7)	C9A-N1A-O1A	113.6(4)		
C7B-C8B	1.308(7)	C9B-N1B-O1B	113.1(4)		
C9A-N1A	1.268(6)	C2A-C1A-C7A	119.6(4)		
C9B-N1B	1.276(6)	C2B-C1B-C7B	119.1(4)		
		C8A-C9A-C10A	121.8(5)		
		C8B-C9B-C10B	122.2(5)		
		C10B-C9B-N1B	124.3(5)		
		C10A-C9A-N1A	124.0(5)		

Table 3. Geometry of intramolecular hydrogen bonds

D-H…A	**D-H, Å**	**H…A, Å**	**D…A, Å**	**θ[DH…A,], º**
O(1A)-H(1)...N(1B)^{i}	0.820(4)	2.061(5)	2.787(7)	147.3(3)
O(1B)-H(2)...N(1A)^{ii}	0.820(4)	2.105(5)	2.819(7)	145.5(3)

Symmetry codes:(i) -*x*+2, -*y*+1, +*z*+1/2 (ii) -*x*+2, -*y*+1, +*z*-1/2

References

[1]Sandier, S.R., Karo, W. *Organic functional group preparations*, 2nd edn. Academic Press: San Diego, **1989,** 431.

[2]Dewan, S.K., Singh, R. and Kumar, A. *Arkivoc*, **2006,** 2006, 41.

[3]Dave, P.R., Forshar, F. *J. Org. Chem*., **1996,** 61,8897.

[4]Ballistreni, F.P., Barbuzzi, E., Tomaselli, G.A. and Toscano, R.M. *Synletters*, **1996,** 11, 1093.

[5]Smith, P.A.S., Gloyer, S.E. *J. Org. Chem*., **1975,** 40, 2508.

[6]Negi, S., Matsukura, M., Mizuno, M., Miyake, K. And Minami, *N. Synthesis*,**1996,** 8, 991.

[7]Narasaka, K. *Pure Appl. Chem*., **2003**, 75, 19.

[8]Dong, W.-K., Sun, Y.-X., He, X.-N., Tong, J.-F. and Wu, J.-C. *Spectrochim. Acta Part A*, **2010,** 76, 476.

[9]Marrs, T. C., Rice, P., Vale, J. A. *Toxicol. Rev*., **2006,** 25, 297.

[10]Fun, H.-K., Loh, W.-S., Kayarmar, R., Dinesha and Nagaraja, G. K. *Acta Cryst*., **2011**, E67, o2332.

[11]El-Sabbagh, Abadi, H. I., Al-Khawad, A. H. and Al Rashood, I. E. K. A. *Arch. Pharm. Pharm. Med. Chem.*, **1990,** 333, 19.

[12]El-Sayed, O. A., El-Semary,M. and Khalid, M. A. *Alex. J. Pharm. Sci.*, **1996,** 10, 43.

[13]Althuis, T. H., Moore, P. F. and Hess, H. J. *J. Med. Chem.* **1979,** 22, 44.

[14]Nargund, L. V. G., Badiger, V. V. and Yarnal, S.M. *J. Pharm. Sci.*, **1992,** 81, 365.

[15]Srivastava, S. K., Yadav, R. and Srivastava, S. D. J. *Indian Chem. Soc*., **2004,** 81,342.

[16]Sheldrick, G. M. *Acta Cryst*.,**2008**, *A64*, 112.

[17]Farrugia, L. J. *J. Appl. Cryst*., **1999**, *32*, 837.

[18]Spek, A. L. *Acta Cryst*., **2009,** *D65*, 148.

[19]Nardelli, M. *J. Appl. Cryst.*, **1995,** *28*, 659.

[20]Allen, F. H., Kennard,O., Watson,D.G., Brammer,L., Orpen,A.G., and Taylor,R. *J. Chem.Soc., Perkin Trans-II*., **1987**, S1

Received: 12.03.2014.
Accepted: 08.04.2014.

MICROWAVE ASSISTED SYNTHESIS OF COBALT PHOSPHATE NANOPARTICLES

Wenying Wang[a][b], Baofeng Zheng[a], Zhu Liu[a] and Guoqiang Zhou[a][b]*

Keywords: Cobalt(II) phosphate; nanoparticles; microwave radiation; X-ray diffraction.

The uniform cobalt phosphate nanoparticles were successfully synthesized by microwave radiation. The effects of microwave irradiation power and reaction time on the treatment process were investigated. The products synthesized were analyzed by field emission scanning electron microscopy, X-ray powder diffraction, Fourier-transform infrared spectroscopy, thermal gravimetric analyses and dynamic light scattering. In this research, the products were cobalt phosphate phase with nanoparticles over the ranges of 60-80 nm. The data revealed that the nearly spherical particle size decreased with increasing irradiation power. The cobalt phosphate nanoparticles were formed after 10 min of microwave irradiation.

* Corresponding Authors
E-Mail: zhougq1982@163.com
[a] College of Chemistry and Environmental Science, Hebei University, Baoding, 071002, China
[b] Key Laboratory of Chemical Biology of Hebei Province, Hebei University, Baoding, 071002, China

Introduction

Nanomaterials are defined as materials which length less than 100 nm at least in one dimension. When the materials enter into nanoscale, they will show special properties which were different from the bulky materials. Nanomaterials have special properties including quantum size effect, surface effect and macroscopic quantum tunneling effect.[1,2] With these physicochemical features, nanomaterials have been used as electronic components, paint, sports equipment, cosmetics and food additives.[3] Cobalt phosphate ($Co_3(PO_4)_2$) was found as violet pigment used in chemical industry in 1895. $Co_3(PO_4)_2$ can be used as catalyst in the oxidation of water in the presence of sun light and for the selective reduction of NO with C_3H_6 or CH_4.[4] The modification with an appropriate amount of $Co_3(PO_4)_2$ could greatly enhance the activity for photoelectrochemical water oxidation of TiO_2.[5] The addition of $Co_3(PO_4)_2$ in Fe_2O_3 enhance the photocatalytic activity of composite electrode for water photooxidation.[6] The properties included catalytic activity, conductivity and electron affinity of $Co_3(PO_4)_2$ nanoparticles were improved by the nanostructure.[7] $Co_3(PO_4)_2$ nanoparticles with novel properties have broad application prospects in battery cathodes usage and catalytic applications.[8]

The traditional preparation method of $Co_3(PO_4)_2$ nanoparticles is the coprecipitation synthesis.[9] Conventional coprecipitation synthesis can yield larger quantities, but it is difficult to achieve a narrow particle size distribution when the particle size less than 100 nm. It also has high reaction temperature, poor reactivity, particle aggregation, broad size distribution and other disadvantages.[10] Microwave radiation technology is widely used to prepare high purity nanoparticles with narrow particle size distribution.

Microwave heating has been known since the early 1940s, and has been used in preparative chemistry and material synthesis since 1986.[11] Compared with the traditional heating method, microwave heating is an internal heat method which has unique features such as fast and uniform heating, no temperature gradient, short reaction time, and high reaction rate.[12] This is beneficial to the formation of uniform nanomaterials. For example, uniform barium carbonate nanoparticles were successfully synthesized using alkaline earth metal nitrate and sodium carbonate in ethylene glycol by a cyclic microwave radiation.[13]

In this study, $Co_3(PO_4)_2$ nanoparticles with different size were synthesized by microwave irradiation method and the influence of microwave power, reaction time on the size control of nanoparticles were investigated.

The synthesized $Co_3(PO_4)_2$ nanoparticles were characterized using X-ray diffraction (XRD), field emission scanning electron microscopy (FE-SEM), fourier transform infrared spectroscopy (FTIR), Thermal gravimetric (TG), differential thermal analyse (DTA) and dynamic light scattering (DLS). The results showed that the particle size could be tuned simply by adjusting the experimental parameters.

Experimental

Chemicals

All the chemicals used in this experiment were analytical grade materials and used without further purification. Cobalt sulfate heptahydrate ($CoSO_4 \cdot 7H_2O$, ≥99 %), sodium dodecylbenzene sulfonate (SDBS, $C_{18}H_{29}NaSO_3$, 99 %), sodium phosphate monobasic dihydrate ($NaH_2PO_4 \cdot 2H_2O$, ≥ 99.0 %) and urea (CON_2H_4, ≥ 98%) were purchased from Aladdin Chemical Reagent. Deionized water was used throughout the reactions. All glasswares were washed with dilute nitric acid (HNO_3) and distilled water, then dried in hot air oven.

Synthesis of $Co_3(PO_4)_2$ nanoparticles

The $Co_3(PO_4)_2$ nanoparticles were synthesized as following process. 100 ml of 3 mM $CoSO_4 \cdot 7H_2O$, 3 mM $NaH_2PO_4 \cdot 2H_2O$, 0.3 mg of $C_{18}H_{29}NaSO_3$ and 6 mg CON_2H_4 were mixed in a beaker to get an aqueous solution. The solution was transferred into a 200 ml beaker and heat-treated in a microwave oven (Galanz 800 W) for different time periods. Then the reactor device was taken out and cooled with water. After the reaction, the resultant product was separated by centrifugation (3000 rpm, 5 min) and washed repeatedly using water and anhydrous ethanol. Then the wet precipitate was dried at 100 °C in an oven for 2 h.

Characterization of nanoparticles

XRD was performed on an X-ray diffractometer employing Cu-Kα radiation with 40 kV and 50 mA (D8 Advance, Bruker, Germany). The typical bonds were detected by fourier transform infrared spectroscopy (Nicolet 380, Thermo, USA). The FTIR spectra obtained using the improved KBr pellet method by grinding down the resin beads prior to recording. Thermal gravimetric (TG) and differential thermal analyses (DTA) were carried out in TG 209F3 instrument (TG 209F3, Netzch, Germany). A known mass of the sample was heated in a silica crucible at a constant heating rate of 10 °C min^{-1} operating in nitrogen atmosphere with a flow rate of 40 mL min^{-1} from 25 to 700 °C and mass loss per time and temperature increment were recorded. The morphology and size of synthesized $Co_3(PO_4)_2$ nanoparticles were measured by FE-SEM (JSM-7500F, JEOL, Japan). A minute drop of nanoparticles solution was cast on to a carbon-coated copper grid and subsequently drying in air before transferring it to the microscope. The size distribution of the nanoparticles in medium was evaluated by DLS (Delsa Nano C, Beckman, USA). Data were analyzed based on six replicated tests.

Results and discussion

Effect of microwave power

The phase composition and structure of obtained samples at different microwave power were examined by XRD (Fig. 1). The reaction time was 15 min. All diffraction peaks can be indexed to the pure monoclinic phase of $Co_3(PO_4)_2$ which belonging to space group *P21/n* with lattice constants *a* = 7.556 Å, *b* = 8.371 Å and *c* = 5.064 Å (JCPDS No. 01-077-0224). No other byproducts can be detected. The intensity of diffraction peaks increased along with increasing irradiation power. This indicated that crystalline phase developed more complete at higher microwave power. Meanwhile, when the irradiation power increased, the width of diffraction peaks increased slightly. This indicated that the particle size decreased slightly along with increasing irradiation power. The above results were also in accordance with the SEM observation (Fig. 4).

FTIR analysis

The FTIR spectra of the synthesized $Co_3(PO_4)_2$ nanoparticles were shown in Figure 2. The triply degenerated asymmetric stretching and bending vibrations of PO_4^{3-} were at 1030 and 570 cm^{-1}. The triply degenerated asymmetric stretching and bending vibrations of PO_4^{3-} were at 1030 and 570 cm^{-1}. The Co-O peaks were at 854 and 703 cm^{-1}. The emergence of the absorption peak of the Co-O and PO_4^{3-} shows that $Co_3(PO_4)_2$nanoparticles have been formed. The peaks at 3000~3500 and 1627 cm^{-1} corresponded to the remaining water.

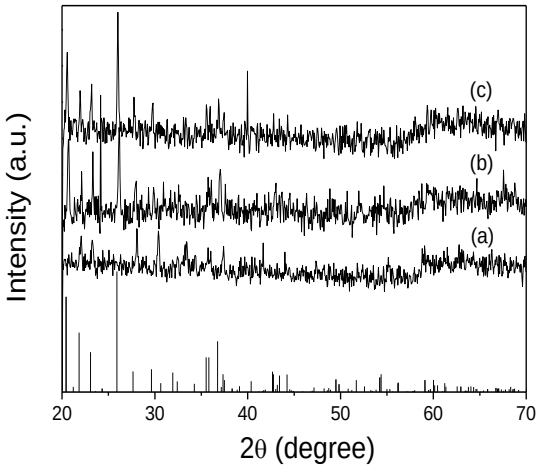

Figure 1. XRD patterns of product obtained at different microwave power. (a) 200 W (b) 500 W (c) 800 W

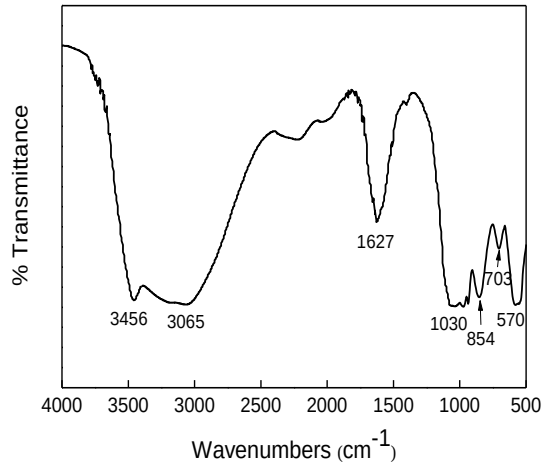

Figure 2. FTIR spectra of sample synthesized by microwave synthesis method.

Thermal gravimetric analysis

TG and DTG curves of the $Co_3(PO_4)_2$ nanoparticles were shown in Figure 3. Two weight losses which corresponding to the removal of physisorbed and interlayer water were observed. The physisorbed and interlayer water molecules which are loosely bound and are mobile that they can be removed by heat treatment below 200 °C. The DTG curve provides more detailed information about the decomposition process. It is possible to distinguish perfectly two peaks in the region below 200 °C, corresponding to the removal first of physisorbed and then of interlayer water. The intensity of the two peaks could be related to the low crystallinity of the compound. It should be noted that the final weight is around 23.4% of the initial weight. The DTA curve of the $Co_3(PO_4)_2$ nanoparticles showed two endothermic peaks corresponding to the above mentioned weight losses.

 DOI: 10.17628/ecb.2014.3.485-488

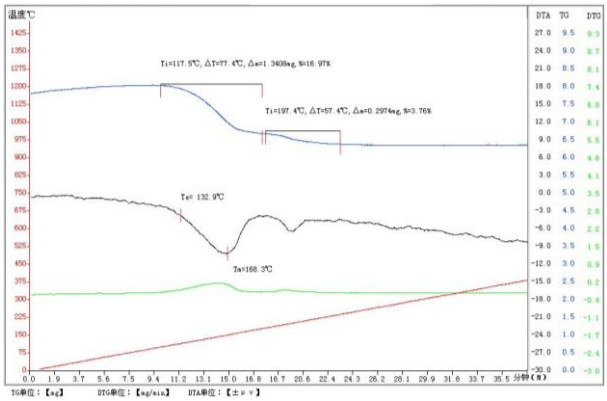

Figure 3. TG and DTG curves of the $Co_3(PO_4)_2$ nanoparticles.

Effect of reaction time

XRD spectra of the $Co_3(PO_4)_2$ nanoparticles prepared at different reaction time were shown in Figure 4. The microwave power was 800 W. The $Co_3(PO_4)_2$ nanoparticles were formed after 10 min of microwave irradiation (Figure 4b). The corresponding SEM micrograph showed that $Co_3(PO_4)_2$ nanoparticles were almost spherical and particle size was about 60 nm (Fig. 5c). The precursors have been converted to $Co_3(PO_4)_2$ when the reaction time was 10 min. The intensity and width of XRD diffraction peaks have no obvious change with extension of microwave irradiation time. This indicated that the particle size remains constant with different reaction times. It may be due to the nucleation and crystallization rate can be greatly accelerated by microwave irradiation method. So the particle size would not change obviously with the extension of reaction time. The above results were also in accordance with the SEM observation (Fig. 5c and 5d). Particle size estimated by XRD was shown in Table 1. The $Co_3(PO_4)_2$ average crystallite size was calculated using Scherrer equation ($R = 0.9\lambda/B\cos\theta_B$), where R is the average particle size (Å), B is the width of the peak at half the peak height (radians), λ is the X-ray wavelength (nm), and θ_B is the Bragg angle (^{o}).

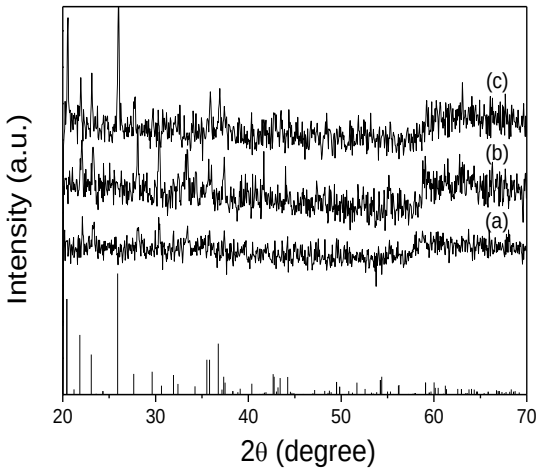

Figure 4. XRD patterns of product obtained from different reaction times. (a) 5 min (b) 10 min (c) 15 min

Table 1. Particle size as estimated from XRD and SEM measurements.

Sample	Microwave power, W	Reaction time, min	Size from XRD, nm	Size from SEM, nm
1	500	10	81	85
2	500	15	78	80
3	800	10	62	65
4	800	15	57	60

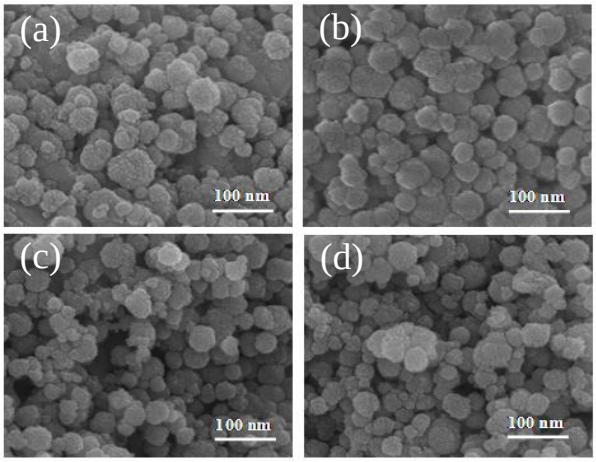

Figure 5. SEM images of $Co_3(PO_4)_2$ nanoparticles obtained from different reaction times and microwave powers. (a) 10 min, 500 W (b) 15 min, 500 W (c) 10 min, 800 W (d) 15 min, 800 W

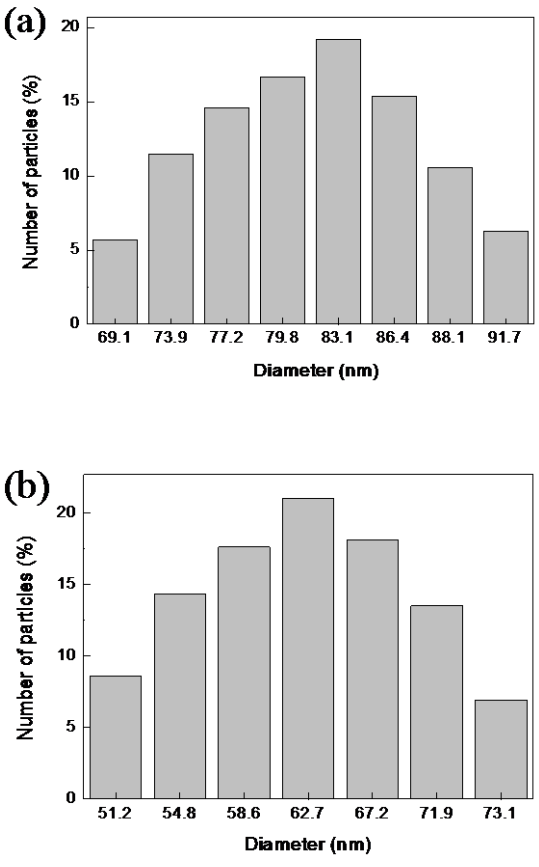

Figure 6. Size distribution of $Co_3(PO_4)_2$ nanoparticles in water measured by DLS. (a) 15 min, 500 W (b) 15 min, 800 W

 DOI: 10.17628/ecb.2014.3.485-488

DLS analysis

The SEM images provided information on the primary size of nanoparticles, however, it could not provide information on whether the nanoparticles existed in single or aggregated forms in the culture medium. The size distribution in the culture medium, therefore, was investigated using a DLS method, which showed that the average size of $Co_3(PO_4)_2$ nanoparticles in the culture medium were 83.5± 11.2 nm and 62.7±9.4 nm, respectively (Fig. 6). The DLS analysis showed that the $Co_3(PO_4)_2$ nanoparticles were homogeneously dispersed in culture medium. The fluid dynamics size of $Co_3(PO_4)_2$ nanoparticles which measured by DLS was in agreement with the primary size obtained by SEM.

Conclusions

In summary, quasi-spherical $Co_3(PO_4)_2$ nanoparticles were synthesized successfully using microwave irradiation method. Average size of the $Co_3(PO_4)_2$ nanoparticles was tunable by simply changing the microwave power and reaction time of the reaction.

The results of characterization showed that the particle size decreased along with increasing irradiation power in the formation of the nanoparticles. $Co_3(PO_4)_2$ nanoparticles with average diameter 80 nm for 500 W and 60 nm for 800 W were highly stable. XRD pattern showed that pure nanostructures with high crystallinity had been made.

Acknowledgments

This research is financially supported by the National Natural Science Foundation of China (21001038).

References

[1]Mahmoudi, M., Azadmanesh, K., Shokrgozar, M. A., Journeay, W. S., Laurent, S., *Chem. Rev*., **2011**, *111*, 3407.

[2]Kostarelos K., *Nat. Biotechnol*., **2008**, *26*, 774.

[3]Farokhzad, O. C., Langer, R., *ACS. Nano*., **2009**, *3*, 16.

[4]Matthew, W. K., Yogesh. S., Daniel. G. N., *Chem. Soc. Rev*., **2009**, *38*, 109.

[5]Liu, D. N., Jing, L. Q., Luan, P., Tang, J. W., Fu, H. G., *ACS. Appl. Mat. Interfaces*., **2013**, *5*, 4046.

[6]Barroso, M., Cowan, A. J., Pendlebury, S. R., Gratzel, M., Klug, D. R., Durrant, J. R., *J. Am. Chem. Soc*., **2011**, *133*, 14868.

[7]Hu, X. L., Piccinin, S., Laio, A., Fabris, S., *ACS. Nano*., **2012**, *6*, 10497.

[8]Lee, M. T., Hwang, D. J., Greif, R., Grigoropoulos, C. P., *Int. J. Hydrogen. Energy*., **2009**, *34*, 1835.

[9]Badsar, M., Edrissi, M., *Mater. Res. Bull*., **2010**, *45*, 1080.

[10]Nelson, J. B., Davis, A. M., Wellman, D. M., *Inorg. Chem*., **2009**, *48*, 10857.

[11]Giguere, R. J., Bray, T. L., Duncan, S. M., Majetich, G., *J. Tetrahedron. Lett*., **1986**, *27*, 4945.

[12]Salavati, N. M.., Banaiean, M. G., Emadi, H., Enhessari, M., *Comptes. Rendus. Chimie*., **2013**, *16*, 929.

[13]Tipcompor, N., Thongtem, T., Phuruangrat, A., Thongtem, S., *Mater. Lett*., **2012**, *87*, 153.

Received: 28.03.2014.
Accepted: 09.04.2014.

MICROWAVE ASSISTED SYNTHESIS, CHARACTERIZATION AND BIOLOGICAL ACTIVITY OF SOME PYRAZOLE AND PYRIMIDINE DERIVATIVES

Kumudini Bhanat[a]*, Bharat Parashar[b] and V. K. Sharma[a]

Keywords: microwave irradiation; pyrazole; pyrimidines; antimicrobial activity.

The synthesis of pyrazoles and pyrimidines can be achieved from different chalcones using microwave irradiation within 5-8 min. Pyrazole and pyrimidine are nitrogen containing heterocyclic rings which are versatile lead compound for designing potent bioactive agents. The structures of the products were supported by IR, ^{1}H NMR, ^{13}C NMR and mass spectral data. The synthesized compounds showed a good antibacterial and antifungal activity.

Corresponding Authors
E-Mail: kumudini23@gmail.com
[a] Microwave Chemistry Laboratory, Department of Chemistry, Mohanlal Sukhadia University, Udaipur - 313 001 (Raj.), India
[b] Department of Pharmacy, M. B. University, Solan (H.P.), India.

INTRODUCTION

Heterocyclic chemistry is currently experiencing a renaissance because of the interest in heterocyclic scaffolds as templates for combinatorial chemistry.[1] As heteroaromatic compounds are present in many natural products,[2] and are constituents of numerous therapeutic agents,[3] they represent ideal drug-like structures for the elaboration of an increase in molecular diversity. Nitrogen containing heterocyclic compounds has received considerable attention due to their wide range of pharmacological activity. The pyrazoles and the pyrimidines constitute interesting class of organic compounds with diverse chemical and biological application. They are known to possess variety of biological activities such as analgesic, anti-inflammatory, protein kinase C inhibitor.[4] Many pyrazole derivatives possess remarkable antiepileptic and antimicrobial,[5] antiamoebic,[6] and antiandrogenic activities.[7] The pyrazole nucleus is a ubiquitous feature of pharmacological interest and has been proven to be a fertile source of medicinal agents. Some of these compounds have also exhibited antidiabetic,[8] anaesthetic[9] properties.

The biological activities of condensed pyrimidines as sedatives and antibacterials are well documented.[10-13] Numerous reports have been patented[14] and have delineated the antiallergic,[15] antiviral,[16] antibacterial,[17] antioxidant[18] and hepatoprotective properties[19] of fused pyrimidines.

The use of microwaves in organic synthesis has increased dramatically in the last years, receiving widespread acceptance and becoming an indispensable tool.[20] Microwave technology has become a powerful tool in organic synthesis, since by employing this technique it is generally possible to prepare organic compounds very fast, with high purity and better yields compared to other more conventional methods.[21-23] So, due to increasing demand and everlasting longing for the biologically active heterocycles, it is considered worthwhile to synthesize some novel pyrimidine and pyrazole moiety, which might possess enhanced biological activity.

EXPERIMENTAL

All the reactions were carried out in a microwave oven (Kenstar, OM26.EGO). Melting points of synthesis compounds were determined in open capillaries in liquid paraffin are uncorrected. Purity of the compounds in addition to elemental analysis were verified by percolated TLC using silica gel G as a adsorbent using ethyl acetate : n-hexane (7:3) as a eluent and spot was detected by using iodine vapors.

The IR (KBr pellets) spectra were recorded on a Perkin Elmer-1800- spectrophotometer and ^{1}H NMR spectra were recorded on BRUKER DRX- 300MHz spectrophotometer, (TMS as a internal reference) and chemical shifts are expressed in δ. MASS spectra were recorded on Jeol D30 spectrophotometer. Elemental analyses for C, H and N were conducted using a Perkin -Elmer CHN analyzer.

General procedure for microwave induced synthesis of 1-(2,4-dinitrophenyl)-3-methyl-1H-pyrazole-5(4H)one (1)

2,4-dinitropheny hydrazine (0.01 mole), ethyl-3-oxobutanoate (0.01 mole) and two to three drops of glacial acetic acid were taken in an Erlenmeyer flask. Then the well-stirred mixture was irradiated in microwave oven for 7 min at 600 W (i.e, 50 % microwave power). The completion of the reaction was monitored by TLC. The solid thus obtained was dried and the product was recrystallized from ethanol to give compound **1**. The physical and spectral data are given in Table 1 and 2.

Table 1. Physical and analytical data of synthesized compound

Compd.	R	Mol. Formula	Mol. Weight	M.P., ºC	Yield, % [Time in min]	Calculated/Found % C,H, and N
1	---	$C_{10}H_8N_4O_5$	264	160-162	85 [6]	45.12/44.13 3.79/4.23 21.05/21.32
2a	4-OH-C_6H_4	$C_{17}H_{12}N_4O_6$	368	250-252	65 [5]	55.14/55.78 3.81/3.34 15.13/15.53
2b	4-Cl-C_6H_4	$C_{17}H_{11}ClN_4O_5$	386	265-267	70 [5]	52.52/52.7 3.37/3.11 14.41/14.76
2c	3-NO_2-C_6H_4	$C_{17}H_{11}N_5O_7$	397	272-274	72 [5]	51.13/51.87 3.28/3.13 17.54/17.9
2d	4-F-C_6H_4	$C_{17}H_{11}FN_4O_5$	370	160-163	75 [5]	54.84/54.46 3.52/3.05 15.05/15.8
3a	4-OH-C_6H_4	$C_{17}H_{14}N_6O_5$	382	105-107	73 [5]	53.12/52.70 4.20/4.69 21.87/20.76
3b	4-Cl-C_6H_4	$C_{17}H_{13}ClN_6O_4$	400	174-176	75 [5]	50.69/50.07 3.75/3.13 20.86/20.09
3c	3-NO_2-C_6H_4	$C_{17}H_{13}N_7O_6$	411	198-200	79 [5]	49.40/48.12 3.66/3.32 23.72/23.03
3d	4-F-C_6H_4	$C_{17}H_{13}FN_6O_4$	384	163-165	78 [5]	52.85/51.89 3.91/3.02 21.75/21.31
4a	4-OH-C_6H_4	$C_{18}H_{14}N_6O_6$	410	90-92	75 [7]	52.43/51.90 3.91/3.09 20.38/21.12
4b	4-Cl-C_6H_4	$C_{18}H_{13}ClN_6O_5$	428	80-82	76 [6]	50.18/50.90 3.51.4.97 19.51/18.87
4c	3-NO_2-C_6H_4	$C_{18}H_{13}N_7O_7$	439	115-117	72 [7]	48.98/48.05 3.43/4.13 22.22/21.87
4d	4-F-C_6H_4	$C_{18}H_{13}FN_6O_5$	412	153-155	70 [8]	52.18/52.98 3.65/4.04 20.18/20.96

Microwave induced synthesis of the chalcones (4-(substituted benzylidene)-1-(2, 4-dinitrophenyl)-3-methyl-1H-pyrazole-5(4H)-one (2a-d)

The chalcones **2a-d** were prepared as starting material to obtain the desired derivatives. Mixture of 2-(2,4-dinitrophenyl)-5-methylpyrazolidine-3-one (0.01 mol) and different aromatic aldehydes (0.01 mol) and KOH (2 to 3 drops) in 30 ml of DMF were taken in an Erlenmeyer flask and mixed thoroughly. The well-stirred mixture was irradiated in microwave oven for 5-6 min at 600 W (i.e. 50 % microwave power). The completion of the reaction was monitored by TLC. The reaction mixture was then cooled at room temperatures and poured into crushed ice. The solid obtained **2a-e** was filtered, washed with water and recrystallized from ethanol. The purity of compounds was analyzed by TLC using ethyl acetate: n-hexane (7: 3) as mobile phase

Microwave induced synthesis of 4-(substituted phenyl)-1-(2,4-dinitrophenyl)-3-methyl-1,3,4,5-tetrahydropyrazolo[3,4-c]pyrazole (3a-d)

Mixture of compound 2 (0.01 mol) and hydrazine hydrate (0.05 mol) in 30 ml of DMF were taken in an Erlenmeyer flask and mixed thoroughly. The well-stirred mixture was irradiated in microwave oven for 7-8 min at 600 W (i.e. 50 % microwave power). The completion of the reaction was monitored by TLC.

The reaction mixture was cooled at room temperatures and poured into crushed ice. The obtained solid was filtered, washed with water and recrystallized from ethanol.

The purity of compounds was analyzed by TLC using ethyl acetate: n-hexane (7: 3) as mobile phase.

Table 2. Spectral data of synthesized compound

Compd.	Spectral data	
1	IR (cm^{-1})	1305(N-N), 1635(C=O), 3252(Ar-CH str.), 3300(N-H str), 1533(N-H bending), 1412(C=C str), 2864(CH_3, sp^3).
	^{1}H NMR (δ)	9.30-8.40 (m, Ar-H), 2.55(s, 2H, CH_2), 1.08(s, 3H, CH_3-methyl).
	^{13}CNMR (δ)	144.1-141.8(C-NO_2),118.4-127.9(CH-Ar),141.9(C-Ar),170.2(C=O), 32.8(CH_2),40.9(CH), 23.5(CH_3)
	Mass (m/z)	264 (M^+), , $[C_9H_6N_4O_5]^+$250, $[C_4H_7N_2O]^+$99, $[C_6H_3N_2O_4]^+$167
2a	IR (cm^{-1})	1310 (N-N), 1638(C=O), 3082(C-H str., Ar-H), 3312(N-H str), 1524(N-H bending), 3052(=C-H, SP^2), 1483 (aromatic ring str.), 2842(CH_3, SP^3), 3410 (OH).
	^{1}H NMR (δ)	9.76-8.83(m, Ar-H), 7.70(s, 1H, CH=), 1.13(s, 3H, CH_3), 6.45-6.83(m, 4H,Ar-H), 5.2(s, 1H, OH).
	^{13}CNMR (δ)	143.1-141.8(C-NO_2), 117.4-127.9(CH-Ar), 141.6(C-Ar), 170.4(C=O), 40.2(CH), 22.6(CH_3), 130.2(C=CH), 137.9(CH), 133.7-133.9(C-Ar), 125.5-129.3(CH-Ar).
	Mass (m/z)	368(M^+), $[C_{17}H_{11}N_4O_5]^+$351, $[C_{11}H_6N_4O_5]^+$274, $[C_{16}H_9N_4O_6]^+$353, $[C_{11}H_9N_2O_2]^+$201, $[C_6H_3N_2O_4]^+$167
2b	IR (cm^{-1})	1312 (N-N), 1722(C=O), 3062(C-H str., Ar-H), 3402(N-H str), 1622(N-H bending), 3154(=C-H, SP^2), 1476(aromatic ring str.), 2710CH_3, SP^3), 664(Cl).
	^{1}H NMR (δ)	9.26-8.3(m, Ar-H), 8.15(s, CH=), 1.25(s, 3H, CH_3), 6.55-7.23(m, 4H, Ar-H).
	^{13}CNMR (δ)	143.12-141.78(C-NO_2), 117.04-127.9(CH-Ar), 141.16(C-Ar), 167.3(C=O), 39.4(CH), 22.8(CH_3), 130.6(C=CH), 137.8(CH), 133.6-129.4(CH-Ar).
	Mass (m/z)	386(M^+),388(M+2), $[C_{17}H_{11}N_4O_5]^+$351, $[C_{11}H_6N_4O_5]^+$274, $[C16H_8N_4O_5]^+$371, $[C_{11}H_{10}ClN_2O]^+$221, $[C_6H_3N_2O_4]^+$167
2c	IR (cm^{-1})	1222 (N-N), 3020 (C-H str., Ar-H), 1645 (C=O str.), 1610(N-H bending), 3175(=C-H, SP^2), 1485 (aromatic ring str.), 2880(CH_3, SP^3), 1550(C-NO_2).
	^{1}H NMR (δ)	9.57-8.77(m, Ar-H), 7.16(s, CH=), 1.18(s, 3H, CH_3), 6.45-6.53(m, 4H, Ar-H).
	^{13}CNMR (δ)	143.12-141.78(C-NO_2), 117.04-127.9(CH-Ar), 141.16(C-Ar), 169.5(C=O), 39.4(CH), 22.6(CH_3), 130.2(C=CH), 138.7(CH), 133.9-127.4(CH-Ar).
	Mass (m/z)	397(M^+), $[C_{17}H_{11}N_4O_5]^+$351, $[C_{11}H_6N_4O_5]^+$274, $[C_{16}H_8N_5O_7]^+$382, $[C_{11}H_{10}N_3O_3]^+$232, $[C_6H_3N_2O_4]^+$167
2d	IR (cm^{-1})	1230 (N-N), 3090 (C-H str., Ar-H), 1694(C=O str.), 1578(N-H bending), 3086(=C-H, SP^2), 1470(aromatic ring str.) 2810(CH_3, SP^3), 812(C-F str.).
	^{1}H NMR (δ)	9.76- 8.85 (m, Ar-H), 7.32(s, CH=), 1.11(s, 3H, CH_3), 7.18-6.83(m, 4H, Ar-H).
	^{13}CNMR (δ)	144.12-142.78(C-NO_2), 118.9-127.9(CH-Ar), 143.16(C-Ar), 169.5(C=O), 39.7(CH), 22.5(CH_3), 130.2(C=CH), 138.5(CH), 133.9-127.4(CH-Ar).
	Mass (m/z)	370(M^+), $[C_{17}H_{11}N_4O_5]^+$351, $[C_{11}H_6N_4O_5]^+$274, $[C_{16}H_8FN_4O_5]^+$355, $[C_{11}H_{10}FN_2O]^+$205, $[C_6H_3N_2O_4]^+$167
3a	IR (cm^{-1})	1556 (C=C ring skeleton Ar. moiety), 1518 (N-H bending), 3210 (N-H str.), 3412 (OH), 2850(CH_3), 1158(C-N str.).
	^{1}H NMR (δ)	9.18-7.80(Ar-H, pyridine), 1.16(s, 3H, CH_3), 6.8 (1H, s, N-H, pyrazole), 2.80(d, 1H, CH), 4.80(d, 1H, CH), 8.08-6.93(m, 4H, Ar-H), 5.8(s, 1H, OH).
	^{13}CNMR (δ)	132.12-139.68(C-NO_2), 115.7-127.9(CH-Ar), 142.1(C-Ar), 154.3(C-pyrazolidine), 42.4-47.2(C-NH), 16.5(CH_3), 54.5(CH-pyrazole), 130.8(C-Ar), 128.6-115.2(CH-Ar), 155.2(C-Ar).
	Mass (m/z)	382(M^+), $[C_{17}H_{13}N_6O_4]^+$365, $[C_{11}H_9N_6O_4]^+$289, $[C_{16}H_{11}N_6O_5]^+$369, $[C_{11}H_{13}N_4O]^+$217, $[C_6H_3N_2O_4]^+$167
3b	IR (cm^{-1})	3410 (N-H stretching), 2788(CH_3), 1595(N-H bending), 1560(C=C), 1148(C-N str.), 747 (C-Cl).
	^{1}H NMR (δ)	9.8-7.7(m, Ar-H), 1.06(s, 3H, CH_3), 7.3 (1H, s, N-H, pyrazole), 2.70(d, 1H, CH), 4.2(d, 1H, CH), 8.8-6.3(m, 4H, Ar-H).
	^{13}CNMR (δ)	133.12-139.68(C-NO_2), 115.7-127.9(CH-Ar), 142.9(C-Ar), 154.4(C-pyrazolidine), 42.4-47.1(C-NH), 16.6(CH), 54.2(CH-pyrazole), 130.5(C-Ar), 128.4-115.1(CH-Ar), 155.2(C-Ar).
	Mass (m/z)	367(M^+),369(M+2),$[C_{17}H_{13}N_6O_4]^+$365,$[C_{11}H_9N_6O_4]^+$289, $[C_{16}H_{10}ClN_6O_4]^+$385, $[C_{11}H_{12}N_4]^+$235, $[C_6H_3N_2O_4]^+$167

Table 2. cont.

3c	IR (cm^{-1})	1565 (C=C ring skeleton Ar. moiety), 1485 (N=N), 3209 (N-H str.), 1610(N-H bending), 2795(CH_3), 1142(C-N str.), 1382 (NO_2).
	^{1}H NMR (δ)	9.50-7.8(m, Ar-H), 1.25(s, 3H, CH_3), 6.6(1H, s, N-H, pyrazole), 2.02(d, 1H, CH), 4.70(d, 1H, CH), 8.5-6.8(m, 4H, Ar-H).
	^{13}CNMR (δ)	133.12-139.68(C-NO_2), 116.7-127.9(CH-Ar), 142.5(C-Ar), 154.3(C-pyrazolidine), 42.2-47.4(C-NH), 16.7(CH_3), 54.5(CH-pyrazole), 130.8(C-Ar), 128.6-115.2(CH-Ar), 155.3(C-Ar).
	Mass (m/z)	411(M^+), $[C_{17}H_{13}N_6O_4]^+$365, $[C_{11}H_9N_6O_4]^+$289, $[C_{16}H_{10}N_7O_6]^+$396, $[C_{11}H_{12}N_5O_2]^+$246 $[C_6H_3N_2O_4]^+$167
3d	IR (cm^{-1})	1568 (C=C), 1585(N-H bending) , 3310 (N-H str.),2792(CH_3), 1142(C-N str.), 1185 (F).
	^{1}H NMR (δ)	9.8-7.8 (m, Ar-H), 1.20(s, 3H, CH_3), 7.2 (1H, s, N-H, pyrazole), 2.6(d, 1H, CH), 4.73(d, 1H, CH), 8.2-6.7(m, 4H, Ar-H).
	^{13}CNMR (δ)	133.02-139.6 (C-NO_2), 115.7-127.9(CH-Ar), 142.0(C-Ar), 154.4(C-pyrazolidine), 42.2-47.2(C-NH), 16.9(CH_3), 54.8(CH-pyrazole), 130.5(C-Ar), 128.5-115.2(CH-Ar), 155.0(C-Ar).
	Mass (m/z)	384(M^+),$[C_{17}H_{13}N_6O_4]^+$365,$[C_{11}H_9N_6O_4]^+$289, $[C_{16}H_{10}FN_6O_4]^+$369,$[C_{11}H_{12}FN_4]^+$219, $[C_6H_3N_2O_4]^+$167
4a	IR (cm^{-1})	1558 (C=C ring skeleton Ar. moiety), 1510 (N-H bending), 1698(C=O), 3210 (N-H str.), 2852(CH_3), 1155(C-N str.), 3410 (OH).
	^{1}H NMR (δ)	9.8-7.80(Ar-H), 2.15(1H, s, NH of Pyrazolidine), 3.5(CH-pyrazolidine), 1.11(CH_3), 2.85(CH), 4.84(CH), 8.08-6.93(m, 4H, Ar-H), 5.6(NH-pyrimidine), 5.7(OH).
	^{13}CNMR (δ)	133.12-139.6(C-NO_2), 115.7-127.9(CH-Ar), 142.0(C-Ar), 163.9(C-pyrazolidine), 164.2(C=O, urea), 49.2(C-CH_3, pyrazolidine), 17.3(CH_3), 51.9(CH), 36.7(CH-NH, pyrimidine), 133.9(C-Ar), 130.3-116.2(CH-Ar), 156.2(C-Ar).
	Mass (m/z)	410(M^+),$[C_{18}H_{13}N_6O_5]^+$393,$[C_{12}H_9N_6O_5]^+$317,$[C_{17}H_{13}N_6O_6]^+$397, $[C_{12}H_{13}N_4O_2]^+$245, $[C_6H_3N_2O_4]^+$167
4b	IR (cm^{-1})	3410 (N-H stretching), 1658 (C=O stretching), 2782(CH_3), 1593(N-H bending), 1562(C=C), 1150(C-N str.), 746 (C-Cl).
	^{1}H NMR (δ)	9.8-7.7(Ar-H), 2.15 (1H, s, NH of Pyrazolidine), 3.8(CH-pyrazolidine), 1.18(CH_3), 2.62(CH), 4.9(CH), 8.9-6.3(m, 4H, Ar-H), 6.5(NH-pyrimidine).
	^{13}CNMR (δ)	134.9-139.6(C-NO_2), 116.7-127.9(CH-Ar), 142.6(C-Ar), 163.4(C-pyrazolidine), 164.5(C=O, urea), 49.5(C-CH_3, pyrazolidine), 17.9(CH_3), 51.5(CH), 36.4(CH-NH, pyrimidine), 133.3(C-Ar), 130.5-116.2(CH-Ar), 156.7(C-Ar).
	Mass (m/z)	428(M^+), 430(M+2), $[C_{18}H_{13}N_6O_5]^+$393, $[C_{12}H_9N_6O_5]^+$317, $[C_{17}H_{12}ClN_6O_5]^+$416, $[C_{12}H_{12}ClN_4O]^+$263, $[C_6H_3N_2O_4]^+$167
4c	IR (cm^{-1})	1565 (C=C ring skeleton Ar. moiety), 1693 (C=O), 3219 (N-H str.), 1612(N-H bending), 2793(CH_3), 1144(C-N str.), 1382 (NO_2).
	^{1}H NMR (δ)	9.50-7.8(Ar-H), 2.37(1H, s, NH of Pyrazolidine), 3.95(CH-pyrazolidine), 1.23(CH_3), 2.71(CH), 4.75(CH), 8.4-6.9(m, 4H, Ar-H), 6.5(NH-pyrimidine).
	^{13}CNMR (δ)	134.02-139.4(C-NO_2), 116.3-127.3(CH-Ar), 142.5(C-Ar), 163.6(C-pyrazolidine), 164.2(C=O, urea), 49.2(C-CH_3, pyrazolidine), 17.2(CH_3), 51.6(CH), 36.6(CH-NH, pyrimidine), 133.5(C-Ar), 130.3-116.6(CH-Ar), 155.2(C-Ar).
	Mass (m/z)	439(M^+), $[C_{18}H_{13}N_6O_5]^+$393, $[C_{12}H_9N_6O_5]^+$317, $[C_{17}H_{12}N_7O_7]^+$427, $[C_{11}H_{10}N_5O_3]^+$260, $[C_6H_3N_2O_4]^+$167
4d	IR (cm^{-1})	1565 (C=C), 1584(N-H bending), 1680 (C=O, 3310 (N-H str.), 2790(CH_3), 1142(C-N str.), 1185 (F).
	^{1}H NMR (δ)	9.8-7.8(Ar-H), 2.51(1H, s, NH of Pyrazolidine), 3.74(CH-pyrazolidine), 1.20(CH_3), 2.83(CH), 4.76(CH), 8.2-6.6(m, 4H, Ar-H), 6.4(NH-pyrimidine).
	^{13}CNMR (δ)	134.12-139.3(C-NO_2), 116.8-127.9(CH-Ar), 142.7(C-Ar), 163.7(C-pyrazolidine), 164.9(C=O, urea), 49.5(C-CH_3, pyrazolidine), 17.9(CH_3), 51.9(CH), 36.5(CH-NH, pyrimidine), 133.9(C-Ar), 130.3-116.0(CH-Ar), 156.3(C-Ar).
	Mass (m/z)	412(M^+), $[C_{18}H_{13}N_6O_5]^+$393, $[C_{12}H_9N_6O_5]^+$317, $[C_{17}H_{12}FN_6O_5]^+$399 $[C_{12}H_{12}FN_4O]^+$247, $[C_6H_3N_2O_4]^+$167

Table 3. Minimum inhibition concentration of synthesized compounds on bacterial and fungal strains (4,5a-d)

Compounds	R	MIC, µg mL^{-1}					
		Bacteria				Fungi	
		E. coli	*P. euroginosa*	*S. aureus*	*S. pyogenus*	*A. nigar*	*C. albicans*
4a	4-HOC$_6$H$_4$	125	250	250	125	250	125
4b	4-ClC$_6$H$_4$	250	125	125	125	250	125
4c	3-NO$_2$C$_6$H$_4$	62.5	125	62.5	125	500	250
4d	4-FC$_6$H$_4$	125	125	100	62.5	500	500
5a	4-HOC$_6$H$_4$	250	125	250	250	250	125
5b	4-ClC$_6$H$_4$	200	100	100	125	250	500
5c	3-NO$_2$C$_6$H$_4$	100	62.5	200	200	125	100
5d	4-FC$_6$H$_4$	62.5	100	125	100	500	100
Amphicilin		100	----	250	100	----	----
Greseofulvin		----	----	----	----	500	100

Microwave induced synthesis of 1-(2,4-dinitrophenyl)-4-(substituted phenyl)-3-methyl-4,5-dihydro-1H-pyrazolo[3,4-d]pyrimidine-6-(3aH)-one (4a-d)

Mixture of compound **2** (0.01 mol) and urea (0.01 mol) with KOH (2-3 drops) in 30 ml of DMF were taken in an Erlenmeyer flask and mixed thoroughly. The well-stirred mixture was irradiated in microwave oven for 7-8 min at 600 W (i.e. 50 % microwave power). The completion of the reaction was monitored by TLC. The reaction mixture was then cooled at room temperatures and poured into crushed ice. The obtained solid was filtered, washed with water and recrystallized from ethanol. The purity of compounds was analyzed by TLC using ethyl acetate: n-hexane (7: 3) as mobile phase.

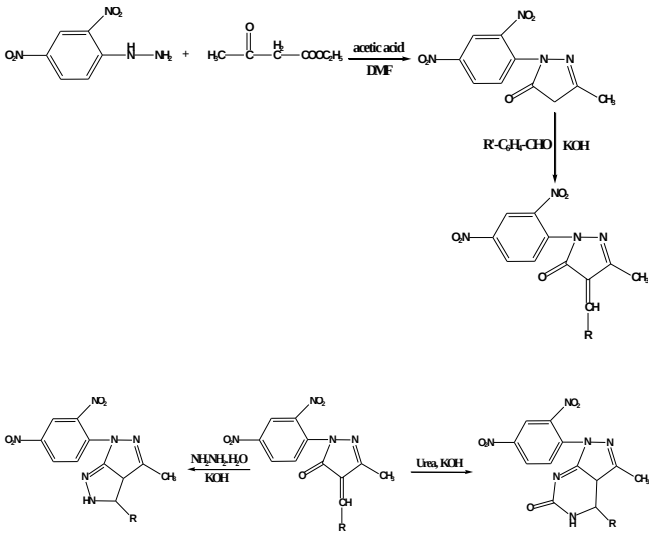

R'= 4-OH, 4-Cl, 3-NO$_2$, 4-F.

R= 4-OH-C$_6$H$_4$, 4-Cl-C$_6$H$_4$, 3-NO$_2$-C$_6$H$_4$, 4-F-C$_6$H$_4$.

Reaction Scheme: Synthesis of pyrazole and pyrimidine derivatives

Antimicrobial Activity

The compounds (**4,5a-d**) were tested for their antimicrobial activities against gram-positive and gram-negative bacterial and fungal strain. The resulting MIC (µg mL^{-1}) values are indicated in Table 3. It was observed that more than half compounds exhibited excellent activity in comparison to standards used, while the remaining were good and one or two of them poor in comparison to the standards. The standard used for antifungal activity was Greseofulvin and Amphicilin were used as a standard for antibacterial assay.

The newly synthesized compounds **(4,5a-d)** were screened for their antibacterial activity against gram-negative bacteria *Escherichia coli* (MTCC 443), *Pseudomonas aeruginosa* (MTCC 441) and gram-positive bacteria *Staphylococcus aureus* (MTCC 96) and *Streptococcus pyogenes* (MTCC 442) and antifungal activity against *A. nigar* and *C. albicans.* The samples were tested by broth dilution method. The screening for antimicrobial activity was carried out by diluting the solution and preparing the sets consecutively from 1000, 500, 250, 200, 100, 50, 25, 12.5, 6.25 micro/ml. The highest dilution showing at least 99 % inhibition zone is taken as MIC. The result of this is much affected by the size of the inoculum. The test mixture should contain 10^8 organism/ml. Among all the synthesized derivatives **4c, 5c** and **5d** were exhibited the best MIC values. **4a, 5a** and **5c** showed equivalent activity to standard and rest of compounds were showed moderate to poor activity.

In fungal activity only **5c** was showed excellent activity against *A. nigar* and **4c, 4d** and **5d** showed equivalent activity to standard and rest of compounds showed moderate to poor activity against fungal standard.

RESULT AND DISCUSSION

Ethyl-3-oxobutanoate on condensation with 2, 4-dinitrophenyl hydrazine in presence of glacial acetic acid in DMF as solvent afforded compound **1.** The compound **1** was characterised by the appearance of IR bands at 3300 cm^{-1} for N-H str., 1635 cm^{-1} for C=O and 1305 cm^{-1} for (N-N).

The compound **1** was treated with various aromatic aldehydes in the presence of KOH to give (4-(substituted benzylidene)-1-(2,4-dinitrophenyl)-3-methyl-1H-pyrazole-5(4H)-one **2a-d.** Compounds **2a-d** were confirmed by disappearance of signal at 2.55 ppm due to CH_2 and appearance of multiplet for five aromatic protons at 7.16-8.15 ppm and =C-H stretching frequency at 3052-3175 cm^{-1}.

Chalcones **2a-d** are convenient starting material for the synthesis of pyrazoles, and pyrimidines due to their α,β-unsaturated moiety.

In first pathway **3a-d** were synthesized by treating compounds **2a-d** with hydrazine hydrate. The formation of pyrazole **3a-d** were explained by the appearance of bands at 1142-1158 cm^{-1} due to (C=N str.) and disappearance of band at 3052-3186 cm^{-1} due to (=C-H) in IR spectrum and singlet at 6.6-7.3 δ due to –NH (pyrazole) in ^1H NMR spectra.

In second pathway formation of pyrimidine derivative were synthesized by compound **2a-d** with urea in basic medium.

Formation of **4a-d** were explained by the appearance of bands at 1142-1155 cm^{-1} due to (C-N str.) and disappearance of band at 3052-3186 cm^{-1} due to (=C-H) in IR spectrum. The compounds were confirmed by the appearance of IR band at 1658-1698 cm^{-1} for C=O stretching. The NMR signal of =C-H at 7.16-8.15 ppm is disappeared and one signal –NH is appeared at 5.6-6.5 ppm. The ^1H NMR and ^{13}C NMR spectroscopic data, as well as IR spectra are in good agreement with the proposed structure of the synthesized compounds.

CONCLUSION

The purpose of the research is the development of new potent bioactive molecules with less toxic, safer and easily available methods. From the literature survey it is evident that Microwave Induced Organic Reaction Enhancement (MORE) chemistry offers a simple, nonconventional technique for the synthesis of wide variety of compounds including biologically important heterocyclic compounds, co-ordination compounds etc. By thorough study of physical, spectral and biological data, it can be concluded that meaningful results were obtained. So pyrimidine and pyrazole moiety were found to possess considerable biological activity, there is a great scope for potent derivatives which can be obtained by structural modifications. As a result, the synthesized derivatives appear to be potential candidates for further exploration.

REFERENCES

[1]Hansford, K. A., Zanzarova, V., Dorr, A., Lubell, W. D., *J. Comb. Chem*. **2004**, *6*, 893.

[2]Heckmann, G., Bach, T., *Angew. Chem. Int. Ed*. **2005**, *44*, 1199.

3Doherty, A. M., *Ann. Rep. Med. Chem*. **2004**, *39*, 335.

[4]Mariappan, G., Saha, B. P., Sutharson, L., Haldar, A., *Ind. J. Chem.*, **2010**, *49B*, 1671.

[5]Anandarajagopal, K., Sunilson, A. J., Illavarasu, A., Thangavelpandian, N., Kalirajan, R., *Int. J. ChemTech. Res.*, **2010**, *2(1)*, 45.

[6]Millan, S. E., Nicholas, D. P., *Bioorg. Med. Chem. Lett.*, **2009**, *19*, 222.

[7]Abid, M., Azam, A., *Bioorg. Med. Chem. Lett.*, **2006**, *16(10)*, 2812.

[8]Amr, Ael-G., Abdel-Lalif, N. A., Abdalla, M. M., *Bioorg. Med. Chem.*, 2006, *14(2)*, 373.

[9]Regaila, H. A., El-Bayonk, A. K., Hammad, M., *Egypt J. Chem.*, **1979**, *20*, 197.

[10]Krishna, R., Pande, B. R., Bharthwal, S. P., Parmar, S. S., *Eur. J. Med. Chem.*, **1980**, *15*, 567.

[11]Ashok, K., Rathod, *Int. J. PharmTech. Res.* **2011**, *3(1)*, 435.

[12]Schimdt, P., Eichenberger, K., Schweizer, E., German Offen., 196908479, *Chem. Abstr*. **1970**, *72*, 31837u .

[13]Eichenberger, K., Schweizer, E., Schimdt, P., US Patent, 262776614, *Chem. Abstr*. **1971**, *74*, 88638w .

[14]Clercq, E. D., Beraaerts, R., *J. Biol. Chem*. **1987**, *262*, 14905.

[15]Ramsey, A. A., US 3830812, *Chem. Abstr*. **1974**, *81*, 136174.

[16]Kitamura, N., Onishi, A., EU 163599, *Chem. Abstr*. **1984**, *104*, 186439.

[17]Tenser, R. B., Gaydos, A., Hay, K. A., *Antimicrob. Agents Chemother*. **2001**, *45*, 3657.

[18]Sharma, P., Rane, N., Gurram, V. K., *Bioorg. Med. Chem. Lett*. **2004**, *14*, 4185.

[19]De la Cruz, J. P., Carrasco, T., Ortega, G. De La Cuesta F. Sanchez, *Lipids*, **1992**, *27*, 192.

[20]Thierney, J. P., Lidstrm, P. Blackwell, *Microwave Assisted Organic Synthesis*, Publishing Ltd; **2005**:296. ISBN 1-405-11560-2.

[21]Loupy, A., *Microwaves in Organic Synthesis, Wiley-VCH, Weinheim*; **2002**.

[22]Hayes, B. L., *Microwave Synthesis: Chemistry at the Speed of Light, CEM Publishing, Matthews NC*, **2002**.

[23]Kappe, C. O., Stadler, A., *Microwaves in Organic and Medicinal Chemistry, Wiley-VCH, Weinheim*, **2005**.

Received: 22.03.2014.
Accepted: 14.04.2014.

ADSORPTIVE REMOVAL OF Pb(II) AND Cr(VI) IONS ON NATROLITE

Uzma Nadeem[a]*

Keywords: natrolite; adsorption; isotherm models; wastewater

Natrolite proved to be an effective adsorbent for the adsorptive removal of lead and chromium ions from aqueous solutions. Adsorption parameters such as pH, adsorbent dose, temperature, and contact time were optimized. For the determination of rate of metal adsorption by natrolite from 50 mL (20 mg L^{-1}), the supernatant was analyzed for residual metals after the contact period of 10-120 min. The effect of pH on metal adsorption by natrolite was determined at values pH 2-8 and the effect of different doses of natrolite from 0.1 to 0.6 was determined, as well as to what extent the adsorption data obey Langmuir and Freundlich adsorption isotherms were also investigated. Thermodynamic studies shows the negative values of ΔG^0 at all the temperature indicates the spontaneous nature of Pb(II) and Cr(VI) ions on natural mineral natrolite. Natrolite has shown good results ans exhibits that the pH plays an important role in adsorption of metal ions.

*Corresponding Authors
E-Mail: uzmanadeem3@gmail.com
[a] Chemistry Department, University of Delhi, Delhi, 110007, India.

Introduction

Heavy metals are common pollutant found in various industrial effluents. The stricter environment regulation on the discharge of heavy metals makes it necessary to develop various technologies for the removal. Waste streams containing low to medium level of heavy metals are often encountered in metal plating facilities, electroplating, mining operations, fertilizer battery manufacture, dyestuffs, chemical pharmaceutical, electronic device manufactures and many others. Most of the heavy metals are highly toxic and are not biodegradable; therefore they must be removed from the polluted streams in order to meet increasingly stringent environmental quality standards. Many methods including chemical precipitation, electro-deposition, ion exchange, membrane separation, and adsorption have been used to treat such streams of these methods, traditional chemical precipitation is the most economic but is inefficient for dilute solution. Ion exchange and reverse osmosis are generally affective but have rather high maintenance and operation costs and subject to fouling. Adsorption is one of the few promising alternatives for this purpose, especially using sorbents such as agricultural wastes, clay materials, zeolites, biomass and sea food processing waste.[1,2]

In the present work, the adsorption behaviour of natural zeolite (natrolite) with respect to Pb(II) and Cr(VI) has been studied in order to consider the application to purify metal containing wastewater. Adsorption parameter such as pH, adsorbent dose, contact time and temperature were optimized in order to explore zeolites application in removal of metals from wastewater. The adsorption equilibrium data were compared to the Langmuir and Freundlich adsorption models. Thermodynamic studies were also performed to evaluate the nature of the adsorption process.

Experimental

Adsorbent

Naturally occurring zeolite (natrolite as a geological specimen, collected from Sinner, Nasik (Maharashtra) and was powdered after cleaning, washing and grinding to very fine white particles and sieved through 100 mesh and then stored in air tight container.

Chemical composition of natural natrolite is given in Table 1.[3] The specimen was further characterized by XRD (X-ray diffraction) and it was established that sample was natrolite.

Table 1. Chemical composition of natural natrolite

Chemical composition	Composition, in %
SiO_2	48.41
Al_2O_3	26.82
Na_2O	16.30
Fe_2O_3	1.12
K_2O	0.20
CaO	0.52
MgO	0.20
H_2O	6.43

Preparation of stock solution

An aqueous solution (1000 mg L^{-1}) of Pb(II) and Cr(VI) was prepared and pH of solution was adjusted using 0.1 M HCl or NaOH. Fresh dilutions were used for each study.

Batch adsorption experiments

The adsorption experiments were carried out in batches of 50 mL of 20 mg L^{-1} metal solution with known amount of natrolite. The solutions were shaken in orbital shaker (Shivam ISO 900/2000) at 120 rpm, at 30 ^oC for a definite period of time, followed by centrifugation.

Eur. Chem. Bull., **2014,** *3(5)*, 495-501 DOI: 10.17628/ecb.2014.3.495-501

The supernatant containing the residual concentration of metals was determined using atomic absorption spectrophotometer (AAS, ECIL-4141). Adsorption parameters such as pH, adsorbent dose, temperature, and contact time were optimized by the method of trial and error. For the determination of rate of metal adsorption by natrolite from 50 mL (20 mg L^{-1}), the supernatant was analyzed for residual metals after the contact period of 10, 20, 30, 60, 90 and 120 min. The effect of pH on metal adsorption by natrolite was determined at values pH 2-8 and the effect of different doses of natrolite from 0.1 to 0.6 was determined. For the adsorption isotherm studies optimized parameters were determined to reach equilibrium for 20 mg L^{-1}, Pb(II) and Cr(VI) ion concentration.

Calculations

The percent removal of metal ions was calculated by using the Equation 1.

$$R(\%) = \frac{C_i - C_f}{C_i} \times 100 \quad (1)$$

where

R is the removal,

C_i is the initial metal concentration and

C_f is the final concentration of the metal ion in mg L^{-1}.

The sorption capacity was calculated from Eqn. 2

$$Q_e = \frac{V(C_i - C_e)}{1000W} \quad (2)$$

where

Q_e is the adsorption capacity (mg g^{-1}),

C_i is the initial metal concentration (mg L^{-1}),

C_e is the equilibrium concentration of metal (mg L^{-1}),

W is the adsorbent dose (g) and

V is the solution volume (mL).

Results and discussion

Effect of pH

pH is an important parameter for adsorption of metal ions because it affects the solubility of the metal ions, concentration of the counter ions on the functional groups of the adsorbent and the degree of ionization of the adsorbate during reaction.

The removal of metal ions from wastewater sample by adsorption is related to the pH of the sample, as the latter affects the surface charge of adsorbents, the degree of ionization, and the species of adsorbate. Adsorption of heavy metals from aqueous solutions depends on properties of adsorbent and molecules of adsorbate transfer from the solution to the solid phase.

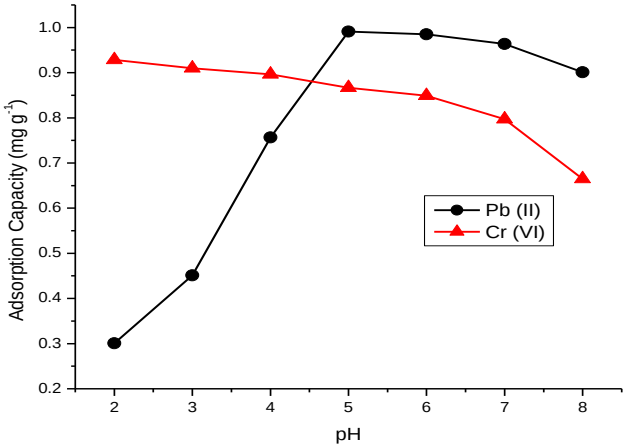

Figure 1. Effect of pH on adsorption capacities of Pb(II) and Cr(VI) ions.

It has been also reported that adsorption capacities for heavy metals are strongly pH sensitive and that adsorption increases as solution pH increases.[4,5] Initial investigation of adsorption capabilities of natrolite for Pb(II) and Cr(VI) ions with the adsorbent dose 0.5 g, per 50 mL of 20 mg L^{-1} metals solution and the role of H^+ concentration was examined at different values of pH 2-8 and Figure 1, showed maximum adsorption capacity for Pb(II) at pH value 5 and whereas Cr(VI) ions shows maximum adsorption capacity at pH value 2.

Zeolites in general, are weakly acidic in nature and sodium form exchanges are selective for hydrogen (R-Na + $H_2O \leftrightarrow RH + Na^+ OH^-$), which leads to high pH values when the exchanger is equilibrated with relatively dilute electrolyte solutions.[6] When the pH of aqueous solution of Pb(II) ion increases, the adsorption capacity increases (Figure 1) sharply up to pH 5. The increase in Pb(II) ion adsorption as pH increases can be explained on the basis of a decrease in competition between proton (H^+) and metal ions on the surface of adsorbent. As pH increased, more adsorbent surface would be exposed and carried negative charges with subsequent attraction of metal ions.[7] However, at pH 4.5 and 5 the hydrolysis of Pb(II) ion starts.[8] The stepwise hydrolysis process could be shown to take place as below.

$$Pb^{2+} + OH^- \rightarrow Pb(OH)^+ \rightarrow Pb(OH)_2$$

The formation of $Pb(OH)^+$ ion makes not only the ion heavier but also reduced charged by one on the ion therefore, the attraction of the ion towards site is not to that extent which explains the slow increase in removal of ions. At a pH where, $Pb(OH)_2$ come out of the solution the removal of lead become difficult. That explains the decrease in adsorption capacity.

At lower pH (pH = 2), dominant form of Cr(VI) is $HCrO_4^-$ while the surface of adsorbent is charged positively. The stable forms of chromium such as H_2CrO_4 and CrO_3 exist as polynuclear species at high chromium concentration and hence the low pH value of 2 results in a higher percentage removal of Cr(VI).[9] Cr(VI) is present in solution as CrO_4^{-2} and $Cr_2O_7^{-2}$ at normal pH values but when pH values are

 DOI: 10.17628/ecb.2014.3.495-501

reduced below 3 then chromium exists in the form of $HCrO_4^-$.[10,11] When adsorbent mixed with chromium solution at low pH values then OH^- group present in adsorbent are replaced by chromate ions in the solution. Since the charge of chromates are negative and the charge of lead ion is positive, it can explain the different trend in adsorption of Cr(VI) ions and Pb(II) at at different pH values. On increase in the pH of the metal solution the acidic sites decreases and increases the Na^+ sites on the natrolite surface. This results into increase in the anionic (alkaline) OH^- sites on Al atoms and increase in the negative charge along with decrease in the positive partial charge on the surface of the adsorbent. When the pH decreases the acidic sites of Si (OHs at Si) increases. This result into decrease in the Na^+ sites and decrease in the Al-OH sites along with increase in the positive charges with decrease in the negative charge on the natrolite cage.

According to Low et al,[12] at low pH values the surface of the adsorbent would be closely associated with hydroxonium ions (H_3O^+), by repulsive force, to the surface functional groups, consequently decreasing the percentage removal of metals. The pH of the aqueous solution is an important controlling parameter in the adsorption process. As the solution pH increase, the onset of the metal hydrolysis and precipitation began at pH >8 and the onset of adsorption therefore occurs before the beginning of hydrolysis.[13] When the pH of the adsorbing medium was increased from 2-8, there was a corresponding increase in de-protonation of the adsorbent surface, leading to decrease in H^+ ion on the adsorbent surface, which favours adsorption of positively charge species and the positive sites on the adsorbent surface.[14-16]

Effect of adsorbent dose

It is important to fix the amount of adsorbent to design the optimum treatment systems and for a quick response of the analysis. To achieve this aim batch experiments were conducted with the adsorbent dose 0.1-0.6 g per 50 mL 20 mg L-1 of metal solution. Figure 2 shows the adsorption of Pb(II) and Cr(VI) with varying weight of the adsorbent. It indicates that the uptake of Pb(II) and Cr(VI) ions increases as the adsorbent dose increases from 0.1 0.6 g per 50 mL of 20 mg L^{-1} metals solution.

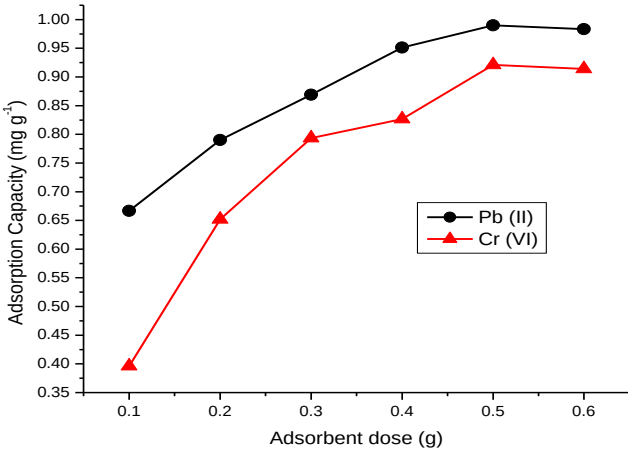

Figure 2. Effect of adsorbent dose on adsorption capacities of Pb(II) and Cr(VI) ions.

Beyond 0.5 g of adsorbent the Pb (II) and Cr(VI) ions removal decreased. According to Shukla et al,[17] the decrease in adsorption with increase in adsorbent dose is due to the high number of unsaturated sites. Based on Figure 2 , an amount of 0.5 g of adsorbent was found to be sufficient to remove Pb (II) and Cr (VI) ions from aqueous solution.

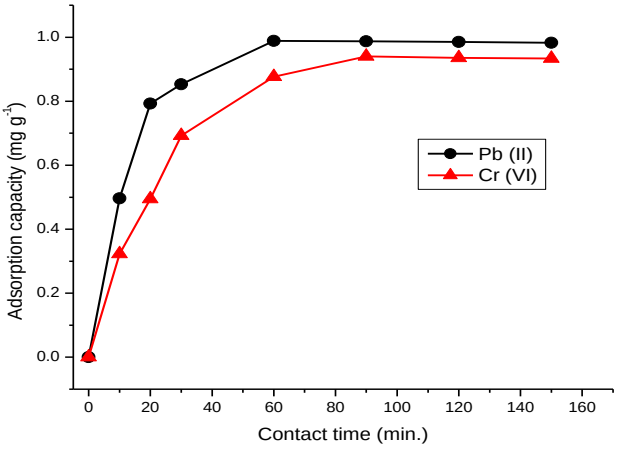

Figure 3. Effect of contact time on adsorption capacities of Pb(II) and Cr(VI) ions.

Effect of contact time

Batch experiments were conducted with the adsorbent dose 0.5 g, per 50 mL of 20 mg L^{-1} of metal solution to study the effect of contact time. Shaking time was varied from 5 minute to 120 min. The Figure 3 shows that the adsorption capacity of natrolite for of Pb(II) and Cr(VI) ions by natrolite was increased with the time of shaking. A sharp increase was observed at 60 min for Pb (II) ions and 90 min for Cr (VI) ions. Hence the contact time of 60 min for Pb (II) ion and 90 min for Cr (VI) ion was set for adsorption isotherm studies.

According to Bhattacharya and Gupta,[18] the initial high rate of metal uptake may be attributed to the existence of the base surface. However the number of available adsorption sites decreased as the number of metal ions adsorbed increases. The enhanced adsorption of metal ion with in agitation time may also in boundary resistance to mass transfer in the bulk solution and an increase in the kinetic energy of hydrated ion.[19] By increasing the agitation time, the boundary layer resistance will be reduced and there will be an increase in the mobility of ions in the solution.

Effect of temperature

Temperature is one of the most important factors in the process of sorption used for wastewater treatment. The net increase or decrease of sorption however, depends upon the nature of the sorbate as well as sorbent. The adsorption process may be either exothermic or endothermic. Temperature increases the rate of removal indicating the process to be endothermic and decrease in the removal indicates exothermic process

Batch experiments were conducted with the adsorbent dose 0.5 g, per 50 mL of 20 mg L^{-1} of metal solution to study the effect of temperature. The effect of temperature on

 DOI: 10.17628/ecb.2014.3.495-501

the adsorption capacity of the Pb(II) and Cr(VI) by the natrolite is shown in Figure 4. It is clear that the uptake of Pb(II) and Cr(VI) ions increased with in an increase in temperature from 20-30 °C.

The adsorption of Pb(II) and Cr(VI) ions may involves chemical bond formation and ion-exchange since the temperature is the main parameter affecting the above two process.[20]

The increase in amount of Pb(II) and Cr(VI) ions adsorbed at equilibrium with increases in temperature may be due to the acceleration of some originally slow adsorption steps or to the creation of some active sites on the adsorbent surface.[21] The increase in uptake of metals with temperature may also due to the change in pore size.[22]

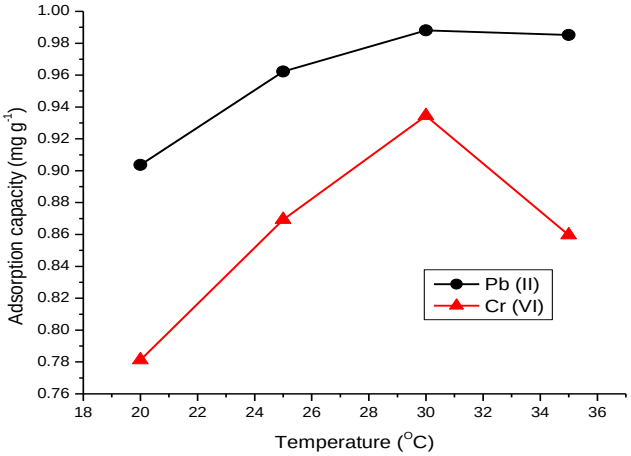

Figure 4. Effect of temperature on adsorption capacities of Pb (II) and Cr(VI) ions.

The amount of Pb(II) and Cr(VI) metals sorbed on natrolite increases by temperature can be explained on the basis of hydrogen binding. In aqueous solutions of metals, there exists extensive hydrogen bonding between the metal molecules and water, resulting in appreciable solubility. This hydrogen bonding get broken at higher temperatures and, this cause metals to be less soluble and, therefore, exhibit a higher tendency to go to the adsorbent surface and adsorbed their rather remaining in the solution.[23]

Adsorption Isotherm Models

The adsorption of a substance from one phase to the surface of another in a specific system leads to a thermodynamically defined distribution of that substance between the phases as the system reaches equilibrium. This distribution can be expressed in terms of adsorption isotherms.[24] Adsorption of Pb(II) and Cr(VI) ions on natrolite was studied in the concentration range 5-20 mg L^{-1} with 0.5 g of adsorbent. The adsorption data were applied to the Langmuir and Freundlich isotherm models.[25, 26] The isotherm constants of Langmuir and Freundlich were calculated using normal linearization method.

Since, the adsorption isotherm is important to describe how adsorbate will interact with adsorbents and so is critical for design purpose, therefore, data using an equation is essential adsorption operation.[27] Modelling of equilibrium data is fundamental for the industrial application of adsorption since it gives information for comparison among different adsorbent under different operational conditions, designing and optimizing operation procedure.[28]

The result of batch equilibrium was used to characterize the equilibrium between the amount of adsorbate that accumulated on the adsorbate and the concentration of dissolve adsorbate. The experimental isotherm data set obtained was fitted using adsorption models including the Langmuir and Freundlich isotherm.

The isotherm constants of Langmuir and Freundlich were calculated using normal linearization method.

Freundlich model

The adsorption data have been fitted to the Freundlich isotherm. Its linearised form is represented by Equation 3.

$$\lg Q_e = \lg K + \frac{1}{n}\lg C_e \qquad (3)$$

where

C_e is the equilibrium concentration (mg L^{-1}),

Q_e is the amount adsorbed (mg g^{-1})

K is adsorption capacity and $1/n$ is adsorption intensity.

A plot of log Q_e versus log C_e (Figure 5) gives a straight line of slope n and intercepts K and the coefficient of determination (R^2).

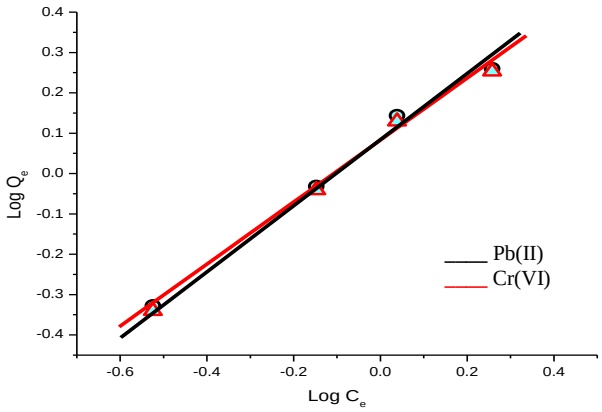

Figure 5. The linearized plot for the Freundlich adsorption isotherm of Pb(II) and Cr (VI) using natrolite.

Langmuir model

The capacity of metal binding was determined by plotting C_e/Q_e against C_e, using the Langmuir equation. The plot of the specific sorption C_e/Q_e against equilibrium concentration C_e gave the linear isotherm parameters Q_{max}, b and the coefficient of determination (R^2).

The linear equation of Langmuir represented as Equation 4.

$$\frac{C_e}{Q_e} = \frac{1}{Q_{max}b} + \frac{C_e}{Q_{max}} \qquad (4)$$

 DOI: 10.17628/ecb.2014.3.495-501

where

C_e is the metal concentration in the solution at equilibrium (mg L^{-1}),

Q_{max} (adsorption capacity) and b (energy of adsorption) are the Langmuir constants.

The essential characteristics of Langmuir equation can be described by dimensionless equilibrium parameter,[29] R_L which is defined as;

$$R_L = \frac{1}{1 + bC_0} \qquad (5)$$

where, b is the Langmuir constant C_0 is the initial metal concentration.

Table 2. Relationship between R_L and type of isotherm

R_L	Type of isotherm
$R_L > 1$	Unfavourable
$R_L = 1$	Linear
$R_L < 1$	Favourable
$R_L = 0$	Irreversible

The values of both Langmuir and Freundlich isotherm parameters were given in Table 3. Examination of correlation coefficient suggests that Freundlich isotherm is a better model for the sorption of Pb(II) and Cr(VI) ions. The values of n that vary between 1 and 10 indicate the favorable adsorption of heavy metals.[30] This isotherm does not predict any saturation of the sorbent by the sorbate; thus infinite surface coverage is predicted mathematically, indicating multilayer adsorption on the surface.[31]

The plots of C_e/Q_e against C_e for adsorption of Pb(II) and Cr(VI) ions gave a straight line are shown in Figure 6. It has seen that the linear fit is fairly good and enables the applicability of the Langmuir model to the Pb(II) and Cr(VI) ions adsorption on the natrolite.

The Langmuir isotherm model effectively describes the sorption with R^2 values. The sorption capacity, Q_{max} which is a measure of maximum adsorption capacity corresponding to complete monolayer coverage showed that natrolite had a mass capacity for Pb(II) and Cr(VI) ions are 4.3956 and 7.0225 mg g^{-1}, respectively. The adsorption coefficient b which is related to the apparent energy of adsorption Pb(II) and Cr(VI) ions are 0.3969 and 0.1602 L mg^{-1} respectively. The high Si/Al ratio of natrolite results in typical low anionic field that gives rise to good selectivity.

The correlation coefficient of data for Langmuir and Freundlich plot give a value which is > 0.9 although this value for Freundlich isotherm is slightly higher than that of Langmuir isotherm since, the correlation coefficient for both are high, it reveals that besides monolayer adsorption there is multilayered adsorption and also suggests that adsorption reaction is physico-chemical type.

Table 3. Langmuir and Freundlich adsorption parameters for the adsorption of Pb(II) and Cr(VI) ions at 30 °C.

Freundlich Parameters	**Pb(II)**	**Cr(VI)**
K	0.8007	0.9519
n	1.1469	1.1555
R^2	0.9990	0.9978
Langmuir Parameters	**Pb(II)**	**Cr(VI)**
Q_{max} (mg g^{-1})	4.3956	7.0225
b (L mg^{-1})	0.3969	0.1602
R^2	0.9641	0.9469

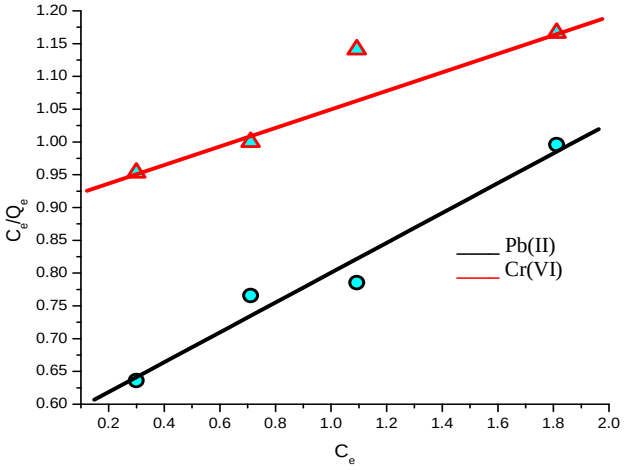

Figure 6. The linearized plot for the Langmuir adsorption isotherm of Pb(II) and Cr(VI) using natrolite

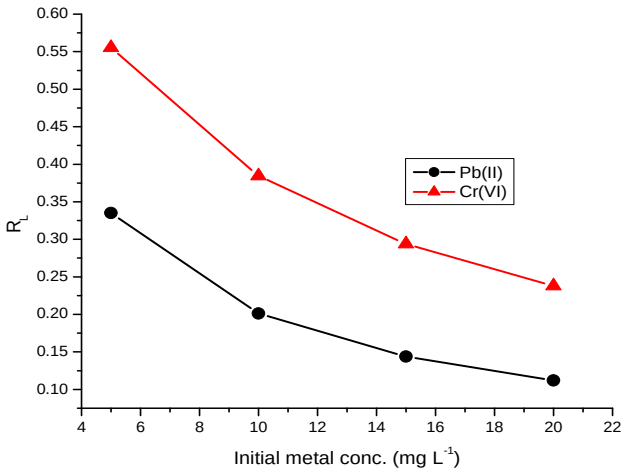

Figure 7. R_L vs initial concentration of metal ion

The R_L values between 0 and 1 indicate favorable adsorption.[32] In the present study the R_L for Pb(II) ions were found to be, 0.3351, 0.2012, 0.1438 and 0.1119 and the R_L for Cr (VI) ions were found to be 0.5552, 0.3843, 0.2938, and 0.2379 as shown in figure- 7, for the initial concentration of Pb (II) and Cr (VI) ions of 5-20 mg L^{-1} indicating that the adsorption of Pb (II) and Cr (VI) ions is favorable. The Langmuir model deals with monolayer coverage and constant adsorption energy while Freundlich equation deals with physicochemical adsorption on heterogeneous surfaces.[33]

 DOI: 10.17628/ecb.2014.3.495-501

In the present study the applicability of both these isotherms to the adsorption of Pb(II) and Cr(VI) adsorption, implies that monolayer adsorption and heterogeneous surfaces conditions exist under the experimental conditions used. The adsorption properties of the adsorbent are thus likely to be complex, involve more than one mechanism.

Zeolites in general, are weakly acidic in nature and sodium form exchanges are selective for hydrogen (R-Na + $H_2O \leftrightarrow RH + Na^+ OH^-$), which leads to high pH values when the exchanger is equilibrated with relatively dilute electrolyte solutions[6] making metal hydroxide precipitate feasible. In natural zeolites these metals seem to reach saturation, which means that the metal had filled possible available sites and adsorption could take place only at new surfaces.

The heavy metal cations are present as hexa aqua complex ions with six surrounding water molecules in the solution and they assed the channel of zeolite in this form.[34] Since the adsorption phenomena depend on the charge density of cations, the diameter of hydrate cations is very important.

It was found that the adsorption equilibrium data was better fitted by the Freundlich isotherm, although it can also be modeled by the Langmuir isotherm in the concentration range studied since it presented the greater coefficient of correlation.

Thermodynamic studies

Thermodynamic parameters such as change in Gibb's free energy ΔG^0, enthalpy ΔH^0 and entropy ΔS^0 were determined using the following Equation 6

$$K_d = \frac{Q_e}{C_e} \qquad (6)$$

where

K_d is the apparent equilibrium constant,

Q_e is the amount of metal adsorbed on the unitary sorbent mass (mmol g^{-1}) at equilibrium and

C_e equilibrium concentrations of metal ions in solution (mmol L^{-1}), when amount adsorbed is equals Q_e.

The thermodynamic equilibrium constants (K_d) of the Pb(II) and Cr(VI) ions adsorption on studied natrolite were calculated by the method suggested by Khan and Singh[35] from the intercept of the plots of $\ln (Q_e/C_e)$ vs. Q_e.

Then, the standard free energy change ΔG^0, enthalpy change ΔH^0 and entropy change ΔS^0 were calculated from the Van't-Hoff Equation 7.

$$\Delta G^0 = -RT \ln K_d \qquad 7$$

where

K_d is the apparent equilibrium constant;

T is the temperature in Kelvin and

R is the gas constant (8.314 $Jmol^{-1} K^{-1}$)

The slope and intercept of the Van't-Hoff plot of ΔG^0 vs T were used to determine the values of ΔH^0 and ΔS^0. The influence of the temperature on the system entropy was evaluated using the equations-8.

$$\Delta G^0 = \Delta H^0 - T\,\Delta S^0 \qquad (8)$$

where

ΔH^0 is the enthalpy change (kJ mol^{-1}) and

ΔS^0 is the entropy change (kJ mol^{-1} K^{-1}).

The values of standard Gibbs free energy change for the adsorption process gained from Equation 8 are listed in Table 4. The negative values of ΔG^0 at all the temperature indicates the spontaneous nature of Pb(II) and Cr(VI) ions on natural mineral natrolite. The negative value of ΔG^0 decrease with increase in temperature, suggests that a better adsorption is actually obtained at higher temperature.

Table 4. Thermodynamic parameters for the equilibrium sorption of Pb(II) and Cr(VI).

Parameters for Pb(II)	**Temperature, K**			
	295	**300**	**305**	**310**
ΔG^0 (kJ mol^{-1})	-1.294	-1.936	-2.242	-2.433
ΔH^0 (kJ mol^{-1})	20.54			
ΔS^0(kJ mol^{-1} K^{-1})	-0.074			
Parameters for Cr(VI)	**Temperature, K**			
	295	**300**	**305**	**310**
ΔG^0 (kJ mol^{-1})	-5.022	-5.505	-6.334	-6.884
ΔH^0 (kJ mol^{-1})	32.87			
ΔS^0(kJ mol^{-1} K^{-1})	-0.128			

The standard enthalpy changes of Pb(II) and Cr(VI) ions adsorption determine from the Equation 8, were 20.54 kJ $mol^{-1}$and 32.87 kJ mol^{-1}, respectively. The changes in entropy of Pb(II) and Cr(VI) ions adsorption were -0.074 kJ mol^{-1} K^{-1} and -0.128 kJ mol^{-1} K^{-1}, respectively.

The negative ΔG^0 values indicates that the adsorption process is exothermic and the negative value of ΔS^0 for both Pb(II) and Cr(VI) ions shows that the exothermic adsorption process occurs with increase in disorder at solid-liquid interface, which suggests that the process is always spontaneous at all temperature.[36]

Conclusions

This work indicates that natrolite can be used for removal of Pb(II) and Cr(VI) ions from wastewater. Both Langmuir and Freundlich isotherm models can be used to estimate maximum metals uptake and the affinity parameter. It was found that the adsorption equilibrium data was better fitted by the Freundlich isotherm; although it can also be modeled by the Langmuir isotherm in the concentration range studied. The negative ΔG^0 values indicate the spontaneous nature of the adsorption and the process is exothermic and also suggests that a better adsorption is actually obtained at higher temperature. The removal of carcinogenic toxicant was found to depend on metal solution pH, adsorbent

 DOI: 10.17628/ecb.2014.3.495-501

dosage, contact time and temperature. Solution pH is an important parameter affecting adsorption of Pb(II) and Cr(VI) ions and maximum removal for Pb(II) ions at pH value 5 and for Cr(VI) ions at pH value 2 was observed. The adsorption mechanism of Pb (II) and Cr (VI) ions on natrolite involves either cation exchange or complexation between the metal cation and the hydroxide ion in the solution. This study shows a new trend for using natrolite for the benefit of environmental pollution control

Acknowledgements

Authors are thankful to the Head, Department of Chemistry, Director, USIC, University of Delhi, and Director of AIRF-Jawaharlal Nehru University for providing instrumentation facilities and UGC [F.15-76/12 (SA-II)] for providing financial assistance.

References

[1]Kesraoui-ouki, S., Cheeseman, C. R. and Perry, R., *J. Chem. Tech. Biol*., **1994**, *59***,** 121-126.

[2]Orhan, Y. and Buyukgungor, H., *Water Sci. Tech*., **1993**, *28(2)*, 247-255.

[3]Kumar, S. and Chattopahdyaya, M. C., *J. Indian Chem. Soc*. **2009**, *86*, 775-782.

[4]Yin, P. H., Yu, Q. M. and Ling, Z.; *Water Res.*, **1999,** *33***,** 1960-1963.

[5]Zhang, L., Zhao, L., Yu, Y. T. and Chen, C. Z.; *Water Res*., **1998**, *32*, 1437-1444.

[6]Leinonen, H. and Lehto, J.; *Waste Manage. Res*., **2001**, *19***,** 45-57.

[7]Brady, D. and Duncan, J. R., *Appl. Microbiol. Biotechnol*., **1994**, *41*, 149-154.

[8]Marques, P., Rosa, M. F. and Pinheiro, H. M., *Bioproc. Biosystems Eng.*, **2000**, *23*, 135-141.

[9]Bayat, B. ; *J. Hazard. Mater*. **2002**, *95*, 275–290.

[10]Demirbas, E.; Kobya, M.; Senturk, E. and Ozkan, T. ; *Water SA*, **2004**, *30*, 533-539

[11]Park, D.; Yun, Y. S.; Lim, S.R. and Park, J.M. ; *J. Microbiol. Biotechnol*., **2006b**, *16(11*), 1720-1727.

[12]Low, K. S.; Lee, C. K. and Leo, A. C. ; *Bioresource Technol*., **1995**, *51***,** 227-231.

[13]Baes G. B. and Mesmer, R. E.; "*Hydrolysis of Cations*", John Wiley and Sons, New York, **1976**.

[14]Ghanem, S. A. and Mikkelsen, D. S.; *Soil Sci.*, **1988**, *146***,** 15-21.

[15] Kadirvelu, K. and Namasivayam, C.; *Adv. Environ. Res*., **2003**, *7*, 471- 478.

[16]Abdus-Salam, N. and Adekola, F. A. ; *AJST*., **2005**, *6*, 55-66.

[17]Shukla, A.; Zhang, Y. H.; Dubey, P.; Margrave, J. L. and Shukla, S. S.; *J. Hazard. Mater.*, **2002**, *B95*, 137-152.

[18]Bhattacharya, K. G. and Gupta, S. S.; *Colloid Surf. A: Physiochem. Eng. Asp*., **2006**, *277*, 191-200.

[19] Horsfall, M. and Abia, A. A., *Water Res*., **2003**, *37*, 4913-4923.

[20]Yubin, T., Fangyan, C. and Honglin, Z., *Adsorpt. Sci. Technol*., **1998**, *16***,** 595-606.

[21]Nassar, M. M. and Magdy, Y. H., *Indian Chem. Eng.*, **1999**, *40(1)*, 27-30.

[22]Pandey, K. K., Prasad, G. and Singh, V. N., *Water Res.*, **1985**, *19*, 869-873.

[23]Jain, A. K., Suhas and Bhatnagar, A., *J. Colloid Inter. Sci.*, **2002**, *251(1)*, 39-45.

[24]Kinniburgh, D. G., *Environ. Sci. Technol*., **1986**, *20*, 895-904.

[25]Langmuir, I., *J. Am. Chem. Soc.*,**1918**, *40*, 1361-1402.

[26,]Freundlich, H., *Z. Physik. Chem*., **1907**, *57*, 385- 470.

[27]Hashem, M. A., Abdelmonem, R. M. and Farrag, T. E.; *Alexandria Eng. J*., **2007**, *1***,** 1-9**.**

[28]Benguella, B. and Benaissa, H., *Water Res*., **2002**, *36*, 2463-2474.

[29]Hall, K. R., Eagleton, I. C., Acrivos, A. and Vermeulen, T., *Ind. Eng. Chem. Fund.*, **1966**, *5***,** 212-223.

[30]Kadirvelu, K. and Namasivayam, C., *Environ. Tech.*, **2000**, *21***,** 1091-1097.

[31]Hasany, S. M., Saeed, M. M., Ahmed, M., *J. Radioanal. Nucl. Chem*., **2002**, *252***,** 477-484.

[32]Ahalya, N., Kanamadi, R. D., Ramachandra, T. V., *Indian J. Chem. Technol*., **2006**, *13*, 122-127.

[33]Singh, K. K.; Singh, A. K. and Hasan, S. H.; *Bioresource Technol*., **2006**, *97***,** 994-1001.

[34]Jama, M. A. and Yucel, H.; *Sep. Sci. Tehnol*., **1990**, *24***,** 1393-1416.

[35]Khan, A. and Singh, R., *Colloids Surfaces*, **1987**, *24*, 33–42.

[36]Kailas, M. D. and Ejazuddin, M. K., *Rev. Environ. Sci. Biotechnol*., **2013**, *12*, 25–44.

Received: 31.03.2014.
Accepted: 14.04.2014.

 DOI: 10.17628/ecb.2014.3.495-501

ENHANCEMENT OF SEED GERMINATION AND PLANT GROWTH OF WHEAT, MAIZE, PEANUT AND GARLIC USING MULTIWALLED CARBON NANOTUBES

Anita Srivastava[a] and D. P. Rao[a]*

Keywords: carbon nanotubes, growth enhancement, MWCNTs.

The uptake of carbon nanomaterials by plants has shown a very recent field of nano-agriculture. This work investigated about the beneficial effects of functionalized multiwalled carbon nanotubes on wheat, maize, peanut and garlic. Here in, we explore the potential influence of 0-50 μg mL^{-1}, the MWCNTs on these different seeds at different concentration. The effects of MWCNTs on root and shoot growth, biomass, number of leaves were investigated. It was hypothesized that MWCNTs were able to penetrate the seed coat by creating new pores; thereby enhancing water uptake. The results of the combined morphological and physiological analysis indicate that after about 5-10 days exposure under our experimental conditions MWCNTs significantly enhances plant growth and biomass compared to control. The number and size of leaves of the MWCNTs treated plants had shown positive effects in a dose dependent manner. Nanotubes exposed seeds sprouted up to three to four times faster than controlled. TEM images of peanut root shows the presence of carbon nanotubes that could explain the enhanced water delivery. Overall after investigation we conclude that low dose MWCNT have seen to be beneficial, improving water absorption, found to accelerate the process of germination by shortening the germination time and higher biomass production.

* Corresponding Authors
E-Mail: devendrapratapraO@yahoo.com
[a] Department of Chemistry, D.A-V. P.G. College, Kanpur-208001, U.P., India

Introduction

Carbon nanotubes are well ordered, high aspect ratio allotropes of carbon having unique physico-chemical characteristics. It has acquired an important status in medicinal and biological application such as gene and drug delivery, tissue engineering, biosensing as well as in diagnostic area.[1-3] Therefore the probability of plant exposure to carbon nanotubes has increased to a greater extent with the rapid growth of research, increasing production and use of nanomaterials in different area.[4]

Changes in agricultural technology have been a major factor shaping modern agriculture, Carbon nanotubes are among the most widely used Carbon based nanomaterial which can easily penetrate membrane like cell wall of plants. As a result CNTs have enormous potential for use in agriculture as directed delivery systems for pesticides, fertilizer and other chemicals. Plant cell wall acts as a barrier for easy entry of any external agent including nanoparticles into plant cells. The sieving properties are determined by pore diameter of cell wall ranging from 5 to 10 nm.[5] Hence only nanoparticles with diameter less than the pore diameter of the cell wall could easily pass through and reach the plasma membrane.[6] There is also a chance for enlargement of pores or induction of new cell wall pores upon interaction with engineered nanoparticles which inturn enhance nanoparticle uptake. Therefore the study on the effects of nanoparticles in plant science is a newly emerging area of research.[7,8] Recently confocal fluorescence image studies have revealed the capacity of single walled carbon nanotubes (SWCNTs) to traverse across both the plant cell wall and cell membrane. Growing interests in applying nanoparticles to plants for agriculture and horticulture[9,10] have shown both positive and negative effects of nanomaterials on the growth and development of seedlings.[11] It is mainly dependent on concentration of nanomaterials delivered to plants. Plants and plant cells showed high tendencies to accumulate CNTs, making plants as an important link in the pathway by which CNTs enter the food chain and biological cycles.[12] Torney and coworkers demonstrated that CNTs can assist the delivery of biological molecules into plant cells.[13] Current literature revealed that the uptake, translocation and accumulation of nanoparticles depend on the species of plant and the size, type, chemical composition, fictionalization and stability of nanoparticles. At the whole plant level a number of researches have reported the dramatic effects on seed germination and plant growth by multi walled carbon nanotubes.[14] More efficient water uptake induced by CNT has been implied as the growth stimulator.[15] On the other hand there exist some contradictory reports that show the toxicity of CNTs to the growth of a number of different plants.[16]

Experimental

The carboxylic acid functionalized multi-walled Carbon nanotubes were purchased from SISCO Research Laboratories Pvt. Ltd. Mumbai. The as-received MWCNTs were powder with 95 % purity, OD 10-20nm and length between 10-30 μm.

Seeds of wheat (*Triticum aestivum*), maize (*Zea mays*), peanut (*Arachis hypogaea*) and garlic bulb (*Allium sativum*) were purchased from local market. These all were washed with deionized water. $MWCNT_S$–COOH in different concentration 20 μg mL^{-1}, 50 μg mL^{-1} were prepared directly in deionized water and dispersed by ultrasonic vibration for one hour. Seeds of all food plant species were soaked in nanoparticle solution for overnight in the dark. Garlic cloves had also kept in solution for 30 minutes. There

garlic cloves were planted into soil about 2 inches deep. In the same way soaked seeds of wheat, maize and peanut were sown, one inch deep in soil. There all were exposed for equal amount of sunlight and equal amount of water was sprinkled on top of soil time to time.

The experiment for wheat seeds was conducted to determine the effects at 20 μg mL^{-1} and 50 μg mL^{-1} and for maize, peanut, garlic at only 50 μg mL^{-1} solution. The controlled sets for germinations were also carried out at the same time along with treated seeds. Every treatment, conducted triplicates each of which 8-10 seeds were maintained and examined for root and shoot development. These results were presented as mean ± SD (Standard deviation). Each of the experimental values was compared to its corresponding control.

Result and Discussion

A significant positive influence on root and shoot elongation was observed for all seeds in compared to those of unexposed control germination. Time of germination, germination percentage, vegetative biomass have shown encouraging results using low concentration of oxidized MWCNTs treated seeds as compared untreated. The effects of the CNTs on growth and development of the germinated sprouts were studied. Root and shoot systems were well recognized as they were fully germination in treated experiments in less time as compared to control.

Growth enhancement of CNTs-treated plants may have been due to the major changes of morphological and well developed root system. Wheat seeds were examined with two different concentration (20 and 50 μg mL^{-1}) of multi-walled Carbon nanotubes and also without MWCNTs. The treated and untreated seeds germinated at 3rd day but percentage of germination was significantly higher in tested medium in comparison to control. Wheat plant grown in 50 μg mL^{-1} possessed well developed long stems compared to the control (Figure 1).

Figure 1. Effect of water-soluble multiwalled carbon nanotubes on the growth of wheat seedling after 5 days

Effects of MWCNTs at different concentration on root and shoot length are shown in Figure 2a and 2b. The influence of MWCNTs solution at 50 μg mL^{-1} on root and shoot growth of maize plantlet varied with exposure time as shown in Figure 3a and 3b.

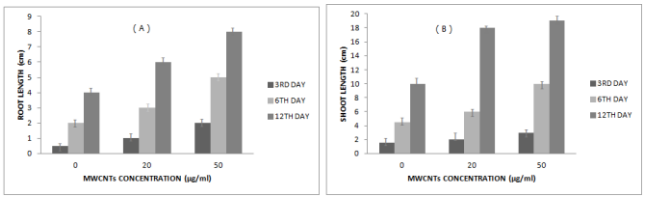

Figure 2. Effect of water-soluble multiwalled carbon nanotubes on wheat seedling. The values are given as mean +/SD (standard deviation) of triplicate samples with 10 seeds each.

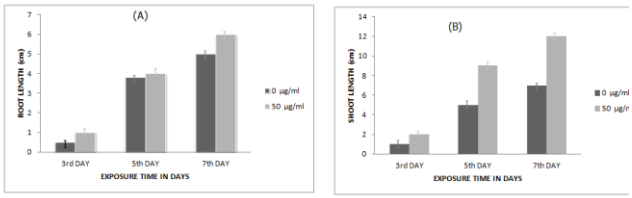

Figure 3. Effect of water-soluble multiwalled carbon nanotubes on germination of maize. The values are given as mean +/SD (standard deviation) of triplicate samples with 8 seeds each.

The well developed long stem and root and an increase in biomass compared to control is shown in Figure 4.

Figure 4. Effect of multiwalled carbon nanotubes on the growth of maize seedling after 5 days

Seed germination and embryo growth was much faster in case of MWCNTs, supplemented peanut seed. On third day it had seen that controlled seed was not germinated while treated seed had showed embryonic growth. There was enhancement of growth rate and biomass production Figure 5a and 5b The root and shoot length enhancement with respect to days is represented in Figure 6a and 6b.

Figure 5. Effect of water soluble carbon nanotubes on germination an growth of peanut seedling. A-without MWCNTs; B-with MWCNTs.

 DOI: 10.17628/ecb.2014.3.502-504

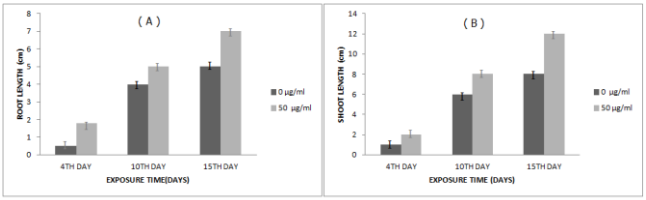

Figure 6. Effect of water soluble multiwalled carbon nanotubes on growth of peanut seedling. The values are given as mean +/SD (standard deviation) of triplicate samples with 8 seeds each.

Garlic cloves which were supplemented with MWCNTs sprouted 90 % till 12th day of sowing while untreated cloves have taken two weeks. There was much difference in root development Figure 7 in tested medium as compared to control. There is good correlation between root and shoot length of garlic plantlet with MWCNTs dose over control Figure 8a and 8b.

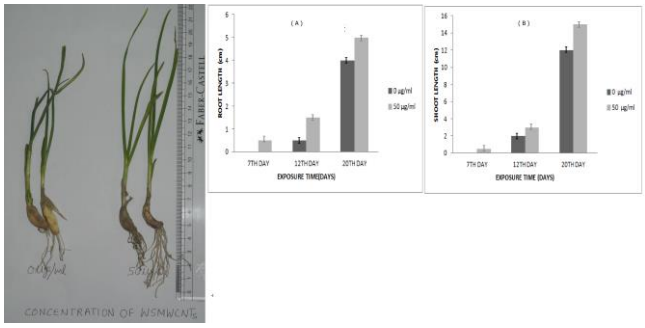

Figure 7. Phenotypes of 20 days old garlic plantlet growing on medium with and without CNTs

Figure 8. Effect of water-soluble multiwalled carbon nanotubes on garlic seedling. The values are given as mean +/SD (standard deviation) of triplicate samples with 10 seeds each.

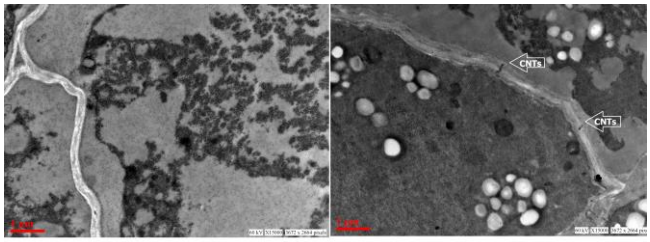

Figure 9. TEM images of the root system of 7 days old peanut seedlings growing on medium without CNTs and with CNTs

MWCNTs, internalization by plants was investigated by TEM (transmission electron microscopy). There is nanotubes accumulation in cell wall and inside the cell in TEM imaging of the root collected from peanut plantlet with and without exposure to MWCNTs. It can be seen in Figure 9 several CNT$_S$ which are completely missing in the images of the control sample. There studies indicate that the CNTs are able to penetrate in seedling as well as the root system and significantly affect their biological activity by enhancing the amount of water that penetrates inside the seed during the germination period.

Conclusions

Our results-demonstrated that all the wheat, maize peanut and garlic seedlings are affected by water soluble multi walled Carbon nanotubes in a concentration dependent manner. Carbon nanotubes can penetrate thick seed coat and support water uptake inside seeds. Lower concentrations are beneficial as they increases growth indices and water contents of the morphological parts most prominently for root which are directly in contact with the medium. The growth and higher biomass production for the plants that were exposed to 50 µg mL^{-1} MWCNTs-COOH, clearly indicate the positive effects of CNTs on seed germination which could have significant economic importance for agriculture.

Acknowledgements

We gratefully acknowledge Prof. L.K.S. Chauhan for TEM imaging at IITR, Lucknow, U.P., India. We are also thankful to University Grants Commission, New Delhi for financial assistance F. No. [39-714/2010].

References

[1]Harrison, B. S., Atala, d A., *Biomaterials*, **2008**, *28*, 344.

[2]Zanello, L. P., Zhao, B., Hu H., Haddon, R. C., *Nano Lett.*, **2006**, *6*, 562.

[3]Panyam, J., Labhasetwar, V., *Adv. Drug Delivery Rev.*, **2003**, *55*, 29.

[4]Joe, E. K., Wei, X., Anderson, R. R., Lin., C. P., *Biophys. J.*, **2003**, *84*, 4023.

[5]Fleischer, M. A., Neil, O., Ehwald, R., *Plant Physiol.*, **1999**, *121*, 829.

[6]Navarro, E., Baun, A., Behra, R., Hartmann, N. B., Filser, J, Miao, A. J., Quigg, A., Santschi, P. H., Sigg, L., *Ecotoxicology*, **2008**, *17*, 372.

[7]Zheng, L., Hong. F., Lu., S., Liu, C., *Biol. Trace Element Res.*, **2005**, *104*, 83.

[8]Lin, D., Xing, B., *Environment. Pollut.*, **2007**, *150*, 243.

[9]Liu, Q. , Chen, B., Wang, Q., Shi, X., Xiao, Z., Lin, J., Fang, X., *Nano Lett.*, **2009**, *9*, 1007.

[10]Khodakovskaya, M., Dervishi, E., Mahmood., M., Xu, Y., Li, Z., Watanabe, F., Biris, S., *ACS Nano*, **2009**, *3*, 3221.

[11]Nowack, B., Bucheli, T. D., *Environment. Pollut.*, **2007**, *150*, 5.

[12]Wierzbicka M., Antosiewicz, D., *Sci. Total Environment Suppl.*, **1993**, *1*, 423.

[13]Torney, F., Trewyn, B., Lin, V. S. Y., Wang, K., *Nanotechnology*, **2007**, *2*, 295.

[14]Serag, M. F., Kaji, N., Tokeshi, M., Yoshinobu, B., *RSC Adv.*, **2012**, *2*, 398.

[15]Villagarcia, H., Dervishi, E., de Silva, K., Biris, A. S., Khodakovskaya, M. V., *Small*, **2012**, *8*, 2328.

[16]Begum, P., Ikhtiari, R., Fugetsu, B., Matsuoka, M., Akasaka T., Watari, F., *Appl. Surf. Sci.*, **2012**, *262*, 120.

Received: 22.03.2014.
Accepted: 15.04.2014.